NATIONAL TECHNICAL UNIVERSITY OF ATHENS

School of Naval Architecture and Marine Engineering

Section of Naval & Marine Hydrodynamics

A Hamiltonian Coupled Mode method for the fully nonlinear water wave problem, including the case of a moving seabed

(Diploma Thesis)

by

Alexis-Tzianni Charalampopoulos

Supervisor: Gerassimos A. Athanassoulis, Professor

Athens, October 2016

This page is left blank intentionally

Acknowledgements

The present thesis may bear my name as author, yet it could not be accomplished without the significant contributions, be it guidance or assistance, from a number of people. For that reason, I would first like to thank Prof. G. Athanassoulis for giving me the opportunity to study such an interesting model (including both theoretical difficulty and applicability) and guiding me throughout the completion of the present work. His suggestions concerning the focus of my thesis not only arose to interesting and fruitful results, but also taught me to function in a more practical and efficient manner. Finally, his undergraduate courses throughout my years of study, enriched my theoretical background and shed light to topics scarcely discussed in most engineering schools. In the same manner, I would also like to thank C. Papoutsellis for his comments and suggestions during my work on this thesis, from the model itself to its numerical study or even to writing a scientific article in a more appropriate manner. In addition, I would also like to thank Prof. T. Gerostathis, who greatly assisted me in learning C++ (a language more or less foreign to me at the beginning of this work) and implementing the problem efficiently in a code. The hours he devoted in helping me fix bugs of the code during all this time, were crucial for the actualization of the current work and without his guidance, this process would be significantly hindered if not brought to a halt. Finally, I would like to thank my family for their unconditional support, be it emotional or material, in all my years of study, allowing me to focus on and pursue my interests.

Alexis-Tzianni Charalampopoulos

Athens, October 2016

Synopsis

Over the last few decades, the study of water waves is becoming relevant for more applications, surpassing their traditional study regarding ships and coastal structures and engulfing relatively new fields such as offshore platforms and energy harvesting from water waves. These problems are usually defined over very large physical domains and hence, the classic and fully nonlinear Navier-Stokes equations have found limited applicability due to their complexity and vast demand of computational time. Hence, the nonlinear irrotational (and inviscid) water wave problem (NLIWW) has been greatly employed for the study of many practical and highly demanding cases, with many new numerical methods arising. The framework of said new methods is the strive for computationally efficient solvers for highly nonlinear and complex problems.

In the first Chapter of this thesis, we present and describe the Hamiltonian Coupled-Mode method (HCM) for the full NLIWW problem. This method was first presented for the fully nonlinear problem in (Athanassoulis & Belibassakis, 2000). For this purpose we utilize an exact vertical eigenfuction series expansion together with Luke's unconstrained variational principle to derive an equivalent variational reformulation of the NLIWW problem. Concerns regarding the validity of this reformulation, which were initially presented in (Athanassoulis et al., 2016), are also addressed. We then proceed to reformulate the Euler-Lagrange equations by using a more computationally efficient system as was presented in (Athanassoulis & Papoutsellis, 2015). In the second Chapter, we calculate analytically the coefficients of the new formulation and present a way their computation can be implemented efficiently. We also present asymptotic results regarding these coefficients and other components of the model. Finally, we describe the truncated system to be used for the numerical implementation and, although we do not prove formally the validity of this truncation, we state some arguments in favor of its usage.

For the numerical part, in Chapter 3, we develop an efficient and parallel implementation of the model utilizing C++. The code can use an arbitrary order for the finite difference method (FDM) with results being presented for schemes from 2^{nd} order up to 12^{th} order. We also analyze the form the discretized system assumes. We then describe the 4^{th} order classical Runge-Kutta method used for the numerical time integration of the solution, completing thus the description of the code. To prove its numerical accuracy and efficiency the code is tested with computationally demanding, highly nonlinear cases. At first the accurate and efficient calculation of the DtN operator is of great importance and a variety of results regarding that matter are presented for a commonly used analytical test case. Following that, we verify the ability of the code to model a variety of complex problems, starting from long-time propagation of solitary waves, reflection of solitary waves on a vertical wall and asymmetric collision of two solitary waves over a flat bottom. We then proceed to present results for seabeds of arbitrary (and quite abrupt) bathymetry with solitary waves propagating over them. Finally, we address the problem of a moving seabed by simulating and presenting results for the experiments executed by Hammack in (Hammack, 1973).

Table of Contents

List of Abbreviations

(BEM) Boundary Element Method

(FDM) Finite Difference Method

(FEM) Finite Element Method

(HCM) Hamiltonian Coupled Mode

(KdV) Korteweg – de Vries

(NLIWW) Nonlinear Irrotational Water Wave

(PDE) Partial Differential Equation

(ZCS) Zakharov Craig Sulem

List of Symbols

Ox_1x_2z	Orthogonal Cartesian coordinate system used for the problem
D_h^η	Domain of the fluid, vertically bounded by the free-surface and the seabed, parametrized by η and h respectively
Γ_h , Γ^η	Vertical boundaries of D_h^η , denoting the seabed and the free-surface respectively
S_a	Excitation lateral boundary of D_h^η
X	Common projection of free-surface and seabed on the horizontal plane $z = 0$.
S^∞	Lateral boundary at infinity of D_h^η
$\boldsymbol{x}$	Horizontal space variables in $\mathbb{R}^2$ with $\boldsymbol{x} = (x_1 , x_2)$ or in $\mathbb{R}$ with $\boldsymbol{x} = x$
z	Vertical space variable
t	Time variable
$\nabla_{\boldsymbol{x}}$	Gradient operator in $\mathbb{R}^2$, with $\nabla_{\boldsymbol{x}} = (\partial_{x_1} , \partial_{x_2})$
∇	Gradient operator in $\mathbb{R}^3$, with $\nabla = (\nabla_{\boldsymbol{x}} , \partial_z)$
∂_t	Time derivative $\partial_t = \frac{d}{dt}$
Δ	Laplace operator in $\mathbb{R}^3$ $\Delta = (\nabla_{\boldsymbol{x}} , \partial_z)$ with or in $\mathbb{R}^2$ with $\Delta = (\partial_x , \partial_z)$
$C^k([a , b])$	Space of k-times continuously differentiable functions defined on $[a , b]$
$L_2(a , b)$	Space of square integrable functions defined on (a , b)

Introduction

In the 5th of July of the year 1687, Isaac Newton publishes his three-volume work *Philosophiae Naturalis Principia Mathematica*, a milestone for the scientific literature, where the Laws of Motion and the theory of differential calculus are first introduced. Yet in Book II, Prop, XLV of his publication, he contributes a less known milestone for the scientific community. He presents the first theory of water waves. It could come as a surprise how can the movement of planets and stars intrigued countless scientists before Newton to write books attempting to predict their behavior, yet no such theory existed for a phenomenon so plainly familiar to them and vital for the sea trade and coastal structures of their era (and ours). This historical oddity can testify for the difficulty that gravity water waves showcase with regard to their theoretical study. Mathematically, the water wave problem cannot be stated as a classical partial differential equations problem, taught in all undergraduate schools of engineering and science, since part of the boundary of the domain, the free-surface, is an unknown field. Physically, water waves exhibit an abundance of complicacies that waves can produce. They can shape steady formations and travel almost unaltered for long distances, they break approaching the shore, disperse in deep water and diffract near objects. Hence, despite their numerous applications, the advancement of the water wave theory for around the next 150 years after Newton's first publication will be limited and mostly confined within the frame of linear water wave theory, (see (Craik, 2004) for a review of the works of that era). Today, water waves draw more attention than ever from the scientific community, playing an essential role for the safety of life at sea and coastal regions, the durability of ships, offshore platforms and coastal structures, the usage of turbine wave energy converters and other important applications. Models for the prediction of their behavior are vital and the advancements of mathematics and computer science can (for around the last 50 years) provide the needed resources for the development and utilization of such models. Yet, even though most recent models have largely abandoned the linear water wave theory, the majority of them work based on the assumptions of an incompressible, irrotational and inviscid flow, assumptions that we shall adopt too. However, such assumptions constitute physical reductions of the problem and not plain mathematical linearizations, and models adopting them have proved their efficiency in many demanding physical problems such as propagation of large amplitude waves over variable bottoms, wave collisions, wave-body interactions and waves over a moving bottom. As a result, a very interesting and open problem for research is the formulation of a water wave model based on the nonlinear irrotational water wave theory (NLIWW) that is computationally efficient. In this diploma thesis, the numerical implementation of such a model, the so called Hamiltonian Coupled Mode method, first presented in (Athanassoulis & Belibassakis, 2000) in its fully nonlinear form, will be presented and tested on demanding and highly nonlinear physical problems. But before we describe in more detail the method utilized here, we shall provide a synoptic review of the general literature in NLIWW theory from when it was initiated and especially for the methods used today.

Models regarding the behavior of nonlinear water waves first emerged during the 19th century. One of the first notable works of the time was (Stokes, 1847) who, employing the

now traditional Stokes-expansion, provided nonlinear solutions of periodic steady waves of small amplitudes. Another significant work of that era came from (Boussinesq, 1872) who derived the two evolution equations-system known as the *Boussinesq equations*, following the observations of Russell with regard to the solitary waves. The work of Boussinesq found applications on the propagation of small amplitude long waves as well as helped to establish the theoretical and physical existence of the solitary waves, a notion that was debated at that time. Although Boussinesq provided an analytic description of the free-surface elevation for solitary waves, he did not provide a simple equation for which the aforementioned free-surface elevation can be derived as a steady solution. This step was completed by (Korteweg & de Vries, 1895) with the development of what is known as the *KdV equation*. Other important simplified models of the time were provided by (Barré de Saint-Venant, 1871) and (Rayleigh, 1876) although their application today are very limited. As can be seen, scientists of that era focused towards the derivations of simple evolution equations that engulf the kinematics and dynamic properties of the (simplified) model (usually for shallow or intermediate depth). This trend can be attributed to the lack of means to solve large systems of partial differential equations (since at that era no computers existed). For that purpose a variety of tools taken from mathematical physics was utilized, including potential theory, Fourier and Laplace transformations, conformal mappings, Green's functions and integral equations as well as petrubation theory. However, the reduced models developed during this era were mainly targeted towards problems with flat bottom and waves of small amplitude, since in other cases the physical properties of the problem became too complex. A detailed review of many of the works described above can be found in the classical books (Stoker, 1957) and (Wehausen & Laitone, 1960).

A new approach towards the fully nonlinear water wave problem was initiated during the 1960's. Considering the case of an irrotational, incompressible and inviscid flow, the main drawback of the classical formulation, computation-wise, was the need to solve the Laplace equation for the interior of the fluid domain. This equation, being a kinematic constraint of the problem, could be reformulated to a more suitable constraint if the water wave problem could be stated through a variational principle. The first publication towards such an approach came from (Petrov, 1964) who derived the dynamic evolution equation as result of a variational principle stated for the Lagrangian of the system. However, his approach requires the solution of the problem to a priori satisfy the kinematic constraints as stated in the classical formulation. As a result Petrov's work drew little attention. Yet, it was only a little later when (Luke, 1967) derived the classical formulation through an unconstrained variational principle. For his method, Luke utilized as an action functional the space-time integral of the pressure in the domain of the field. It was shown then that the Euler-Lagrange equations of the functional correspond to the classical hydrodynamic water wave problem. Although Luke's Functional did not originate from the traditional Hamiltonian formulation, its unconstrained nature (excluding the irrotationality of the flow) was to become a milestone for models derived in the future. The practical importance of Luke's approach was first noticed by (Whitham, 1967) who utilized the variational principle by exploiting an asymptotic expansion of the potential of the fluid and derived the Boussinesq equations. A little later, (Zakharov, 1968) derived the Hamiltonian reformulation of the problem, by using

the total energy of the system as the Hamiltonian. Zakharov's variational principle used as variables the free-surface elevation of the system together with the trace of the velocity potential on the free-surface, variables who Zakharov proved to be canonical for the water wave problem. Continuing Petrov's Hamiltonian approach, while utilizing his transformation, Zacharov's approach set as possible to derive the free-surface evolution equations under the kinematic constraints in the interior and other boundaries of the fluid. The system was now written as a couple of evolution equations defined on the free-surface with variables being the free-surface elevation and the trace of the potential that was also defined upon the free-surface. Hence, the only obstacle preventing the evolution equations from being a closed problem was the need to calculate the normal (to the free-surface) derivative of the potential defined on the free-surface. This unknown field had to be calculated through the kinematic constraints of the fluid. The significance of this reformulation was further magnified with (Craig & Sulem, 1993) who introduced formally the Dirichlet to Neumann operator that corresponds to the normal velocity of the fluid on the free-surface. Due to their contribution, the Hamiltonian approach for the water waves is usually referred to as the Zakharov Craig Sullem formulation (ZCS). It was now apparent that a numerical approach of the nonlocal problem of the ZCS formulation required an accurate and efficient method for the calculation of the DtN operator, regardless of whether the operator itself was explicitly defined in the numerical approach or not.

Today, the literature regarding the NLIWW problem can be separated into methods that target on solving the full problem without further mathematical or physical simplifications and simplified models based on asymptotic expansions and assumptions regarding the shallowness, nonlinearity and bottom variation of the problem. The latter models comprise the most popular line of work throughout the history of the nonlinear water wave theory. Today they are utilized due to their extremely fast numerical solution, given that most of them comprise entirely of one or two evolution equations, and due to their well-studied mathematical behavior. However, their practical applicability is limited to problems with a weakly varying seabed and generally not significant dispersion or nonlinearity. Important such models are the so called Boussinesq Type models (inspired by the work of Boussinesq), that either eliminate the vertical variable from the flow equations or assign a simplified prescribed behavior to them, see for example (Serre, 1953), (Green & Naghdi, 1976) (Nwogu, 1993), (Mitsotakis, Dutykh, & Carter, 2014). Other such models are the shallow water equations initiated by (Barré de Saint-Venant, 1871) with other models seen in (Xing & Shu, 2005) & (Dutykh & Clamond, 2012) and the mild slope equations with such models seen in (Berkhoff, 1972), (Isobe & Abohadima, 1998), (Klopman, Van Groesen, & Dingemans, 2010). A detailed and mathematical description of many of the above models can be found in the book (Lannes, 2013). As for the fully nonlinear models, most of them can be assigned to either direct numerical methods, or the so called Higher Order Spectral Methods, models that will be described below.

Advancements in the computational capability of computers, have allowed the implementation of a variety of direct numerical methods. Such methods, have been mainly used for calculating wave-body interactions, with many applications found in the prediction

of wave forces on marine installations. From these models, the most widespread one is the boundary element method (BEM) (Longuet-Higgins & Cokelet, 1976), (Grilli et al., 1994), (Clamond & Grue, 2001). The main idea behind this method is the exploitation of Green's theorem to project the problem defined on the water domain, onto the boundary of the fluid. This technique allows for the dimensional reduction of the problem at the cost of projecting it at a generally more complex subdomain and forming a discretized approximation that requires the inversion of a full matrix. As a result, in case of large and complex boundary geometries, 3D direct numerical methods can be competitive (with regard to the computational time) with BEM. The most straightforward of these methods is the finite difference method (FDM) whose simplicity in implementation has drawn recently attention to the method (Bingham & Zhang, 2007), (Engsig-Karup, Bingham, & Lindberg, 2009). Furthermore, numerical evidences imply that high-order direct numerical models are more efficient than low-order ones for water wave problems (Kreiss & Oliger, 1972). As a result finite element methods have been studied on the scope of gravitational water waves (Cai et al., 1998), (Rycroft & Wilkening, 2013), (Gagarina et al., 2014), noting that these methods treat the weak formulation of the NLIWW problem. The main trait of this approach is its inherent flexibility with respect to adaptive grids and high-order approximations. The main downside of this approach is the need of regridding at each time step, a problem that is general handled with the help of a time-dependent mapping of the water domain onto a simple stationary solution domain (for the Laplace equation).

A class of models extensively used for solving the fully nonlinear water wave problem, are the so called *Higher Order Spectral methods* (HOS), with first numerical results presented in (West *et al.*, 1987) and (Dommermuth & Yue, 1987) for the flat bottom case. These models are based on an expansion for the free-surface elevation and vertical velocity in a way where the evaluation of the DtN operator becomes efficient. Such methods were extended in the sloping bottom case in (Liu & Yue, 1998). In a similar approach (Craig & Sulem, 1993) expanded the DtN operator in the form of a functional Volterra-Taylor series in powers of the free-surface elevation, in the Fourier space. This numerically efficient new description of the DtN operator is the main innovation of the aforementioned paper, while its applicability is constrained in spatially periodic surface waves and domains. Finally, a recent implementation of such a method for cases with a variable bottom can be found in (Gouin et al., 2015).

In the theory of (both linear and nonlinear) water waves, many authors utilized vertical eigenfunction expansions for the dimensional reduction of the problem. This expansion could either be applied to the velocity potential, for the case of water waves, or to the pressure field for the case of acoustic waves. As a result the field in discussion is expressed in a way were its vertical structure is a priori known and its horizontal behavior is dependent on a series of introduced modal amplitudes, each corresponding to one eigenfunction of the expansion. This technique of dimensional reduction is generally referred to as the *coupled mode method* in the literature. For acoustic waves within a medium whose properties and boundaries vary slowly with the horizontal variables, i.e. a stratified medium, (Pierce, 1965) provided such a vertical series expansion of normal modes. His method was based on the assumption that the normal modes are uncoupled, an assumption inspired from the mathematically equivalent Born-

Oppenhaimer approximation for the Schrodinger's equation regarding the separation of electronic and nuclear motions. The uncoupling of the modes is assumed for the purpose of retaining the needed calculations for the system manageable for the hardware of the time. Furthermore, (Milder, 1969) investigated channel classes of non-uniformities, regarding the sound-velocity profile, for which the normal mode assumption is applicable. For the case of water waves, such representation are presented in (Massel, 1993) and (Porter & Staziker, 1995) in the context of extending the applicability of the mild slope equation. In these papers the assumption of uncoupled modes used for the aforementioned acoustic models is not used. However, even though all these models are presented for the case of varying bottoms, the expansions used for the problem cannot comply with the sloping bottom boundary condition in a truncated form. As a result, such models were not accurate for cases with a sloping bottom and hence did not satisfy the conservation of energy.

With this initiative, prof. Athanassoulis and prof. Belibassakis commenced a new line of work with the paper (Athanassoulis, Belibassakis, & Livaditi, 1998) and the application of their method on acoustic waves. In that paper, an enhanced local mode representation (derived from a regular Sturm-Liouville problem) of the pressure is utilized together with a variational principle applied to the transmission problem. The idea behind the method is to subtract from the velocity potential a suitable function so that the difference satisfies the boundary conditions of the Sturm-Liouville problem and thus ensuring the rapid convergence of the method. Hence, a new enhanced coupled-mode system of equations arise. The big contribution of this paper was the introduction of the sloping bottom mode (and as a result an additional equation) which makes the model consistent with the bottom boundary condition and the conservation of energy. However, no evidence is given concerning the independence of the terms of the expansion (and as a result the validity of the variational formulation). With (Athanassoulis & Belibassakis, 1998) & (Athanassoulis & Belibassakis, 1999) the method is now applied to water waves over variable bathymetry. This time the series expansion is applied to the velocity potential of the field. Again, this method provided a model consistent with the sloping bottom boundary conditions and conservation of energy. The new variational formulation is based on the linearized Luke's variational principle. Yet, since a truncation of this model cannot comply with the free-surface evolution equations of the full water-wave problem, the method was restricted to the linear water-wave theory. Also, in the aforementioned paper a theorem is stated concerning the admissible function space for the potential, for the representation to form a basis. Numerical results for scattered linear waves over an arbitrary bottom were presented in (Belibassakis *et al.*, 2001) & (Belibassakis *et al.*, 2011) while results for weakly nonlinear waves were presented in (Athanassoulis & Belibassakis, 2002).

In the paper (Athanassoulis & Belibassakis, 2000) the *free-surface mode* is introduced, allowing a truncation of the model to adapt to the free-surface boundary conditions. As a result, the model is reformulated as a nonlinear coupled-mode system of 2^{nd} order differential equations in the propagation space, fully accounting for the effects of the nonlinearity and dispersion. Furthermore, a theorem is stated without proof concerning the admissible space for the velocity potential in order for the newly enhanced series to converge uniformly. The

modal amplitudes needed for the representation of the velocity potential are first presented here. The coupled mode system presented in this paper comprises of two evolutionary equations, one algebraic and one vector-equation. We should also mention that in that paper there was not given a proof for the term-wise differentiability of the infinite series, since the asymptotic behavior $\|\varphi_n\|_\infty \sim O\left(n^{-4}\right)$ was only validated numerically and not rigorously. The first proof for the term-wise differentiability of the infinite series representation arises at (Athanassoulis & Belibassakis, 2003). The theorem presented in that paper proves the enhanced series expansion twice term-by-term differentiability up to and including the boundary. The main essential advantage of this approach is the rapid convergence of the expansion throughout the domain and as a result the need for a little number of modes in order to simulate challenging problems without simplifications. We therefore obtain an exact reformulation of the fully nonlinear irrotational and inviscid problem and not a simplification of any kind (excluding the assumption that the waves will not break, an assumption essential for all such models and not limited to the current method). This trait counters the computationally challenging form of the system presented in the aforementioned two papers, a form that was revised in the papers we will presented below.

A first reformulation of the fully nonlinear system is presented in (Athanassoulis & Belibassakis, 2007). The idea behind the simplification is the calculation of the modal amplitudes, at a specific time instant, through a system of partial differential equations. This subproblem corresponds to the kinematic constraints of the problem and practically is associated with the calculation of the Dirichlet to Neumann operator. As a result, the free-surface evolution equations are drastically simplified since the problem can be solved (at each discrete time-step) in two steps, solving the substrate problem for the modal amplitudes and advancing the solution through the free-surface evolution equations. We should also note that in that paper the equivalent steady problem for calculating periodic solutions of the model on a periodic cell, is first introduced. For a more detailed discussion on the equivalent steady problem see (Papoutsellis, 2016). The reformulation of the problem is advanced even further, following the same idea, in (Athanassoulis & Papoutsellis, 2015) were both the substrate problem and the evolution equations are drastically simplified. The paper also provides a formula for the calculation of the Dirichlet to Neumann operator linking the operator only with the free-surface modal amplitude and no other modal amplitude.

PART I.

Implementation of the HCM method using Finite Differences

Chapter 1: Analytic Formulation of the Problem

1.1 Geometric configuration of the Problem

Consider an orthogonal Cartesian co-ordinate system Ox_1x_2z, with the z-axis being the vertical axis, facing upwards, and the still water level corresponding to $z=0$. We investigate the motion of an incompressible, inviscid and homogenous fluid with a free-surface $z=\eta(\boldsymbol{x},t)$ over a variable and possibly time dependent bathymetry $z=-h(\boldsymbol{x},t)$. The flow is assumed irrotational, therefore enabling the expression of the fluid velocity as the gradient of a scalar velocity potential $\Phi(x,z,t)$.

The horizontal domain of the fluid is the half plane $X=\{\boldsymbol{x}=(x_1,x_2)\in\mathbb{R}^2 : x_1\geq a\}$, where a is an arbitrary real number. The vertical fluid extent is the strip defined by the graphs:

$$\Gamma^{\eta}(X,t) = \{(\boldsymbol{x},z)\in X\times\mathbb{R} : \boldsymbol{x}\in X,\ z = \eta(\boldsymbol{x},t)\} \tag{1.1a}$$

$$\Gamma_h(X,t) = \{(\boldsymbol{x},z)\in X\times\mathbb{R} : \boldsymbol{x}\in X,\ z = -h(\boldsymbol{x},t)\} \tag{1.1b}$$

where $\Gamma_h(X,t)$ represents the time-dependent seabed and $\Gamma^{\eta}(X,t)$ represents the unknown, time-dependent free-surface of the fluid. Therefore, the problem in discussion is defined on a non-uniform, strip-like domain:

$$D_h^{\eta}(X,t) = \{(\boldsymbol{x},z)\in X\times\mathbb{R} : \boldsymbol{x}\in X,\ -h(\boldsymbol{x},t) < z < \eta(\boldsymbol{x},t)\} \tag{1.1c}$$

Furthermore, we define the vertically closed domain $\bar{D}_h^{\eta}(X,t)$:

$$\bar{D}_h^{\eta}(X,t) = \{(\boldsymbol{x},z)\in X\times\mathbb{R} : \boldsymbol{x}\in X,\ -h(\boldsymbol{x},t) \leq z \leq \eta(\boldsymbol{x},t)\} \tag{1.1d}$$

which will be used in the sections to follow.

The lateral boundary of the fluid domain $D_h^{\eta}(X,t)$ can be split into the following parts:

The first part is denoted as the *excitation boundary* and is the subset S_a of the vertical plane $\{x_1=a\}$ defined by

$$S_a = \{(\boldsymbol{x},z) : x_1 = a,\ x_2\in\mathbb{R},\ -h(a,x_2,t)\leq z\leq\eta(a,x_2,t)\}. \tag{1.1e}$$

The second part, is a conventional *boundary-at-infinity*, denoted by S^{∞} and defined as:

$$(\boldsymbol{x},z)\in S^{\infty} \Leftrightarrow \begin{cases} x_1\geq a, & (x_1^2+x_2^2)^{1/2}\to\infty, \\ -h_{\infty}\leq z\leq 0. \end{cases} \tag{1.1e}$$

with h_∞ is the constant depth at infinity.

The local total depth $H(\boldsymbol{x},t) = \eta(\boldsymbol{x},t) + h(\boldsymbol{x},t)$ is assumed smooth, finite and strictly positive everywhere. The reason behind this restriction will be explained further below.

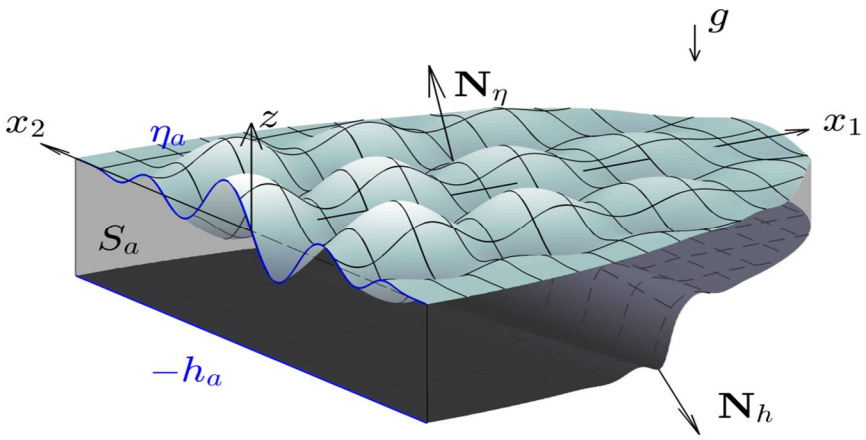

Fig 1. The geometric configuration of the fluid domain, Figure taken from (Papoutsellis, 2016)

Remark regarding the physical assumptions: Apart from the assumption that the local depth $H(\boldsymbol{x},t)$ is finite and strictly positive, there is another more subtle assumption we made. It is the assumption that the free-surface η and the bottom bathymetry h remain always single-valued functions of the $\boldsymbol{x}$ variable. These assumptions, combined with a certain needed smoothness from the aforementioned functions, will be explained in detail in the subsequent sections. Although the smoothness assumption may be overlooked as non restrictive, the other two assumptions cannot. As a result the method to be analyzed in the sequel cannot solve problems involving phenomena like wave-breaking and geometries that contain shores (zero bathymetry).

Remark regarding the excitation boundary: The excitation boundary is introduced here for the purpose of presenting in the following sections the correct boundary conditions the model can assume in case of an incident wave. Yet, in the numerical implementation we will not examine in detail the case of excitation boundary conditions. This neglect is done because results for such cases have been presented in detail before, see e.g (Athanassoulis & Papoutsellis, 2015) and are investigated even more thoroughly in (Papoutsellis, 2016). In this thesis we focus our numerical results to initial value problem test cases that present high nonlinearity and very large horizontal domains. This way we can showcase the efficiency and accuracy of the designed code. Furthermore, in the absence of excitation we can easily test the ability of the model to conform to the conservation of energy and mass, attributes vital for long-time simulations. Hence, incident wave problems and problems regarding imposed free-surface pressure will be presented synoptically in this work. However, this limited presentation regarding these problems should not undermine the ability of the model to simulate effectively and easily such cases.

1.2 Classical formulation, Luke's principle & other important contributions

Classical differential formulation of the water-wave problem with lateral excitation

The classical formulation describing the water wave evolution with respect to the free-surface elevation $\eta = \eta(\boldsymbol{x},t)$ and the wave potential $\Phi = \Phi(\boldsymbol{x},z,t)$ is generally stated as (see e.g. (Stoker, 1957), (Wehausen & Laitone, 1960), (Johnson, 1997))

$$\Delta\Phi = \nabla_{\boldsymbol{x}}^2\Phi + \partial_z^2\Phi = 0 \qquad \text{in} \quad D_h^\eta(X,t), \quad t_0 \le t \le t_1 \tag{1.2a}$$

$$\boldsymbol{N}_h \cdot \nabla\Phi = \partial_t h, \qquad \text{on} \quad \Gamma_h(X), \quad t_0 \le t \le t_1 \tag{1.2b}$$

$$\partial_t\eta - \boldsymbol{N}_\eta \cdot \nabla\Phi = 0 \qquad \text{on} \quad \Gamma^\eta(X,t), \quad t_0 \le t \le t_1 \tag{1.2c}$$

$$\partial_t\Phi + \frac{1}{2}(\nabla\Phi)^2 + g\eta + \frac{p_{\text{surf}}}{\rho} = 0 \quad \text{on} \quad \Gamma^\eta(X,t), \quad t_0 \le t \le t_1 \tag{1.2d}$$

where $\nabla_{\boldsymbol{x}} = (\partial_{x_1},\partial_{x_2})$ is the horizontal (2D) gradient, $\nabla = (\nabla_{\boldsymbol{x}},\partial_z) = (\partial_{x_1},\partial_{x_2},\partial_z)$ is the corresponding three-dimensional (3D) gradient, $\nabla_{\boldsymbol{x}}^2 = (\partial_{x_1}^2,\partial_{x_2}^2)$ is the horizontal Laplacian, ∂_t denotes the time derivative, $\boldsymbol{N}_h = (-\nabla_{\boldsymbol{x}}h,-1)$ and $\boldsymbol{N}_\eta = (-\nabla_{\boldsymbol{x}}\eta,1)$ are the outward (with respect to the fluid) normal (but not necessary of unit length) vectors on $\Gamma_h(X)$ and $\Gamma^\eta(X,t)$ respectively, and $p_{\text{surf}}(\boldsymbol{x},t)$ denotes any externally applied pressure. Furthermore, g is the acceleration due to gravity, and ρ is the (constant) density of the fluid. Eqs (1.2c), (1.2d) express the kinematic and dynamic free-surface conditions, respectively. Eq (1.2b) is the impermeability condition on the seabed, and Eq (1.2a) is the Laplace equation, accounting for the irrotationality and incompressibility of the fluid flow.

For Eqs (1.2a)-(1.2d) to yield a unique solution, they should be complemented by appropriate conditions on the lateral boundaries and initial conditions for the free-surface elevation and the potential at the free-surface and the lateral boundary S_a.

Lateral conditions for the problem under consideration can be of the form:

$$\eta(a,x_2,t) = \eta_a(x_2,t) \equiv \eta_a, \qquad x_2 \in \mathbb{R}, \quad t_0 \le t \le t_1 \tag{1.2e}$$

$$\left\{ \begin{array}{ll} \text{either} & \partial_{x_1}\Phi(a,x_2,z,t) = V_a(x_2,z,t) \equiv V_a \\ \text{or} & \Phi(a,x_2,z,t) = \Phi_a(x_2,z,t) \equiv \Phi_a \end{array} \right\}, \quad \boldsymbol{x} \in S_a. \quad t_0 \le t \le t_1 \tag{1.2f}$$

$$\eta(\boldsymbol{x},t),\ \nabla\Phi(\boldsymbol{x},z;t) \to 0, \qquad \boldsymbol{x} \in S^\infty, \quad t_0 \le t \le t_1 \tag{1.2g}$$

The lateral conditons of Eqs (1.2e) & (1.2f) represent, respectively, the free-surface elevation and the values of the normal velocity (or, alternatively, the values of the wave potential) on

the excitation boundary S_a at each time instance t. The data η_a and V_a (or Φ_a) are known functions. Eq (1.2g) supplements the problem with a radiation condition at infinity.

Furthermore, the initial prescribed data can be written concisely in the form:

$$\begin{aligned} &\eta(\boldsymbol{x}, t_0) = \eta_0(\boldsymbol{x}), \quad \Phi(\boldsymbol{x}, z = \eta_0(\boldsymbol{x}), t_0) = \Phi_0(\boldsymbol{x}, z), \\ &\text{and specify (compatible) data on the boundary of } D_h^{\eta}(X, t_0). \end{aligned} \tag{1.2h}$$

Collectively, Eqs (1.2) define the classical differential formulation of the non-linear irrotational water wave problem (or NLIWW problem, for abbreviation). The 2D formulation (one horizontal dimension) of the problem can easily be derived from Eqs (1.2), assuming that the unknown fields (η, Φ) and the data functions $(\eta_a, V_a$ or $\Phi_a, p_{\text{surf}})$ are independent of the variable x_2. In this case, the fluid domain $D_h^{\eta}(X, t) \subset \mathbb{R}^2$ takes the form of a half-strip with arbitrary, yet single-valued, (upper and lower) boundaries, while S_a and S^{∞} become vertical intervals at $x_1 = a$ and $x_1 \to \infty$, respectively.

Notational remark: As a compromise between clarity and conciseness, from now on the boundary values (traces) of the various fields will be represented by using brackets with a sub-script denoting the boundary. For example, Eqs (1.2b) will be written as $\boldsymbol{N}_h \cdot \left[\nabla \Phi \right]_{z=-h} = 0$. Keeping explicitly track of the boundary values is important in the present problem since, on the free surface and the seabed, the trace of horizontal differential operators on fields depend on the order of application of differentiation and taking the trace. For example, $\left[\nabla_{\boldsymbol{x}} \Phi \right]_{z=\eta} \neq \nabla_{\boldsymbol{x}} \left[\Phi \right]_{z=\eta}$.

Luke's Variational Principle

An unconstrained variational principle for irrotational water waves was introduced in (Luke, 1967), by Luke. In that paper Luke provided an unconditional variational principle for the NLIWW problem in a horizontally unbounded fluid. In this approach, the fluid pressure was exploited as a Lagrangian density, with the assumption of zero free-surface pressure. As seen in (Athanassoulis & Papoutsellis 2015), the Lagrangian density of this principle, augmented by two simple terms accounting for the presence of applied pressure and lateral excitation, is given below:

$$\begin{aligned} &L\left[\eta, \Phi\right] = L(\eta(\mathbf{x}, t), \Phi(\mathbf{x}, \cdot, t)) = \\ &= \int_{-h}^{\eta} \left(\partial_t \Phi + \frac{1}{2} |\nabla_{\boldsymbol{x}} \Phi|^2 + \frac{1}{2} (\partial_z \Phi)^2 + g z \right) dz + \frac{p_{\text{surf}}}{\rho} \eta + \begin{cases} \int_{-h_a}^{\eta_a} V_a \left[\Phi \right]_{x_1 = a} dz \\ 0 \end{cases} \end{aligned} \tag{1.3a}$$

The last term of Eq. (1.3a) highlights the fact that the excitation of the fluid domain may occur either by specifying the normal velocity V_a or the values the potential Φ_a there. The respective action functional is defined by integrating $L[\eta,\Phi]$ over the region $X\times[t_0,t_1]$:

$$\mathcal{S}[\eta,\Phi]=\int_{t_0}^{t_1}\int_X L[\eta,\Phi]d\boldsymbol{x}\,dt \tag{1.3b}$$

Luke's variational principle states that the two fields η,Φ satisfy the NLIWW problem, Eqs (1.2a)-(1.2d) & (1.2f), if and only if they render the functional $S[\eta,\Phi]$ stationary. As can be found in many books of Calculus of Variations (see e.g (Gelfand & Fomin, 1963), (Elsgolc, 1961)) the above statement corresponds to the variational equation:

$$\delta\mathcal{S}[\eta,\Phi;\delta\Phi,\delta\eta]=\delta_\Phi\mathcal{S}[\eta,\Phi;\delta\Phi]+\delta_\eta\mathcal{S}[\eta,\Phi;\delta\eta]=0\,, \tag{1.4}$$

for all admissible variations $\delta\eta,\delta\Phi$. Here $\delta_\Phi\mathcal{S}[\eta,\Phi;\delta\Phi]$ and $\delta_\eta\mathcal{S}[\eta,\Phi;\delta\eta]$ denote the first partial variations (functional derivatives) of $S[\eta,\Phi]$ with respect to the potential Φ and the free surface elevation η in the directions $\delta\Phi$ and $\delta\eta$, respectively, They are derived by adapting the classical procedure (see e.g. (Luke, 1967), or (Whitham, 1974)) by guarding the lateral term at S_a after the integration by parts. However, the variational derivatives calculated in this Section differ from the ones presented in (Athanassoulis & Papoutsellis, 2015), due to the time-dependent sloping-bottom. By direct application of the theory of variational calculus we get:

$$\begin{aligned}\delta_\eta\mathcal{S}[\eta,\Phi;\delta\eta]&=\mathcal{S}[\eta+\delta\eta,\Phi]-\mathcal{S}[\eta,\Phi]=\\&=\int_{t_0}^{t_1}\int_X\left\{\left[\partial_t\Phi+\frac{1}{2}|\nabla_{\boldsymbol{x}}\Phi|^2+\frac{1}{2}(\partial_z\Phi)^2+g\,z\right]_{z=\eta}+g\eta+\frac{p_{\text{surf}}}{\rho}\right\}\delta\eta\,d\boldsymbol{x}\,dt\end{aligned} \tag{1.5a}$$

$$\begin{aligned}\delta_\Phi\mathcal{S}[\eta,\Phi;\delta\Phi]&=\mathcal{S}[\eta,\Phi+\delta\Phi]-\mathcal{S}[\eta,\Phi]=\\&=\int_{t_0}^{t_1}\int_X\left\{\int_{-h}^{\eta}\left(\partial_t\delta\Phi+|\nabla_{\boldsymbol{x}}\Phi\,\nabla_{\boldsymbol{x}}\delta\Phi|+(\partial_z\Phi\,\partial_z\delta\Phi)\right)dz\right\}d\boldsymbol{x}\,dt+\\&\quad+\begin{cases}\int_{-h_a}^{\eta_a}V_a\left[\delta\Phi\right]_{x_1=a}dz\\0\end{cases}\end{aligned} \tag{1.5b}$$

Equation (1.5b) needs further treatment since it contains derivatives of the increment $\delta\Phi$.

Utilizing Leibniz's rule for the part of the integral with kernel $\partial_t\delta\Phi$, and using the Green-Gauss theorem for the part of the integral with kernel $|\nabla_{\boldsymbol{x}}\Phi\,\nabla_{\boldsymbol{x}}\delta\Phi|+(\partial_z\Phi\,\partial_z\delta\Phi)$ we get:

$$\begin{aligned}\delta_{\Phi} S\left[\eta,\Phi;\delta\Phi\right] = \int_{t_0}^{t_1}\int_X \Big\{ &\Big(-\partial_t\eta + \boldsymbol{N}_\eta\cdot\left[\nabla\Phi\right]_{z=\eta}\Big)\left[\delta\Phi\right]_{z=\eta} \\ &+ \Big(-\partial_t h + \boldsymbol{N}_h\cdot\left[\nabla\Phi\right]_{z=-h}\Big)\left[\delta\Phi\right]_{z=-h} - \int_{-h}^{\eta}\Delta\Phi\,\delta\Phi\,dz\Big\}\,d\boldsymbol{x}\,dt \\ &+ \int_{t_0}^{t_1}\int_{\mathbb{R}}\int_{-h_a}^{\eta_a}\Big(-\left[\partial_{x_1}\Phi\right]_{x_1=a} + V_a\Big)\left[\delta\Phi\right]_{x_1=a}\,dz\,dx_2\,dt\,,\end{aligned} \tag{1.5c}$$

Note: In Eq (1.5c) we took into account the lateral conditions the velocity potential and the free-surface elevation must satisfy. For the excitation boundary S_a we have the conditions $\left[\delta\eta\right]_{x=x_\alpha} = \left[\delta\Phi\right]_{x=x_\alpha} = 0$ because the velocity potential is given there. For the boundary at infinity S_∞ we assumed that $\eta,\Phi\to 0$ and as a result $\left[\delta\eta\right]_{S_\infty} = \left[\delta\Phi\right]_{S_\infty} = 0$. These conditions are needed for the correct application of the Green-Gauss theorem.

As said, Eq (1.5c) differs from the formulae given by (Athanassoulis & Papoutsellis, 2015). Yet, it can easily be seen that assuming a time-independent bottom bathymetry, the above formula transforms to the variational derivative presented in the aforementioned paper.

The significance of Luke's principle lies in the ability to express the fully nonlinear water wave problem through a variational principle free of *a priori* stated kinematic constraints (except for the assumption of irrotationality). Since the entirety of the water wave problem is derived through a variational principle, this method allows us to reformulate the classical problem by choosing different representations (i.e a series expansion) for the velocity potential or the free-surface. Hence, utilizing for example, as will be shown in this chapter, a vertical series expansion, we can easily derive a dimensionally reduced reformulation of the fully nonlinear water wave problem and thus replace the computationally demanding Laplace equation throughout the interior of the fluid's domain, with a different system of equations, that can be much more efficient to solve computationally-wise.

Zakharov-Craig-Sulem Hamiltonian formulation

As seen in the introduction, it was (Petrov, 1964) who provided directly the validity of Hamilton's principle for free-surface flows for the first time, yet it was Zakharov (Zakharov, 1968) who first recognized that the free-surface elevation $\eta(\boldsymbol{x},t)$ and the trace of the velocity potential on the free-surface:

$$\psi(\boldsymbol{x},t) = \Phi\left(\boldsymbol{x},z=\eta(\boldsymbol{x},t),t\right) = \left[\Phi\right]_{z=\eta} \tag{1.6}$$

are conjugate canonical variables, for the NLIWW problem and formulated it as an evolutionary Hamiltonial system on (η,ψ). Much later, Craig & Sulem (Craig & Sulem, 1993) introduced the Dirichlet to Neumann operator (DtN) and extended the Hamiltonian formulation in the finite depth case. It is easy to extend further this approach including lateral excitation. However, the great contribution of that paper was the formal definition of the

Dirichlet to Neumann operator for the water wave problem. Including lateral excitation, the DtN operator is defined as:

$$G\left[\eta, h, V_a\right]\psi = \boldsymbol{N}_\eta \cdot \left[\, \nabla\Phi \,\right]_{z=\eta} = -\nabla_{\boldsymbol{x}}\eta \cdot \left[\, \nabla_{\boldsymbol{x}}\Phi \,\right]_{z=\eta} + \left[\, \partial_z \Phi \,\right]_{z=\eta} \tag{1.7}$$

where Φ satisfies the Laplace equation (1.2a) in $D_h^\eta(X,t)$, the Neumann condition, Eqs (1.2b), on the moving bottom surface $\Gamma_h(X,t)$, the Dirichlet condition (1.6) on the free-surface $\Gamma_\eta(X,t)$ and one of the lateral conditions on $S_h^\eta(a)$ (see Eq (1.2f)). Using the modified DtN operator (1.7), the Zakharov-Craig-Sulem (ZCS) Hamiltonian equations take the form:

$$\partial_t \eta = \frac{\delta H}{\delta \psi} = G[\eta, h, V_a]\psi \tag{1.8a}$$

$$\partial_t \psi = -\frac{\delta H}{\delta \eta} = -g\eta - \frac{1}{2}(\nabla_{\boldsymbol{x}}\psi)^2 + \frac{(G[\eta, h, V_a]\psi + \nabla_{\boldsymbol{x}}\eta \cdot \nabla_{\boldsymbol{x}}\psi)^2}{2(1+|\nabla_{\boldsymbol{x}}\eta|^2)} - \frac{p_{\text{surf}}}{\rho} \tag{1.8b}$$

where H is the Hamiltonian of the system, given by

$$H[\eta,\psi] = \int_X \left(\frac{1}{2}\psi\, G[\eta, h, V_a]\psi + \frac{1}{2} g\eta^2 + \frac{p_{\text{surf}}}{\rho}\eta \right) d\boldsymbol{x} \tag{1.9}$$

and $\delta/\delta\psi$, $\delta/\delta\eta$ denote the variational (Volterra) derivatives. Equations (1.8) should be supplemented by boundary and initial data. This new form of the evolution equations shows that we only require the calculation of the DtN operator in order to solve Eqs. (1.8) (complemented with appropriate initial data). Therefore it is clear that any reformulation of the kinematic constraints of the problem, focuses strongly on calculating efficiently and accurately the DtN operator at every time step.

1.3 Representation of the velocity potential by a vertical series expansion

Luke's variational principle showcased, as was first noticed by (Whitham, 1967), that by introducing an expansion of the velocity potential we can reformulate the fully nonlinear water wave problem into a new system of equations in favor of computational efficiency. This methodology found use in two approaches, the first and most popular being the replacement of the potential through an approximate expansion and as a result deriving a simplified form of the problem, while the second being the representation of the potential by an exact reformulation. A few notable such approximate expansions can be found in (Isobe & Abohadima, 1998), (Klopman, Van Groesen, & Dingemans, 2010), (Yates & Benoit, 2015). The expansion presented here follows the second approach, being an exact representation of the potential, and was first presented in its complete form in (Athanassoulis & Belibassakis, 2000) for the fully nonlinear water wave problem, although it was previously utilized in a slightly (yet essentially) different form for the linear water wave problem in (Athanassoulis & Belibassakis, 1999). The aforementioned expansion was the first exact representation of the velocity potential to be employed for the exact variational reformulation of the fully nonlinear water wave problem. All the models described above are rendered possible by the unconstrained nature of Luke's principle. It is this critical characteristic that enables the introduction of various convenient representations for the velocity potential $\Phi = \Phi(\boldsymbol{x}, z, t)$, without the need to a priori consider the kinematic aspects of the problem, described in Eqs (1.2). The stepping stone for any such model is the analysis of the potential Φ by a vertical series expansion (assuming that it is well represented by such an expansion) that contains unknown horizontal functions and suitably prescribed vertical ones. Some exploited functions for the vertical structure of the potential are polynomials (Klopman et al., 2010), hyperbolic functions (Isobe & Abohadima, 1998) and enhanced eigenfunction series (Athanassoulis & Belibassakis, 1999). Nonetheless, in its more general form the vertical expansion of the potential can be expressed as:

$$\Phi(\mathbf{x}, z, t) = \sum_n \varphi_n(\boldsymbol{x}, t)\, Z_n(z; \eta(\boldsymbol{x}, t), h(\boldsymbol{x}, t)) \tag{1.10}$$

where the functions Z_n explicitly prescribed vertical functions and $\varphi_n(\boldsymbol{x}; t)$ are the time-dependent modal amplitudes, dependent only on the horizontal space-coordinates. It should be also noted that functions Z_n can also be implicitly time-dependent through their η and h dependency.

The motivation for utilizing such a representation greatly influences the choice of functions to be used as well as the difficulty of the matter. Whether the goal of the representation is the extraction of an approximate water wave model or the derivation of an exact variational reformulation of the fully nonlinear water wave problem the nature of the series to be used is crucial. The first case is the most commonly encountered in the literature and it encompasses the representation of Φ through a finite series, neglecting any discussions concerning convergence. As a result, said models exclusively rely on their numerical performance (and some asymptotic arguments) to showcase their effectiveness at describing nonlinear water-

wave phenomena. For the second case, which is the one described here, we search an infinite and convergent series, that can exactly represent the velocity potential throughout the fluid domain up to and including the boundaries. Furthermore, since the classical formulation of the problem requires a certain level of smoothness from the velocity potential, this series must conform with said requirements regardless of the fact that the free-surface boundary conditions and the Laplace equation are satisfied by the variational principle without a priori consideration. Therefore, we require, and hence must prove, the infinite series to be term-by-term differentiable up to and including the boundary and to provide continuous second space derivatives for the velocity potential as well as a continuous trace of the derivatives on the boundaries. Without the above restrictions, Luke's variational principle cannot be rendered exact when applied to the functional variables $(\eta, \{\varphi_n\}_n)$.

Note: Even though an exact representation of the velocity potential must utilize an infinite series, a numerical implementation of such a method would require its truncation. However, such a finite-dimensional problem would still be distinct from any finite-dimensional approximate representation of the velocity potential in the sense that the equations of the problem will arise as a truncation of an exact reformulation of the problem, rendering the model much more capable of describing nonlinear phenomena. Of course comparisons about its numerical efficiency (in terms of computational time) with approximate models cannot be made a priori.

In what is to follow, we will construct in detail a uniformly convergent series expansion of the form (1.10), as seen in (Athanassoulis & Papoutsellis, 2015). Said series will represent exactly the velocity potential $\Phi(\boldsymbol{x}, z, t)$ and its first and second derivatives, throughout the fluid domain $\overline{D_h^\eta}(X, t)$ at every given time $t \geq t_0$. It should be noted that the proof of convergence properties for the series is based on the assumption that the classical formulation has a solution.

The vertical functions used here are indexed by the set $n \in \{-2, -1, 0, 1, 2, ...\}$. The subset $\{Z_n,\ n \geq 0\}$ was first presented (with different indexing) in (Athanassoulis & Belibassakis, 1999) and is defined as the set of the eigenfunctions derived from the *local regular Sturm-Liouville* problem:

$$\partial_{zz} Z_n(z) - \lambda^2 Z_n(z) = 0, \quad -h(\boldsymbol{x},t) < z < \eta(\boldsymbol{x},t) \tag{1.11a}$$

$$[(\partial_z - \mu_0) Z_n]_{z=\eta} = 0 \tag{1.11b}$$

$$[\partial_z Z_n]_{z=-h} = 0 \tag{1.11c}$$

where the parameter μ_0 is a positive constant, whose choice will be discussed further below. The eigenvalues $\lambda = k_n$, $n \geq 0$ of the above *Sturm-Liouville* problem are defined as the positive roots of the equations:

$$\mu_0 - k_0 \tanh[k_0(\eta+h)] = 0 \tag{1.12a}$$

$$\mu_0 + k_n \tan[k_n(\eta+h)] = 0\,,\ n \geq 1 \tag{1.12b}$$

and the corresponding eigenfunctions, normalized so that $\left[Z_n\right]_{z=\eta} = 1\,,\ n \geq 0$ are given by the formulae:

$$Z_0(z;\eta,h) = \frac{\cosh[k_0(z+h)]}{\cosh[k_0(\eta+h)]} \tag{1.13a}$$

$$Z_n(z;h,\eta) = \frac{\cos[k_n(z+h)]}{\cos[k_n(\eta+h)]}\,,\ n \geq 1 \tag{1.13b}$$

An important detail is the implicit dependence of the eigenvalues $\{k_n\,,\ n \geq 0\}$ on $\boldsymbol{x}$ and t through their dependence on functions $h(\boldsymbol{x},t)$ and $\eta(\boldsymbol{x},t)$. This dependence shall not be simplified throughout the following Chapters, in opposition to all existing approximate theories (for example (Klopman et al., 2010)).

From the theory of regular Sturm-Liouville problems (see e.g (Birkhoff & Rota, 1989), (Coddington & Levinson, 1955)) the system $\{Z_n(z)\,,\ n \geq 0\}$ constitutes an orthogonal L^2-basis for functions defined on the instantaneous vertical segment $[-h(\boldsymbol{x},t),\eta(\boldsymbol{x},t)]$. As such, an expansion of the form $\Phi = \sum_{n=0}^{\infty} \varphi_n\, Z_n$ has been used previously by (Massel, 1993), (Porter & Staziker, 1995), (Chamberlain & Porter, 1995) and others to develop monochromatic, linear extended mild-slope model equations, or other linearized models in acoustics (Athanassoulis, Belibassakis, & Livaditi, 1998) or gravity waves (Athanassoulis & Belibassakis, 1999). Thus, such an expansion seems to be a possible candidate for the series expansion (1.10). Another testimony towards that belief is the following lemma, which is produced as a direct application of Theorem 4.1, page 197 from (Coddington & Levinson, 1955), to the current problem. This lemma proves that under certain conditions the convergence of the series is uniform: The proof of this lemma is omitted.

Lemma 1: *Let* $\Phi(\boldsymbol{x},.,t) \in L^2([-h,\eta])$ *on* $[-h(\boldsymbol{x},t),\eta(\boldsymbol{x},t)]$ *for each fixed* $(\boldsymbol{x},t) \in X \times [t_0,t_1]$ *and satisfy the boundary conditions* (1.11b), (1.11c). *Then on* $[-h(\boldsymbol{x},t),\eta(\boldsymbol{x},t)]$ Φ *admits the representation:*

$$\Phi(\boldsymbol{x},z,t) = \sum_{n=0}^{\infty} \big(\Phi, Z_n(z;\eta,h)\big) Z_n(z;\eta,h)$$

where the series converges uniformly.

However, the above Lemma shows that such an expansion cannot be applied successfully outside of the mild-slope bathymetry spectrum, even in the linearized regime since we generally lose the uniform convergence of the expansion. This observation is reinforced by the need for a truncation of the series in order to obtain a numerical solution. For that case, we can easily note that such a truncated series cannot approximate effectively the velocity potential for the nonlinear case. Our claim can be proved just by noting that the boundary conditions, the potential will satisfy, on the free-surface and the sloping-bottom, are:

$$\partial_z \Phi - \mu_0 \Phi = 0 \qquad \text{on} \quad \Gamma^{\eta}\left(\boldsymbol{x}, t\right) \tag{1.14a}$$

$$\partial_z \Phi = 0 \qquad \text{on} \quad \Gamma_h\left(\boldsymbol{x}, t\right) \tag{1.14b}$$

meaning that it does not even satisfy the linearized free-surface condition $\partial_{tt}\Phi + g\Phi = 0$ and the bottom impermeability conditionof Eq (1.2b). To improve the situation it is necessary to enhance the series expansion giving it the ability to converge to the correct boundary conditions. This is done by introducing two additional modes, as was first implemented in (Athanassoulis & Belibassakis, 1999) for the *sloping bottom mode* $Z_{-1}\varphi_{-1}$ and (Athanassoulis & Belibassakis, 2000) for the *free-surface mode* $Z_{-2}\varphi_{-2}$, without a clear theoretical justification. In accordance with the above discussion, the two new vertical functions Z_{-2} and Z_{-1} are selected to satisfy the boundary conditions:

$$[Z_{-2}]_{z=\eta} = 1 \qquad [(\partial_z - \mu_0) Z_{-2}]_{z=\eta} = 1/h_0 \tag{1.15a,b}$$

$$[\partial_z Z_{-2}]_{z=-h} = 0 \tag{1.15c}$$

$$[Z_{-1}]_{z=\eta} = 1 \qquad [(\partial_z - \mu_0) Z_{-1}]_{z=\eta} = 0 \tag{1.16a,b}$$

$$[\partial_z Z_{-1}]_{z=-h} = 1/h_0 \tag{1.16c}$$

where the constant h_0 denotes a reference depth and is introduced for dimensional consistency. Conditions (1.15b), (1.16c) are critical in the sense that they ensure $[(\partial_z - \mu_0) Z_{-2}]_{z=\eta} \neq 0$ and $[\partial_z Z_{-1}]_{z=-h} \neq 0$, thus permitting the functions Z_{-2} and Z_{-1} to account for inhomogeneities on the boundaries $\Gamma^{\eta}\left(\boldsymbol{x}, t\right)$ and $\Gamma_h\left(\boldsymbol{x}, t\right)$ respectively. Conditions (1.15c), (1.16b) are introduced to separate the influence of the two functions on one vertical boundary each (yet for the right-hand sides of these conditions any basis of the $\mathbb{R}^2$ is a valid choice). Because the above conditions do not uniquely define said functions, we pick out the solutions corresponding to the least degree polynomials (in the vertical variable) which leads to the following results:

$$Z_{-2}(z;\eta,h) = \frac{\mu_0 h_0 + 1}{2 h_0} \frac{(z+h)^2}{(\eta+h)} - \frac{\mu_0 h_0 + 1}{2 h_0}(\eta + h) + 1 \tag{1.17a}$$

$$Z_{-1}(z;\eta,h)=\frac{\mu_0 h_0-1}{2h_0}\frac{(z+h)^2}{(\eta+h)}+\frac{1}{h_0}(z+h)-\frac{\mu_0 h_0+1}{2h_0}(\eta+h)+1 \tag{1.17b}$$

The motivation behind the introduction of these two modes can be traced to the fact that series expansion of the Sturm-Liouville problem (1.11), converges uniformly to $\left[-h(x,t),\eta(x,t)\right]$ if the function it represents, satisfies the same boundary conditions as the Sturm-Liouville problem. As a result, by subtracting from the velocity potential these functions (complemented by their corresponding modal amplitudes $\varphi_{-1},\varphi_{-2}$) we achieve just that in a relatively easy manner.

Previously, we stated that the solution of the Sturm-Liouville problem constitutes a basis in for the space $L^2([-h,\eta])$. Hence, logically the question for what space does the new enhanced series constitutes a basis arises. A rigorous proof concerning this question has not been published yet. This question is not only of formal importance, but of essential importance too, since if this representation is not a basis of the space we search for solutions, the change of variables $[\eta,\Phi]\rightarrow[\eta,\varphi_{-2},\varphi_{-1},\varphi_0,...]$ that will be shown in Section 1.4 for the variational principle is invalid. Yet, it can be shown that the aforementioned series forms a basis for the Sobolev space $H^2([\eta,-h])$ (locally for every horizontal point). Although this question will remain unanswered here, a more practical question that we shall answer is whether this representation converges rapidly to the solution of the problem. This question was first answered without a proof in (Athanassoulis & Belibassakis, 2000). A detailed proof concerning the admissible space the velocity potential belongs to, is first supplied in (Athanassoulis et al., 2015) and is presented below:

Theorem 1 (Athanassoulis et al., 2015): *Let* Φ *be a function defined on* $\bar{D}_h^{\eta}(X)\times[t_0,t_1]$, *and assume that for each* $(\boldsymbol{x},t)\in X\times[t_0,t_1]$ *the* $z-$*function* $\Phi(\boldsymbol{x},\cdot,t)\in C^2([-h,\eta])$. *Then* Φ *admits the series expansion:*

$$\Phi(\boldsymbol{x},z,t)=\varphi_{-2}(\boldsymbol{x},t)Z_{-2}(z;\eta,h)+\varphi_{-1}(\boldsymbol{x},t)Z_{-1}(z;\eta,h)+\\ +\sum_{n=0}^{\infty}\varphi_n(\boldsymbol{x},t)Z_n(z;\eta,h) \tag{1.18}$$

where the modal amplitudes $\varphi_n(\boldsymbol{x},t)$, $n\geq-2$ *are related with* $\Phi(\boldsymbol{x},z,t)$ *by the equations*

$$\varphi_{-2}(\boldsymbol{x},t)=h_0\left([\partial_z\Phi]_{z=\eta}-\mu_0[\Phi]_{z=\eta}\right)\qquad \varphi_{-1}(\boldsymbol{x},t)=h_0[\partial_z\Phi]_{z=-h} \tag{1.19a,b}$$

$$\varphi_n(\boldsymbol{x},t)=\left\|Z_n\right\|_2^{-2}\int_{-h}^{\eta}\Phi^*(\boldsymbol{x},z,t)Z_n(z;\eta,h)\,dz\ ,\ n\geq 0 \tag{1.19c}$$

where $\|\Phi\|_2$ *stands for the usual* L^2-norm *of the function* Φ. *The series is uniformly convergent for* $z\in[-h(\boldsymbol{x}),\eta(\boldsymbol{x},t)]$.

Proof: Our goal is to obtain a new 'velocity potential' Φ^* from Φ and the functions Z_{-2}, Z_{-1} that will satisfy the boundary conditions of the Sturm-Liouville problem (1.11) and the smoothness requirements of Lemma 1. These properties will enable as to use Lemma 1 on Φ^*, which in sequence, will prove the theorem for function Φ .

Thus, given Φ, the parameters (h_0,μ_0) and the vertical functions Z_{-2}, Z_{-1}, we define the function:

$$\begin{aligned}\Phi^*(\boldsymbol{x},z,t) = \Phi(\boldsymbol{x},z,t) - h_0\left([\partial_z\Phi]_{z=\eta}-\mu_0[\Phi]_{z=\eta}\right)Z_{-2}\\ - h_0[\partial_z\Phi]_{z=-h}Z_{-1}\end{aligned} \tag{1.20}$$

Applying the boundary operators $[\partial_z]_{z=-h}$ and $[\partial_z-\mu_0]_{z=-h}$ to both members of Eq. (1.20) and taking into account the boundary conditions of functions Z_{-2}, Z_{-1}, we easily obtain:

$$[\partial_z\Phi^*]_{z=-h} = 0 \quad \text{and} \quad [(\partial_z-\mu_0)\Phi^*]_{z=\eta} = 0 \tag{1.21a,b}$$

Thus, $\Phi^*(\boldsymbol{x},z,t)$ as a function of the vertical coordinate z, satisfies the same boundary conditions as the eigenfunctions $Z_n(z)$, $n\geq 0$, of the regular Sturm-Liouville problem (1.11) and $\Phi^*(\boldsymbol{x},.,t)\in C^2([-h,\eta])$. Applying now Lemma 1 we conclude that, for each fixed $(\boldsymbol{x},t)\in X\times[t_0,t_1]$, function $\Phi^*(\boldsymbol{x},z,t)$ admits the following, uniformly convergent, series expansion:

$$\Phi^*(\mathbf{x},z,t)=\sum_{n=0}^{\infty}\varphi_n(\boldsymbol{x},t)\,Z_n(z;\eta,h) \tag{1.22}$$

where $\varphi_n(\boldsymbol{x},t)$, $n\geq 0$ are given by Eq (1.19c). Substituting Eq (1.20) to Eq (1.22) and solving for $\Phi(\boldsymbol{x},z,t)$ we obtain the needed wanted series expansion □

From the analysis done up to now, we can deduct that the constant $\mu_0>0$ serves the purpose of defining the auxiliary Sturm-Liouville problem (1.11a)-(1.11c) in a convenient way. Let it be stressed that the validity and the uniform convergence of the series expansion (1.18) is not affected by the choice of the parameter. However from the point of view of the numerical treatment of the problem, optimal choices of h_0 and μ_0 do exist (See Section 3.2 for a numerical argument concerning the matter).

Furthermore, the term $\varphi_{-2} Z_{-2}$ will be referred to as the *free-surface mode*, the term $\varphi_{-1} Z_{-1}$ as the *sloping-bottom mode*, term $\varphi_0 Z_0$ as the propagating mode and $\varphi_n Z_n \;\; n \geq 1$ as the evanescent modes. It should be noted though that the names propagating and evanescent do not imply that the physical notions of these modes correspond to the classical propagating and evanescent modes of the water wave theory . For example the field strength of the evanescent modes presented here does not vanish exponentially in the horizontal direction (nor does it vanish in general).

Finally, for us to use the calculus of variations for a reformulation of the problem we must ensure that the infinite series representation is at least twice term-wise differentiable with respect to the horizontal variables (x_1, x_2) and once term-wise differentiable with respect to the time variable t and the vertical variable z. It is known that an infinite series of the form $f(x) = \sum_{n=1}^{\infty} u_n(x),\ x \in X$ is term-wise differentiable if (but not only if) we can find a convergent series $\sum_{n=1}^{\infty} M_n$ such that $\|u_n(x)\|_{\infty} \leq M_n \;\; \forall\ n \in \mathbb{N}$. Such a proof was first presented in (Athanassoulis & Belibassakis, 2003) and stated that under certain smoothness assumptions regarding $\Phi(\boldsymbol{x}, z, t)$ the modal amplitudes φ_n decay at a rate of n^{-4}.

Theorem 2 (Athanassoulis et al,. 2003): *Let* Φ *be defined on* $\bar{D}_h^{\eta} \times [t_0, t_1]$ *and assume that*

$$\Phi(\cdot,\cdot,t) \in C^4(D_h^{\eta}) \cap C^3(\bar{D}_h^{\eta}) \qquad \|\Phi(\cdot,\cdot,t)\|_{C^4(D_h^{\eta}) \cap C^3(\bar{D}_h^{\eta})} \to 0 \;\; \textit{for} \;\; \boldsymbol{x} \in S^{\infty} \tag{1.23}$$

and $\Phi(\boldsymbol{x}, z, \cdot) \in C^1([t_0, t_1])$. *Then, the modal amplitudes* $\varphi_n(\boldsymbol{x}, t)$ *satisfy the estimate:*

$$\|\varphi_n\|_{\infty,\, X \times I} = \max\{\, |\varphi_n(\boldsymbol{x}, t)|\,,\ \boldsymbol{x} \in X,\ t \in I = [t_0, t_1]\,\} = O(n^{-4}) \tag{1.24}$$

Proof: Using Eq (1.11a), we reformulate Eq (1.19c) as:

$$\varphi_n(\boldsymbol{x}, t) = \|Z_n\|_2^{-2}\, k_n^{-2} \int_{-h}^{\eta} \Phi^*\, \partial_{zz} Z_n \, dz \tag{1.25}$$

where Φ^* is defined from Eq (1.20). Integrating by parts two times, we obtain

$$\varphi_n(\boldsymbol{x}, t) = \|Z_n\|_2^{-2} k_n^{-2} \left([\Phi^*\, \partial_z Z_n]_{-h}^{\eta} - [\partial_z \Phi^*\, Z_n]_{-h}^{\eta} + \int_{-h}^{\eta} \partial_{zz} \Phi^*\, Z_n \, dz \right)$$

Using the boundary conditions of Φ^* and Z_n, we see that the boundary terms cancel out, and

$$\varphi_n(\boldsymbol{x}, t) = \|Z_n\|_2^{-2} k_n^{-2} \left(\int_{-h}^{\eta} \partial_{zz} \Phi^*\; Z_n \, dz \right) \tag{1.26}$$

Integrating by parts twice again, Eq (1.26) we obtain:

$$\varphi_n(\boldsymbol{x},t) = \left\| Z_n \right\|_2^{-2} k_n^{-4} \left([\partial_z^2 \Phi^* \partial_z Z_n]_{-h}^{\eta} - [\partial_z^3 \Phi^* Z_n]_{-h}^{\eta} + \int_{-h}^{\eta} \partial_z^4 \Phi^* Z_n \, dz \right)$$

which, after applying the boundary conditions of Φ^* and Z_n reduces to

$$\varphi_n(\boldsymbol{x},t) = \left\| Z_n \right\|_2^{-2} k_n^{-4} \left(\begin{array}{r} [(\partial_z^2 \Phi^* \mu_0 - \partial_z^3 \Phi^*) Z_n]_{z=\eta} - [\partial_z^3 \Phi^* Z_n]_{z=-h} + \\ + \int_{-h}^{\eta} \partial_z^4 \Phi^* Z_n \, dz \end{array} \right) \tag{1.27}$$

The last formula is an estimate of the magnitude of $\left|\varphi_n(\boldsymbol{x},t)\right|$. Invoking eigenvalue-asymptotics for large values of n, one can easily find that $k_n = \pi n/(\eta+h) + O(n^{-1}) = O(n)$ and we readily confirm that

$$Z_n(z=\eta) = 1 \qquad Z_n(z=-h)| = O(1) \qquad |Z_n\|_2 = O(1). \tag{1.28}$$

Furthermore, $\left|\partial_z^2 \Phi^*\right|, \left|\partial_z^3 \Phi^*\right|, \left|\partial_z^4 \Phi^*\right|$ are uniformly bounded on $C^4(D_h^{\eta}) \cap C^3(\bar{D}_h^{\eta})$ from the assumptions declared above. Thus we obtain $\left|\varphi_n(\boldsymbol{x},t)\right| \leq A\, n^{-4}$ uniformly on X which proves the theorem. □

1.4 Variational reformulation of problem

In this Section, we exploit the representation of the velocity potential, presented in Section 1.3, to derive a variational reformulation of the nonlinear irrotational water wave (NLIWW) problem. In the first part of this Section we will formulate the *Euler-Lagrange* equations of the variational problem without explicitly referring to the vertical expansion of Section 1.3 given by Eqs (1.13) & (1.17), but only utilizing an expansion of the form (1.18). As a result, the derived Euler-Lagrange equations will hold for any arbitrary vertical expansion of the velocity potential (finite or infinite, approximate or exact). In the last part of this Section we will exploit the discussed series expansion and reformulate the *Euler-Lagrange* equations to a new, numerically efficient, system that is equivalent to the classical NLIWW problem, first presented in (Athanassoulis & Papoutsellis, 2015).

Replacing Eq (1.18) to Luke's action functional, would mean that a change of functional variables has taken place in the form of $(\eta,\Phi)\rightarrow(\eta,\boldsymbol{\varphi})$ where $\boldsymbol{\varphi}\equiv\boldsymbol{\varphi}(\boldsymbol{x},t)=\{\varphi_n(\boldsymbol{x},t)\}_n$. To simplify notation, we rewrite Eq (1.18) as $\Phi(\boldsymbol{x},z,t)=\boldsymbol{\varphi}^{\mathrm{T}}\boldsymbol{Z}$ with $\boldsymbol{Z}=\boldsymbol{Z}(z,\eta,h)\equiv\{Z_n(z;\eta(\boldsymbol{x},t),h(\boldsymbol{x},t))\}_n$. This manipulation of the action functional denotes a Kantorovich-type dimensional reduction of the NLIWW problem (see (Kantorovich & Krylov, 1958) & (Athanassoulis & Belibassakis, 2000)). In more detail, the fact that the vertical structure of the velocity potential is a priori known, transforms the 3D NLIWW problem to one solely defined on the horizontal plane. In addition, this dimensional reduction is not of the same nature as the one imposed by a Boundary Element Method (Grilli, Skourup, & Svendsen, 1989). In such a method the problem is projected onto the boundary of the domain, and although the reformulated problem is defined on a surface as well, said surface can assume a much more arbitrary form since it is defined on $\mathbb{R}^3$. Another problem is the fact that such a surface is time-dependent since it encompasses the free-surface elevation. As a result, implementing a Boundary Element Method for solving the NLIWW problem would require computations to be done using curvilinear coordinates, continuous re-meshing of the domain (Grilli *et al.*, 2001) as well as the arithmetic calculation of surface integrals, all tasks that are very time consuming. To surpass the problem of recreating the grid at every time-step, many models incorporate a time-independent transformation of the domain at the expense of formulating new systems with time-dependent coefficients (Bridges & Donaldson, 2011). On the other hand the current method simply projects the problem to the horizontal plane. Thus the new domain is a time-independent area of the horizontal plane. However, this quality comes at an expense, since it is exactly this form of dimensional reduction that requires the free-surface elevation and the sloping bottom to be single-valued functions of the horizontal space variables. More on this subject will be said in following Chapters.

The new action functional $\tilde{\mathcal{S}}[\eta,\boldsymbol{\varphi}]=\mathcal{S}[\eta,\boldsymbol{\varphi}^{\mathrm{T}}\boldsymbol{Z}(\eta)]$ can be explicitly calculated from Eqs (1.3a), (1.3b), by substituting Eq (1.18) and utilizing the notation introduced above:

$$\tilde{\mathcal{S}}[\eta,\boldsymbol{\varphi}] = \int_{t_0}^{t_1}\left\{\int_X\left(\int_{-h}^{\eta}\partial_t(\boldsymbol{\varphi}^{\mathrm{T}}\boldsymbol{Z}(\eta))\,dz + \tilde{\mathcal{K}}[\eta,\boldsymbol{\varphi}] + \frac{1}{2}g\eta^2 + \frac{p_{\mathrm{surf}}}{\rho}\eta\right)d\boldsymbol{x}\right\}dt + \begin{cases} \displaystyle\int_{t_0}^{t_1}\int_{\mathbb{R}}\int_{-h_a}^{\eta_a} V_a\left[\boldsymbol{\varphi}^{\mathrm{T}}\boldsymbol{Z}(\eta)\right]_{x_1=a} dz\,dx_2\,dt \\ 0 \end{cases} \tag{1.29a}$$

where $\tilde{\mathcal{K}}[\eta,\boldsymbol{\varphi}] = \mathcal{K}[\eta,\boldsymbol{\varphi}^{\mathrm{T}}\boldsymbol{Z}(\eta)]$ is the transformed kinetic energy density. given by:

$$\tilde{\mathcal{K}}[\eta,\boldsymbol{\varphi}] = \frac{1}{2}\int_{-h}^{\eta}|\nabla(\boldsymbol{\varphi}^{\mathrm{T}}\boldsymbol{Z}(\eta))|^2\,dz \tag{1.29b}$$

Assuming that the transformation $(\eta,\Phi)\to(\eta,\boldsymbol{\varphi})$ is regular and invertible, the critical points of $\mathcal{S}[\eta,\Phi]$ and $\tilde{\mathcal{S}}[\eta,\boldsymbol{\varphi}]$ are essentially the same in the sense that:

$$\delta\mathcal{S}[\eta,\Phi;\delta\Phi,\delta\eta] = 0 \quad\Leftrightarrow\quad \delta\tilde{\mathcal{S}}[\eta,\boldsymbol{\varphi};\delta\eta,\delta\boldsymbol{\varphi}] = 0 \tag{1.30}$$

Accordingly, the NLIWW problem is transformed through the new functional variables, to the following variational equation:

$$\delta\tilde{\mathcal{S}}[\eta,\boldsymbol{\varphi};\delta\eta,\delta\boldsymbol{\varphi}] = \delta_\eta\tilde{\mathcal{S}}[\eta,\boldsymbol{\varphi};\delta\eta] + \sum_{m=-2}^{\infty}\delta_{\varphi_m}\tilde{\mathcal{S}}[\eta,\boldsymbol{\varphi};\delta\varphi_m] = 0 \tag{1.31}$$

where $\delta_\eta\tilde{\mathcal{S}}[\eta,\boldsymbol{\varphi};\delta\eta]$ and $\delta_{\boldsymbol{\varphi}}\tilde{\mathcal{S}}[\eta,\boldsymbol{\varphi};\delta\boldsymbol{\varphi}]$ are the partial variations of the functional $\tilde{\mathcal{S}}[\eta,\boldsymbol{\varphi}]$ in the directions $\delta\eta$ and $\delta\boldsymbol{\varphi}$ respectively. The variations $(\delta\eta,\delta\boldsymbol{\varphi})$ are arbitrary, admissible functions of $(\boldsymbol{x};t)$, that satisfy the following constraints:

(i) The isochronality constraint

(ii) The vanishing at infinity constraint at a rate ensuring the convergence of the integrals appearing in the right-hand side of Eq (1.29a)

(iii) constraint $\left[\delta\eta\right]_{x_1=a} = 0$ since the free surface elevation is assumed known on the excitation boundary

(iv) constraint $\left[\delta\varphi_m\right]_{x_1=a} = 0$ in case of Dirichlet lateral conditions for the potential.

The next step for the derivation of the new formulation, is the explicit calculation of the variational partial derivatives appearing in Eq (1.31). This task can be done in many ways, yet we can utilize the chain rule for functional derivatives (see (Gasinski & Papageorgiou, 2006), Prop. 4.1.12), as a tool that will greatly simplify our calculations. The following proposition, taken from the book cited above, comes especially handy:

Proposition 1 (Gasinski et al. 2006): *Let* $X, Y, Z,$ *be Banach spaces. Furthermore, let the following be true:*

mapping $f : X \to Y$, is Gâteaux differentiable at $x \in X$, with $\delta f(x;h)$ denoting its Gâteaux derivative with respect to the increment $h \in X$.

mapping $g : Y \to Z$, is Fréchet differentiable at $f(x) \in Y$, with $Dg(y)$ denoting its Fréchet derivative.

Then the mapping $k \triangleq g \circ f : X \to Z$ is Gâteaux differentiable at $x \in X$ with

$$\delta k(x;h) = \delta g(f(x);\delta f(x;h)) = Dg(f(x))\,\delta f(x;h)$$

The following Lemma, proven in (Athanassoulis et al., 2015), derives the needed formulae for the partial variational derivatives of Eq (1.31) utilizing the aforementioned Proposition:

Lemma 1 (Athanassoulis et al,. 2015): *The partial variations* $\delta_\eta \tilde{\mathcal{S}}[\eta, \boldsymbol{\varphi}; \delta\eta]$ *and* $\delta_{\varphi_m} \tilde{\mathcal{S}}[\eta, \boldsymbol{\varphi}; \delta\varphi_m]$ *appearing in* Eq (1.30) *are calculated by the following formulae:*

$$\delta_\eta \tilde{\mathcal{S}}[\eta, \boldsymbol{\varphi}; \delta\eta] = \delta_\eta \mathcal{S}[\eta, \boldsymbol{\varphi}^{\mathrm{T}} \boldsymbol{Z}(\eta); \delta\eta] + \delta_\Phi \mathcal{S}[\eta, \boldsymbol{\varphi}^{\mathrm{T}} \boldsymbol{Z}(\eta); (\boldsymbol{\varphi}^{\mathrm{T}} \partial_\eta \boldsymbol{Z}(\eta))\delta\eta] \tag{1.31a}$$

$$\delta_{\varphi_m} \tilde{\mathcal{S}}[\eta, \boldsymbol{\varphi}; \delta\varphi_m] = \delta_\Phi \mathcal{S}[\eta, \boldsymbol{\varphi}^{\mathrm{T}} \boldsymbol{Z}(\eta); Z_m(\eta)\delta\varphi_m] \tag{1.31b}$$

where the variations $\delta_\eta \mathcal{S}[\eta, \Phi; \delta\eta]$ *and* $\delta_\Phi \mathcal{S}[\eta, \Phi; \delta\Phi]$ *are given by* Eqs (1.5a) & (1.5b) *respectively.*

Proof: We start by applying the chain rule for composite operators as described in Proposition 1. In our case $x = (x_1, x_2) = (\eta, \boldsymbol{\varphi})$ and $y = (y_1, y_2) = (\eta, \Phi)$. As a result

mapping f represents the transformation $(\eta, \boldsymbol{\varphi}) \to (\eta, \Phi)$ and can be rewritten as $f(\eta, \boldsymbol{\varphi}) = (f_1(\eta, \boldsymbol{\varphi}), f_2(\eta, \boldsymbol{\varphi})) = (\eta, \Phi)$.

Applying Proposition 1, for the directions f_1 and f_2 separately, we get:

$$\delta_\eta k(x;\delta\eta) = \delta_\eta g(f(x);\delta_\eta f_1(x;\delta\eta)) + \delta_\Phi g(f(x);\delta_\eta f_2(x;\delta\eta)) \tag{1.32a}$$

$$\delta_{\boldsymbol{\varphi}} k(x;\delta\boldsymbol{\varphi}) = \delta_\eta g(f(x);\delta_{\boldsymbol{\varphi}} f_1(x;\delta\boldsymbol{\varphi})) + \delta_\Phi g(f(x);\delta_{\boldsymbol{\varphi}} f_2(x;\delta\boldsymbol{\varphi})) \tag{1.33b}$$

Now implementing the fact that:

mapping g represents the action functional $\mathcal{S}[\eta, \Phi]$

mapping k represents the new action functional $\tilde{\mathcal{S}}[\eta, \boldsymbol{\varphi}]$

$$f_1(\eta,\boldsymbol{\varphi}) = \eta \qquad \text{and} \qquad f_2(\eta,\boldsymbol{\varphi}) = \boldsymbol{\varphi}^{\mathrm{T}}\mathbf{Z}(\eta)$$

we get from Eqs (1.32a) & (1.32b):

$$\delta_\eta \tilde{\mathcal{S}}[\eta,\boldsymbol{\varphi};\delta\eta] = \delta_\eta \mathcal{S}[\eta,\boldsymbol{\varphi}^{\mathrm{T}}\boldsymbol{Z}(\eta);\delta\eta] + \delta_\Phi \mathcal{S}[\eta,\boldsymbol{\varphi}^{\mathrm{T}}\boldsymbol{Z}(\eta);(\boldsymbol{\varphi}^{\mathrm{T}}\partial_\eta \boldsymbol{Z}(\eta))\delta\eta] \tag{1.33a}$$

$$\delta_{\boldsymbol{\varphi}} \tilde{\mathcal{S}}[\eta,\boldsymbol{\varphi};\delta\boldsymbol{\varphi}] = \delta_\Phi \mathcal{S}[\eta,\boldsymbol{\varphi}^{\mathrm{T}}\boldsymbol{Z}(\eta);\boldsymbol{Z}(\eta)^{\mathrm{T}}\delta\boldsymbol{\varphi}] \tag{1.33b}$$

Eq (1.33a) is identical to (1.31a). To prove Eq (1.31b), we invoke the linearity of the variation with respect to the increment, i.e $\delta_{\boldsymbol{\varphi}} \tilde{\mathcal{S}}[\eta,\boldsymbol{\varphi};\delta\boldsymbol{\varphi}] = \sum_{m=-2}^{\infty} \delta_{\varphi_m} \tilde{\mathcal{S}}[\eta,\boldsymbol{\varphi};\delta\varphi_m]$. The Fréchet differentiability of the action functional $\mathcal{S}[\eta,\Phi]$ implies that $\delta_\Phi \mathcal{S}[\eta,\Phi;\cdot]$ is a linear operator on $\delta\Phi$. Therefore, we can write:

$$\delta_{\boldsymbol{\varphi}} \tilde{\mathcal{S}}[\eta,\boldsymbol{\varphi};\delta\boldsymbol{\varphi}] = \sum_{m=-2}^{\infty} \delta_{\varphi_m} \tilde{\mathcal{S}}[\eta,\boldsymbol{\varphi};\delta\varphi_m] = \sum_{m=-2}^{\infty} \delta_\Phi \mathcal{S}[\eta,\boldsymbol{\varphi}^{\mathrm{T}}\boldsymbol{Z}(\eta);Z_m(\eta)\delta\varphi_m] \tag{1.33c}$$

Thus, Eq (1.31b) follows by using the arbitrariness of the increments $\delta\varphi_m$, completing the proof. □

Euler-Lagrange equations derived from an arbitrary vertical series expansion

In this subsection, we will calculate the variations of Eqs (1.30) and derive the corresponding *Euler-Lagrange* equations, hence allowing us to obtain a new formulation of the NLIWW problem. The equations we shall obtain were first presented in (Athanassoulis & Belibassakis, 2000), however as will be seen later this form will not be the final model we will discretize and solve numerically. Notice that in the current subsection the vertical series representation (1.13), (1.17) of Section 1.3, will not be explicitly used. As a result the Euler-Lagrange equations we will derive can be used by any kind of vertical expansion of the form (1.18), approximate or exact. Furthermore the index of the vertical functions need not be $\mathbb{N}\cup\{-2,-1\}$ but any arbitrary subset of $\mathbb{Z}$. These calculations were first presented in detail in (Athanassoulis et al., 2015). The exploitation of the vertical functions as calculated in Section 1.3 will be done in the following subsection.

We start by calculating the variation $\delta_\eta \tilde{S}[\eta,\boldsymbol{\varphi};\delta\eta]$. Utilizing Eq (1.31a) we substitute $\Phi = \boldsymbol{\varphi}^{\mathrm{T}}\boldsymbol{Z}(\eta)$ in Eq (1.5a) & Eq (1.5c) and $\delta\Phi = \partial_\eta Z_m(\eta)\delta\eta$ in Eq (1.5c), obtaining:

$$\begin{aligned}\delta_\eta \tilde{\mathcal{S}}[\eta,\boldsymbol{\varphi};\delta\eta] = & \int_{t_0}^{t_1}\int_X \Big\{\Big[\partial_t\big(\boldsymbol{\varphi}^{\mathrm{T}}\boldsymbol{Z}(\eta)\big)+\frac{1}{2}|\nabla_{\boldsymbol{x}}\big(\boldsymbol{\varphi}^{\mathrm{T}}\boldsymbol{Z}(\eta)\big)|^2 + \\ & +\frac{1}{2}(\partial_z\big(\boldsymbol{\varphi}^{\mathrm{T}}\boldsymbol{Z}(\eta)\big))^2+g\,z\Big]_{z=\eta}+g\,\eta+\frac{p_{\mathrm{surf}}}{\rho}\Big\}\delta\eta\,d\boldsymbol{x}\,dt \\ & +\sum_{m=-2}^{\infty}\int_{t_0}^{t_1}\int_X\Big\{\Big(-\partial_t\eta+\boldsymbol{N}_\eta\cdot\Big[\nabla\big(\boldsymbol{\varphi}^{\mathrm{T}}\boldsymbol{Z}(\eta)\big)\Big]_{z=\eta}\Big)\Big[\,\varphi_m\,\partial_\eta Z_m(\eta)\delta\eta\,\Big]_{z=\eta} \\ & +\Big(-\partial_t h+\boldsymbol{N}_h\cdot\Big[\nabla\big(\boldsymbol{\varphi}^{\mathrm{T}}\boldsymbol{Z}(\eta)\big)\Big]_{z=-h}\Big)\Big[\,\varphi_m\,\partial_\eta Z_m(\eta)\delta\eta\,\Big]_{z=-h} \\ & +\int_X\Delta\big(\boldsymbol{\varphi}^{\mathrm{T}}\boldsymbol{Z}(\eta)\big)\varphi_m\,\partial_\eta Z_m(\eta)\delta\eta\,dz\Big\}d\boldsymbol{x}\,dt \\ & +\int_{t_0}^{t_1}\int_X\int_{-h_a}^{\eta_a}\Big(-\Big[\,\partial_{x_1}\big(\boldsymbol{\varphi}^{\mathrm{T}}\boldsymbol{Z}(\eta)\big)\Big]_{x_1=a}+V_a\Big)\Big[\,\varphi_m\,\partial_\eta Z_m(\eta)\delta\eta\,\Big]_{x_1=a}dz\,dx_2\,dt\end{aligned} \tag{1.39}$$

Continuing on the derivation of the Euler-Lagrange equations, we want to simplify Eq (1.3). In order to do that, we expand the following terms:

$$\begin{aligned}\sum_{n=-2}^{\infty}\int_{-h}^{\eta}\Delta\big(\boldsymbol{\varphi}^{\mathrm{T}}\boldsymbol{Z}(\eta)\big)\varphi_m\,\partial_\eta Z_m(\eta)\delta\eta\,dz = & \;\delta\eta\Big\{\sum_{n=-2}^{\infty}\Delta_{\boldsymbol{x}}\varphi_n\int_{-h}^{\eta}Z_n\,\partial_\eta Z_m\,dz + \\ & +2\sum_{n=-2}^{\infty}\big(\nabla_{\boldsymbol{x}}\varphi_n,0\big)\int_{-h}^{\eta}\big(\nabla_{\boldsymbol{x}},\partial_z\big)Z_n\,\partial_\eta Z_m\,dz+\sum_{n=-2}^{\infty}\varphi_n\int_{-h}^{\eta}\big(\Delta_{\boldsymbol{x}},\partial_z^2\big)Z_n\,\partial_\eta Z_m\,dz\Big\}\Rightarrow\end{aligned}$$

$$\begin{aligned}\sum_{n=-2}^{\infty}\int_{-h}^{\eta}\Delta\big(\boldsymbol{\varphi}^{\mathrm{T}}\boldsymbol{Z}(\eta)\big)\varphi_m\,\partial_\eta Z_m(\eta)\delta\eta\,dz = & \;\delta\eta\Big\{\sum_{n=-2}^{\infty}\Delta_{\boldsymbol{x}}\varphi_n\int_{-h}^{\eta}Z_n\,\partial_\eta Z_m\,dz + \\ & +2\sum_{n=-2}^{\infty}\nabla_{\boldsymbol{x}}\varphi_n\int_{-h}^{\eta}\nabla_{\boldsymbol{x}}Z_n\,\partial_\eta Z_m\,dz+\sum_{n=-2}^{\infty}\varphi_n\int_{-h}^{\eta}\big(\Delta_{\boldsymbol{x}}Z_n+\partial_z^2Z_n\big)\partial_\eta Z_m\,dz\Big\}\end{aligned} \tag{1.40a}$$

and

$$\begin{aligned}\boldsymbol{N}_h\cdot\Big[\nabla\big(\boldsymbol{\varphi}^{\mathrm{T}}\boldsymbol{Z}(\eta)\big)\varphi_m\,\partial_\eta Z_m(\eta)\delta\eta\Big]_{z=-h} = & \\ =-\delta\eta\,\nabla_{\boldsymbol{x}}h\cdot\sum_{n=-2}^{\infty}\Big(\nabla_x\varphi_n\big[Z_n\big]_{z=-h}+\varphi_n\big[\nabla_{\boldsymbol{x}}Z_n\big]_{z=-h}\Big)-\delta\eta\sum_{n=-2}^{\infty}\varphi_n\big[\partial_z Z_n\big]_{z=-h}\end{aligned} \tag{1.40b}$$

From Eqs (1.40a) & (1.40b), we can define the following operators:

$$l_{mn}\big[\eta,h\big]=a_{mn}\,\Delta+\boldsymbol{b}_{mn}\cdot\nabla_x+c_{mn}\;,\;m,n\geq-2 \tag{1.41a}$$

where $a_{mn}(\eta,h)$, $\boldsymbol{b}_{mn} = \left(b_{mn}^{(1)}, b_{mn}^{(2)} \right)$ and $c_{mn}(\eta,h)$, with $m, n \geq -2$, are matrix coefficients defined by the following formulae:

$$a_{mn}(\eta,h) = \int_{-h}^{\eta} Z_n \, \partial_\eta Z_m \, dz \tag{1.41b}$$

$$\boldsymbol{b}_{mn}(\eta,h) = \left(b_{mn}^{(1)}, b_{mn}^{(2)} \right) = 2\int_{-h}^{\eta} \nabla_{\boldsymbol{x}} Z_n \, \partial_\eta Z_m \, dz + \nabla_{\boldsymbol{x}} h \left[Z_n \, \partial_\eta Z_m \right]_{z=-h} \tag{1.41c}$$

$$c_{mn}(\eta,h) = \int_{-h}^{\eta} \left(\Delta_x Z_n + \partial_z^2 Z_n \right) \partial_\eta Z_m dz - N_h \cdot \left[(\nabla_x Z_n, \partial_z Z_n) \partial_\eta Z_m \right]_{z=-h} \tag{1.41d}$$

Invoking Eqs (1.40) and (1.41) we can derive the following relation:

$$\begin{aligned} \sum_{m=-2}^{\infty} \sum_{n=-2}^{\infty} \ell_{mn}[\eta,h] \varphi_n \varphi_m \; = \; & \int_{-h}^{\eta} \Delta\left(\boldsymbol{\varphi}^T \boldsymbol{Z} \right) \left(\boldsymbol{\varphi}^T \, \partial_\eta \boldsymbol{Z} \right) dz - \\ & - \boldsymbol{N}_h \cdot \left[\left| \nabla \left(\boldsymbol{\varphi}^T \boldsymbol{Z} \right) \right| \left(\boldsymbol{\varphi}^T \, \partial_\eta \boldsymbol{Z} \right) \right]_{z=-h} \end{aligned} \tag{1.42}$$

Finally Eq (1.39) is reformulated as:

$$\begin{aligned} & \delta_\eta \tilde{\mathcal{S}}[\eta, \boldsymbol{\varphi}; \delta\eta] = \\ & = \int_{t_0}^{t_1} \int_X \left\{ \left[\partial_t (\boldsymbol{\varphi}^{\mathrm{T}} \mathbf{Z}) \right]_{z=\eta} + \frac{1}{2} \left[\nabla (\boldsymbol{\varphi}^{\mathrm{T}} \boldsymbol{Z}) \right]_{z=\eta}^2 + g\eta - \sum_{m=-2}^{\infty} \sum_{n=-2}^{\infty} \ell_{mn}[\eta,h] \varphi_n \varphi_m \right. \\ & \qquad \left. + \left(-\partial_t \eta + \mathbf{N}_\eta \cdot \left[\nabla (\boldsymbol{\varphi}^{\mathrm{T}} \boldsymbol{Z}) \right]_{z=\eta} \right) \left[\boldsymbol{\varphi}^{\mathrm{T}} \partial_\eta \mathbf{Z} \right]_{z=\eta} + \frac{p_{\mathrm{surf}}}{\rho} \right\} \delta\eta \, d\mathbf{x} \, dt \, , \end{aligned} \tag{1.43}$$

Next, we calculate the variations $\delta_{\varphi_m} \tilde{\mathcal{S}}[\eta, \boldsymbol{\varphi}; \delta\boldsymbol{\varphi}_m]$. Utilizing Eq (1.31b) we substitute the $\Phi = \boldsymbol{\varphi}^{\mathrm{T}} \boldsymbol{Z}(\eta)$ and $\delta\Phi = Z_m(\eta) \delta\varphi_m$ in Eq (1.5c), obtaining:

$$\begin{aligned} \delta_{\varphi_m} \tilde{\mathcal{S}}[\eta, \boldsymbol{\varphi}; \delta\varphi_m] = & \int_{t_0}^{t_1} \int_X \left\{ \left(-\partial_t \eta + \boldsymbol{N}_\eta \cdot \left[\nabla \left(\boldsymbol{\varphi}^{\mathrm{T}} \boldsymbol{Z}(\eta) \right) \right]_{z=\eta} \right) \left[Z_m(\eta) \delta\varphi_m \right]_{z=\eta} \right. \\ & + \left(-\partial_t h + \boldsymbol{N}_h \cdot \left[\nabla \left(\boldsymbol{\varphi}^{\mathrm{T}} \boldsymbol{Z}(\eta) \right) \right]_{z=-h} \right) \left[Z_m(\eta) \delta\varphi_m \right]_{z=-h} \\ & \left. - \int_{-h}^{\eta} \Delta \left(\boldsymbol{\varphi}^{\mathrm{T}} \boldsymbol{Z}(\eta) \right) Z_m(\eta) \delta\varphi_m \, dz \right\} d\mathbf{x} \, dt \\ + \int_{t_0}^{t_1} \int_{\mathbb{R}} \int_{-h_a}^{\eta_a} & \left(- \left[\partial_{x_1} \left(\boldsymbol{\varphi}^{\mathrm{T}} \boldsymbol{Z}(\eta) \right) \right]_{x_1=a} + V_a \right) \left[Z_m(\eta) \delta\varphi_m \right]_{x_1=a} dz \, dx_2 \, dt \, , \; m \geq -2 \end{aligned} \tag{1.44}$$

In the same direction as with the partial variation $\delta_\eta \widetilde{S}[\eta,\boldsymbol{\varphi};\delta\eta]$, we expand the following terms:

$$\sum_{n=-2}^{\infty}\int_{-h}^{\eta}\Delta\left(\boldsymbol{\varphi}^{\mathrm{T}}\boldsymbol{Z}(\eta)\right)\varphi_m Z_m(\eta)\delta\varphi_m\,dz = \left\{\sum_{n=-2}^{\infty}\left(\int_{-h}^{\eta} Z_n Z_m\,dz\right)\Delta_{\boldsymbol{x}}\varphi_n + \right.$$
$$\left. + \sum_{n=-2}^{\infty} 2\left(\int_{-h}^{\eta}\left(\nabla_{\boldsymbol{x}} Z_n, \partial_z Z_n\right) Z_m\,dz\right)\cdot\left(\nabla_{\boldsymbol{x}}\varphi_n, 0\right) + \sum_{n=-2}^{\infty}\left(\int_{-h}^{\eta}\left(\nabla_{\boldsymbol{x}}^2 Z_n + \partial_z^2 Z_n\right) Z_m\,dz\right)\varphi_n\right\}\delta\varphi_m \Rightarrow$$

$$\int_{-h}^{\eta}\Delta(\boldsymbol{\varphi}^{\mathrm{T}}\boldsymbol{Z}) Z_m\,\delta\varphi_m\,dz = \left\{\sum_{n=-2}^{\infty}\Delta_{\boldsymbol{x}}\varphi_n\left(\int_{-h}^{\eta} Z_n Z_m\,dz\right) + \right.$$
$$\left. + \sum_{n=-2}^{\infty} 2\left(\int_{-h}^{\eta}\nabla_{\boldsymbol{x}} Z_n Z_m\,dz\right)\cdot\nabla_{\boldsymbol{x}}\varphi_n + \sum_{n=-2}^{\infty}\left(\int_{-h}^{\eta}\left(\nabla_{\boldsymbol{x}}^2 Z_n + \partial_z^2 Z_n\right) Z_m\,dz\right)\varphi_n\right\}\delta\varphi_m \tag{1.45a}$$

and

$$\mathbf{N}_h\cdot\left[\nabla(\boldsymbol{\varphi}^{\mathrm{T}}\mathbf{Z}) Z_m\,\delta\varphi_m\right]_{z=-h} =$$
$$= \left\{\sum_{n=-2}^{\infty} -\nabla_{\mathbf{x}} h\cdot\left(\nabla_{\mathbf{x}}\varphi_n\left[Z_n\right]_{z=-h} + \varphi_n\left[\nabla_{\mathbf{x}} Z_n\right]_{z=-h}\right) - \left[\partial_z Z_n\right]_{z=-h}\varphi_n\right\}\delta\varphi_m. \tag{1.45b}$$

From Eqs (1.45a) & (1.45b), we can define the following operators:

$$\mathrm{L}_{mn}[\eta,h] = \mathrm{A}_{mn}(\eta,h)\nabla_{\mathbf{x}}^2 + (\mathrm{B}^1_{mn}(\eta,h)\,,\,\mathrm{B}^2_{mn}(\eta,h))\cdot\nabla_{\mathbf{x}} + \mathrm{C}_{mn}(\eta,h) \tag{1.46a}$$

where $\mathrm{A}_{mn}(\eta,h), \mathbf{B}_{mn}(\eta,h) = (\mathrm{B}^1_{mn}(\eta,h)\,,\,\mathrm{B}^2_{mn}(\eta,h))$ and $\mathrm{C}_{mn}(\eta,h)$, with $m, n \geq -2$, are matrix coefficients defined by the following formulae:

$$\mathrm{A}_{mn} = \int_{-h}^{\eta} Z_n Z_m\,dz \tag{1.46b}$$

$$\mathbf{B}_{mn} = 2\int_{-h}^{\eta}\nabla_{\boldsymbol{x}} Z_n Z_m\,dz + \nabla_{\boldsymbol{x}} h\left[Z_m Z_n\right]_{z=-h} \tag{1.46c}$$

$$\mathrm{C}_{mn} = \int_{-h}^{\eta}\left(\nabla_{\boldsymbol{x}}^2 Z_n + \partial_z^2 Z_n\right) Z_m\,dz - \boldsymbol{N}_h\cdot\left[\left(\nabla_{\boldsymbol{x}} Z_n, \partial_z Z_n\right) Z_m\right]_{z=-h} \tag{1.46d}$$

Invoking Eqs (1.45) and (1.46) we can derive the following relation:

$$\sum_{n=-2}^{\infty} \mathrm{L}_{mn}[\eta,h]\varphi_m = \int_{-h}^{\eta} \Delta\left(\boldsymbol{\varphi}^T \boldsymbol{Z}\right)\delta\varphi_m Z_m\, dz - \\ - \boldsymbol{N}_h \cdot \left[\left|\nabla\left(\boldsymbol{\varphi}^T \boldsymbol{Z}\right)\right|\delta\varphi_m Z_m\right]_{z=-h} \tag{1.47}$$

Finally Eq (1.44) is reformulated as:

$$\delta_{\varphi_m}\tilde{\mathcal{S}}[\eta,\boldsymbol{\varphi};\delta\varphi_m] = \int_{t_0}^{t_1}\int_X \left\{\left(-\partial_t\eta + \boldsymbol{N}_\eta\cdot\left[\nabla\left(\boldsymbol{\varphi}^{\mathrm{T}}\boldsymbol{Z}(\eta)\right)\right]_{z=\eta}\right)\left[Z_m(\eta)\delta\varphi_m\right]_{z=\eta}\right. \\ \left. - \partial_t h\left[Z_m(\eta)\delta\varphi_m\right]_{z=-h} - \int_{-h}^{\eta}\sum_{n=-2}^{\infty}\mathrm{L}_{mn}[\eta,h]\varphi_m\,\delta\varphi_m\,dz\right\} d\boldsymbol{x}\,dt \tag{1.48}$$
$$+\int_{t_0}^{t_1}\int_{\mathbb{R}}\int_{-h_a}^{\eta_a}\left(-\left[\partial_{x_1}\left(\boldsymbol{\varphi}^{\mathrm{T}}\boldsymbol{Z}(\eta)\right)\right]_{x_1=a} + V_a\right)\left[Z_m(\eta)\delta\varphi_m\right]_{x_1=a} dz\,dx_2\,dt,\ m\geq -2$$

Having replaced the derivatives of the variations $(\delta\eta,\delta\boldsymbol{\varphi})$ we can now invoke the arbitrariness of the variations $(\delta\eta,\delta\boldsymbol{\varphi})$, and derive the following *Euler-Lagrange* equations for the functional $\tilde{\mathcal{S}}[\eta,\boldsymbol{\varphi}]$:

$$\delta\eta: \quad \left[\partial_t(\boldsymbol{\varphi}^{\mathrm{T}}\boldsymbol{Z})\right]_{z=\eta} + g\eta + \frac{1}{2}\left[\nabla(\boldsymbol{\varphi}^{\mathrm{T}}\boldsymbol{Z})\right]^2_{z=\eta} - \sum_{m=-2}^{\infty}\left(\sum_{n=-2}^{\infty}\ell_{mn}[\eta,h]\varphi_n\right)\varphi_m \\ +\left(-\partial_t\eta + \boldsymbol{N}_\eta\cdot\left[\nabla(\boldsymbol{\varphi}^{\mathrm{T}}\boldsymbol{Z})\right]_{z=\eta}\right)\left(\boldsymbol{\varphi}^{\mathrm{T}}\left[\partial_\eta\boldsymbol{Z}\right]_{z=\eta}\right) = -\frac{p_{\mathrm{surf}}}{\rho}, \tag{1.49a}$$

$$\delta\varphi_m: \quad \left(\partial_t\eta - \boldsymbol{N}_\eta\cdot\left[\nabla(\boldsymbol{\varphi}^{\mathrm{T}}\boldsymbol{Z})\right]_{z=\eta}\right)\left[Z_m\right]_{z=\eta} + \\ + \sum_{n=-2}^{\infty}\mathrm{L}_{mn}[\eta,h]\varphi_n = -\partial_t h[Z_m]_{z=-h}, \tag{1.49b}$$

$$\left[\delta\varphi_m\right]_{x_1=a}: \quad \sum_{n=-2}^{\infty}\left(\left[\partial_{x_1}\varphi_n\right]_{x_1=a}\mathrm{A}^{(a)}_{mn} + \left[\varphi_n\right]_{x_1=a}\mathrm{B}^{(a)}_{mn}\right) = g_m \tag{1.49c}$$

where

$$\mathrm{A}^{(a)}_{mn} = \int_{-h_a}^{\eta_a}\left[Z_n Z_m\right]_{x_1=a} dz \tag{1.50a}$$

$$\mathrm{B}_{mn}^{(a)} = \int_{-h_a}^{\eta_a} \left[\partial_{x_1} Z_n \, Z_m \right]_{x_1 = a} dz \tag{1.50b}$$

$$g_m = \int_{-h_a}^{\eta_a} V_a \left[Z_m \right]_{x_1 = a} dz \tag{1.50c}$$

Eq (1.49c) corresponds to a Neumann lateral condition on the line $\{x_1 = a\}$. In case of Dirichlet excitation, Eq (1.49c) is replaced by the following lateral condition:

$$\left[\varphi_n \right]_{x_1 = a} = \varphi_n^a \ , \ n \geq -2 \tag{1.49d}$$

where φ_n^a , $n \geq -2$ are known values.

The system defined by (1.49), together with an initial condition and a radiation condition at infinity is equivalent the classical formulation of the NLIWW and could be used to implement such problems. This system has the form of two nonlinear evolutionary equations, one scalar (1.49a) and one vector (1.49b). Such systems have been extensively used for the derivation of approximate models from Luke's variational principle (see e.g. (Isobe & Abohadima, 1998), (Klopman, Van Groesen, & Dingemans, 2010)). This models however, is an exact reformulation of the NLIWW problem and as such it is expected to behave better than the corresponding approximate models. It should also be noted that the approximate models cited above can be derived from the Euler-Lagrange equations (1.49) with the proper representations of the vertical structure of the velocity potential and the corresponding linearizations. As a result, system (1.49) has a much more general meaning and actually the approximate models cited above can be derived from system (1.49) with the proper linearizations and explicit representation of the vertical structure of the velocity potential.

Hamiltonian reformulation of the NLIWW

In this subsection we will explicitly utilize the vertical series expansion presented in Section 1.3, Eqs (1.13), (1.17). Hence, the reformulation of the problem that will be presented here is not generally true for an arbitrary vertical expansion (1.18) of the velocity potential.

As up to now in the process of deriving the new formulation of the NLIWW, we have transformed the classical problem to a pair of equations (one scalar and one vector) defined on the free-surface combined with lateral boundary conditions from Eq (1.48). The current state of the problem is not numerically efficient, in the sense that it couples two systems:

$$\sum_{m=-2}^{\infty} \sum_{n=-2}^{\infty} \ell_{mn}[\eta, h] \varphi_n \varphi_m = \int_{-h}^{\eta} \Delta\left(\boldsymbol{\varphi}^T \boldsymbol{Z}\right)\left(\boldsymbol{\varphi}^T \partial_\eta \boldsymbol{Z}\right) dz - \boldsymbol{N}_h \cdot \left[\left| \nabla\left(\boldsymbol{\varphi}^T \boldsymbol{Z}\right) \right| \left(\boldsymbol{\varphi}^T \partial_\eta \boldsymbol{Z}\right) \right]_{z=-h}$$

$$\sum_{n=-2}^{\infty} \mathrm{L}_{mn}[\eta,h]\varphi_m = \int_{-h}^{\eta} \Delta\left(\boldsymbol{\varphi}^T \boldsymbol{Z}\right) Z_m \, dz - \boldsymbol{N}_h \cdot \left[\left| \nabla\left(\boldsymbol{\varphi}^T \boldsymbol{Z}\right) \right| Z_m \right]_{z=-h}$$

together with the nonlinear classical evolutionary equations of the free-surface. Thus, even though the new formulation is defined in a dimensionally reduced space, in comparison with the classical formulation, it still presents many difficulties regarding its arithmetical treatment. This is understood from the fact that the numerical simulation of nonlinear and time-dependent systems is very time consuming and in many cases unstable. A first reformulation of these equations was first provided in (Athanassoulis & Belibassakis, 2007) however the form of the evolution equations was still relative complex. A second reformulation of the problem was presented in (Athanassoulis & Papoutsellis, 2015) where the numerically inefficient evolution equations of Eqs. (1.49) were transformed to two simple evolution equations coupled with a substrate problem of partial differential equations (in which essentially all the numerical complexity lies). Also, in this new form explicit use of the DtN operator is used to represent the coupling between the substrate problem and the evolution equations. We shall derive and present this model in the current Section.

Noticing that the nonlinearity of Eqs (1.49a) and (1.49b) is restrained only in the terms that correspond to the classical free-surface equations, we search a way to decouple the linear systems defined above with the free-surface equations. The following Lemma will help us in achieving this goal:

Lemma 2 (Athanassoulis et al., 2015): *Let* $\boldsymbol{\varphi} = \{\varphi_n(\boldsymbol{x};t)\}_{n=-2}^{\infty}$ *satisfies* Eqs (1.47) *at every* $t \in [t_0, t_1]$. *Then, the function* $\Phi = \boldsymbol{\varphi}^{\mathrm{T}} \boldsymbol{Z}$, *where the vertical functions* $\boldsymbol{Z}$ *are given by* Eqs (1.13), (1.17), *satisfies the Laplace equation* (1.2a) *and the bottom impermeability condition* (1.2b).

Proof: Let us fix an $m = m_*$. Subtracting from Eqs (1.49a) the m_*^{th} equation, we get the relation:

$$\sum_{n=-2}^{\infty} \left(\mathrm{L}_{mn}[\eta,h] - \mathrm{L}_{m_* n}[\eta,h]\right)\varphi_n = -\partial_t h \left[Z_m - Z_{m_*} \right]_{z=-h} \,, \; m \geq -2 \tag{1.51a}$$

But by utilizing Eq (1.47), we also get the formula:

$$\begin{aligned} \sum_{n=-2}^{\infty} \left(\mathrm{L}_{mn}[\eta,h] - \mathrm{L}_{m_* n}[\eta,h]\right)\varphi_n = & \int_{-h}^{\eta} \Delta\Phi\left(Z_m - Z_{m_*}\right) dz \\ & - \boldsymbol{N}_h \cdot \left[\nabla\Phi\left(Z_m - Z_{m_*}\right) \right]_{z=-h} \end{aligned} \tag{1.51b}$$

Combining Eqs(1.51a) with (1.51b) we get:

$$\int_{-h}^{\eta} \Delta\Phi\,(Z_m - Z_{m_*})\,dz \;=\; -\big(\partial_t h - \boldsymbol{N}_h\cdot\nabla\Phi\big)\big[Z_m - Z_{m_*}\big]_{z=-h} \tag{1.52}$$

Consider now a function $\delta\Psi$, defined on the closed domain $\overline{D_h^\eta}(X,t)$, which is zero on the boundaries Γ^η and S^∞, and arbitrary (admissibly smooth) in the open domain $D_h^\eta(X,t)$ and on the seabed boundary Γ_h. Applying Theorem 1 of Section 1.3, we conclude that there exists an admissible sequence $\delta\boldsymbol{\psi} = \{\delta\psi_m(\boldsymbol{x};t)\}_{m=-2}^{\infty}$ such that $\delta\Psi = \sum_{m=-2}^{\infty} \delta\psi_m Z_m$. The fact that $\|\delta\psi_m\|_\infty = O\big(n^{-4}\big)$ makes the series rapidly convergent and thus, the various term-by-term operations made below are justified. Multiplying the m^{th} equation (1.52) by $\delta\psi_m$ and integrating over X, and summing over m, we obtain:

$$\begin{aligned}&\int_X\int_{-h}^{\eta} \Delta\Phi \sum_{m=-2}^{\infty} \delta\psi_m (Z_m - Z_{m_*})\,dz\,d\boldsymbol{x} + \\ &+\int_X \big(\partial_t h - \boldsymbol{N}_h\cdot\nabla\Phi\big)\sum_{m=-2}^{\infty}\delta\psi_m\Big[\,Z_m - Z_{m_*}\,\Big]_{z=-h} d\boldsymbol{x} = 0.\end{aligned} \tag{1.53}$$

Consider now the function $\delta\tilde{\Psi} = \sum_{m=-2}^{\infty} \delta\psi_m (Z_m - Z_{m_*})$. Since

$$\delta\tilde{\Psi} \;=\; \sum_{m=-2}^{\infty}\delta\psi_m Z_m - Z_{m_*}\sum_{m=-2}^{\infty}\delta\psi_m \;=\; \delta\Psi - Z_{m_*}\big[\,\delta\Psi\,\big]_{z=\eta},$$

and $[\![\delta\Psi]\!]_{z=\eta} = 0$ by construction, we conclude that $\delta\tilde{\Psi} = \delta\Psi$. Consequently, we also have

$$\sum_{m=-2}^{\infty}\delta\psi_m\Big[\,Z_m - Z_{m_*}\,\Big]_{z=-h} = \left[\sum_{m=-2}^{\infty}\delta\psi_m (Z_m - Z_{m_*})\right]_{z=-h} = \big[\,\delta\tilde{\Psi}\,\big]_{z=-h} = \big[\,\delta\Psi\,\big]_{z=-h}$$

Thus, identity (1.53) takes the form

$$\int_X\int_{-h}^{\eta}\Delta\Phi\,\delta\Psi\,dz\,d\boldsymbol{x} - \int_X \big(\partial_t h - \boldsymbol{N}_h\cdot\nabla\Phi\big)\big[\delta\Psi\big]_{z=-h}\,d\boldsymbol{x} = 0 \tag{1.54}$$

Since $\delta\Psi$ is arbitrary in the open domain $D_h^\eta(X,t)$ and on the seabed boundary Γ_h, we conclude that the function $\Phi = \boldsymbol{\varphi}^{\mathrm{T}}\boldsymbol{Z}$ satisfies the Laplace equation and the bottom impermeability condition, by using the standard arguments of the calculus of variations. □

Lemma 2 allows us to simplify our formulation of the system by rewriting Eqs (1.49) as two couple problems. In more detail, the equations $\Delta(\boldsymbol{\varphi}^{\mathrm{T}}\boldsymbol{Z})=0$ in $D_h^{\eta}(X,t)$ and $\boldsymbol{N}_h\cdot\nabla(\boldsymbol{\varphi}^{\mathrm{T}}\boldsymbol{Z})=\partial_t h$ on Γ_h, established by Lemma 2, in conjunction with the identities (1.42) and (1.47), lead to the much more numerically efficient new identities:

$$\sum_{n=-2}^{\infty}\mathrm{L}_{mn}[\eta,h]\varphi_n = -\partial_t h\left[Z_m\right]_{z=-h},, \qquad \sum_{n=-2}^{\infty}\ell_{mn}[\eta,h]\varphi_n = 0,\ldots m\geq -2, \tag{1.55a,b}$$

joined with the new evolutionary equations of the free-surface

$$\partial_t\eta - \boldsymbol{N}_{\eta}\cdot\left[\nabla(\boldsymbol{\varphi}^{\mathrm{T}}\boldsymbol{Z})\right]_{z=\eta}=0 \tag{1.56a}$$

$$\left[\partial_t(\boldsymbol{\varphi}^{\mathrm{T}}\boldsymbol{Z})\right]_{z=\eta}+g\eta+\frac{1}{2}\left[\nabla(\boldsymbol{\varphi}^{\mathrm{T}}\boldsymbol{Z})\right]^2_{z=\eta}=-\frac{p_{\mathrm{surf}}}{\rho} \tag{1.56b}$$

In this way. the infinite system of Eqs (1.49a) is split into one scalar evolution equation (1.56a) which corresponds to the kinematic free-surface condition and an infinite system of time-independent equations, given by (1.55a). Furthermore, Eq (1.49) is drastically simplified (dynamic free-surface condition). This reformulation is very practical for the numerical implementation of the problem since the nonlinearity of the problem is only located on the free-surface equations, while the infinite system of boundary conditions of (1.55a) is linear (of course in any numerical implementation of the problem the system should be truncated, yet the above statement will still stand).

The physical interpretation of the aforementioned infinite system of Eq (1.55a) is not clear at this point, but it will be presented in the following Lemma. For reasons of notation we first introduce the trace of the wave potential:

$$\psi(\boldsymbol{x},t)=\Phi\left(\boldsymbol{x},z=\eta(\boldsymbol{x},t),t\right)=\left[\Phi\right]_{z=\eta}=\boldsymbol{\varphi}^{\mathrm{T}}\left[\boldsymbol{Z}\right]_{z=\eta}=\sum_{n=-2}^{\infty}\varphi_n \tag{1.57}$$

Lemma 3 (Athanassoulis et al. 2015): *For each* $t\in[t_0,t_1]$ *the infinite system of PDEs*

$$\sum_{n=-2}^{\infty}\mathrm{L}_{mn}[\eta,h]\varphi_n = -\partial_t h\left[Z_m\right]_{z=-h},, \qquad m\geq -2, \quad \boldsymbol{x}\in X \tag{1.58}$$

supplemented with the boundary condition (1.49c) *or* (1.49d) *on the excitation boundary, the vanishing at-infinity conditions* $\eta,\varphi_n\to 0$ *for* $\boldsymbol{x}\in S^{\infty}$, *and the algebraic constraint* (1.57), *is equivalent to the boundary value problem*

$$\Delta\Phi=0, \qquad (\boldsymbol{x},z)\in D_h^{\eta}(X,t) \tag{1.59a}$$

$$\boldsymbol{N}_h \cdot \left[\nabla \Phi \right]_{z=-h} = 0, \qquad \boldsymbol{x} \in X \tag{1.59b}$$

$$\left[\Phi \right]_{z=\eta} = \psi, \qquad \boldsymbol{x} \in X \tag{1.59c}$$

$$\left[\partial_{x_1} \Phi \right]_{x_1=a} = V_a \quad \text{or} \quad \left[\Phi \right]_{x_1=a} = \Phi_a, \qquad (x_2, z) \in S_h^{\eta}(a) \tag{1.59d}$$

$$\Phi \to 0, \qquad \boldsymbol{x} \in S^{\infty} \tag{1.59e}$$

Proof: Let Φ be the unique classical solution of problem (1.58), with $\boldsymbol{\varphi}^{\mathrm{T}} \boldsymbol{Z}$ being its modal expansion, in accordance to Theorem 1 of Section 1.3. Then, we readily see that Eqs. (1.59c) and (1.59e) yield directly Eq. (1.57) and the radiation conditions $\varphi_n \to 0$ for $\boldsymbol{x} \in S^{\infty}$. Furthermore, in view of identity (1.47), $\boldsymbol{\varphi} = \{\varphi_n\}_{n=-2}^{\infty}$ satisfies Eq. (1.58). In order to obtain the conditions (1.49c) on the excitation boundary, we multiply the first of Eqs. (1.59d) by Z_m, integrating over $[-h_a, \eta_a]$ and expand $\Phi = \boldsymbol{\varphi}^{\mathrm{T}} \boldsymbol{Z}$.

Now suppose that the admissible sequence $\boldsymbol{\varphi} = \{\varphi_n\}_{n=-2}^{\infty}$ satisfies Eqs (1.58) and consider the field $\Phi = \boldsymbol{\varphi}^{\mathrm{T}} \boldsymbol{Z}$. Then, using Eqs. (1.57) and (1.59d), we see at once that Φ satisfies Eqs. (1.58c) and (1.58e). In order to prove (1.58a,b) take an arbitrary admissible function $\delta\Psi$, defined on the closed domain $\overline{D_h^{\eta}}(X,t)$. Applying Theorem 1 of Section 1.3, we conclude that there exists an admissible sequence $\delta\boldsymbol{\psi} = \{\delta\psi_m(\boldsymbol{x};t)\}_{m=-2}^{\infty}$ such that $\delta\Psi = \sum_{m=-2}^{\infty} \delta\psi_m Z_m$. Multiplying the m^{th} Eq. (1.58) by $\delta\psi_m$ integrating over X, and summing over m, we obtain an equation like Eq. (1.54). Then, we continue by using variational arguments, as in Lemma 1. The lateral excitation condition (1.58d) [either the Neumann or the Dirichlet one] is also easily obtained by using (1.49c) or (1.49d), and the series expansion. Thus the theorem is proved □

Anyone of the two equivalent problems (1.59) or [(1.58), (1.57) & (1.49c) or (1.49d)] will be called the *substrate problem*. The former will be referred to as the *classical* and the later as the *modal* form of the substrate problem. The solution of this problem determines the DtN operator, which permits us to close the two evolution equations (1.56a) & (1.56b). In many works dealing with the study of the NLIWW problem, the DtN operator is defined by means of a problem like (1.59) (usually under the assumptions of a flat horizontal seabed and spatial periodicity instead of the lateral conditions (1.59d,e)) and treated by operator expansion techniques (see e.g.). Our next step is the explicit introduction of the DtN operator in the free-surface equations as well as their restatement in a form that contains only the free-surface fields (η, ψ). The following Lemma helps us towards this transformation.

Lemma 4 (Athanassoulis et al., 2015): *Assuming that* $\varphi_n = \varphi_n(\boldsymbol{x},t)$ *and* $Z_n = Z_n(z;\eta(\boldsymbol{x},t),h(\boldsymbol{x},t))$, *and that the series* $\boldsymbol{\varphi}^{\mathrm{T}}\boldsymbol{Z}$ *is appropriately convergent (or finite), the following equations hold true:*

$$\left[\partial_t(\boldsymbol{\varphi}^{\mathrm{T}}\boldsymbol{Z})\right]_{z=\eta} = \partial_t\left[\boldsymbol{\varphi}^{\mathrm{T}}\boldsymbol{Z}\right]_{z=\eta} - \boldsymbol{\varphi}^{\mathrm{T}}\left[\partial_z\boldsymbol{Z}\right]_{z=\eta}\partial_t\eta \tag{1.60a}$$

$$\left[\nabla_{\boldsymbol{x}}(\boldsymbol{\varphi}^{\mathrm{T}}\boldsymbol{Z})\right]_{z=\eta} = \nabla_{\boldsymbol{x}}\left[\boldsymbol{\varphi}^{\mathrm{T}}\boldsymbol{Z}\right]_{z=\eta} - \boldsymbol{\varphi}^{\mathrm{T}}\left[\partial_z\boldsymbol{Z}\right]_{z=\eta}\nabla_{\boldsymbol{x}}\eta \tag{1.60b}$$

$$\left[\partial_z(\boldsymbol{\varphi}^{\mathrm{T}}\boldsymbol{Z})\right]_{z=\eta} = \boldsymbol{\varphi}^{\mathrm{T}}\left[\partial_z\boldsymbol{Z}\right]_{z=\eta} \tag{1.60c}$$

In the case where $Z_n = Z_n(z;\eta(\boldsymbol{x},t),h(\boldsymbol{x},t))$, $n \geq -2$, *are given by* Eqs (1.13), (1.17), *the last equation can be also written by the simpler form:*

$$\left[\partial_z(\boldsymbol{\varphi}^{\mathrm{T}}\boldsymbol{Z})\right]_{z=\eta} = h_0^{-1}\varphi_{-2} + \mu_0\psi \tag{1.60d}$$

Proof: To prove Eq. (1.60a) calculate first $\partial_t(\boldsymbol{\varphi}^{\mathrm{T}}\boldsymbol{Z})$ at an interior $-h < z < \eta$, $\partial_t(\boldsymbol{\varphi}^{\mathrm{T}}\boldsymbol{Z}) = \partial_t\boldsymbol{\varphi}^{\mathrm{T}}\boldsymbol{Z} + \boldsymbol{\varphi}^{\mathrm{T}}\partial_\eta\boldsymbol{Z}\left(\partial_t\eta + \partial_t h\right)$, and, then, take the limit as $z \to \eta$, obtaining

$$\left[\partial_t(\boldsymbol{\varphi}^{\mathrm{T}}\boldsymbol{Z})\right]_{z=\eta} = \partial_t\boldsymbol{\varphi}^{\mathrm{T}}\left[\boldsymbol{Z}\right]_{z=\eta} + \boldsymbol{\varphi}^{\mathrm{T}}\left[\partial_\eta\boldsymbol{Z}\right]_{z=\eta}\partial_t H$$

On the other hand, since $\left[\boldsymbol{Z}\right]_{z=\eta} = \boldsymbol{Z}(z=\eta(\boldsymbol{x},t);\eta(\boldsymbol{x},t),h(\boldsymbol{x},t))$, we have

$$\partial_t\left[\boldsymbol{\varphi}^{\mathrm{T}}\boldsymbol{Z}\right]_{z=\eta} = \partial_t\boldsymbol{\varphi}^{\mathrm{T}}\left[\boldsymbol{Z}\right]_{z=\eta} + \boldsymbol{\varphi}^{\mathrm{T}}\left(\left[\partial_z\boldsymbol{Z}\right]_{z=\eta}\partial_t\eta + \left[\partial_\eta\boldsymbol{Z}\right]_{z=\eta}\partial_t H\right)$$

Subtracting the latter equation from the former, we obtain Eq. (1.60a). Eq. (1.60b) is proved similarly, while Eq. (1.60c) is obvious since $\boldsymbol{\varphi}$ is z independent. To prove Eq. (1.60d), use is made of the equations $\left[Z_n\right]_{z=\eta} = 1$, $\left[\partial_z Z_{-2}\right]_{z=\eta} = \mu_0 + h_0^{-1}$ and $\left[\partial_z Z_n\right]_{z=\eta} = \mu_0$, $n \geq -1$, which hold for the specific choice of vertical functions . □

Assuming that the surface fields (η,ψ) are known, at any specific time t, the sequence of modal amplitudes $\boldsymbol{\varphi} = \{\varphi_n\}_{n=-2}^{\infty}$ can be determined by solving the modal substrate problem. What is most important, for the specific choice of vertical functions $\{Z_n\}_{n\geq -2}$, is that the substrate problem communicates with the dynamic evolution Eqs. (1.56) only by means of the free surface mode φ_{-2} (as seen by combining Eqs. (1.56) and (1.60)), which becomes the modal alternative of the usual DtN operator. Clearly φ_{-2} as all modes $\{\varphi_n\}_{n=-2}^{\infty}$, depends on

η, h, ψ and the lateral excitation V_a or Φ_a applied on $S_h^\eta(a)$. To emphasize this fact we introduce the notation

$$\varphi_{-2} = \begin{cases} \mathcal{F}[\eta, h, V_a]\psi \\ \mathcal{F}[\eta, h, \Phi_a]\psi \end{cases} = \mathcal{F}_a[\eta, h]\psi \tag{1.61}$$

Now substituting (1.60) in Eqs (1.56), and taking into account Eq. (4.24) we arrive at the following:

Lemma 5 (Athanassoulis et al. 2015): *The NLIWW problem is equivalent with the following system of two nonlinear evolution equations*

$$\partial_t \eta = -(\nabla_{\boldsymbol{x}} \eta)\cdot(\nabla_{\boldsymbol{x}} \psi) + (|\nabla_{\boldsymbol{x}} \eta|^2 + 1)\left(h_0^{-1}\mathcal{F}_a[\eta, h]\psi + \mu_0 \psi\right) \tag{1.62a}$$

$$\partial_t \psi = -g\eta - \frac{1}{2}(\nabla_{\boldsymbol{x}} \psi)^2 + \frac{1}{2}(|\nabla_{\boldsymbol{x}} \eta|^2 + 1)\left(h_0^{-1}\mathcal{F}_a[\eta, h]\psi + \mu_0 \psi\right)^2 - \frac{p_{\text{surf}}}{\rho} \tag{1.62b}$$

where $\mathcal{F}_\alpha[\eta, h]\psi = \varphi_{-2}(\boldsymbol{x}, t)$ *is the first element of the modal sequence* $\{\varphi_n(\boldsymbol{x}; t)\}_{n=-2}^{\infty}$ *obtained by solving the modal substrate problem* {(1.57), (1.58), (1.49c) or (1.49d).

Proof: For Eq. (1.62a) we invoke Eq. (1.56a) together with Lemma 4 while taking into account that the normal outer-vector of the free-surface is written as $\boldsymbol{N}_\eta = (-\nabla_{\boldsymbol{x}} \eta, 1)$:

$$\partial_t \eta - (-\nabla_{\boldsymbol{x}} \eta, 1)\cdot\left(\nabla_{\boldsymbol{x}}\left[\boldsymbol{\varphi}^{\mathrm{T}}\boldsymbol{Z}\right]_{z=\eta} - \boldsymbol{\varphi}^{\mathrm{T}}\left[\partial_z \boldsymbol{Z}\right]_{z=\eta}\nabla_{\boldsymbol{x}} \eta\ ,\ \boldsymbol{\varphi}^{\mathrm{T}}\left[\partial_z \boldsymbol{Z}\right]_{z=\eta}\right) = 0$$

Introducing also the representation of (1.57): $\psi(\boldsymbol{x}, t) = \boldsymbol{\varphi}^{\mathrm{T}}\left[\boldsymbol{Z}\right]_{z=\eta}$, we have:

$$\partial_t \eta - (-\nabla_{\boldsymbol{x}} \eta, 1)\cdot\left(\nabla_{\boldsymbol{x}} \psi - \boldsymbol{\varphi}^{\mathrm{T}}\left[\partial_z \boldsymbol{Z}\right]_{z=\eta}\nabla_{\boldsymbol{x}} \eta\ ,\ \boldsymbol{\varphi}^{\mathrm{T}}\left[\partial_z \boldsymbol{Z}\right]_{z=\eta}\right) = 0$$

Furthermore, calculating the formulas: $\left[\partial_z Z_{-2}\right]_{z=\eta} = \mu_0 + h_0^{-1}\left[\partial_z Z_{-1}\right]_{z=\eta} = \mu_0$

$\left[\partial_z Z_n\right]_{z=\eta} = \mu_0$, $n \geq 0$ we arrive to the following formula:

$$\partial_t \eta + \nabla_{\boldsymbol{x}} \eta\ \nabla_{\boldsymbol{x}} \psi + \left|\nabla_{\boldsymbol{x}} \eta\right|^2\left(h_0^{-1}\varphi_{-2} + \mu_0 \sum_{n=-2}^{\infty}\varphi_n\right) + h_0^{-1}\varphi_{-2} + \mu_0 \sum_{n=-2}^{\infty}\varphi_n = 0 \Rightarrow$$

$$\partial_t \eta = -(\nabla_{\boldsymbol{x}} \eta)\cdot(\nabla_{\boldsymbol{x}} \psi) + (|\nabla_{\boldsymbol{x}} \eta|^2 + 1)\left(h_0^{-1}\mathcal{F}_a[\eta, h]\psi + \mu_0 \psi\right)$$

where $\psi(\boldsymbol{x}, t) = \sum_{n=-2}^{\infty}\varphi_n$ and $\mathcal{F}_a[\eta, h]\psi = \varphi_{-2}$

Now to prove Eq. (1.62b), we invoke Eq. (1.56b) and follow the same process as before, to obtain:

$$\partial_t \left[\boldsymbol{\varphi}^{\mathrm{T}} \boldsymbol{Z} \right]_{z=\eta} - \boldsymbol{\varphi}^{\mathrm{T}} \left[\partial_z \boldsymbol{Z} \right]_{z=\eta} \partial_t H + g\eta + \frac{1}{2} \left[\left[\nabla_{\boldsymbol{x}} (\boldsymbol{\varphi}^{\mathrm{T}} \boldsymbol{Z}) \right]_{z=\eta}^2 + \left[\partial_z (\boldsymbol{\varphi}^{\mathrm{T}} \boldsymbol{Z}) \right]_{z=\eta}^2 \right] = - \frac{p_{\mathrm{surf}}}{\rho}$$

and using Lemma 4, together with Eq. (1.57) we get:

$$\partial_t \psi - \left(h_0^{-1} \varphi_{-2} + \mu_0 \psi \right) \partial_t \eta + g\eta + \\ + \frac{1}{2} \left[\left(\nabla_{\boldsymbol{x}} \psi - \left(h_0^{-1} \varphi_{-2} + \mu_0 \psi \right) \nabla_{\boldsymbol{x}} \eta \right)^2 + \left(h_0^{-1} \varphi_{-2} + \mu_0 \psi \right)^2 \right] = - \frac{p_{\mathrm{surf}}}{\rho} \Rightarrow$$

$$\partial_t \psi - \left(\partial_t \eta + \nabla_{\boldsymbol{x}} \psi \nabla_{\boldsymbol{x}} \eta \right) \left(h_0^{-1} \varphi_{-2} + \mu_0 \psi \right) + g\eta + \\ + \frac{1}{2} \left[\left| \nabla_{\boldsymbol{x}} \psi \right|^2 + \left(h_0^{-1} \varphi_{-2} + \mu_0 \psi \right)^2 \left(\left| \nabla_{\boldsymbol{x}} \eta \right|^2 + 1 \right) \right] = - \frac{p_{\mathrm{surf}}}{\rho}$$

Invoking the already proved Eq (1.62a) and $\mathcal{F}_a [\eta, h] \psi = \varphi_{-2}$ we have:

$$\partial_t \psi - (|\nabla_{\boldsymbol{x}} \eta|^2 + 1) \left(h_0^{-1} \mathcal{F}_a [\eta, h] \psi + \mu_0 \psi \right)^2 + g\eta + \\ + \frac{1}{2} \left[\left| \nabla_{\boldsymbol{x}} \psi \right|^2 + \left(h_0^{-1} \mathcal{F}_a [\eta, h] \psi + \mu_0 \psi \right)^2 \left(\left| \nabla_{\boldsymbol{x}} \eta \right|^2 + 1 \right) \right] = - \frac{p_{\mathrm{surf}}}{\rho}$$

or better written as:

$$\partial_t \psi = - g\eta - \frac{1}{2} (\nabla_{\boldsymbol{x}} \psi)^2 + \frac{1}{2} (|\nabla_{\boldsymbol{x}} \eta|^2 + 1) \left(h_0^{-1} \mathcal{F}_a [\eta, h] \psi + \mu_0 \psi \right)^2 - \frac{p_{\mathrm{surf}}}{\rho}$$

Thus, the proof is complete. □

Lemma 5, allows us to write our exact reformulation of the NLIWW problem, collectively, in the following form:

The free-surface evolution equations:

$$\partial_t \eta = - (\nabla_{\boldsymbol{x}} \eta) \cdot (\nabla_{\boldsymbol{x}} \psi) + (|\nabla_{\boldsymbol{x}} \eta|^2 + 1) \left(h_0^{-1} \mathcal{F}_a [\eta, h] \psi + \mu_0 \psi \right) \tag{1.63a}$$

$$\partial_t \psi = - g\eta - \frac{1}{2} (\nabla_{\boldsymbol{x}} \psi)^2 + \frac{1}{2} (|\nabla_{\boldsymbol{x}} \eta|^2 + 1) \left(h_0^{-1} \mathcal{F}_a [\eta, h] \psi + \mu_0 \psi \right)^2 - \frac{p_{\mathrm{surf}}}{\rho} \tag{1.63b}$$

complemented with the infinite-dimensional substrate problem:

$$\sum_{n=-2}^{\infty} \mathrm{L}_{mn} [\eta, h] \varphi_n = - \partial_t h \left[Z_m \right]_{z=-h}, \qquad m \geq -2 \qquad \boldsymbol{x} \in X \tag{1.63c}$$

and the algebraic constraint:

$$\sum_{n=-2}^{\infty} \varphi_n = \left[\Phi\right]_{z=\eta} = \psi(\boldsymbol{x},t) \tag{1.63d}$$

supplemented with the Neumann boundary conditions on the excitation boundary

$$\sum_{n=-2}^{\infty} \left(\left[\partial_{x_1} \varphi_n\right]_{x_1=a} \mathrm{A}_{mn}^{(a)} + \left[\varphi_n\right]_{x_1=a} \mathrm{B}_{mn}^{(a)} \right) = g_m \ , \ n \geq -2 \tag{1.63e1}$$

or the Dirichlet boundary conditions on the excitation boundary

$$\left[\varphi_n\right]_{x_1=a} = \varphi_n^a \ , \ n \geq -2 \tag{1.63e2}$$

and the vanishing at-infinity condition:

$$\eta(\boldsymbol{x},t) \ , \ \nabla\varphi_m(\boldsymbol{x},z;t) \rightarrow 0 \ , \ m \geq -2 \qquad \text{on} \qquad x \in S_\infty \tag{1.63f}$$

The numerical implementation of the system, of Eqs. (1.63), will be analyzed in Chapters 2 and 3 together will results for various highly nonlinear and computationally demanding test cases. Also comparison with accuracy of other methods implemented for the NLIWW problem will be done in Chapter 3.

Remark: Having formed the HCM system of Eqs. (1.63) a logical question that arises is how this system is compared in terms of numerical efficiency with regard to approximate models that were derived through some variational principle. A lot of these models, due to their approximate nature devise the vertical expansion in a way that significantly reduces the numerical cost of the resulting model while also trying to limit the physical simplifications (see for example (Klopman et al., 2010)). Hence, such models are expected a priori to be much faster than the current model, yet they should not be able to simulate cases with high nonlinearity due to their physical reductions. However, simplified approximate models exist whose system assumes schematically the same form as ours (two free-surface evolution equations coupled with a substrate problem) and thus cannot be a priori assumed more efficient (numerically) than the model presented here (see for example (Isobe & Abohadima, 1998)). The same can also be seen for models without explicit physical reductions that however utilized an approximate representation of the velocity potential (Yates & Benoit, 2015).

Chapter 2: Analytic Treatment of the HCM System

In the end of the previous Chapter, we derived a reformulation of the classical NLIWW problem in the form of Eqs. (1.63). Having done so, we now turn our attention towards the numerical implementation of the aforementioned system. The first part of any numerical implementation for such a system is its analytic treatment. In more detail, we need to derive explicit formulae for the coefficients of the equations of the problem, derive a finite and efficient truncation of the infinite system and study the asymptotic behavior of the truncated system as well as the behavior of the infinite system. These aspects of the system will be analyzed in the current Chapter.

2.1 . Analytic calculation of the spatial derivatives of the vertical basis $Z_n, n \geq -2$

Before we can formulate a numerical implementation of the HCM system, we need to explicitly calculate the matrix coefficients $A_{m,n}, B_{m,n}, C_{m,n}$ of the substrate problem of Eq. (1.63c). Yet, the calculation of the matrix coefficients $A_{m,n}, B_{m,n}, C_{m,n}$, given by Eqs. (1.46b)-(1.46d), requires the derivation of analytic expressions of the spatial derivatives of $Z_n, n \geq -2$. More specifically, the calculation of the vertical integrals appearing in B_{mn} and C_{mn} can be executed only when explicit expression for the gradient $\nabla_{\boldsymbol{x}} Z_n$ and the horizontal Laplacian $\Delta_{\boldsymbol{x}} Z_n$ are available. The purpose of this section is to derive in a systematic way such expressions. A part of these calculations ($n \geq 1$) have been derived in (Athanassoulis & Papoutsellis, 2016). For a detailed derivation of these results see Appendices A & B.

Spatial Derivatives for $n = -2, -1$

The horizontal gradients of the *free-surface mode* Z_{-2}, Eq. (1.17a), and the *sloping-bottom mode* Z_{-1}, Eq. (1.17b), are easily found by straightforward differentiation. The results can be conveniently expressed as follows

$$\nabla_{\boldsymbol{x}} Z_n = \boldsymbol{F}_n^{(0)}(\boldsymbol{x},t) + \boldsymbol{F}_n^{(1)}(\boldsymbol{x},t)\,(z+h) + \boldsymbol{F}_n^{(2)}(\boldsymbol{x},t)\,(z+h)^2, n = -2,-1, \quad (2.1a)$$

where the $\boldsymbol{F}_n^{(k)}-$coefficients are $(\boldsymbol{x},t)-$dependent (vector) fields, given by

$$\boldsymbol{F}_{-2}^{(0)} = -a_2 \nabla_{\boldsymbol{x}} H, \qquad \boldsymbol{F}_{-2}^{(1)} = \frac{2a_2}{H}\nabla_{\boldsymbol{x}} h, \qquad \boldsymbol{F}_{-2}^{(2)} = -\frac{a_2}{H^2}\nabla_{\boldsymbol{x}} H, \quad (2.1b)$$

$$\boldsymbol{F}_{-1}^{(0)} = \frac{1}{h_0}\nabla_{\boldsymbol{x}} h - a_2 \nabla_{\boldsymbol{x}} H, \; \boldsymbol{F}_{-1}^{(1)} = \frac{2a_1}{H}\nabla_{\boldsymbol{x}} h, \qquad \boldsymbol{F}_{-1}^{(2)} = -\frac{a_1}{H^2}\nabla_{\boldsymbol{x}} H, \quad (2.1c)$$

The horizontal Laplacians of Z_{-2} and Z_{-1} are similarly derived, and they can be expressed in the form:

$$\Delta_{\boldsymbol{x}} Z_n = G_n^{(0)}(\boldsymbol{x},t) + G_n^{(1)}(\boldsymbol{x},t)\big(z+h\big) + G_n^{(2)}(\boldsymbol{x},t)\big(z+h\big)^2, \qquad n = -2,-1, \quad (2.2a)$$

where the $G_n^{(k)}-$coefficients are $(\boldsymbol{x},t)-$dependent (scalar) fields, given by

$$G_n^{(0)} = \nabla_{\boldsymbol{x}} \cdot \boldsymbol{F}_n^{(0)} + \boldsymbol{F}_n^{(1)} \cdot \nabla_{\boldsymbol{x}} h, \qquad G_n^{(1)} = \nabla_{\boldsymbol{x}} \cdot \boldsymbol{F}_n^{(1)} + 2\,\boldsymbol{F}_n^{(2)} \cdot \nabla_{\boldsymbol{x}} h, \quad (2.2b)$$

$$G_n^{(2)} = \nabla_{\boldsymbol{x}} \cdot \boldsymbol{F}_n^{(2)}, \qquad n = -2,-1. \quad (2.2c)$$

Finally, the first and second vertical derivatives of Z_{-2} and Z_{-1} are given below:

$$\partial_z Z_{-1} = \frac{2a_1}{H}(z+h) + \frac{1}{h_0}, \qquad \partial_z Z_{-2} = \frac{2a_2}{H}(z+h), \tag{2.3a}$$

$$\partial_z^2 Z_{-1} = \frac{2a_1}{H}, \qquad \partial_z^2 Z_{-2} = \frac{2a_2}{H}. \tag{2.3b}$$

Spatial Derivatives for $n = 0$

The calculation of the gradient of the *propagating mode* Z_0, Eq. (1.13a), is more involved. The $\boldsymbol{x}-$dependence of Z_0 comes through its dependence on the free-surface elevation $\eta(\boldsymbol{x};t)$, the bottom bathymetry $h(\boldsymbol{x},t)$, and the parameter $k_0 = k_0(\boldsymbol{x},t) = k_0\big(H(\boldsymbol{x},t)\big)$, which is implicitly defined by means of Eq. (1.12a). Therefore, such a calculation requires the use of the implicit function theorem (to calculate the derivative of $k_0\big(H(\boldsymbol{x},t)\big)$), and the chain rule (to pass from the derivatives with respect to η, h and k_0 to the $\boldsymbol{x}-$gradient). Since $H(\boldsymbol{x},t) = \eta(\boldsymbol{x},t) + h(\boldsymbol{x},t)$, it follows that $\partial_\eta k_0 = \partial_h k_0 = \partial_H k_0$. Using the implicit function theorem we can easily prove the following Proposition that first appeared in (Athanassoulis & Papoutsellis, 2016).

Proposition 1: *For* $n \geq 0$*, the first and second derivatives of* $k_n(H)$ *are given by the following equations:*

$$\partial_\eta k_n = \partial_h k_n = \partial_H k_n = \begin{cases} -\dfrac{k_0(k_0^2 - \mu_0^2)}{\mu_0 + H(k_0^2 - \mu_0^2)}, & n = 0 \\ \dfrac{k_n(k_n^2 + \mu_0^2)}{\mu_0 - H(k_n^2 + \mu_0^2)}, & n \geq 1 \end{cases} \tag{2.4a}$$

$$\partial_H^2 k_n = -2\,\partial_H k_n \left\{ \mu_0 + \frac{\partial_H k_n}{k_n}\big(H\mu_0 - 1\big)\left(2 + H\,\frac{\partial_H k_n}{k_n}\right)\right\}, \quad n \geq 0 \tag{2.4b}$$

$$\nabla_{\boldsymbol{x}} k_n = \partial_H k_n \cdot \nabla_{\boldsymbol{x}} H, \qquad \Delta_{\boldsymbol{x}} k_n = \partial_H^2 k_n \Delta_{\boldsymbol{x}} H + \partial_H k_n \big(\nabla_{\boldsymbol{x}} H\big)^2, \tag{2.4c,d}$$

A detailed proof of Proposition 1 can be found in Appendix A and as a result will not be presented here.

Furthermore, in order to write the space derivatives of the $Z_n, n \geq 0$ functions in a simpler manner, we introduce the functions

$$W_0 = \frac{\sinh[k_0(z+h)]}{\cosh(k_0 H)}, \qquad W_n = -\frac{\sin[k_n(z+h)]}{\cos(k_n H)}, \quad n \geq 1. \tag{2.5a,b}$$

Having these comments in mind, we proceed in the calculation of $\nabla_{\boldsymbol{x}} Z_0$ as follows:

$$\nabla_{\boldsymbol{x}} Z_0 = \left(\partial_\eta Z_0 + \partial_{k_0} Z_0 \, \partial_H k_0\right)(\nabla_{\boldsymbol{x}} \eta) + \left(\partial_h Z_0 + \partial_{k_0} Z_0 \, \partial_H k_0\right)(\nabla_{\boldsymbol{x}} h). \quad (2.6)$$

The partial derivative $\partial_\eta Z_0$ is easily calculated by direct differentiation of Eq. (1.13a), and use of the local dispersion relation, Eq. (1.12a), leading to

$$\partial_\eta Z_0 = -\frac{k_0 \cosh[k_0(z+h)] \sinh(k_0 H)}{\cosh^2(k_0 H)} = -\mu_0 Z_0. \quad (2.7a)$$

Working similarly, we find

$$\partial_h Z_0 = k_0 W_0 - \mu_0 Z_0, \quad (2.7b)$$

$$\partial_{k_0} Z_0 = (z+h) W_0 - \frac{H \mu_0}{k_0} Z_0, \quad (2.7c)$$

where W_0 is the conjugate of Z_0, as defined in Eq. (2.5a). Substituting the derivatives $\partial_\eta Z_0$, $\partial_h Z_0$, $\partial_{k_0} Z_0$ from Eqs. (2.7a,b,c) into Eq. (2.6), we obtain

$$\nabla_{\boldsymbol{x}} Z_0 = -\mu_0 \left(1 + H \frac{\partial_H k_0}{k_0}\right)(\nabla_{\boldsymbol{x}} H) Z_0 + \partial_H k_0 (\nabla_{\boldsymbol{x}} H)(z+h) W_0 + k_0 (\nabla_{\boldsymbol{x}} h) W_0. \quad (2.8)$$

Finally, we can write the gradient of the *propagating mode* Z_0 in the following form:

$$\nabla_{\boldsymbol{x}} Z_0 = \boldsymbol{F}_0^{(1)}(\boldsymbol{x}, t) Z_0 + \boldsymbol{F}_0^{(2)}(\boldsymbol{x}, t) W_0 + \boldsymbol{F}_0^{(3)}(\boldsymbol{x}, t)(z+h) W_0, \quad (2.9)$$

where the vector fields $\boldsymbol{F}_0^{(1)}$, $\boldsymbol{F}_0^{(2)}$, $\boldsymbol{F}_0^{(3)}$ are given by

$$\boldsymbol{F}_0^{(1)} = -\mu_0 \left(1 + \frac{H \, \partial_H k_0}{k_0}\right) \nabla_{\boldsymbol{x}} H = -\mu_0 \frac{\nabla_{\boldsymbol{x}} (k_0 H)}{k_0}, \quad (2.10a)$$

$$\boldsymbol{F}_0^{(2)} = k_0 \nabla_{\boldsymbol{x}} h, \qquad \boldsymbol{F}_0^{(3)} = \partial_H k_0 \, \nabla_{\boldsymbol{x}} H = \nabla_{\boldsymbol{x}} k_0. \quad (2.10b,c)$$

For the second horizontal derivatives, the gradient of the conjugate function W_0 is required. The $\boldsymbol{x}-$dependence of W_0 is of the same structure as for Z_0. Thus, working similarly as above, one can easily derive the formula:

$$\nabla_{\boldsymbol{x}} W_0 = (\partial_\eta W_0 + \partial_{k_0} W_0 \, \partial_H k_0)(\nabla_{\boldsymbol{x}} \eta) + (\partial_h W_0 + \partial_{k_0} W_0 \, \partial_H k_0)(\nabla_{\boldsymbol{x}} h). \quad (2.11)$$

Further, by direct differentiation of Eq. (2.5a) and use of Eq. (1.12a), we obtain

$$\partial_\eta W_0 = -\mu_0 W_0, \quad (2.12a)$$

$$\partial_h W_0 = k_0 Z_0 - \mu_0 W_0, \quad (2.12b)$$

$$\partial_{k_0} W_0 = (z+h) Z_0 - \frac{H \mu_0}{k_0} W_0, \quad (2.12c)$$

Substituting now the derivatives $\partial_\eta W_0$, $\partial_h W_0$ and $\partial_{k_0} W_0$ from Eqs. (2.12a,b,c) into Eq. (2.11), we find

$$\nabla_{\boldsymbol{x}} W_0 \;=\; -\mu_0 \left(1 + H \frac{\partial_H k_0}{k_0} \right) (\nabla_{\boldsymbol{x}} H) W_0 \;+\; \partial_H k_0 \, (\nabla_{\boldsymbol{x}} H)(z+h) Z_0 + k_0 \, (\nabla_{\boldsymbol{x}} h) Z_0 , \quad (2.13)$$

which can also be written in the form

$$\nabla_{\boldsymbol{x}} W_0 \;=\; \boldsymbol{F}_0^{(1)}(\boldsymbol{x},t)\, W_0 \;+\; \boldsymbol{F}_0^{(2)}(\boldsymbol{x},t)\, Z_0 \;+\; \boldsymbol{F}_0^{(3)}(\boldsymbol{x},t)(z+h)\, Z_0 , \quad (2.14)$$

where the fields $\boldsymbol{F}_0^{(1)}$, $\boldsymbol{F}_0^{(2)}$, $\boldsymbol{F}_0^{(3)}$ are given by Eqs. (2.10a,b,c).

To obtain the Laplacian of the *propagating mode*, we take the gradient of both members of Eq. (2.9)

$$\begin{aligned}
\Delta_{\boldsymbol{x}} Z_0 \;&=\; \nabla_{\boldsymbol{x}} \cdot (\nabla_{\boldsymbol{x}} Z_0) \\
&=\; \nabla_{\boldsymbol{x}} \cdot \left(\boldsymbol{F}_0^{(1)} Z_0 \;+\; \boldsymbol{F}_0^{(2)} W_0 \;+\; \boldsymbol{F}_0^{(3)} (z+h) W_0 \right) = \\
&=\; \left(\nabla_{\boldsymbol{x}} \cdot \boldsymbol{F}_0^{(1)} \right) Z_0 \;+\; \boldsymbol{F}_0^{(1)} \cdot (\nabla_{\boldsymbol{x}} Z_0) \;+\; \left(\nabla_{\boldsymbol{x}} \cdot \boldsymbol{F}_0^{(2)} \right) W_0 \;+\; \boldsymbol{F}_0^{(2)} \cdot (\nabla_{\boldsymbol{x}} W_0) \\
&\qquad +\; \left(\nabla_{\boldsymbol{x}} \cdot \boldsymbol{F}_0^{(3)} \right) (z+h) W_0 \;+\; \boldsymbol{F}_0^{(3)} \cdot (\nabla_{\boldsymbol{x}} h)\, W_0 \;+\; \boldsymbol{F}_0^{(3)} (z+h) (\nabla_{\boldsymbol{x}} W_0)
\end{aligned}$$

Utilizing again Eqs. (2.9), (2.13) for $\nabla_{\boldsymbol{x}} Z_0$ and $\nabla_{\boldsymbol{x}} W_0$ in the above equation and performing a simple rearrangement we get

$$\Delta_{\boldsymbol{x}} Z_0 \;=\; G_0^{(1)} Z_0 + G_0^{(2)} (z+h) Z_0 + G_0^{(3)} (z+h)^2 Z_0 + G_0^{(4)} W_0 + G_0^{(5)} (z+h) W_0 \quad (2.15)$$

with

$$G_0^{(1)} \;=\; \left| \boldsymbol{F}_0^{(1)} \right|^2 \;+\; \left| \boldsymbol{F}_0^{(2)} \right|^2 \;+\; \nabla_{\boldsymbol{x}} \cdot \boldsymbol{F}_0^{(1)} , \quad (2.16a)$$

$$G_0^{(2)} \;=\; 2\, \boldsymbol{F}_0^{(2)} \cdot \boldsymbol{F}_0^{(3)} , \quad (2.16b)$$

$$G_0^{(3)} \;=\; \left| \boldsymbol{F}_0^{(3)} \right|^2 , \quad (2.16c)$$

$$G_0^{(4)} \;=\; 2\, \boldsymbol{F}_0^{(2)} \cdot \boldsymbol{F}_0^{(1)} \;+\; \nabla_{\boldsymbol{x}} \cdot \boldsymbol{F}_0^{(2)} \;+\; \boldsymbol{F}_0^{(3)} \cdot (\nabla_{\boldsymbol{x}} h) , \quad (2.16d)$$

$$G_0^{(5)} \;=\; 2\, \boldsymbol{F}_0^{(3)} \cdot \boldsymbol{F}_0^{(1)} \;+\; \nabla_{\boldsymbol{x}} \cdot \boldsymbol{F}_0^{(3)} , \quad (2.16e)$$

Finally, the first and second vertical space derivatives of the *propagating mode* are easily found to be:

$$\partial_z Z_0 = k_0 W_0 , \quad (2.17a)$$

$$\partial_z^2 Z_0 = k_0^2 Z_0 , \quad (2.17b)$$

Spatial Derivatives for $n \geq 1$

The calculation of the gradient of the *evanescent modes* follows the same process as the one for the *propagating mode*. For this reason, the derivation of the space derivatives for the evanescent modes is omitted here but can be found in Appendix B. Similarly as before we can easily calculate the horizontal gradient of the functions $Z_n, n \geq 1$ as:

$$\nabla_{\boldsymbol{x}} Z_n = \boldsymbol{F}_n^{(1)}(\boldsymbol{x},t) Z_n + \boldsymbol{F}_n^{(2)}(\boldsymbol{x},t) W_n + \boldsymbol{F}_n^{(3)}(\boldsymbol{x},t)(z+h) W_n, \quad n \geq 1, \tag{2.18}$$

where:

$$\boldsymbol{F}_n^{(1)} = -\mu_0 \left(1 + H \frac{\partial_H k_n}{k_n}\right) \nabla_{\boldsymbol{x}} H, \quad \boldsymbol{F}_n^{(2)} = k_n \nabla_{\boldsymbol{x}} h, \quad \boldsymbol{F}_n^{(3)} = \partial_H k_n \nabla_{\boldsymbol{x}} H, n \geq 0 \tag{2.19}$$

Before we calculate the horizontal Laplacian of the functions Z_n, we need the gradient of the functions W_n, $n \geq 0$. In fact, by use of chain rule, while following the same steps of the calculations for W_0 the following Proposition can be proven:

Proposition 2: *The horizontal gradient of the functions* W_n, $n \geq 0$ *is given by the following formula:*

$$\nabla_{\boldsymbol{x}} W_n = \boldsymbol{F}_n^{(1)}(\boldsymbol{x},t)\, W_n + \boldsymbol{F}_n^{(2)}(\boldsymbol{x},t)\, Z_n + \boldsymbol{F}_n^{(3)}(\boldsymbol{x},t)(z+h)\, Z_n \tag{2.20}$$

where the functions $\boldsymbol{F}_n^{(i)}(\boldsymbol{x},t)$, $i = 1,2,3$ *are given by Eqs.* (2.10) *for* $n = 0$ *and by Eqs.* (2.19) *for* $n \geq 1$*, respectively.*

For a proof of this Proposition see Appendix B.
Differentiating one more time, the second horizontal derivatives of Z_n arise in the form

$$\begin{aligned} \Delta_{\boldsymbol{x}} Z_n = {} & G_n^{(1)}(\boldsymbol{x},t) Z_n + G_n^{(2)}(\boldsymbol{x},t)\big(z+h\big) Z_n + G_n^{(3)}(\boldsymbol{x},t)\big(z+h\big)^2 Z_n \\ & + G_n^{(4)}(\boldsymbol{x},t) W_n + G_n^{(5)}(\boldsymbol{x},t)\big(z+h\big) W_n, \quad n \geq 1 \end{aligned} \tag{2.21}$$

where:

$$G_n^{(1)} = \left|\boldsymbol{F}_n^{(1)}\right|^2 - \left|\boldsymbol{F}_n^{(2)}\right|^2 + \nabla_{\boldsymbol{x}} \cdot \boldsymbol{F}_n^{(1)}, \tag{2.22a}$$

$$G_n^{(2)} = -2\, \boldsymbol{F}_n^{(2)} \cdot \boldsymbol{F}_n^{(3)}, \tag{2.22b}$$

$$G_n^{(3)} = -\left|\boldsymbol{F}_n^{(3)}\right|^2, \; n \geq 0 \tag{2.22c}$$

$$G_n^{(4)} = 2\, \boldsymbol{F}_n^{(2)} \cdot \boldsymbol{F}_n^{(1)} + \nabla_{\boldsymbol{x}} \cdot \boldsymbol{F}_n^{(2)} + \nabla_{\boldsymbol{x}} h \cdot \boldsymbol{F}_n^{(3)}, \tag{2.22d}$$

$$G_n^{(5)} = 2\, \boldsymbol{F}_n^{(3)} \cdot \boldsymbol{F}_n^{(1)} + \nabla_{\boldsymbol{x}} \cdot \boldsymbol{F}_n^{(3)}, \quad n \geq 0 \tag{2.22e}$$

Finally, the first and second vertical derivatives of the *evanescent modes* take the form:

$$\partial_z Z_n = k_n W_n \ , n>0 \tag{2.23a}$$

$$\partial_z^2 Z_n = -k_n^2 Z_n \ , n>0 \tag{2.23b}$$

Our persistence in expressing the space derivatives of the $Z_n, n \geq -2$ functions in such a manner has a very specific reason. These formulas visibly separate the $z-$ dependence of the functions $\nabla_{\boldsymbol{x}} Z_n$ and $\Delta_{\boldsymbol{x}} Z_n$. Such a representation will later make the analytic calculation of the matrix coefficients $A_{m,n}, B_{m,n}, C_{m,n}$ a lot easier. Another, desirable trait of this representation is the expression of the $z-$ dependence of the space derivatives of the functions $Z_n, n \geq -2$ as a linear (at every horizontal point) combination of the functions $(z+h)^s$, $(z+h)^s Z_n$ and $(z+h)^s W_n$ with $s = 0,1,2$. As a result the matrix coefficients of the substrate problem can be written as a linear combination of the above functions and products of them. Hence, as will be shown in the next Section, we can significantly decrease the computational time needed for the calculation of the matrix coefficients, by calculating the vertical integrals of the functions given above instead of directly calculating the vertical integrals that appear in the matrix coefficients.

2.2 Analytic calculation of the matrix coefficients for the substrate modal problem.

In this Section, explicit expressions of the matrix coefficients $A_{m,n}$, $B_{m,n}$, $C_{m,n}$ $m, n \geq -2$ are derived.

The choice of the procedure used for the calculation of aforementioned coefficients, although insignificant for the theoretical formulation of the problem, is quite important for the implementation of the HCM method to a program. For the calculation of the matrix coefficients to be computationally efficient it must have little computational cost time-wise as well as regarding its memory needs (total amount of data needed to be stored). A very important quality of the HCM reformulation is that the matrix coefficients at every horizontal point $\boldsymbol{x}_* \in X$, need only information defined on said horizontal point (more specifically $\eta(\boldsymbol{x}_*, t)$, $h(\boldsymbol{x}_*, t)$, k_n and their spatial derivatives). In other words, in an implementation of the problem using the Finite Difference Method, the matrix coefficients of every horizontal point, of the discretized domain, can be calculated locally. This property allows for easy parallelization of the problem (a very important trait for large scale simulations) as well as practically diminishing the memory needs for the calculation of the matrix coefficients. As we will see in Chapter 3, we don't have to first calculate all the matrix coefficients of the discretized system and then create the matrix of the discretized (and truncated) substrate problem. On the contrary, we can built the matrix of the linear system point by point, while storing only the matrix coefficients of the horizontal point we currently do calculations on. Hence our only concern in this Section is the derivation of a way to calculate the matrix coefficients, in the spirit of minimizing the computational cost required for their numerical evaluation.

To do so, we will exploit the representation of the spatial derivatives of the functions $Z_n, n \geq -2$, presented in Section 2.1 to express the matrix coefficients, as a linear combination of a few *basic integrals*. The matrix coefficients are revisited below:

$$A_{m,n} = \int_{-h}^{\eta} Z_n Z_m \, dz \,, \tag{2.24a}$$

$$\boldsymbol{B}_{m,n} = 2\int_{-h}^{\eta} (\nabla_{\boldsymbol{x}} Z_n) Z_m \, dz + (\nabla_{\boldsymbol{x}} h) \left[Z_m Z_n \right]_{z=-h}, \quad i = 1, 2 \,, \tag{2.24b}$$

$$C_{m,n} = \int_{-h}^{\eta} (\nabla_{\boldsymbol{x}}^2 Z_n + \partial_z^2 Z_n) Z_m \, dz - \boldsymbol{N}_h \cdot \left[(\nabla_{\boldsymbol{x}} Z_n, \partial_z Z_n) Z_m \right]_{z=-h}, \tag{2.24c}$$

We can also separate the integral and the boundary terms of the above coefficients writing them as:

$$A_{m,n} = A_{m,n}^{\text{int}} \quad , \qquad \boldsymbol{B}_{m,n} = \boldsymbol{B}_{m,n}^{\text{int}} + \boldsymbol{B}_{m,n}^{\text{b}} \quad , \qquad C_{m,n} = C_{m,n}^{\text{int}} + C_{m,n}^{\text{b}}$$

with

$$A^{\text{int}}_{m,n} = \int_{-h}^{\eta} Z_n Z_m \, dz$$

$$\boldsymbol{B}^{\text{int}}_{m,n} = 2\int_{-h}^{\eta} (\nabla_{\boldsymbol{x}} Z_n) Z_m \, dz \;, \qquad \boldsymbol{B}^{\text{b}}_{m,n} = (\nabla_{\boldsymbol{x}} h)\left[Z_m Z_n \right]_{z=-h}$$

$$C^{\text{int}}_{m,n} = \int_{-h}^{\eta} (\nabla^2_{\boldsymbol{x}} Z_n + \partial^2_z Z_n) Z_m \, dz \;, \qquad C^{\text{b}}_{m,n} = \boldsymbol{N}_h \cdot \left[(\nabla_{\boldsymbol{x}} Z_n, \partial_z Z_n) Z_m \right]_{z=-h}$$

Substitution of the expressions for the first horizontal gradients, Eqs (2.1a), (2.9), (2.18),the expressions for the horizontal Laplacian, Eqs (2.3a), (2.15), (2.21), and vertical derivatives (2.3), (2.17), (2.23), leads to the following formulae:

$$A_{m,n} = J(0; Z_m, Z_n) \;, n, m \geq -2 \,, \tag{2.25}$$

$$\boldsymbol{B}^{\text{int}}_{m,-2} = \boldsymbol{F}^{(0)}_{-2} J(0; Z_m) + \boldsymbol{F}^{(1)}_{-2} J(1; Z_m) + \boldsymbol{F}^{(2)}_{-2} J(2; Z_m) \,, \tag{2.26a}$$

$$\boldsymbol{B}^{\text{int}}_{m,-1} = \boldsymbol{F}^{(0)}_{-1} J(0; Z_m) + \boldsymbol{F}^{(1)}_{-1} J(1; Z_m) + \boldsymbol{F}^{(2)}_{-1} J(2; Z_m) \,, \tag{2.26b}$$

$$\boldsymbol{B}^{\text{int}}_{m,0} = 2\left(\boldsymbol{F}^{(1)}_{0} J(0; Z_0 Z_m) + \boldsymbol{F}^{(2)}_{0} J(0; W_0 Z_m) + \boldsymbol{F}^{(3)}_{0} J(1; W_0 Z_m) \right), \tag{2.26c}$$

$$\boldsymbol{B}^{\text{int}}_{m,n} = 2\left(\boldsymbol{F}^{(1)}_{n} J(0; Z_n Z_m) - \boldsymbol{F}^{(2)}_{n} J(0; W_n Z_m) - \boldsymbol{F}^{(3)}_{n} J(1; W_n Z_m) \right) \;, n \geq 1 \,. \tag{2.26d}$$

$$\boldsymbol{B}^{\text{b}}_{m,n} = \nabla_{\boldsymbol{x}} h \left[Z_m Z_n \right]_{-h} \;, m, n \geq -2 \,, \tag{2.26e}$$

$$C^{\text{int}}_{m,-2} = \left(G^{(0)}_{-2} + \frac{2a_2}{H} \right) J(0; Z_m) + G^{(1)}_{-2} J(1; Z_m) + G^{(2)}_{-2} J(2; Z_m) \;, m \geq -2 \,, \tag{2.27a}$$

$$C^{\text{int}}_{m,-1} = \left(G^{(0)}_{-1} + \frac{2a_1}{H} \right) J(0; Z_m) + G^{(1)}_{-1} J(1; Z_m) + G^{(2)}_{-1} J(2; Z_m) \;\; m \geq -2 \,, \tag{2.27b}$$

$$\begin{aligned} C^{\text{int}}_{m,n} = {} & G^{(1)}_{n} J(0; Z_n Z_m) + G^{(2)}_{n} J(1; Z_n Z_m) + G^{(3)}_{n} J(2; Z_n Z_m) + \\ & + G^{(4)}_{n} J(0; W_n Z_m) + G^{(5)}_{n} J(1; W_n Z_m) \;\; m \geq -2 \text{ and } n \geq 0 \end{aligned} \,, \tag{2.27c}$$

$$C^{\text{b}}_{m,n} = -\nabla_{\boldsymbol{x}} h \cdot \begin{cases} \boldsymbol{F}^{(0)}_{n} \left[Z_m \right]_{-h} \;, & n = -2, -1 \\ \boldsymbol{F}^{(1)}_{n} \left[Z_n Z_m \right]_{-h} \;, & n \geq 0 \end{cases} \tag{2.27d}$$

where the following notation has been used for brevity

$$J\left(s; f(\boldsymbol{x}, z, t)\right) = \int_{-h(\boldsymbol{x},t)}^{\eta(\boldsymbol{x},t)} (z + h(\boldsymbol{x},t))^s f(\boldsymbol{x}, z, t)\, dz \tag{2.28}$$

with

$$J\left(s; f(\boldsymbol{x}, z, t)\right) = \left((z + h)^s, f(\boldsymbol{x}, z, t)\right) = \left(u^s, f\right)$$

Integrals of the form (2.28) that appear in Eqs. (2.25), (2.26), (2.27), will be called *basic integrals* and their systematic calculation is the goal of the next two subsections.

Formulae (2.25-2.27) indicate that the use of direct analytic formulae for the calculation of every matrix coefficient may be computationally inefficient since a lot of them share quantities, like the functions $\boldsymbol{F}_n^{(i)}$ and $G_n^{(i)}$, as well as some basic integrals, with each other. Since the goal of this Section is to present a numerically efficient method for computing the matrix coefficients we will utilize the representation of Eqs. (2.25), (2.26) and (2.27) that allows us to reduce calculations by storing extra quantities (i.e. the basic integrals) that will be used for the computation of many matrix coefficients. In a sense, this new representation trades computational time for additional needed storage of information (the storage of the basic integrals). Yet, this is a trade-off we gladly make due to the fact that (as stated in the beginning of the Section) the memory needs for such calculations are too little (with or without the storage of the basic integrals), and as a result we are interested only in the decrease of the of computational time.

Note: Some reasons for utilizing such a systematic approach, for the matrix coefficients, concern the practicality of the approach. Such a representation can be checked methodically and part-by-part in a program, while long analytic expressions for the matrix coefficients would be much more difficult to do so. Furthermore, this method can lead to a simpler way of calculating the asymptotic behavior of said coefficients. Yet, it should be noted that the reason behind our implementation of the calculation of the matrix coefficients in this way is done only for reasons of computational efficiency and not for the two traits discussed here.

Following this trail of thought, we can further decrease the needed computational time by utilizing recursive relations for the basic integrals with functions $f \in \{Z_n Z_m\}_{m=0,n=-2}^{\infty}$ or $f \in \{Z_n W_m\}_{m=0,n=-2}^{\infty}$, with respect to the polynomial degree s. These relations will result to a reformulation of Eqs. (2.26) & (2.27) that will include such basic integrals only for $s = 0$. This way, we will reduce the number of the basic integrals needed to be calculated. For the computation of the basic integrals, at first we take on the simpler case where $f \in \left\{\{Z_n\}_{n=-2}^{\infty}, \{W_n\}_{n=0}^{\infty}\right\}$. Next we address the more intricate case $f \in \{Z_n Z_m\}_{m,n=-2}^{\infty}$ or $f \in \{Z_n W_m\}_{m=0,n=-2}^{\infty}$ and when it is possible recursive relations are derived, allowing the corresponding integrals to be evaluated in terms of the previously calculated ones.

Calculation of basic integrals $J(s;Z_n)$ and $J(s;W_n)$

The basic integrals where f is one of the vertical polynomial functions $Z_n, n=-2,-1$,are calculated in a straightforward manner even for arbitrary s

$$J(s;Z_{-2}) = \frac{1}{1+s}H^{s+1} - \frac{2a_2}{(3+s)(1+s)}H^{s+2}, \tag{2.29}$$

$$J(s;Z_{-1}) = \frac{1}{1+s}H^{s+1} + \left(\frac{1}{(2+s)h_0} + \frac{a_1}{3+s} - \frac{a_2}{1+s}\right)H^{s+2}. \tag{2.30}$$

On the other hand, integrals involving the implicitly defined functions Z_n, W_n, $n \geq 0$ are less transparent and deserve more attention. Let us start off with the easy case $s=0$. Integrating by parts and taking into account that $Z_0 = (1/k_0)\partial_z W_0$, $Z_n = -(1/k_n)\partial_z W_n$, $n \geq 0$ and that $[W_0]_{z=\eta} = [W_n]_{z=\eta} = 0$ we obtain

$$J(0;Z_0) = \frac{1}{k_0}[W_0]_{z=\eta} = \frac{\tanh(k_0 H)}{k_0} = \frac{\mu_0}{k_0^2} \tag{2.31a}$$

$$J(0;Z_n) = \frac{1}{k_n}[W_n]_{-h}^{\eta} = \frac{\tan(k_n H)}{k_n} = -\frac{\mu_0}{k_n^2}, \; n \geq 1 \tag{2.31b}$$

where the relations (1.12a), (1.12b) have been used in obtaining the last equalities in (2.31a,b). In the same manner the next formulas can be calculated

$$J(0;W_0) = \frac{[Z_0]_{z=-h}^{z=\eta}}{k_0} = \frac{1-\dfrac{1}{\cosh(k_0 H)}}{k_0} \tag{2.32a}$$

$$J(0;W_n) = -\frac{[Z_n]_{z=-h}^{z=\eta}}{k_n} = \frac{\dfrac{1}{\cos(k_n H)}-1}{k_n} \tag{2.32b}$$

For $s \geq 1$ use will be made of the following recursive relations

$$J(s;Z_0) = H^s J(0;Z_0) - \frac{s}{k_0}J(s-1;W_0), \tag{2.33a}$$

$$J(s;Z_n) = -H^s J(0;Z_n) - \frac{s}{k_n}J(s-1;W_n), \tag{2.33b}$$

$$J(s;W_0) = H^s J(0;W_0) - \frac{s}{k_0} J(s-1;Z_0), \tag{2.34a}$$

$$J(s;W_n) = H^s J(0;W_n) + \frac{s}{k_n} J(s-1;Z_n), \tag{2.34b}$$

Eq. (2.33a) is readily verified using integration by parts as in the derivation of (2.31a)($s = 0$). Indeed one easily finds that

$$J(s;Z_0) = \frac{1}{k_0}\left\{ H\left[W_0\right]_{z=\eta} - s\int_{-h}^{\eta} (z+h)^{s-1} Z_0\, dz \right\},$$

which upon using the left equality of (2.31a) and the notation (2.28) yields (2.33a). The derivation of Eqs. (33b) and (34a,b) is similar and is omitted. The usefulness of Eqs. (2.33-2.34) is clear once it is noted that their right hand sides are given as a simple linear combination of the already calculated basic integrals Eqs. (2.31-2.32) and already calculated integrals of (2.33-2.34).

Calculation of the basic integrals $J(s;Z_n Z_m)$ *and* $J(s;Z_n W_m)$

We start with the calculation of integrals involving polynomial functions Z_{-2}, Z_{-1}. Taking into account the definitions (1.17a), (1.17b) of Z_{-2}, Z_{-1} and the notation (2.28) one easily verifies that for $n \geq -2$ the following identities hold

$$J(s;Z_{-2}Z_n) = \frac{a_2}{H} J(s+2;Z_n) + (1 - a_2 H) J(s;Z_n), \ , \tag{2.35a}$$

$$J(s;Z_{-1}Z_n) = \frac{a_1}{H} J(s+2;Z_n) + \frac{1}{h_0} J(s+1;Z_n) + (1 - a_2\ H) J(s;Z_n), \tag{2.35b}$$

$$J(s;W_n Z_{-2}) = \frac{a_2}{H} J(s+2;W_n) + (1 - a_2 H) J(s;W_n), \quad n \geq 0. \tag{2.36a}$$

$$J(s;W_n Z_{-1}) = \frac{a_1}{H} J(s+2;W_n) + \frac{1}{h_0} J(s+1;W_n) + (1 - a_2 H) J(s;W_n), \quad n \geq 0 \tag{2.36b}$$

For the rest of these basic integrals we will derive recursive relations. Before we do this, we must calculate said integrals for $s = 0$.

In the case $m, n \geq 0$ and $s = 0$ we have

$$J(0; Z_0 Z_0) = \frac{\mu_0 + H(k_0^2 - \mu_0^2)}{2k_0^2} \tag{2.37a}$$

$$J(0; Z_m Z_m) = \frac{H}{2} + \frac{-\mu_0 + H\mu_0^2}{2}\frac{1}{k_m^2}, \; m \geq 1 \tag{2.37b}$$

$$J(0; Z_n Z_m) = J(0; Z_m Z_n) = 0, \; n, m \geq 0 \wedge n \neq m \tag{2.37c}$$

for the basic integrals with integral kernel of the form $f \in \left\{\{Z_n Z_m\}_{m,n=0}^{\infty}\right\}$. Eq (2.37b) is readily verified utilizing integration by parts by noting that $Z_n = -(1/k_n)\partial_z W_n$ and furthermore utilizing the fact that $W_m^2 = Z_m^2 - 1$, as well as the dispersion relation of Eq. (1.12b), which result to the formula:

$$J(0; Z_m, Z_m) = \frac{-\mu_0}{k_m^2} + \int_{-h}^{\eta}\left[\frac{1}{\cos^2(k_m H)} - Z_m^2\right]dz$$

and Eq. (2.37b) follows with simple calculus. For a detailed derivation of Eqs. (2.37) see Appendix C.

For the basic integrals with integral kernel of the form $f \in \left\{\{Z_n W_m\}_{m=0,n=0}^{\infty}\right\}$, we have:

$$J(0; W_0 Z_0) = \frac{\mu_0^2}{2k_0^3} \tag{2.38a}$$

$$J(0; W_0 Z_m) = -\frac{\mu_0^2}{(k_0^2 + k_m^2)k_0} + \frac{k_0}{k_0^2 + k_m^2}\left(1 - \frac{1}{\cosh(k_0 H)\cos(k_m H)}\right), \; m \geq 1, \tag{2.38b}$$

$$J(0; W_n Z_0) = -\frac{\mu_0^2}{(k_n^2 + k_0^2)k_n} - \frac{k_n}{k_n^2 + k_0^2}\left(1 - \frac{1}{\cos(k_n H)\cosh(k_0 H)}\right), \; n \geq 1, \tag{2.38c}$$

$$J(0; W_n Z_m) = \frac{\mu_0^2}{(k_n^2 - k_m^2)k_n} - \frac{k_n}{k_n^2 - k_m^2}\left(1 - \frac{1}{\cos(k_n H)\cos(k_m H)}\right), \quad n, m \geq 1, \; n \neq m \tag{2.38d}$$

$$J(0; W_m Z_m) = -\frac{\mu_0^2}{2k_m^3}, \; m \geq 1, \tag{2.38e}$$

The analytic derivation of these integrals can be found in Appendix C. To synoptically present one case of these calculations, i.e Eq. (2.38e), we use integration by parts to derive the formula:

$$J(0;W_m,Z_m) = \frac{\left[W_m W_m\right]_{z=-h}^{z=\eta}}{k_m} - \int_{-h}^{\eta} Z_m W_m \, dz$$

Utilizing the dispersion relation of Eq. (1.12b) we easily get the wanted result.

Lastly, we calculate the following integrals that will be used later for the recursive relations that will be derived for $s \geq 1$.

$$J(0;W_0 W_0) = \frac{\mu_0 - H(k_0^2 - \mu_0^2)}{2k_0^2} \tag{2.39a}$$

$$J(0;W_n W_0) = -\frac{\mu_0}{k_0 k_n} \ , n>0 \tag{2.39b}$$

$$J(0;W_m W_m) = \frac{\mu_0 + H(k_m^2 + \mu_0^2)}{2k_m^2} \ , m>0 \tag{2.39c}$$

$$J(0;W_n W_m) = \frac{\mu_0}{k_m k_n} \ , n,m>0 \ , \ n \neq m \tag{2.39d}$$

In order to derive the recursive relations, integration by parts will be used. Another significant note is that we will replace the boundary terms that arise from the integration by parts with the formulae (2.37), (2.38), (2.39)& (2.31), (2.32). The results are derived in detail in Appendix C.

For $s \geq 1$ integration by parts in conjunction with notation (2.28) yields the following identities:

$$J(s;Z_0 Z_0) = -\frac{s}{2k_0} J(s-1;W_0 Z_0) + \frac{H^s}{s+1} J(0;Z_0 Z_0) + \frac{s H^s}{2(s+1)} J(0;Z_0), \tag{2.40a}$$

$$J(s;Z_m Z_m) = -\frac{s}{2k_m} J(s-1;W_m Z_m) + \frac{H^s}{s+1} J(0;Z_m Z_m) + \frac{s H^s}{2(s+1)} J(0;Z_m) \tag{2.40b}$$

$$J(s;Z_0\,Z_n) \;=\; -s\frac{k_n\,J(s-1;W_n\,Z_0)+k_0\,J(s-1;Z_n\,W_0)}{k_0^2+k_n^2},\;\; n\geq -2\,, \tag{2.40c}$$

$$J(s;Z_m\,Z_n) \;=\; s\frac{k_n\,J(s-1;W_n\,Z_m)-k_m\,J(s-1;Z_n\,W_m)}{k_m^2-k_n^2}\,,\; n,m\geq 1\,,\; n\neq m\,, \tag{2.40d}$$

For basic integrals with $f \in \left\{\{Z_n\,Z_m\}_{m,n=0}^{\infty}\right\}$. And for basic integrals of the form $J(s;W_n\,Z_m)$ we have:

$$J(s;W_0\,Z_0) \;=\; -\frac{s}{2\,k_0}J(s-1;W_0\,W_0)+H^s\,J(0;W_0\,Z_0)\,, \tag{2.41a}$$

$$J(s;W_n\,Z_0) \;=\; \frac{k_0\left(H^{s-1}\,J(0;W_n\,W_0)-s\,J(s-1;W_n\,W_0)\right)}{k_0^2+k_n^2} - \frac{2\,H^{s-1}k_n\,J(s;\,Z_0\,Z_0)}{k_0^2+k_n^2}\,, \tag{2.41b}$$

$$J(s;W_0\,Z_m) \;=\; \frac{2\,H^{s-1}k_0\,J(0;\,Z_0\,Z_0)}{k_m^2+k_0^2} + \frac{k_m\left(H^{s-1}J(0;W_0\,W_m)-s\,J(s-1;W_0\,W_m)\right)}{k_m^2+k_0^2}\,, \tag{2.41c}$$

$$J(s;W_n\,Z_m) \;=\; \frac{k_m\left(J(0;W_n\,W_m)H^{s-1}-s\,J(s-1;W_n\,W_m)\right)-2k_n\,H^{s-1}J(0;\,Z_n\,Z_n)}{k_m^2-k_n^2}\,, \tag{2.41d}$$

$$J(s;W_m\,Z_m) \;=\; -H^s\,J(0;W_m\,Z_m)-\frac{s}{2\,k_m}J(s-1;W_m\,W_m)\,, \tag{2.41e}$$

Eqs.(2.40-2.41) in conjunction with Eqs.(2.37-2.29) permits us to calculate all the remaining integrals required in Eqs.(2.25-2.27). This fact allows us to calculate the matrix coefficients in a manner that requires less calculations and therefore less computational time.

A reformulation of Eqs (26-27)*, for the calculation of the matrix coefficients.*

In this subsection, we will combine Eqs. (2.26-2.27) and the recursive relations of the former subsection to calculate in a more efficient manner the integral part of the coefficients $\boldsymbol{B}_{m,n}$ and $C_{m,n}$ (i.e. $\boldsymbol{B}^{\text{int}}_{m,n}$ and $C^{\text{int}}_{m,n}$). The boundary terms of these coefficients need not to change.

The calculation of the A_{mn} can be readily done by using Eqs. (2.25) and Eqs. (2.31), (2.37) so no further treatment is needed for these coefficients.

Reformulation of coefficients $\boldsymbol{B}_{m,n}$:

We begin by stating that Eqs (2.26a), (2.26b) need not to be changed since they can directly be calculated from Eqs. (2.29), (2.30), (2.31).

Eqs. (2.26c) can be reformulated using Eqs. (2.37a)-(2.38c) (and taking into account Eqs. (2.41e)) to:

$$\boldsymbol{B}^{\text{int}}_{0,0} = 2\left(\boldsymbol{F}_0^{(1)} J(0;Z_0\,Z_0) + \left(\boldsymbol{F}_0^{(2)} + \boldsymbol{F}_0^{(3)} H\right) J(0;W_0\,Z_0) - \frac{1}{2k_0}\,\boldsymbol{F}_0^{(3)} J(0;W_0\,W_0)\right) \tag{2.42a}$$

$$\boldsymbol{B}^{\text{int}}_{m,0} = 2\left(\boldsymbol{F}_0^{(2)} J(0;W_0\,Z_m) + \frac{2k_0}{k_m^2 + k_0^2}\boldsymbol{F}_0^{(3)} J(0;Z_0\,Z_0)\right),\ m \geq -2,\ m \neq 0 \tag{2.42b}$$

Eqs (2d) can be reformulated using Eqs (37b), (38d), (41e):

$$\boldsymbol{B}^{\text{int}}_{m,n} = 2\left(-\boldsymbol{F}_n^{(2)} J(0;W_n\,Z_m) + \frac{2k_n}{k_m^2 - k_n^2}\boldsymbol{F}_n^{(3)} J(0;Z_n\,Z_n)\right),\ m,n \geq 1 \wedge m \neq n, \tag{2.42c}$$

$$\boldsymbol{B}^{\text{int}}_{m,m} = 2\left(\boldsymbol{F}_m^{(1)} J(0;Z_m\,Z_m) + \left(\boldsymbol{F}_m^{(3)} - \boldsymbol{F}_m^{(2)}\right) J(0;W_m\,Z_m) + \frac{1}{2k_m}\boldsymbol{F}_m^{(3)} J(0;W_m\,W_m)\right),\ m \geq 1 \tag{2.42d}$$

$$\boldsymbol{B}^{\text{int}}_{0,n} = 2\left(-\boldsymbol{F}_n^{(2)} J(0;W_n\,Z_0) + \frac{k_n}{k_0^2 + k_n^2}\boldsymbol{F}_n^{(3)} J(0;Z_n\,Z_n)\right),\ n \geq 1 \tag{2.42e}$$

Reformulation of coefficients C_{mn}:

We begin by stating that Eqs (27a), (27b) need not to be changed since they can directly be calculated from Eqs (5a), (5d), (6a) & (6b).

Eqs (3c) can be reformulated using Eqs (8a)-(8e) to:

$$C_{0,0}^{\text{int}} = \left(G_0^{(1)} + G_0^{(2)}\frac{H}{2} + G_0^{(3)}\frac{H^2}{3}\right)J(0;Z_0\,Z_0) + \left(G_0^{(2)}\frac{H}{4} + G_0^{(3)}\frac{H^2}{3}\right)J(0;Z_0)$$
$$+\left(-G_0^{(2)}\frac{1}{2k_0} - G_0^{(3)}\frac{H}{k_0} + G_0^{(4)} + G_0^{(5)}H\right)J(0;W_0\,Z_0) - \quad , \quad (2.43a)$$
$$-\left(G_0^{(5)}\frac{1}{2k_0} - G_0^{(3)}\frac{1}{2k_0^2}\right)J(0;W_0\,W_0)$$

$$C_{0,n}^{\text{int}} = \left(G_n^{(3)}4\frac{k_n^2}{\left(k_0^2+k_n^2\right)^2} - G_n^{(5)}\frac{k_n}{k_0^2+k_n^2}\right)J(0;Z_n\,Z_n)$$
$$-G_n^{(3)}4\frac{k_0^2}{\left(k_0^2+k_n^2\right)^2}J(0;Z_0\,Z_0) - G_n^{(2)}\frac{k_0}{k_0^2+k_n^2}J(0;Z_n\,W_0)\ , \quad (2.43b)$$
$$+\left(-G_n^{(2)}\frac{k_n}{k_0^2+k_n^2} + G_n^{(4)}\right)J(0;W_n\,Z_0)\ ,\ n\geq 1$$

$$C_{m,0}^{\text{int}} = \left(-G_0^{(3)}\frac{4k_0^2}{\left(k_0^2+k_m^2\right)^2} + G_0^{(5)}\frac{2k_0}{k_m^2+k_0^2}\right)J(0;Z_0\,Z_0)$$
$$+G_0^{(3)}\frac{4k_m^2}{\left(k_0^2+k_m^2\right)^2}J(0;Z_m\,Z_m) + \left(-G_0^{(2)}\frac{k_0}{k_0^2+k_m^2} + G_0^{(4)}\right)J(0;W_0\,Z_m), \quad (2.43c)$$
$$-G_0^{(2)}\frac{k_m}{k_0^2+k_m^2}J(0;W_m\,Z_0)\ \ m\geq 0\ m\neq 0$$

$$C_{m,n}^{\text{int}} = -\left(G_n^{(3)}\frac{4k_n^2}{\left(k_m^2-k_n^2\right)^2} + G_n^{(5)}\frac{2k_n}{k_m^2-k_n^2}\right)J(0;Z_n\,Z_n)$$
$$+\left(G_n^{(2)}\frac{k_n}{k_m^2-k_n^2} + G_n^{(4)}\right)J(0;W_n\,Z_m) - G_n^{(2)}\frac{k_m}{k_m^2-k_n^2}J(0;Z_n\,W_m), \quad (2.43d)$$
$$-G_n^{(3)}\frac{4k_m^2}{\left(k_m^2-k_n^2\right)^2}J(0;Z_m\,Z_m)\ \ m,\ n\geq 1\ ,\ m\neq n$$

$$C_{m,m}^{\text{int}} = \left(G_m^{(1)} + G_m^{(2)} \frac{H}{2} + G_m^{(3)} \frac{H^2}{3} \right) J(0; Z_m Z_m) + \left(G_m^{(2)} \frac{H}{4} + G_m^{(3)} \frac{H^2}{3} \right) J(0; Z_m)$$
$$+ \left(-G_m^{(2)} \frac{1}{2k_m} + G_m^{(3)} \frac{H}{k_m} + G_m^{(4)} - G_m^{(5)} H \right) J(0; W_m Z_m) + \tag{2.43e}$$
$$+ \left(G_m^{(3)} \frac{1}{2k_m^2} - G_m^{(5)} \frac{1}{2k_m} \right) J(0; W_m W_m) \quad m \geq 1$$

2.3 Asymptotic behavior of the vertical integral coefficients

The asymptotic behavior of the matrix coefficients $A_{m,n}$, $B_{m,n}$, $C_{m,n}$, $m,n \geq -2$, and the system in general, is insignificant for the procedure of implementing the HCM system into a code. However, the accuracy of such a code, as well as properties like convergence of the code, in a methodical study of any case, are heavily influenced by the asymptotic behavior of the substrate problem, and as a result from the asymptotic behavior of the vertical integral coefficients. Moreover, any study that needs to be done, that concerns the convergence of a truncated model of the infinite-HCM system, or existence of the solution of the full HCM system have such calculations as prerequisites. Hence, we believe that it is of good use, to calculate and present in this Section the asymptotic behavior of the matrix coefficients. In order to derive such calculations easily, we will first present the asymptotic behavior of the basic integrals of Section 2.2. Such calculations in turn require the knowledge of the asymptotic behavior of a few quantities related to the wave numbers k_n, $n \geq 1$. The following Proposition, will give as this needed information concerning this matter.

Proposition 1: *The asymptotic behavior of the wave numbers* k_n, $n \geq 1$ *is given by the relation:*

$$k_n = \frac{n\pi}{H} - \frac{\mu_0}{n\pi} + O\left(n^{-2}\right) \tag{2.44a}$$

Moreover the following limiting formula holds:

$$\frac{1}{\cos(k_n H)} = (-1)^n \left[1 + \frac{\mu_0^2 H^2}{4\pi^2 n^2} + O\left(n^{-4}\right)\right] \tag{2.44b}$$

Proof: To prove the first scale of the proposition, we utilize the dispersion relation of the evanescent modes: $k_n \tan(k_n H) = -\mu_0$, or written in a slightly different way

$$\tan(k_n H) = -\frac{\mu_0 H}{k_n H}$$

Setting $x = k_n H$, and approximating locally, around $n\pi$ the function $\tan(x)$, by the two-term Taylor series expansion: $\tan(x) = (x - n\pi) + \frac{1}{3}(x - n\pi)^3 + \ldots$, we get the algebraic equation:

$$(x - n\pi) + \frac{1}{3}(x - n\pi)^3 = -\frac{\mu_0 H}{x}$$

Finally, solving the above equation by means of the petrubation approach we get the solution:

$$x \simeq n\pi - \frac{\mu_0 H}{n\pi} + O\left(n^{-2}\right) \quad \text{or} \qquad k_n \simeq \frac{n\pi}{H} - \frac{\mu_0}{n\pi} + O\left(n^{-2}\right)$$

and since the Taylor expansion of $\tan(x)$ we used is valid only as $n \to \infty$,we arrive at the desired conclusion.

As for the second part of the Proposition, we use the Taylor series

$$\frac{1}{\cos(x)} = (-1)^n \left[1 + \frac{1}{2}(x - n\pi)^2 + \frac{5}{24}(x - n\pi)^4 \right], \text{ around } n\pi \text{ which results to}$$

$$\frac{1}{\cos(k_n H)} = (-1)^n \left[1 + \frac{1}{2}(k_n H - n\pi)^2 + \frac{5}{24}(k_n H - n\pi)^4 \right] \Rightarrow$$

$$\frac{1}{\cos(k_n H)} = (-1)^n \left[1 + \frac{1}{2}(n\pi - \frac{\mu_0 H}{n\pi} - n\pi)^2 + \frac{5}{24}(n\pi - \frac{\mu_0 H}{n\pi} - n\pi)^4 \right] \Rightarrow$$

$$\frac{1}{\cos(k_n H)} = (-1)^n \left[1 + \frac{\mu_0^2 H^2}{4\pi^2 n^2} + O\left(n^{-4}\right) \right]$$

and thus the proposition is proved. □

Note: At this point, it is highlighted that the goal of this section is a synoptic presentation of the asymptotic behavior of the matrix coefficients of the substrate problem. We desire to sustain the coherence of the Chapter and not confuse the reader with a detailed derivation of the asymptotic formulas to be presented below. As a result, most of the proofs of these formulas have been moved to Appendix D.

Having done so we can easily derive the asymptotic behavior of the vertical functions Z_n, $n \geq 1$ and theirs conjugate functions W_n, $n \geq 1$. For both group of functions we use Eqs. (2.44) to derive the formulae:

$$Z_n = \frac{\cos[k_n(z+h)]}{\cos(k_n H)} = (-1)^n \left[1 + \frac{\mu_0^2 H^2}{4\pi^2 n^2} + O\left(n^{-4}\right) \right] \cos[n\pi \frac{(z+h)}{H}] \tag{2.45a}$$

$$W_n = \frac{\sin[k_n(z+h)]}{\cos(k_n H)} = (-1)^n \left[1 + \frac{\mu_0^2 H^2}{4\pi^2 n^2} + O\left(n^{-4}\right) \right] \sin[n\pi \frac{(z+h)}{H}] \tag{2.45b}$$

We now move forward to the calculation of the asymptotic behavior of the spatial derivatives of the Z_n , $n \geq 1$ functions. For the horizontal gradient and the horizontal Laplacian of said functions, we implore Eqs. (2.18) and (2.21) respectively. As a result we also need the asymptotic behavior of the functions $\boldsymbol{F}_n^{(i)}$, $n \geq 1$, $i = 1, 2, 3$, given by Eqs. (2.19), and of the functions $G_n^{(i)}$, $n \geq 1$, $i = 1, ..., 5$ given by Eqs (2.22). To calculate said asymptotics, we will make use of the following proposition that shows the asymptotic behavior of the first and second partial derivatives of the wave numbers k_n , $n \geq 1$ with respect to the total bathymetry $H(\boldsymbol{x}, t)$.

Proposition 2: *The asymptotic behavior of the partial derivatives* $\partial_H k_n$ *and* $\partial_H^2 k_n$ *are given by the following relations:*

$$\partial_H k_n = -\frac{n\pi}{H^2} - \frac{H\mu_0^2}{n\pi} + O(n^{-2}), \tag{2.46a}$$

$$\partial_H^2 k_n = 2\frac{n\pi}{H^3} + O(1), \tag{2.46b}$$

The following limits are also true:

$$\lim_{n\to\infty} \frac{\partial_H k_n}{k_n} = -\frac{1}{H}, \qquad \lim_{n\to\infty} \frac{\nabla_{\boldsymbol{x}} k_n}{k_n} = -\frac{\nabla_{\boldsymbol{x}} H}{H}, \tag{2.46c}$$

$$\lim_{n\to\infty} \frac{\partial_H^2 k_n}{k_n} = \frac{2}{H^2}, \qquad \lim_{n\to\infty} \frac{\Delta_{\boldsymbol{x}} k_n}{k_n} = \frac{2(\nabla_{\boldsymbol{x}} H)^2}{H^2} - \frac{\Delta_{\boldsymbol{x}} H}{H}, \tag{2.46d}$$

A detailed proof of Proposition 2 is presented in Appendix D.

A detailed derivation of these formulas can also be found in Appendix D: For the $\boldsymbol{F}_n^{(i)}$, $n \geq 1$, $i = 1, 2, 3$, we have:

$$\boldsymbol{F}_n^{(1)} = -\mu_0\left(1 + H\frac{\partial_H k_n}{k_n}\right)\nabla_{\boldsymbol{x}} H = \frac{H^3\mu_0^3}{n^2\pi^2}\nabla_{\boldsymbol{x}} H + O\left(n^{-4}\right), \tag{2.47a}$$

$$\boldsymbol{F}_n^{(2)} = k_n \nabla_{\boldsymbol{x}} h = \frac{n\pi}{H}\nabla_{\boldsymbol{x}} h - \frac{\mu_0 H}{n\pi}\nabla_{\boldsymbol{x}} h + O\left(n^{-2}\right), \tag{2.47b}$$

$$\boldsymbol{F}_n^{(3)} = \partial_H k_n \nabla_{\boldsymbol{x}} H = -\frac{n\pi}{H^2}\nabla_{\boldsymbol{x}} H - \frac{H\mu_0^2}{n\pi}\nabla_{\boldsymbol{x}} H + O\left(n^{-2}\right), \tag{2.47c}$$

And for the $G_n^{(i)}$, $n \geq 1$, $i = 1, \ldots, 5$ functions we have:

$$G_n^{(1)} = \left|\boldsymbol{F}_n^{(1)}\right|^2 - \left|\boldsymbol{F}_n^{(2)}\right|^2 + \nabla_{\boldsymbol{x}} \cdot \boldsymbol{F}_n^{(1)} = \frac{n^2\pi^2}{H^2}\left(\nabla_{\boldsymbol{x}} h\right)^2 + O(1), \tag{2.48a}$$

$$G_n^{(2)} = -2\boldsymbol{F}_n^{(2)} \cdot \boldsymbol{F}_n^{(3)} = 2\frac{n^2\pi^2}{H^3}\nabla_{\boldsymbol{x}} H \cdot \nabla_{\boldsymbol{x}} h + O(1), \tag{2.48b}$$

$$G_n^{(3)} = -\left|\boldsymbol{F}_n^{(3)}\right|^2 = -\frac{n^2\pi^2}{H^4}\left(\nabla_{\boldsymbol{x}} H\right)^2 + O(1), \tag{2.48c}$$

$$G_n^{(4)} = 2\boldsymbol{F}_n^{(2)} \cdot \boldsymbol{F}_n^{(1)} + \nabla_{\boldsymbol{x}} \cdot \boldsymbol{F}_n^{(2)} + \nabla_{\boldsymbol{x}} h \cdot \boldsymbol{F}_n^{(3)} = \frac{n\pi}{H^2}\left[\Delta_{\boldsymbol{x}} H + \nabla_{\boldsymbol{x}} H \cdot \nabla_{\boldsymbol{x}} h\right] + O(1), \tag{2.48d}$$

$$G_n^{(5)} = 2\boldsymbol{F}_n^{(3)}\cdot\boldsymbol{F}_n^{(1)} + \nabla_{\boldsymbol{x}}\cdot\boldsymbol{F}_n^{(3)} = \frac{n\pi}{H^2}\left[\Delta_{\boldsymbol{x}}H + 2\left(\nabla_{\boldsymbol{x}}H\right)^2\right] + O(1), \tag{2.48e}$$

For these Calculations, Proposition 2 was used as well as Eqs. (2.45).

We will now briefly show the asymptotics of the basic integrals presented in Section 2.2. For a detailed derivation of the formulae to follow, see Appendix D.

Asymptotics of basic integrals $J(s;Z_n)$ and $J(s;W_n)$

We first prove the asymptotic formulae of the above integrals for $s = 0$ by utilizing Proposition 1 of this Section.

$$J(0;Z_n) = -\frac{\mu_0}{k_n^2} = -\frac{\mu_0 H^2}{n^2\pi^2} + O(n^{-4}) \tag{2.49a}$$

$$J(0;W_n) = \frac{\frac{1}{\cos\left(k_n H\right)} - 1}{k_n} = \begin{cases} \dfrac{\mu_0^2 H^3}{4n^3\pi^3} + O(n^{-5}) & ,n \text{ even} \\ -\dfrac{2H}{n\pi} + O(n^{-3}) & ,n \text{ odd} \end{cases} \tag{2.49b}$$

For $s \geq 1$ we present the following Proposition, which is proven in Appendix D:

Proposition 3: *The asymptotic behavior of basic integrals $J(s;Z_n)$ and $J(s;W_n)$ with $s \geq 1$ is given by the following formulae:*

$$J(s;Z_n) = \begin{cases} -\dfrac{\mu_0 H^{s+2}}{n^2\pi^2} + O(n^{-4}) & ,n \text{ even} \\ -\dfrac{H^{s+1}}{n^2\pi^2}\left(\mu_0 H + 2s\right) + O(n^{-4}) & ,n \text{ odd} \end{cases} \tag{2.50a}$$

$$J(s;W_n) = \begin{cases} \dfrac{\mu_0 H^{s+2}}{n^3\pi^3}\left(\dfrac{\mu_0 H}{4} + s\right) + O(n^{-4}) & ,n \text{ even} \\ -\dfrac{2H^{s+1}}{n\pi} + O(n^{-4}) & ,n \text{ odd} \end{cases} \tag{2.50b}$$

We then proceed to calculate the asymptotic behavior of the remaining basic integrals, by means of formulae (2.49) and Propositions 1, 2, 3 of current Section.

Asymptotic behavior of basic integrals $J(0;Z_n\,Z_m)$, $J(0;Z_n\,W_m)$ *and* $J(0;W_n\,W_m)$

1. Asymptotic behavior of Basic integrals $J(0;Z_m,Z_n)$. For these basic integrals we take into account the symmetry of their kernel with respect to the indexes m,n reducing the number of cases we have to consider:

$$J(0;Z_{-2},Z_n)=O\left(n^{-2}\right),\qquad J(0;Z_{-1},Z_n)=O\left(n^{-2}\right),\quad \text{as } n\to\infty \tag{2.51a,b}$$

For $m\neq n, m\geq 0$, $J(0;Z_m,Z_n)=0$, (2.51c)

$$J(0;Z_n,Z_n)=\frac{H}{2}+O\left(n^{-2}\right),\qquad \text{as } n\to\infty \tag{2.51d}$$

2. Asymptotic behavior of Basic integrals $J(0;W_m,Z_n)$:

$$J(0;W_n,Z_m)=\begin{cases}O\left(n^{-3}\right), n \text{ even}\\ O\left(n^{-1}\right), n \text{ odd}\end{cases},\quad \text{with } m=-2,-1 \text{, as } n\to\infty \tag{2.52a}$$

$$J(0;W_n,Z_0)=O\left(n^{-1}\right),\qquad \text{as } n\to\infty \tag{2.52b}$$

$$J(0;W_n,Z_n)=O\left(n^{-3}\right),\qquad \text{as } n\to\infty \tag{2.52c}$$

$$J(0;W_n,Z_m)=O\left(m^{-2}\right),\qquad \text{as } m\to\infty \tag{2.52d}$$

$$J(0;W_n,Z_m)=O\left(n^{-2}\right),\qquad \text{as } n\to\infty \tag{2.52e}$$

$$J(0;W_n,Z_m)=?,\qquad \text{as } n-m=c, n\to\infty \tag{2.52f}$$

3. Asymptotic behavior of Basic integrals $J(0;W_m,W_n)$. Here too, we take into account the symmetry of the basic integrals with respect to the indexes m,n.

$$J(0;W_n,W_0)=O(n^{-1}),\qquad \text{as } n\to\infty \tag{2.53a}$$

$$J(0;W_n,W_m)=O(n^{-1}),\qquad \text{as } n\to\infty \tag{2.53b}$$

$$J(0;W_n,W_m)=O(m^{-1}),\qquad \text{as } m\to\infty \tag{2.53c}$$

$$J(0;W_n,W_m)=O(n^{-2}),\qquad \text{as } n-m=c, n\to\infty \tag{2.53d}$$

$$J(0;W_n,W_n)=\frac{H}{2}+O\left(n^{-2}\right)\qquad \text{as } n\to\infty \tag{2.53e}$$

Asymptotic behavior of matrix coefficients $A_{m,n}$, $B_{m,n}$, $C_{m,n}$

We now proceed to the final part of this Section, which is the presentation of the asymptotic behavior of the matrix coefficients $A_{m,n}$, $B_{m,n}$, $C_{m,n}$ of the substrate problem. The asymptotic behavior of the coefficients $A_{m,n}$ can be taken directly from Eqs. (2.51) and therefore there is no need to rewrite them.

Asymptotic behavior of coefficients $\boldsymbol{B}_{mn}$

$$B_{m,n} = (-1)^m (1 - a_2 H)\nabla_{\boldsymbol{x}} h + O(m^{-2}), \text{ with } n = -2,-1, \quad \text{as } m \to \infty \tag{2.54a}$$

$$B_{m,0} = (-1)^m \frac{\nabla_{\boldsymbol{x}} h}{\cosh(k_0 H)}, \quad \text{as } m \to \infty \tag{2.54b}$$

$$B_{m,n} = O(1), \quad \text{with } m = -2,-1, \quad \text{as } n \to \infty \tag{2.54c}$$

$$B_{0,n} = \left[2 + \frac{(-1)^n}{\cosh(k_0 H)}\right]\nabla_{\boldsymbol{x}} h - \nabla_{\boldsymbol{x}} H, \quad \text{as } n \to \infty \tag{2.54d}$$

$$B_{m,n} = (-1)^m \frac{\nabla_{\boldsymbol{x}} h}{\cos(k_n H)}, \quad \text{as } m \to \infty \tag{2.54e}$$

$$B_{m,n} = 2\nabla_{\boldsymbol{x}} H - 2\nabla_{\boldsymbol{x}} h, \quad \text{as } n \to \infty \tag{2.54f}$$

$$B_{m,n} = \begin{cases} \dfrac{nH}{c}\nabla_{\boldsymbol{x}} H + O(1) & ,c \text{ even} \\ \dfrac{n}{c}\left[H\nabla_{\boldsymbol{x}} H + 2\nabla_{\boldsymbol{x}} h\right] + O(n^{-2}) & ,c \text{ odd} \end{cases} , \text{as } m = n - c,\ n \to \infty \quad , \tag{2.54g}$$

$$B_{m,m} = \nabla_{\boldsymbol{x}} h - \frac{1}{2}\nabla_{\boldsymbol{x}} H, \quad \text{as } m \to \infty \tag{2.54h}$$

For the asymptotic behavior of the coefficients C_{mn}

$$C_{m,n} = -(-1)^m \nabla_{\boldsymbol{x}} h \cdot \boldsymbol{F}_n^{(0)}, \quad \text{with } n = -2,-1, \quad \text{as } m \to \infty \tag{2.55a}$$

$$C_{m,0} = -(-1)^m \nabla_{\boldsymbol{x}} h \cdot \frac{\boldsymbol{F}_0^{(1)}}{\cosh(k_0 H)}, \quad \text{as } m \to \infty \tag{2.55b}$$

$$C_{m,n} = O(1), \quad \text{with } m = -2,-1 \quad \text{as } n \to \infty \tag{2.55c}$$

$$C_{0,n} = -\Delta_x h[1 - \frac{(-1)^n}{\cosh(k_0 H)}] - \Delta_x H, \qquad \text{as } n \to \infty \qquad (2.55d)$$

$$C_{m,n} = O(1), \qquad \text{as } n \to \infty \qquad (2.55e)$$

$$C_{m,n} = O(1), \qquad \text{as } m \to \infty \qquad (2.55f)$$

$$C_{m,n} = \begin{cases} \frac{n^2}{c^2 H}\left|\nabla_x H\right|^2 + O(n^{-2}) & , c \text{ even} \\ \frac{n^2}{c^2 H}\left[\left|\nabla_x H\right|^2 + 2\nabla_x H \cdot \nabla_x h\right] + O(n^{-2}) & , c \text{ odd} \end{cases} \quad \text{as } m = n - c, \ n \to \infty \qquad (2.55g)$$

$$C_{n,n} = O(n^2), \qquad \text{as } n \to \infty \qquad (2.55h)$$

2.4 Truncation of the infinite-dimensional HCM system

In the previous sections we presented a way to evaluate the matrix coefficients of the infinite substrate problem efficiently. However, any numerical implementation of the method requires the truncation of the infinite series representation and of the infinite substrate problem as well. The first step we take towards this goal is to truncate the vertical velocity potential series expansion from the infinite series

$$\Phi(\boldsymbol{x}, z, t) = \sum_{n=-2}^{\infty} \big(\Phi, Z_n(z;\eta,h)\big) Z_n(z;\eta,h)$$

to

$$\Phi(\boldsymbol{x}, z, t) = \sum_{n=-2}^{M} \big(\Phi, Z_n(z;\eta,h)\big) Z_n(z;\eta,h), \text{ with } M \in \mathbb{N} \tag{2.56}$$

The second, and much more unintuitive, step is the truncation of the infinite dimensional substrate problem:

$$\sum_{n=-2}^{\infty} \mathrm{L}_{mn}[\eta,h]\varphi_n = -\partial_t h\big[Z_m\big]_{z=-h}, \qquad m \geq -2 \qquad \boldsymbol{x} \in X \tag{2.57a}$$

complemented with the algebraic constraint:

$$\sum_{n=-2}^{\infty} \varphi_n = \big[\Phi\big]_{z=\eta} = \psi(\boldsymbol{x}, t) \tag{2.57b}$$

Such a task can be accomplished in many ways that will produce different results concerning the efficiency and convergence of the algorithm to be created. In addition, a formal truncation of an infinite system requires a proof that the truncated system's solution converges to the solution of the infinite system. Yet, this question is a very difficult mathematical question to answer and it is common practice to be omitted during the early stages of a model. As a result, we will not concern ourselves with such questions here. The infinite system in discussion is not a simple infinite-dimension system of linear pdes, but a system of pdes coupled with an algebraic constraint. The asymptotic properties of such systems have not been studied methodically, and no satisfactory literature could be found concerning this matter for the time being. Hence, no attempt is made to answer such questions. On the other hand, we concern ourselves with truncating the problem in such a way that minimizes the computational effort (given a constant amount of degrees of freedom) and produce solutions that converge as the number of used modes increases.

The task of the truncated substrate problem of the HCM model, is the computation of an approximation of the nonlocal DtN operator:

$$G^{(M)}[\eta,\psi]\psi = -\nabla_{\boldsymbol{x}}\eta\,\nabla_{\boldsymbol{x}}\psi + \left[\left(\nabla_{\boldsymbol{x}}\eta\right)^2 + 1\right]\left[\, h_0^{-1}\varphi_{-2}^{(M)} + \mu_0\psi \,\right],$$

where $\varphi_{-2}^{(M)}$ denotes the approximation of the free-surface modal amplitude.

The truncated version of the model we shall utilize in this thesis is the following:

$$\sum_{n=-2}^{M} \mathrm{L}_{mn}[\eta,h]\varphi_n = -\partial_t h[Z_m]_{z=-h}, \qquad -2 \le m \le M-1 \qquad \boldsymbol{x} \in X, \tag{2.58a}$$

$$\sum_{n=-2}^{M} \varphi_n = [\Phi]_{z=\eta} = \psi(\boldsymbol{x},t), \tag{2.58b}$$

This truncation is not more theoretically justified than any other truncations of the substrate problem. Other truncations have also been utilized for this reason, yet this truncation seems to be satisfactory regarding computational efficiency and accuracy. A truncation that theoretically more consistently calculates the DtN operator is the system:

$$\sum_{n=-2}^{M} \mathrm{L}_{mn}[\eta,h]\varphi_n = -\partial_t h[Z_m]_{z=-h}, \quad -2 \le m \le M \qquad \boldsymbol{x} \in X \tag{2.59a}$$

$$\sum_{n=-2}^{M} \varphi_n = [\Phi]_{z=\eta} = \psi(\boldsymbol{x},t) \tag{2.59b}$$

This truncated model allows us to minimize the approximate Hamiltonian of the system and as a result appears to be a likely candidate for our numerical scheme since no theoretical error is inserted in the calculation of the approximate DtN operator. Yet, the substrate system that is formed is overdetermined. As a result we require the use of a least square (approximate) method to solve the system. Such a method cannot yield an exact solution for the linear system but an approximate one. Hence the actual numerical solution we will derive from such a model will significantly diverge from the theoretical solution. Furthermore, such linear solvers are based on a transformation of the overdetermined system $A\cdot X = B$, where A is a $(M+4)\times(M+3)$ matrix, to a determined system of the form $A^T A\cdot X = A^T B$. Hence, except for the time needed to solve a linear system, these methods require time for a matrix multiplication. As a result the required computational time for such a method is almost double than the required time for a determined system of the same dimension. On the other hand the truncated system of Eqs. (2.58) is determined and as a result requires much less computational time. Furthermore solvers for such systems are much more accurate than least-square solvers. However, the solution of such a system does not minimize the corresponding Hamiltonian of

the truncated potential. As a result such a model has inherent error inserted to it. However, it can be assumed that using enough modes this error can be rendered indifferent for us. Finally, other truncations can be used, i.e introduction of a Lagrange multiplier to the aforementioned overdetermined system (with the Lagrange multiplier being the DtN operator itself) or even subtracting on equation of (2.59a) from the rest. Yet, these truncations have not been studied thoroughly enough to be described here.

Remark on truncations: In both the truncated models presented above the modal amplitude of the free-surface mode, the sloping bottom mode, the propagating mode and the first evanescent mode are included for any truncation. As a result the truncations refer to $M \geq 1$. Furthermore, the first 3 equations of the substrate problem together with the algebraic constraint of the problem are always included in the truncation.

Chapter 3: Implementation of the HCM method using FDM

3.1 Discretizing the HCM system using Finite Differences

With the setup and truncation of the HCM system complete, we now focus on the discretization of the system in order to implement the model to a computer program. For this purpose, we utilize finite differences as our first approach due to their easy and straightforward actualization, which would allow us to quickly generate an algorithm for the problem and test it on an abundance of different cases. We should mention however, that even though in Chapters 1 and 2, we presented the model and its analytical aspects for a 3D space domain (2 horizontal dimensions and 1 vertical), the code that is developed using a FD scheme strictly addresses problems defined on a 2D space domain. This restriction is imposed due to the fact that Finite Differences are not optimal for the case of a 3D domain. They are computationally inefficient compared to more advanced methods like Finite Elements and handle with more difficulty domains of arbitrary shape. One should notice, that the domain on which we solve the problem is not the actual domain of the physical problem, but its projection on the horizontal axis or plane. Considering this fact we understand that in a 2D space problem, the actual domain of the model will always be an interval of the $x-$ axis. As a result, there is no complexity in the representation of the domain and we can easily create the needed horizontal grid for the discretization. However, in the case of a 3D domain, its projection on the horizontal plane can assume a very arbitrary shape and even though the architecture of the scheme is essentially the same in both dimensions, the creation of the grid is a much more demanding task (due to its restrictive topology). Hence, for the case of a 3D domain, the implementation of the Finite Element Method appears to be a much more promising solution for the problem. Such an implementation has been carried out for the substrate problem of the HCM method, yet it will not be presented here.

In this section, we present in detail the discretization to be done for the numerical scheme. The aforementioned process is divided into three subsections. In the first one, we deal only with the space discretization and the substrate problem, thus restricting ourselves to a fixed time t^*. In the second one we examine the time-discretization and describe the time-stepping method used to solve the free-surface boundary equations in the time domain. Finally, we address a more subtle numerical aspect of the model, that of the calculation of the eigenvalues k_n , $n \geq 0$ of the Sturm-Liouville problem, as were discussed in Section 1.3.

Space discretization and the Finite Difference Method

Finite difference methods are numerical discretization schemes used for the purpose of solving differential equations by approximating them with difference equations. In these new equations, finite differences approximate the derivatives. Towards this goal, we utilize a Taylor series expansion for the fields in question:

$$f\left(x_i + h\right) = f\left(x_i\right) + \frac{f^{'}\left(x_i\right)}{1!}h + \frac{f^{(2)}\left(x_i\right)}{2!}h^2 + ... + \frac{f^{(n)}\left(x_i\right)}{n!}h^n + R_n\left(x_i\right), \qquad (3.1)$$

where $n!$ denotes the factorial of n and $R_n\left(x_i\right)$ is a remainder term, denoting the difference between the Taylor polynomial of degree n and the original function.

The first step of the finite difference method is the discretization of the horizontal domain of the problem. In our case, the continuous horizontal domain of the problem $\left[a,b\right]$ is replaced by the discretized domain with a finite number of points $\left\{x_i\right\}_{i=1}^{N_X} \in \left[a,b\right]$, where $x_1 = a$, $x_{N_X} = b$ and $x_i = a + \Delta x\, i$, $i \in \left\{1,2,...,N_X\right\}$ with $\Delta x = \frac{b-a}{N_X - 1}$. Having done so, the fields η and $\left\{\varphi_n\right\}_{n=-2}^{M}$ are substituted by their discretized counterparts that consist of their values at the (discretized) horizontal domain. The next step, is to replace the horizontal derivatives with their finite difference approximates. The algorithm we will construct and show, works for an arbitrary order of the FD scheme to be used. However, for the presentation to be more concise we will present the finite difference approximates for 4$^{\text{th}}$ order finite difference schemes. This order is chosen because, as will be shown in later sections, it seems to be the most efficient in terms of accuracy and computational cost for the problem. Throughout the domain, whenever possible we utilize central differences. The representation of the first and second horizontal derivatives for the modal amplitudes of the problem $\partial_x \varphi_m\left(x_i, t^*\right) = \partial_x \varphi_m\left(x_i\right)$, $\partial_x^2 \varphi_m\left(x_i, t^*\right) = \partial_x^2 \varphi_m\left(x_i\right)$

where $i = 3,4,...,N_X - 2$ by 4th order central differences can be calculated as follows, using a Taylor expansion:

$$\varphi_m\left(x_{i-2}\right) = \sum_{n=0}^{4} \frac{\partial_x^n \varphi_m\left(x_i\right)}{n!}\left(-2\Delta x\right)^n + O\left(\Delta x^5\right) \qquad (3.2a)$$

$$\varphi_m\left(x_{i-1}\right) = \sum_{n=0}^{4} \frac{\partial_x^n \varphi_m\left(x_i\right)}{n!}\left(-\Delta x\right)^n + O\left(\Delta x^5\right) \qquad (3.2b)$$

$$\varphi_m\left(x_{i+1}\right) = \sum_{n=0}^{4} \frac{\partial_x^n \varphi_m\left(x_i\right)}{n!}\left(\Delta x\right)^n + O\left(\Delta x^5\right) \qquad (3.2c)$$

$$\varphi_m\left(x_{i+2}\right) = \sum_{n=0}^{4} \frac{\partial_x^n \varphi_m\left(x_i\right)}{n!}\left(2\Delta x\right)^n + O\left(\Delta x^5\right) \qquad (3.2d)$$

To calculate the representation of the first horizontal derivative we need to calculate a linear combination of Eqs. (3.2) that will eliminate higher order horizontal derivatives. One can easily find the linear combination:

$$\varphi_m(x_{i-2}) - 8\varphi_m(x_{i-1}) + 8\varphi_m(x_{i+1}) - \varphi_m(x_{i+2}) = \sum_{n=0}^{4}\frac{\partial_x^n\varphi_m(x_i)}{n!}(-2\Delta x)^n - 8\sum_{n=0}^{4}\frac{\partial_x^n\varphi_m(x_i)}{n!}(-\Delta x)^n + 8\sum_{n=0}^{4}\frac{\partial_x^n\varphi_m(x_i)}{n!}(\Delta x)^n - \sum_{n=0}^{4}\frac{\partial_x^n\varphi_m(x_i)}{n!}(2\Delta x)^n + O(\Delta x^5)$$

which results to:

$$\partial_x\varphi_m(x_i) = \frac{\varphi_m(x_{i-2}) - 8\varphi_m(x_{i-1}) + 8\varphi_m(x_{i+1}) - \varphi_m(x_{i+2})}{12\Delta x}$$

In a similar manner we can calculate the representation of the second horizontal derivative as:

$$\partial_x^2\varphi_n(x_i) = \frac{-(\varphi_m(x_{i-2}) + \varphi_m(x_{i+2})) + 16(\varphi_m(x_{i-1}) + \varphi_m(x_{i+1})) - 30\varphi_m(x_i)}{12\Delta x^2}$$

These formulas are used throughout the discretized domain in the case of periodic boundary conditions, where $\varphi_m(x_{-1}) = \varphi_m(x_{N_X-1})$, $\varphi_m(x_{-2}) = \varphi_m(x_{N_X-2})$. However, in the case of wall conditions, central differences cannot be used for $i = 1, 2, N_X-1, N_X$. For these cases we shall use asymmetric differences as well as forward and backward differences. For the case of the 4th order formulas in a similar manner as before we get:

4th-order Forward finite difference scheme:

$$\partial_x\varphi_n(x_1) = \frac{-25\varphi_m(x_1) + 48\varphi_m(x_2) - 36\varphi_m(x_3) + 16\varphi_m(x_4) - 3\varphi_m(x_5)}{12\Delta x}$$

$$\partial_x^2\varphi_n(x_1) = \frac{45\varphi_m(x_1) - 154\varphi_m(x_2) + 214\varphi_m(x_3) - 156\varphi_m(x_4)}{12\Delta x^2} + \frac{61\varphi_m(x_5) - 10\varphi_m(x_6)}{12\Delta x^2}$$

4th-order Asymmetric (1-4) finite difference scheme:

$$\partial_x\varphi_n(x_2) = \frac{-3\varphi_m(x_1) - 10\varphi_m(x_2) + 18\varphi_m(x_3) - 6\varphi_m(x_4) + \varphi_m(x_5)}{12\Delta x}$$

$$\partial_x^2\varphi_n\left(x_2\right)=\frac{10\varphi_m\left(x_1\right)-15\varphi_m\left(x_2\right)-4\varphi_m\left(x_3\right)+14\varphi_m\left(x_4\right)}{12\Delta x^2}+$$
$$+\frac{-6\varphi_m\left(x_5\right)+\varphi_m\left(x_6\right)}{12\Delta x^2}$$

4th-order Asymmetric (4-1) finite difference scheme:

$$\partial_x\varphi_n\left(x_{N_X-1}\right)=\frac{3\varphi_m\left(x_{N_X}\right)+10\varphi_m\left(x_{N_X-1}\right)-18\varphi_m\left(x_{N_X-2}\right)+6\varphi_m\left(x_{N_X-3}\right)-\varphi_m\left(x_{N_X-4}\right)}{12\Delta x}$$
$$\partial_x^2\varphi_n\left(x_{N_X-1}\right)=\frac{10\varphi_m\left(x_{N_X}\right)-15\varphi_m\left(x_{N_X-1}\right)-4\varphi_m\left(x_{N_X-2}\right)+14\varphi_m\left(x_{N_X-3}\right)}{12\Delta x^2}+$$
$$+\frac{-6\varphi_m\left(x_{N_X-4}\right)+\varphi_m\left(x_{N_X-5}\right)}{12\Delta x^2}$$

4th-order Backward finite difference scheme:

$$\partial_x\varphi_n\left(x_{N_X}\right)=\frac{25\varphi_m\left(x_{N_X}\right)-48\varphi_m\left(x_{N_X-1}\right)+36\varphi_m\left(x_{N_X-2}\right)-16\varphi_m\left(x_{N_X-3}\right)+3\varphi_m\left(x_{N_X-4}\right)}{12\Delta x}$$
$$\partial_x^2\varphi_n\left(x_{N_X}\right)=\frac{45\varphi_m\left(x_{N_X}\right)-154\varphi_m\left(x_{N_X-1}\right)+214\varphi_m\left(x_{N_X-2}\right)-156\varphi_m\left(x_{N_X-3}\right)}{12\Delta x^2}+$$
$$+\frac{61\varphi_m\left(x_{N_X-4}\right)-10\varphi_m\left(x_{N_X-5}\right)}{12\Delta x^2}$$

We turn our attentions on constructing the new discretized substrate problem. The goal of a finite difference scheme is to replace a system of linear partial differential equations with a linear system of the form $A\cdot X=B$ where X consists of the discretized counterparts of the fields we want to find, A is a square matrix with known elements and B is a vector with known elements. Essential for the construction of the new system are the lateral conditions we will impose on it. The two cases we will showcase are the periodic lateral conditions and the case of two fully reflecting walls.

1. Periodic Lateral Conditions

The discretization of the substrate problem that is complemented with periodic lateral conditions is easier compared to the substrate problem with other lateral conditions. This is because central finite differences can be used to approximate the first and second derivatives of the $\varphi_n\left(x_i,t^*\right)$ functions in the entirety of the discretized domain. The discretized model for this case is presented below:

$$\sum_{n=-2}^{M} \mathrm{L}_{mn}[\eta,h]\varphi_n\left(x_i,t^*\right) = -\partial_t h[Z_m]_{z=-h},\ x \in \left\{x_i\right\}_{i=1}^{N_X} \tag{3.3a}$$

$$\sum_{n=-2}^{M} \varphi_n\left(x_i,t^*\right) = \left[\Phi\right]_{z=\eta} = \psi(x_i,t)\ \ x \in \left\{x_i\right\}_{i=1}^{N_X} \tag{3.3b}$$

Substituting the formulas of the 4th-order central finite difference scheme give us:

$$\begin{aligned}\sum_{n=-2}^{M} \mathrm{L}_{mn}[\eta,h]\varphi_n\left(x_i,t^*\right) = \sum_{n=-2}^{M}\Bigg\{&\left[\mathrm{C}_{mn} - \mathrm{A}_{mn}\frac{30}{12\Delta x^2}\right]\varphi_m\left(x_i\right) + \\ &+\left[-\mathrm{B}_{mn}\frac{8}{12\Delta x} + \mathrm{A}_{mn}\frac{16}{12\Delta x^2}\right]\varphi_m\left(x_{i-1}\right) + \left[\mathrm{B}_{mn}\frac{8}{12\Delta x} + \mathrm{A}_{mn}\frac{16}{12\Delta x^2}\right]\varphi_m\left(x_{i+1}\right) \\ &+\left[\mathrm{B}_{mn}\frac{1}{12\Delta x} - \mathrm{A}_{mn}\frac{1}{12\Delta x^2}\right]\varphi_m\left(x_{i-2}\right) + \left[-\mathrm{B}_{mn}\frac{1}{12\Delta x} - \mathrm{A}_{mn}\frac{1}{12\Delta x^2}\right]\varphi_m\left(x_{i+2}\right)\Bigg\} = -\partial_t h\left[Z_m\right]_{z=-h},\end{aligned}$$

As a result, the system is transformed into a linear system of the form $A\cdot X = B$ where X consists of the discretized counterparts of the fields we want to find. The matrix of the system consists of $(M+3)\times(M+3)$ blocks. The last $M+3$ blocks correspond to the algebraic constraint and as a result are identity matrices. The other blocks correspond to the substrate equations and are of the form:

$$X_{mn} = \begin{pmatrix}
\Phi_{m,n}^{1,3} & \Phi_{m,n}^{1,4} & \Phi_{m,n}^{1,5} & 0 & 0 & 0 & 0 & \dots & \Phi_{m,n}^{1,1} & \Phi_{m,n}^{1,2} & 0 \\
\Phi_{m,n}^{2,2} & \Phi_{m,n}^{2,3} & \Phi_{m,n}^{2,4} & \Phi_{m,n}^{2,5} & 0 & 0 & 0 & \dots & 0 & \Phi_{m,n}^{2,1} & 0 \\
\Phi_{m,n}^{3,1} & \Phi_{m,n}^{3,2} & \Phi_{m,n}^{3,3} & \Phi_{m,n}^{3,4} & \Phi_{m,n}^{3,5} & 0 & 0 & \dots & 0 & 0 & 0 \\
0 & \Phi_{m,n}^{4,1} & \Phi_{m,n}^{4,2} & \Phi_{m,n}^{4,3} & \Phi_{m,n}^{4,4} & \Phi_{m,n}^{4,5} & 0 & \dots & 0 & 0 & 0 \\
0 & 0 & \Phi_{m,n}^{5,1} & \Phi_{m,n}^{5,2} & \Phi_{m,n}^{5,3} & \Phi_{m,n}^{5,4} & \Phi_{m,n}^{5,5} & \dots & 0 & 0 & 0 \\
 & & & & & \dots & & & & & \\
0 & 0 & 0 & \dots & \Phi_{m,n}^{N_x-4,1} & \Phi_{m,n}^{N_x-4,2} & \Phi_{m,n}^{N_x-4,3} & \Phi_{m,n}^{N_x-4,4} & \Phi_{m,n}^{N_x-4,5} & 0 & 0 \\
0 & 0 & 0 & \dots & 0 & \Phi_{m,n}^{N_x-3,1} & \Phi_{m,n}^{N_x-3,2} & \Phi_{m,n}^{N_x-3,3} & \Phi_{m,n}^{N_x-3,4} & \Phi_{m,n}^{N_x-3,5} & 0 \\
0 & 0 & 0 & \dots & 0 & 0 & \Phi_{m,n}^{N_x-2,1} & \Phi_{m,n}^{N_x-2,2} & \Phi_{m,n}^{N_x-2,3} & \Phi_{m,n}^{N_x-2,4} & \Phi_{m,n}^{N_x-2,5} \\
0 & \Phi_{m,n}^{N_x-1,5} & 0 & \dots & 0 & 0 & 0 & \Phi_{m,n}^{N_x-1,1} & \Phi_{m,n}^{N_x-1,2} & \Phi_{m,n}^{N_x-1,3} & \Phi_{m,n}^{N_x-1,4} \\
0 & \Phi_{m,n}^{N_x,4} & \Phi_{m,n}^{N_x,5} & \dots & 0 & 0 & 0 & 0 & \Phi_{m,n}^{N_x,1} & \Phi_{m,n}^{N_x,2} & \Phi_{m,n}^{N_x,3}
\end{pmatrix}$$

where:

$$\Phi_{m,n}^{i,1} = \mathrm{B}_{mn}\frac{1}{12\Delta x} - \mathrm{A}_{mn}\frac{1}{12\Delta x^2}, \tag{3.4a}$$

$$\Phi_{m,n}^{i,2} = -\mathrm{B}_{mn}\frac{8}{12\Delta x} + \mathrm{A}_{mn}\frac{16}{12\Delta x^2}, \tag{3.4b}$$

$$\Phi_{m,n}^{i,3} = \mathrm{C}_{mn} - \mathrm{A}_{mn}\frac{30}{12\Delta x^2}, \tag{3.4c}$$

$$\Phi_{m,n}^{i,4} = \mathrm{B}_{mn}\frac{8}{12\Delta x} + \mathrm{A}_{mn}\frac{16}{12\Delta x^2}, \tag{3.4d}$$

$$\Phi_{m,n}^{i,5} = -\mathrm{B}_{mn}\frac{1}{12\Delta x} - \mathrm{A}_{mn}\frac{1}{12\Delta x^2}, \tag{3.4e}$$

and the right hand side vector is of the form

$$B = \left[\left\{-\partial_t h\left[Z_{-2}\right]_{z=-h}\right\},\left\{-\partial_t h\left[Z_{-1}\right]_{z=-h}\right\},\ldots,\left\{-\partial_t h\left[Z_M\right]_{z=-h}\right\},\{-\psi\}\right]$$

As we can see the resulting matrix of the system is sparse and its of the blocks described before are banded. This result is essential for the numerical efficiency of the method. The fact that the matrix is sparse and with an a priori known pattern (which can easily be calculated for every order of finite differences) allows as to store the data using sparse matrix representation i.e. storing only the nonzero elements and their global place on the matrix. Furthermore, the fact that the matrix is sparse and almost banded block-wise, allows us to utilize sparse matrix solvers which solve the linear system a lot faster than the normal methods used for full matrices. The biggest benefit of the sparse methods, is that the computational time required to solve the system raises linearly as the size of the square matrix raises. On the contrary methods used for full matrices usually follow a law of $T = c\,n^3$ regarding the size of the size of the matrix n and the computation time needed for the solution of the system T.

2. Fully-reflecting Wall Lateral Conditions

The construction of this discretized problem requires except of the use of central finite differences the use of asymmetric and forward and backward finite difference schemes. The discretized model in the case of fully-reflecting wall lateral conditions is presented below:

$$\sum_{n=-2}^{M}\left(\partial_x\varphi_n\left(x_i,t^*\right)\mathrm{A}_{mn}^{(a)} + \varphi_n\left(x_i,t^*\right)\mathrm{B}_{mn}^{(a)}\right) = 0,\ M > m \geq -2,\ i = 1, N_X \tag{3.5a}$$

$$\sum_{n=-2}^{M}\mathrm{L}_{mn}[\eta,h]\varphi_n\left(x_i,t^*\right) = -\partial_t h\left[Z_m\right]_{z=-h},\ x \in \left\{x_i\right\}_{i=1}^{M-1} \tag{3.5b}$$

$$\sum_{n=-2}^{M}\varphi_n\left(x_i,t^*\right) = \left[\Phi\right]_{z=\eta} = \psi(x_i,t),\ x \in \left\{x_i\right\}_{i=0}^{M} \tag{3.5c}$$

In a similar fashion as before we can easily see that the matrix of the system consists of $(M+3)\times(M+3)$ blocks. The last $M+3$ correspond to the algebraic constraint and as a result are identity matrices. The other blocks correspond to the substrate equations and are of the form:

$$X_{mn}=\begin{pmatrix}
\Phi_{m,n}^{1,1} & \Phi_{m,n}^{1,2} & \Phi_{m,n}^{1,3} & \Phi_{m,n}^{1,4} & \Phi_{m,n}^{1,5} & 0 & 0 & \dots & 0 & 0 & 0 \\
\Phi_{m,n}^{2,1} & \Phi_{m,n}^{2,2} & \Phi_{m,n}^{2,3} & \Phi_{m,n}^{2,4} & \Phi_{m,n}^{2,5} & \Phi_{m,n}^{2,6} & 0 & \dots & 0 & 0 & 0 \\
\Phi_{m,n}^{3,1} & \Phi_{m,n}^{3,2} & \Phi_{m,n}^{3,3} & \Phi_{m,n}^{3,4} & \Phi_{m,n}^{3,5} & 0 & 0 & \dots & 0 & 0 & 0 \\
0 & \Phi_{m,n}^{4,1} & \Phi_{m,n}^{4,2} & \Phi_{m,n}^{4,3} & \Phi_{m,n}^{4,4} & \Phi_{m,n}^{4,5} & 0 & \dots & 0 & 0 & 0 \\
0 & 0 & \Phi_{m,n}^{5,1} & \Phi_{m,n}^{5,2} & \Phi_{m,n}^{5,3} & \Phi_{m,n}^{5,4} & \Phi_{m,n}^{5,5} & \dots & 0 & 0 & 0 \\
 & & & & & \dots & & & & & \\
0 & 0 & 0 & \dots & \Phi_{m,n}^{N_x-4,1} & \Phi_{m,n}^{N_x-4,2} & \Phi_{m,n}^{N_x-4,3} & \Phi_{m,n}^{N_x-4,4} & \Phi_{m,n}^{N_x-4,5} & 0 & 0 \\
0 & 0 & 0 & \dots & 0 & \Phi_{m,n}^{N_x-3,1} & \Phi_{m,n}^{N_x-3,2} & \Phi_{m,n}^{N_x-3,3} & \Phi_{m,n}^{N_x-3,4} & \Phi_{m,n}^{N_x-3,5} & 0 \\
0 & 0 & 0 & \dots & 0 & 0 & \Phi_{m,n}^{N_x-2,1} & \Phi_{m,n}^{N_x-2,2} & \Phi_{m,n}^{N_x-2,3} & \Phi_{m,n}^{N_x-2,4} & \Phi_{m,n}^{N_x-2,5} \\
0 & 0 & 0 & \dots & 0 & \Phi_{m,n}^{N_x-1,1} & \Phi_{m,n}^{N_x-1,2} & \Phi_{m,n}^{N_x-1,3} & \Phi_{m,n}^{N_x-1,4} & \Phi_{m,n}^{N_x-1,5} & \Phi_{m,n}^{N_x-1,6} \\
0 & 0 & 0 & \dots & 0 & 0 & \Phi_{m,n}^{N_x,1} & \Phi_{m,n}^{N_x,2} & \Phi_{m,n}^{N_x,3} & \Phi_{m,n}^{N_x,4} & \Phi_{m,n}^{N_x,5}
\end{pmatrix}$$

Notice that due to the use of asymmetrical finite difference schemes at the points x_2 , x_{N_X-1} the second and N_X-1 rows of each block has one more nonzero (in general) element than the other rows. This happens because for the asymmetrical finite differences to be of the same order as the central and forward and backward, use of more adjacent points is required.

Finally we should mention that the same form have the blocks of the substrate problem if we use the lateral condition:

$$\sum_{n=-2}^{\infty}\left(\left[\partial_{x_1}\varphi_n\right]_{x_1=a}\mathrm{A}_{mn}^{(a)}+\left[\varphi_n\right]_{x_1=a}\mathrm{B}_{mn}^{(a)}\right)=g_m\ ,\ n\geq -2$$

which, as explained is Section 1.4, is a Neumann condition representing an excitation boundary. Hence, such a problem would be an incident wave problem and not an initial wave problem. This kind of conditions are not examined here in detail for two reasons. First the form of the linear system, concerning the pattern of the nonzero elements, is the same as the above case. Second, problems with excitation boundary require the use of incident layers and maybe even sponge layers. These kind of layers are artificial and hence effectively hinder the conservation properties of the model. As a result, and because they are utilized only for incident value problems, we will not delve into their implementation. Finally, we present the algorithm used to build the matrix of the system for the case of periodic lateral conditions (we don't present the blocks corresponding to the algebraic constraint since they are identity matrices):

```
for (int cpoint=0; cpoint<nx; cpoint++){ // Loop over all the horizontal points of the domain.



hcmArray ind(order+1); // The positions of the nonzero elements at every block.
hcmArray D1(order+1), D2(order+1); // The coefficients of the finite differences for the 1st & 2nd derivatives.
temp_size = (order+1)*modes;

// Calculate local column-positions of nonzero elements of iith row in the mth row of blocks.
for(int kk=0; kk<order+1; kk++){ // index loop start.

        ind[kk] = cpoint -order/2 +kk;
        if (ind[kk] < 0) ind[kk] = ind[kk] +nx-1; // Check if index[ii] < 0.
        else if (ind[kk] > nx-1) ind[kk] = ind[kk] -nx+1; // Check if index[ii] > nx-1.

} // index loop end.


for(int mm=0; mm<modes-1; mm++){ // Row-block loop start.

        line_counter = cpoint +nx*mm; // Calculate global number of row to be calculated.
        lines[mm] = line_counter; // Store the global number of the row to be calculated.

        for(int nn=0; nn<modes; nn++){ // Column-block loop start.

                for (int kk=0; kk<order+1; kk++){ // index loop start.

                        col_counter  = ind[kk] +nx*nn; // Calculate global column-position of the element to
be calculated.
                        temp_counter = nn*(order+1) +kk; // Calculate number of non-zero element to be
calculated mth row.
                        cols[temp_counter] = col_counter; // Store the global column-position of the element
to be calculated.

                        / Store non-zero element.
                        if (kk == order/2) temp[temp_counter] = AA(mm,nn)*D2[kk] +BB(mm,nn)*D1[kk]
+CC(mm,nn);
                        else temp[temp_counter] = AA(mm,nn)*D2[kk] +BB(mm,nn)*D1[kk];

                } // index loop end.

        } // Column-block loop end.

        MatSetValues(FCM1,1,&line_counter,temp_size,cols,temp,INSERT_VALUES); // Store the calculate
row to the matrix.

} // Row-block loop end.
} // cpoint-loop end.
```

Time Discretization and time-stepping algorithm

Having finished the discretization of the substrate problem and described the means to solve it, we now deal with the time discretization and the method used to advance the solution in the time domain. We introduce a time step dt and the time grid $t_n = n\,dt$, $n = 0,1,2,...,N_T$. The time-stepping problem can be described as: given a fixed time value t_n for which we know the free-surface elevation $\eta(x;t_n)$ and the free-surface potential $\psi(x;t_n)$ and have calculated the Dirichlet to Neumann operator $G(x;t_n)$ or more specifically the free-surface modal amplitude $\varphi_{-2}(x;t_n)$, we need a way to calculate the free-surface elevation and free-surface potential at the next time value $t_{n+1} = t_n + \Delta t$, by means of the free-surface kinematic and dynamic equations:

$$\partial_t \eta = -(\nabla_{\boldsymbol{x}} \eta)\cdot(\nabla_{\boldsymbol{x}} \psi) + (|\nabla_{\boldsymbol{x}} \eta|^2 + 1)\left(h_0^{-1}\varphi_{-2} + \mu_0 \psi\right), \tag{3.6a}$$

$$\partial_t \psi = -g\eta - \frac{1}{2}(\nabla_{\boldsymbol{x}} \psi)^2 + \frac{1}{2}(|\nabla_{\boldsymbol{x}} \eta|^2 + 1)\left(h_0^{-1}\varphi_{-2} + \mu_0 \psi\right)^2 - \frac{p_{\text{surf}}}{\rho}, \tag{3.6b}$$

For the discretization of these equations, we search for a high order method (which would yield high accuracy solutions) that also preserves quantities such as the Hamiltonian and the total mass of the system. These traits are a necessity since we want the model to handle long-time simulations. By means of testing we reach the conclusion that the explicit 4th-order Runge-Kutta numerical method is a good solution. Although, methods like the Adams-Bashforth predictor-corrector method are 4th order and require almost half the computational time, they do not conserve the energy and the mass of the system. As a result these methods cannot be used for long time simulations. We should however mention that the Runge-Kutta method is a dissipative numerical method in the sense that it gradually decreases the total energy and mass of the system. On the other hand, the rate of said dissipation is very slow and doesn't actually hinders the effectiveness of the algorithm in long-time simulations. Furthermore, we should mention that the model developed is non-dissipative as a Hamiltonian system. All the dissipation the system experiences in long-time simulations is entirely artificial and has no physical interpretation since it does not constitute a trait of the model. This method is used as follows:

Runge-Kutta methods are defined for initial value problem of the form:

$$\frac{d}{dt}u = f(u;t),\ u(t_0) = u_0$$

It is assumed that the first time derivative of the function y is dependent only on time and the function u. Notice that in our case $u = [\eta, \psi]^T$. Then, picking a step size Δt, for the classical 4th order Runge-Kutta method we define:

$$u_{n+1} = u_n + \frac{\Delta t}{6}\left(k_1 + 2k_2 + 2k_3 + k_4 \right), \tag{3.7a}$$

where:

$$u_i = u\left(t_i\right) \text{ and } t_i = t_0 + i\,\Delta t, \tag{3.7b}$$

$$k_1 = f\left(t_n, u_n \right), \tag{3.7c}$$

$$k_2 = f\left(t_n + \frac{\Delta t}{2}, u_n + \frac{\Delta t}{2} k_1 \right), \tag{3.7d}$$

$$k_3 = f\left(t_n + \frac{\Delta t}{2}, u_n + \frac{\Delta t}{2} k_2 \right), \tag{3.7e}$$

$$k_4 = f\left(t_n + \Delta t, u_n + \Delta t\, k_3 \right), \tag{3.7f}$$

This Runge-Kutta method is a 4th-order method, meaning that the local truncation error is on the order of $O\left(\Delta t^5\right)$ while the total accumulated error is of order $O\left(\Delta t^4\right)$. The algorithm of the problem is presented below:

```
t_temp = t_current;

parallel_system_constructor(..., uutemp, uutempdx,...); // Construct Initial linear system at time t = t_temp
parallel_system_solver(..., uutemp, t_temp,...); // Solve initial linear system at time t = t_temp
parallel_DtN_calculation(..., uutemp, t_temp,...); // Calculation of DtN.
// Calculation of right hand side of evolutionary equations (k1 vector).
parallel_rhs_calculation(..., uutemp, uutempdx, t_temp, k1,...);

// Set uu for calculation of k2
for(int ii=0; ii<2*nx; ii++) uutemp[ii] = uu[ii] +0.5*dt*k1[ii];
t_temp = t_current +dt/2.;


parallel_system_constructor(..., uutemp, uutempdx,...); // Construct Initial linear system at time t = t_temp
parallel_system_solver(..., uutemp, t_temp,...); // Solve initial linear system at time t = t_temp
parallel_DtN_calculation(..., uutemp, t_temp,...); // Calculation of DtN.
// Calculation of right hand side of evolutionary equations (k2 vector).
parallel_rhs_calculation(..., uutemp, uutempdx, t_temp, k2,...);


// Set uu for calculation of k3
for(int ii=0; ii<2*nx; ii++) uutemp[ii] = uu[ii] +0.5*dt*k2[ii];
t_temp = t_current +dt/2.;


parallel_system_constructor(..., uutemp, uutempdx,...); // Construct Initial linear system at time t = t_temp
parallel_system_solver(..., uutemp, t_temp,...); // Solve initial linear system at time t = t_temp
parallel_DtN_calculation(..., uutemp, t_temp,...); // Calculation of DtN.
// Calculation of right hand side of evolutionary equations (k3 vector).
parallel_rhs_calculation(..., uutemp, uutempdx, t_temp, k3,...);
```

```
// Set uu for calculation of k4
for(int ii=0; ii<2*nx; ii++) uutemp[ii] = uu[ii] +dt*k3[ii];
t_temp = t_current +dt;


parallel_system_constructor(..., uutemp, uutempdx,...); // Construct Initial linear system at time t = t_temp
parallel_system_solver(..., uutemp, t_temp,...); // Solve initial linear system at time t = t_temp
parallel_DtN_calculation(..., uutemp, t_temp,...); // Calculation of DtN.
// Calculation of right hand side of evolutionary equations (k4 vector).
parallel_rhs_calculation(..., uutemp, uutempdx, t_temp, k4,...);


// Set solution of the next time-step.
for(int ii=0; ii<2*nx; ii++) uutemp[ii] = uu[ii] + dt*(k1[ii] + 2.*k2[ii] + 2.*k3[ii] + k4[ii]);
```

The function parallel_system_constructor() contains the construction of the matrix and the right hand side of the substrate problem. This function was analyzed in the before subsection. The function parallel_system_solver() contains the solver of the linear system created by the discretized substrate problem. This function does not contain some interesting aspect of the model but only technicalities concerning the solution of the linear system. The function parallel_DtN_calculation is responsible for the calculation of the Dirichlet to Neumann operator for at a specific time. It contains the following algorithm:

```
for(int ii=0; ii<nx; ii++) DtN[ii] = -uudx[ii]*uudx[ii+nx] +(uudx[ii]*uudx[ii]      +1.)*(fullSolution[ii]/h0
+m0*uu[ii+nx]);
```

where fullSoution[1:nx-1] corresponds to the discretized mode φ_{-2}.

The function parallel_rhs_calculation is responsible for the calculation of the right-hand side of the evolutionary free-surface equations at a specific time. The following algorithm is contained in the function:

```
for(int ii=0; ii<nx; ii++){
// deta/dt = DtN equation
RHS[ii] = DtN[ii] +layer[ii]*(uu_inc[ii] -uu[ii]);
// dpot/dt = -g*eta -0.5*(dpot/dx)^2 -psurf/r +0.5*(DtN +deta/dx*dpot/dx)^2 /( (deta/dx)^2 +1 ) equation
RHS[nx+ii] = -g*uu[ii] -pp[ii] -0.5*uudx[ii+nx]*uudx[ii+nx] + \
0.5*pow(DtN[ii]+uudx[ii]*uudx[ii+nx],2.)/(uudx[ii]*uudx[ii]+1.)  +layer[ii]*(uu_inc[ii+nx] -uu[ii+nx]);
}
```

A note on the calculation of the eigenvalues k_n , $0 \le n \le N$

To close this section we shed some light to the numerical calculation of the eigenvalues k_n , $0 \le n \le M$ (of the Sturm-Liouville problem) that are derived as roots of the transcendental equations:

$$\mu_0 - k_0 \tanh[k_0(\eta + h)] = 0, \tag{3.8a}$$

$$\mu_0 + k_n \tan[k_n(\eta + h)] = 0, \; n \ge 1, \tag{3.8b}$$

The calculation of these eigenvalues is accomplished by using the Newton-Raphson numerical method. This iterative root-finding method is defined as follows:

Let $f : [a, b] \longrightarrow \mathbb{R}$ be a differentiable function and x^* one of its roots. Furthermore, we assume that there exists an interval that includes x^* such that $f'(x) \neq 0$ for all the values in this intervals. Let x_0 be an initial estimation of a root x^* of the function. We suppose that the initial estimation is close enough to the root, so the function can be approximated between these two values as:

$$y = f'(x_0)(x - x_0) + f(x_0), \tag{3.9}$$

Then a better approximation for the root can be calculated by the formula:

$$x_1 = x_0 - \frac{f'(x_0)}{f(x_0)}, \tag{3.10a}$$

or for the nth step:

$$x_{n+1} = x_n - \frac{f'(x_n)}{f(x_n)}, \tag{3.10b}$$

For the case of a root with multiplicity one, one can see that this method will converge at least quadratically, making it quite efficient.

For initial estimation of these eigenvalues we use the values:

$$k_0 = \mu_0, \quad \text{and} \quad k_n = \pi n / H \;, n \ge 1$$

The algorithm for the iterative Newton-Raphson is presented below for the case of the eigenvalue of the propagating mode:

```
// The approximation of the k0 that is to be return from the function.
double k0_value = m0; // Initial estimation for propagating mode.
// A variable that stores the value of the function f0=k0*tanh(k0*H)-m0, for every iteration.
double ff0_value =m0 -k0_value*tanh(k0_value*bathymetry);
// A variable that stores the value of the function df0 = d(f0)/dk0, for every iteration.
double dff0_value = -( m0 + bathymetry*(k0_value*k0_value - m0*m0) )/k0_value;
// A variable used for checking whether the wanted margin of error has been achieved or the maximum number //
of iterations has been surpassed. While the conditions for the function to stop are not satisfied, checker = true, //
otherwise checker = false.
bool checker = true;
// A variable used for counting the number of iterations we made at each step.
int iter_counter = 0;

// Check if the initial estimation satisfies the given margin of error for f0.
if (fabs(ff0_value) < ff_marg) checker = false;

while (checker){
        // Calculate the df0/dk0 function.
        dff0_value = -( m0 + bathymetry*(k0_value*k0_value - m0*m0) )/k0_value;
        // Use Newton-Raphson method to calculate the next estimation of k0.
        k0_value = k0_value - ff0_value/dff0_value;

        // Recalculate the f0 function for the new k0.
        ff0_value =m0 -k0_value*tanh(k0_value*bathymetry);

        // Check if the current k0-estimation satisfies the error-margin for the f0 function.
        if (fabs(ff0_value) < ff_marg) checker = false;

        iter_counter = iter_counter + 1; // Add the executed iteration to the iteration counter.
        // Checking if we surpassed the maximum number of iterations.
        if (iter_counter == max_iter) checker = false;
}

return k0_value; // Return final estimation of the k0 value.
```

In a similar manner the method for the evanescent modes can be written. Since the function $f(x)$ and it derivative can be calculated analytically this method does not suffer from implicit error estimates concerning numerical differentiation or approximation of the function itself. However, the major drawback of this method is the need to calculate the values of $\tanh[x_n(\eta+h)]$ and $\tan[x_n(\eta+h)]$ for every iteration. These functions are very costly computation-wise to be calculated numerically in a program. Yet the method was shown to converge fairly fast, in only a few iterations for up to accuracy of 10^{-14}. In general the calculation of these eigenvalues only consumes a minor percentage of the total computational time of the program compared to that of solving the substrate problem.

3.2 Numerical Simulation of the HCM system using analytic solutions

With the discussion on the numerical scheme used for the simulation completed, we now want to test the accuracy and efficiency of the created model. To make the examination of the system more concise, it is desirable to test each of the components of the problem separately. Since the model itself is decomposed to two coupled problems (the substrate problem and the free-surface evolution equations) we can first examine the efficiency of the substrate problem (i.e. the calculation of the DtN operator). Such a test case will only require the calculation of the DtN operator of the problem given a free-surface elevation and free-surface potential (Dirichlet data) at a fixed time. This way we can focus on the ability of the code to efficiently and accurately calculate the Neumann data of the problem (free-surface normal potential derivative) given the corresponding Dirichlet data. To do so, we shall use a problem that has an easy to find closed-form solution. It should be noted though that such a problem has no physical interpretation. The accuracy of the code will be tested by calculating the L^2-error of the numerically computed Dirichlet to Neumann operator and the modal amplitudes $\{\varphi_n\}_{n=-2}^{M}$ of the substrate problem, with their analytical counterparts. The error for the above fields will be calculated as

$$E_2[F] = \frac{\left\| F_{numerical}(x) - F_{analytical}(x) \right\|_2}{\left\| F_{analytical}(x) \right\|_2}, \tag{3.11}$$

where $\|.\|_2$ is the L^2-norm and $F(x)$ is the field in discussion.

The efficiency of the system concerns the number of modes and the number of horizontal points required to reach the accuracy threshold of the problem (or at least a satisfactory accuracy) concerning the DtN operator and the modal amplitudes $\{\varphi_n\}_{n=-2}^{M}$. We will furthermore examine the effect of the order of the finite difference scheme to the accuracy of the results. The efficiency of the code is a crucial wanted trait, since otherwise long-time simulations of large (in the sense of the horizontal discretization) problems will be rendered practically impossible. For that purpose we shall showcase the results of the simulations for a large variety of the number of horizontal points, used modes and orders of finite difference schemes. It should be noted that the accuracy threshold that was mentioned above is not a trait of the system that is theoretically predicted. Most numerical schemes either exhibit a threshold of accuracy or, if the discretization grid becomes too fine, a blow-up of the relative error. This can easily be seen in the current model since the elements of the matrix, produced by the discretized substrate problem, contain the quantities $\frac{1}{\Delta x^i}$, $i = 1,2$, see Eqs. (3.4), and as a result approach infinity as $\Delta x \longrightarrow 0$. Therefore, it becomes obvious that there exist a constraint concerning the ability to refine the space discretization. Furthermore, adding additional modes raises the dimension of the linear system to be solved and subsequently its condition number. As a result, inclusion of more modes (and as a results more equations of the substrate problem) can only improve the accuracy of the method up to a point. These

effects can be schematically understood through a methodical study of a simple mathematical, in the sense that it has no direct physical counterpart, example.

The case to be tested comprises of a laterally periodic initial value problem. The horizontal domain is the interval $[0, 2\pi]$. The bottom is flat with depth $h(x) = 1$. The free-surface elevation is the periodic function $\eta(x) = e_0 \cos(x)$ while the potential throughout the domain is:

$$\Phi^{EX}(x, z) = \cosh(z + h)\cos(x), \tag{3.12}$$

This case has been presented in various papers, first introduced in (Nicholls & Reitich, 2001) and further exploited in (Fazioli & Nicholls, 2010), where the efficiency of calculating DtN operators is tested. This function can be easily shown to comply with the Laplace equation, the impermeability condition and the periodicity of the domain: $\Phi^{EX}(0, z) = \Phi^{EX}(2\pi, z)$. Given the above problem, we can now calculate the analytical formulae of the DtN operator and the HCM system's modes:

a. The free-surface modal amplitude, as seen in Section 1.3 is defined from the following relation:

$$\begin{aligned} \varphi_{-2}(x) &= h_0\left(\left[\partial_z \Phi^{EX}\right]_{z=\eta} - \mu_0\left[\Phi^{EX}\right]_{z=\eta}\right) = \\ &= h_0\left[\sinh(\kappa H) - \mu_0 \cosh(H)\right]\cos(x) \end{aligned}, \tag{3.13}$$

b. For the case of a flat bottom domain, the sloping bottom modal amplitude is zero everywhere:

$$\varphi_{-1}(x) = 0, \tag{3.14}$$

Since the sloping bottom amplitude is zero globally, we could neglect the sloping bottom mode from the equations and reduce the substrate system. This way we could also potentially raise the accuracy of the solution since the system's dimension would be decreased as well as the error produced by the sloping bottom amplitude (numerically it could never be zero) would be neglected. Yet, this approach does not seem desirable since we would be unaware of the error in the calculation of the sloping bottom amplitude, an error very important in cases where the bottom is not flat. As this case constitutes the first test of the numerical behavior of the substrate system it would not be wise to a priori demand the system to behave as its theoretical counterpart. Instead we should observe its efficiency in complying with said traits. As a result the sloping bottom amplitude is kept throughout the problem as a field to be found.

c. From Section 1.3, we can easily get the following formula for the propagating modal amplitude of the system:

$$\varphi_0(x) = \frac{1}{A_{00}}\int_{-h}^{\eta}\left(\Phi^{EX} - \varphi_{-2}Z_{-2}\right)Z_0 dz = \frac{1}{A_{00}}\left[\int_{-h}^{\eta}\Phi^{EX}\,Z_0\,dz - \int_{-h}^{\eta}\varphi_{-2}\,Z_{-2}\,Z_0 dz\right]$$

Separating the integral in two terms and calculating the first term of the right side gives us:

$$\int_{-h}^{\eta}\Phi^{EX}Z_0 dz = \int_{-h}^{\eta}\cosh(z+h)\cos(x)\frac{\cosh\left[k_0(z+h)\right]}{\cosh(k_0 H)}dz \Rightarrow$$

$$\int_{-h}^{\eta}\Phi^{EX}Z_0 dz = \frac{\cos(x)}{\cosh(k_0 H)}\int_{-h}^{\eta}\cosh(z+h)\cosh\left[k_0(z+h)\right]dz$$

Making the substitution of variables: $u = \frac{z+h}{H} \Rightarrow dz = du\,H$ within the integral, we have:

$$\int_{-h}^{\eta}\Phi^{EX}Z_0 dz = \frac{H\cos(x)}{\cosh(k_0 H)}\int_0^1\cosh(Hu)\cosh(k_0 Hu)\,du \Rightarrow$$

$$\int_{-h}^{\eta}\Phi^{EX}Z_0 dz = \frac{H\cos(x)}{\cosh(k_0 H)}\left.\frac{\dfrac{\sinh\left[Hu(1-k_0)\right]}{1-k_0} + \dfrac{\sinh\left[Hu(1+k_0)\right]}{1+k_0}}{2H}\right|_{u=0}^{u=1}$$

Using the trigonometric formula: $\sinh(x \pm y) = \sinh(x)\cosh(y) \pm \cosh(x)\sinh(y)$, while also utilizing the dispersion relation $\mu_0 - k_0\tanh[k_0(\eta+h)] = 0$ corresponding to the propagating eigenvalue and gathering the terms together we have;

$$\int_{-h}^{\eta}\Phi^{EX}Z_0 dz = \frac{\left[\sinh(H) - \mu_0\cosh(H)\right]\cos(x)}{1-k_0^2} \Rightarrow$$

or utilizing the analytic expression of the free-surface mode of Eq. (2), we have:

$$\int_{-h}^{\eta}\Phi^{EX}Z_0 dz = \frac{\varphi_{-2}(x)}{h_0\left(1-k_0^2\right)}, \tag{3.15a}$$

Calculating the second term of the right side of the initial equation:

$$\int_{-h}^{\eta}\varphi_{-2}\,Z_{-2}\,Z_0 dz = \varphi_{-2}\int_{-h}^{\eta}\left[a_2\frac{(z+h)^2}{H} + 1 - a_2 H\right]\frac{\cosh\left[k_0(z+h)\right]}{\cosh(k_0 H)}dz \Rightarrow$$

Similarly, substituting $u = \frac{z+h}{H} \Rightarrow dz = du\,H$ and calculating the integrals:

$$\int_{-h}^{\eta} \varphi_{-2}\, Z_{-2}\, Z_0 dz = \frac{a_2\, \varphi_{-2}\, H^2}{\cosh\left(k_0 H\right)} \left| \frac{\left(H^2 k_0^2 u^2 + 2\right)\sinh\left(k_0 H u\right) - 2 H k_0 u \cosh\left(k_0 H u\right)}{H^3 k_0^3} \right|_{u=0}^{u=1} +$$

$$+ \varphi_{-2} \frac{1 - a_2 H}{\cosh\left(k_0 H\right)} H \left| \frac{\sinh\left(k_0 H u\right)}{H k_0} \right|_{u=0}^{u=1} \Rightarrow$$

Following the same steps described for the first term of Eq. (4) we arrive at the result:

$$\int_{-h}^{\eta} \varphi_{-2}\, Z_{-2}\, Z_0 dz = \varphi_{-2} \left[\frac{2\mu_0\, a_2}{H k_0^4} + \frac{-2\, a_2}{k_0^2} + \frac{\mu_0}{k_0^2} \right], \tag{3.15b}$$

Finally replacing the above formulas to Eq. (4) and noting that $a_2 = \dfrac{\mu_0 h_0 + 1}{2 h_0}$, we have:

$$\varphi_0\left(x\right) = \frac{\varphi_{-2}\left(x\right)}{A_{00}} \left[\frac{1}{h_0\left(k_0^2 - k_0^4\right)} - \frac{2\mu_0\, a_2}{H k_0^4} \right], \tag{3.15c}$$

d. Calculation for Evanescent modal amplitudes:

$$\varphi_n\left(x\right) = \frac{1}{A_{nn}} \int_{-h}^{\eta} \left(\Phi^{EX} - \varphi_{-2} Z_{-2}\right) Z_n dz$$

As before we calculate the two terms of the integral independently, utilizing the substitution of variables $u = \dfrac{z+h}{H} \Rightarrow dz = du\, H$, the dispersion relation $\mu_0 + k_n \tan[k_n(\eta + h)] = 0$ as well as the trigonometric formula: $\sin\left(x \pm y\right) = \sin\left(x\right)\cos\left(y\right) \pm \cos\left(x\right)\sin\left(y\right)$, we can easily derive the formulae:

$$\int_{-h}^{\eta} \Phi^{EX} Z_n dz = \cos\left(x\right) \frac{\kappa \sinh\left(H\right) - \mu_0 \cosh\left(H\right)}{k_n^2 + \kappa^2} = \frac{\varphi_{-2}}{h_0\left(k_n^2 + 1^2\right)}, \tag{3.16a}$$

$$\int_{-h}^{\eta} \varphi_{-2} Z_{-2} Z_n dz = \frac{1}{h_0} \frac{\varphi_{-2}}{k_n^2} + \frac{2 a_2 \varphi_{-2} \mu_0}{H k_n^4}, \tag{3.16b}$$

$$\varphi_n\left(x;t\right) = \frac{\varphi_{-2}}{A_{nn}} \left[\frac{-1}{h_0\left(k_n^4 + k_n^2\right)} - \frac{2 a_2 \mu_0}{H} \frac{1}{k_n^4} \right], \tag{3.16c}$$

Finally we can calculate the form of the Dirichlet to Neumann operator from the expression:

$$G = (-\partial_x\eta, 1)\cdot\left(\left[\partial_x\Phi^{EX}\right]_{z=\eta} - \left[\partial_z\Phi^{EX}\right]_{z=\eta}\partial_x\eta\,,\left[\partial_z\Phi^{EX}\right]_{z=\eta}\right) =$$

$$= -\partial_x\eta\left[\partial_x\Phi^{EX}\right]_{z=\eta} + \left[(\partial_x\eta)^2 + 1\right]\left[\partial_z\Phi^{EX}\right]_{z=\eta}$$

or utilizing Eq. (2) we have:

$$G = -\partial_x\eta\,\partial_x\psi + \left[(\partial_x\eta)^2 + 1\right]\left(\frac{\varphi_{-2}}{h_0} + \mu_0\psi\right), \tag{3.17}$$

We shall compare the numerical results with the analytical expression derived above. We will run multiple simulations for many values of the order of finite difference schemes, the number of modes used and the space discretization scheme.

We start by presenting some results for 4th order finite differences:

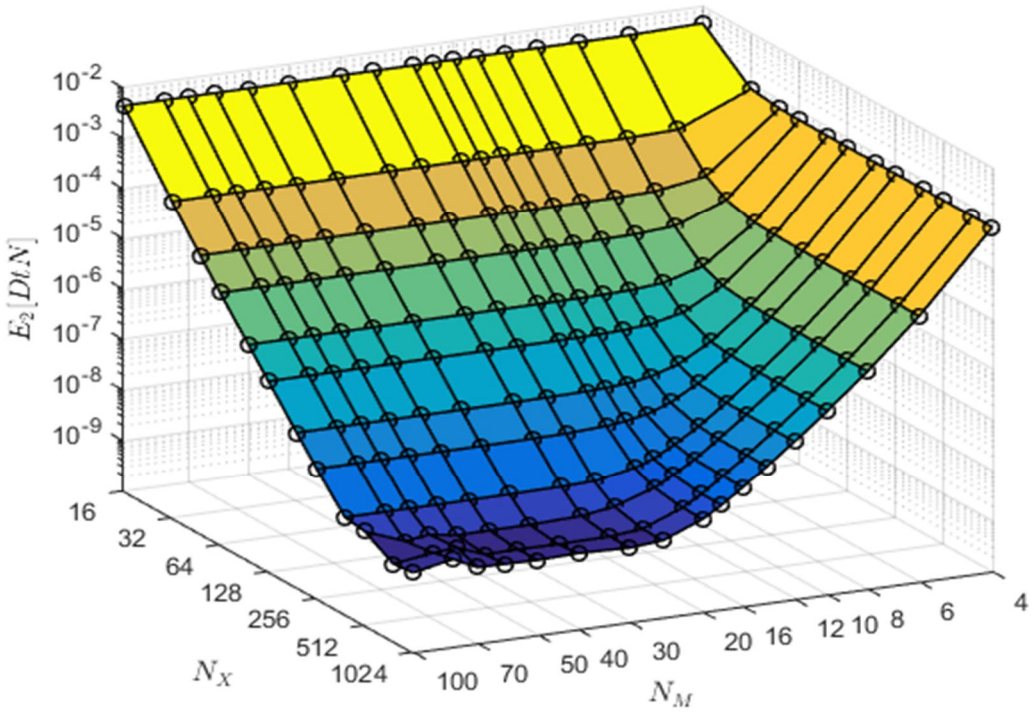

Figure 2: Relative L^2-error of the DtN operator with regard to the number of horizontal points N_X and total modes N_M used for the simulation.

As can be seen from the above Figure, the numerical calculation of the DtN operator reaches a plateau of accuracy, as expected, that is near to 10^{-9}. It should be noted that for the simulation we used *long double* variables for the C++ program. The rate at which the simulation reaches this plateau seems to be more rapid while we increase the number of modes rather than while we refine the discretization. However, concerning the computational time of the simulation, raising these two parameters by the same percentage does not result in

the same raise of the computational cost. This assertion can easily be validated by simply examining the change in the matrix created by the substrate problem and presented in Section 3.1. At a first glance we see that by raising either parameter by a factor of a in both cases the dimension of the matrix will change from $N_X N_M$ to $a N_X N_M$. The run-time required for a linear solver algorithm is dependent on the number of floating point operations needed. For the case of full matrices, this number has a $1-1$ correlation with the size of the matrix, but for the case of sparse matrices, that is not the case since we also need to know the raise of the number of nonzero elements. As can be seen in the books (Saad, 2003) and (Davis, 2006) most sparse algorithms have a run-time of the form $O(N)$ or $O(N \log N)$, where N is the number of nonzero elements of the matrix. Then, for the case of a refinement of the horizontal discretization, we have more horizontal points and as a result the equations of the system must be satisfied on all of them, while the total number of block matrices of the total matrix does not change. Hence, because the number of nonzero elements at every row of a block of the matrix depends only on the order of the finite difference scheme (and the lateral conditions) the nonzero elements at every row remain the same. As a result, for a refinement of the horizontal discretization by a factor of a the number of nonzero elements is raised by a factor of a. In a more practical manner we can state that this happens because the number of rows of the matrix is increased by a, while the number of nonzero elements at every row remains the same. On the other hand, for the case of an increase in the number of modes, not only we increase the number of unknown fields (and as a result the size of the linear system) but we also increase the number of substrate problem equations (we take a higher truncation of the infinite system) for the discretization of the system. As a result this yields a total increase on the number of the nonzero elements of the matrix in the order of a^2, and as a result a similar increase in the computational time. Hence, it is expected a raise of modes to yield higher run-times than a raise of the used horizontal points. We showcase these observation at the Table below:

Run-time calculations with a 4th-order FD scheme on 1 core of an *Intel Core i5-4210U CPU*							
Matrix dim = 5,120		Matrix dim = 10,240		Matrix dim = 20,480		Matrix dim = 40,960	
N_X / N_M	T [sec]	N_X / N_M	T [sec]	N_X / N_M	T [sec]	N_X / N_M	T [sec]
256 / 20	1.055	256 / 40	4.550	256 / 80	22.434	256 / 160	104.608
512 / 10	0.894	1024 / 10	1.313	2048 / 10	2.718	4096 / 10	6.014

Table 1: Comparing run-time results for horizontal grid refinement and raising modes.

Another important result of the Figure 1, is the fact that if too few horizontal points or modes are used the simulation cannot reach the optimal plateau of accuracy no matter how much we raise the other parameter. Such a result is also expected since no accurate results can arise from simulation that correspond to a very small truncation of the system or too little horizontal points (therefore, poor representation of the initial data). Finally, we should state that in simulations concerning large problems we are only interested in the results presented at the top corners of Figure 1. The horizontal domain of the problem presented here corresponds entirely to one wavelength (not in a literal sense since the free-surface elevation presented

does not correspond to a real wave) and as a result the entirety of the horizontal grid simulates just that. However, in a case that corresponds to a practical problem, the domain's length is tenths or hundreds if not thousands of wavelengths long (taking the wavelength of a wave present in the problem as a guide). Hence, it is not realistic to assume that we can represent a single wave with a few hundreds or even thousands of horizontal points. Furthermore, usage of as many as a few tens of modes will render the needed time of the simulation totally impractical for a simple computer to handle. However, we can see that even for 4 modes and 16 horizontal points the total L^2-error is approximately 10^{-4} and with a horizontal discretization of a few tens of points and 6-10 modes we can achieve results with satisfactory accuracy. Hence, these results will be taken into account for the choice of the parameters for simulations to follow.

Moving forward we now present the L^2-error of some modes of the problem.

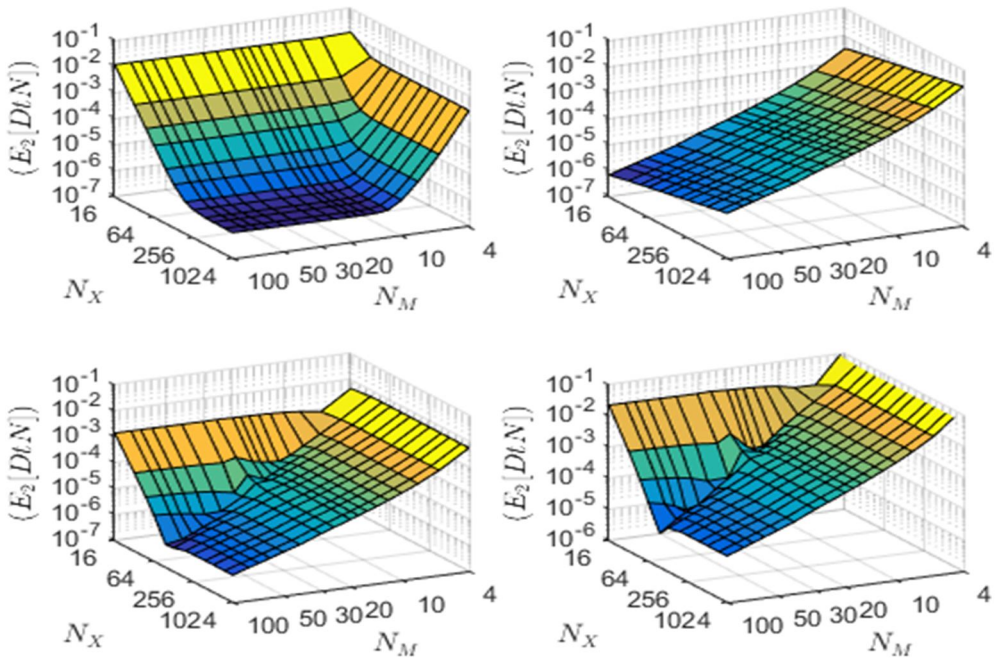

Figure 3: Relative L^2-error of the modes φ_{-2}, φ_{-1}, φ_0, φ_1 with regard to the number of horizontal points and total modes used for the simulation.

The relative error of the *free-surface mode* φ_{-2} is similar to the error of the DtN operator, an expected result since the Dirichlet to Neumann operator is given by the Eq. (3.16). The relative error of the *sloping bottom mode* φ_{-1} displays a different behavior than the one of the free-surface mode. Here, the defining criterion for the error is the number of modes used, while the number of horizontal points does not seem to matter much in the relative error. This behavior is not assumed to be general for this mode but an exception for this case, since the bottom of the problem is flat. As a result, the bottom geometry is always described exactly by the approximation, no matter how many points are used, while the *sloping bottom mode* is

equal to $\varphi_{-1}(x) = 0$. We also observe a slight increase of the relative error for raising control points while keep fixed number of modes for a case of large modes. This effect may be attributed to the raise of the condition number of the system while the control points are increasing. The relative error of the propagating mode φ_0 and the first evanescent mode φ_{-1} behave similarly but with the error of the evanescent mode being bigger. This can be attributed to the fact that the absolute error of the two modes are approximately equal but, because the propagating mode takes much larger values, its relative error is smaller. The aforementioned note combined with the fact that the measure of the evanescent modes decreases by a value of $O\left(n^{-4}\right)$, may lead us to assume that there is a specific number of modes we can actually calculate satisfactory and this could potentially lead to a breakdown of the method. The next Figure addresses this concern:

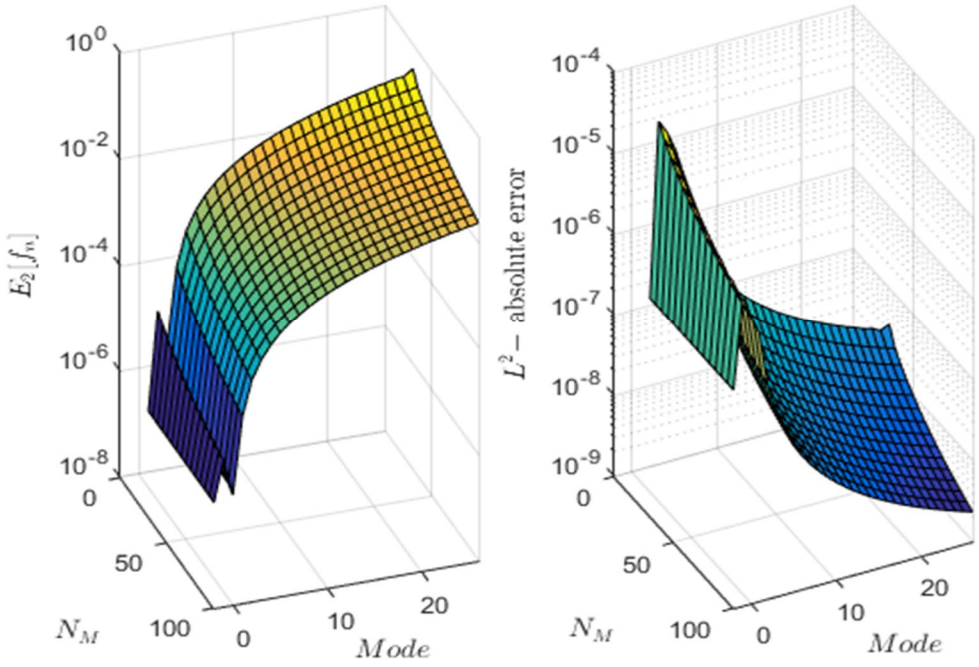

Figure 4: L^2-relative and absolute error of the first 29 modes of the system with regard to the number of total modes used, for 512 control points.

From the left plot of Figure 3 it is clear that the modes we can calculate with the biggest relative accuracy is the free-surface mode φ_{-2} and the propagating mode φ_0. The evanescent modes exhibit a steadily decreasing accuracy of the relative L^2-error although this error drops as we refine the grid. However the right plot of Figure 3 showcases that the absolute L^2-error of the evanescent modes actually decreases as n rises. By absolute error we mean the quantity $\left\|F_{numerical}(x) - F_{analytical}(x)\right\|_2$. Hence, no problem should arise from using many modes since the accuracy of the model is not hindered. The decrease of the relative error for the modal amplitudes of the evanescent modes is simply a result of the rapidly decaying field

strength. This observation combined with the results of Table 1, make us assume that the optimal number of modes to be used for simulations would be 6-12 modes in total.

To observe this result from a different view we also present the norm of the modal amplitudes. For this case we use the C^2 – norm since the substrate problem id dependent up to the second horizontal derivatives of the modal amplitudes. This norm is defined by the relation:

$$\left\|\varphi_n\right\|_{C^2} = \left\|\varphi_n\right\|_\infty + h_0^{-1}\left\|\partial_x\varphi_n\right\|_\infty + h_0^{-2}\left\|\partial_x^2\varphi_n\right\|_\infty, \tag{3.18}$$

an expression that can be analytically calculated for all the modal amplitudes. The results are presented in the following figure:

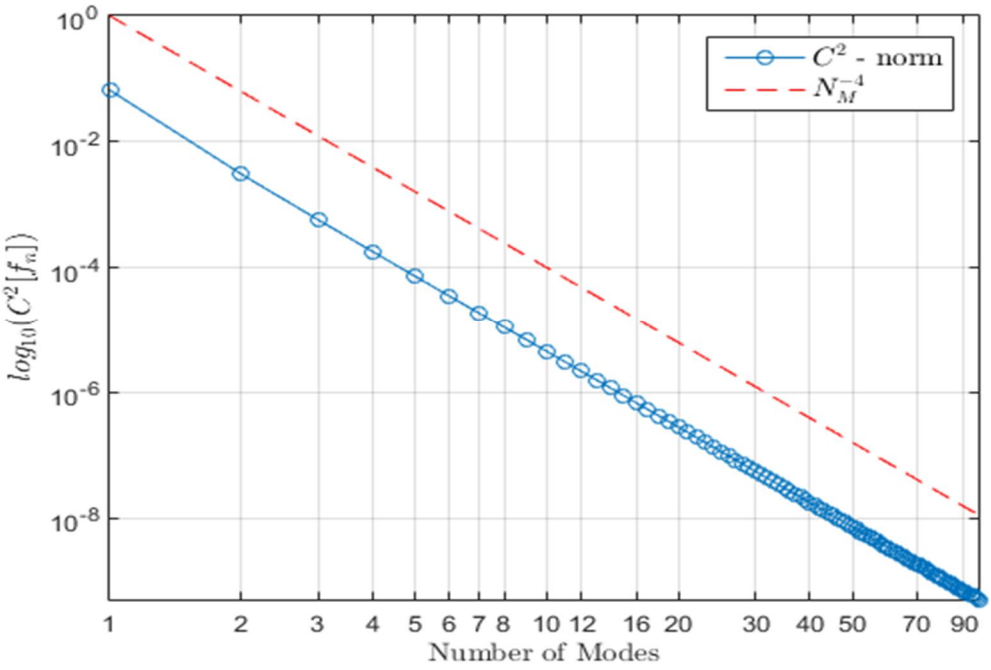

Figure 5: Presentation of the $C^2(X)$ – norm of various modal amplitudes of the system

From this figure we can deduce that evanescent modes of large number do note effect the equations of the substrate problem significantly. Hence, the increasing relative error for these modes is not important for the efficiency of the code. Furthermore, one can observe that in Figure 3 we did not show the 30th mode even though all simulations have at least 30 modes. This happened because in every simulation the last mode used is not calculated correctly since the substrate equation that it corresponds to is not included in the truncation of the problem. This behavior is visible in the following Figure:

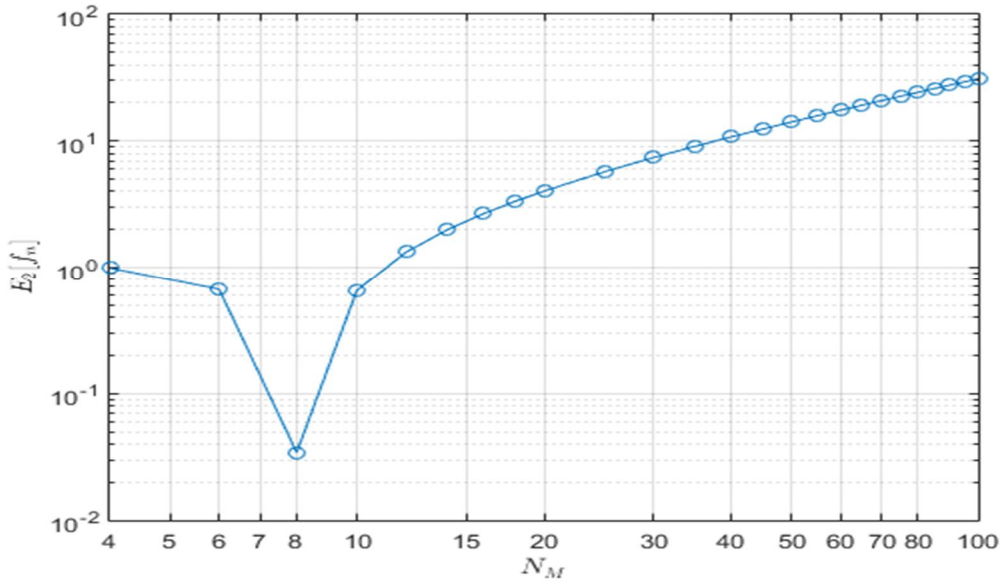

Figure 6: Presentation of the L^2-error of the last mode of a number of simulations.

As it can be seen, this behavior is limited for the case where $N_M \leq 10$,and is more visible as the number of total modes increases. Of course, this diagram does not imply that the absolute error for the last mode increases as the number N_M . Since we know that $\|\varphi_n\|_\infty = O\left(n^{-4}\right)$ as n goes to infinity, it simply means that the magnitude of the absolute error, is one or more orders bigger than the measure of the mode.

For now we only checked the spatial accuracy of the method for changing the total number of horizontal grid points. However, spatial accuracy of the model is also related to the order of the finite difference scheme we utilize. For this purpose, we now proceed to calculate the relative L^2-error of the DtN operator while implementing the finite difference scheme with a variety of orders. We run a number of simulations for 2nd, 4^{th} and up to 12^{th} order schemes parametrized by the number of total used modes or the number of horizontal points (while keeping constant the other factor). We begin our examination with the case where we keep a constant number of horizontal points and raise the number of used modes within the interval $N_M \in [\,4, 70\,]$. Even if our current study is limited to a domain of small horizontal length we want to be able to utilize the results here for larger cases. As a result, the number of horizontal grid points should not be too large since it would not be able to correspond to practical cases and also the problem would reach fast its plateau of accuracy for all the schemes. For this reason we choose to run the simulations with 64 horizontal points as a logical degree of detail. The results of these simulations concerning the L^2-error of the DtN operator are displayed in the Figure below:

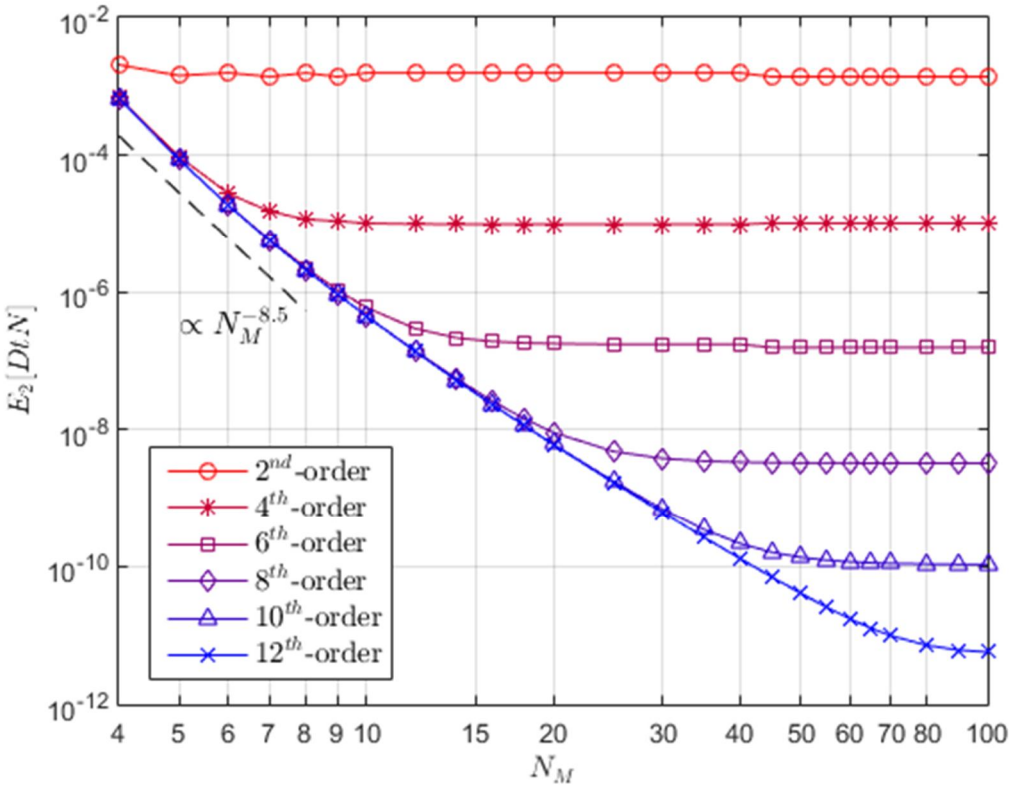

Figure 7a: Presentation of the L^2-error of the DtN operator for 6 different orders of finite difference schemes with $N_X = 64$.

Firstly, we observe that each method reaches a different plateau of accuracy, logically, smaller as we raise the order. We also note that high order schemes reached, for the current horizontal discretization, a relative error so low that the 4th order scheme cannot reach no matter how many horizontal points or modes we use. This can be explained from the fact that high order schemes calculate the spatial derivatives of the problem with much higher precision than their lower-order counterparts. Hence, this results can act as another way of ensuring that the model has no errors in its implementation and the numerical threshold of the 4th order is related to some kind of bug in the code or inherent error of the model. We should however mention that for practical applications, 4th order and 6th order schemes seem to be the best in balancing computational time and accuracy of results while higher order finite differences find little application. We could although utilize higher order schemes for cases where a wave will pass over a very abrupt change of bathymetry (only during these moments) in an attempt to better calculate the spatial derivatives of the model better during that time.

We now run another series of simulations, for many orders of finite differences, where we change the number of horizontal points while keeping constant the number of used modes to $N_M = 12$. This number of modes again corresponds to a value that can be utilized for problems with time-evolution and large horizontal domains. The results of these simulations concerning the L^2- error of the DtN operator are displayed in the Figure below:

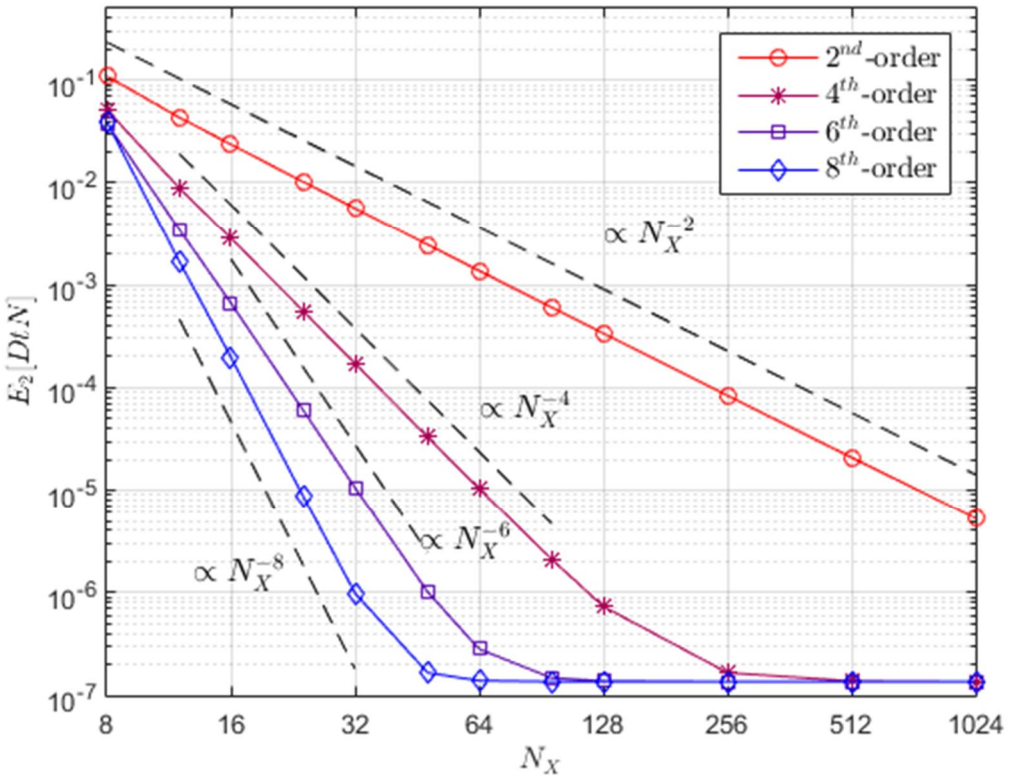

Figure 7b: Presentation of the L^2 – error of the DtN operator for 4 different orders of finite difference schemes with $N_M = 12$

In contrast with the case where we kept constant the number of horizontal points, we now observe that all the schemes converge (except for the 2nd order that has yet to converge) to the same accuracy threshold. This can easily be explained from the fact that both raising the order of the model as well as raising the number of horizontal points, only effect the spatial accuracy of the model. Hence, by keeping the number of used modes constant we always use the same truncated sets of partial differential equations for the substrate problem and this threshold corresponds to exactly that accuracy threshold of the truncated substrate problem.

Finally, we study the effect of the amplitude e_0 of the free-surface elevation of the wave, with regard to the accuracy of the calculation of the DtN operator for the system. For this purpose, we multiple run simulations with the free-surface elevation given by the formula $\eta = e_0 \cos(x)$ and parameter values $e_0 = 0.1, 0.3, 0.5, 0.7, 0.9$. A 4th order finite difference scheme will be utilized and a total of 256 horizontal points. The total number of modes will be from 4 to 50. The results are presented in the figure below:

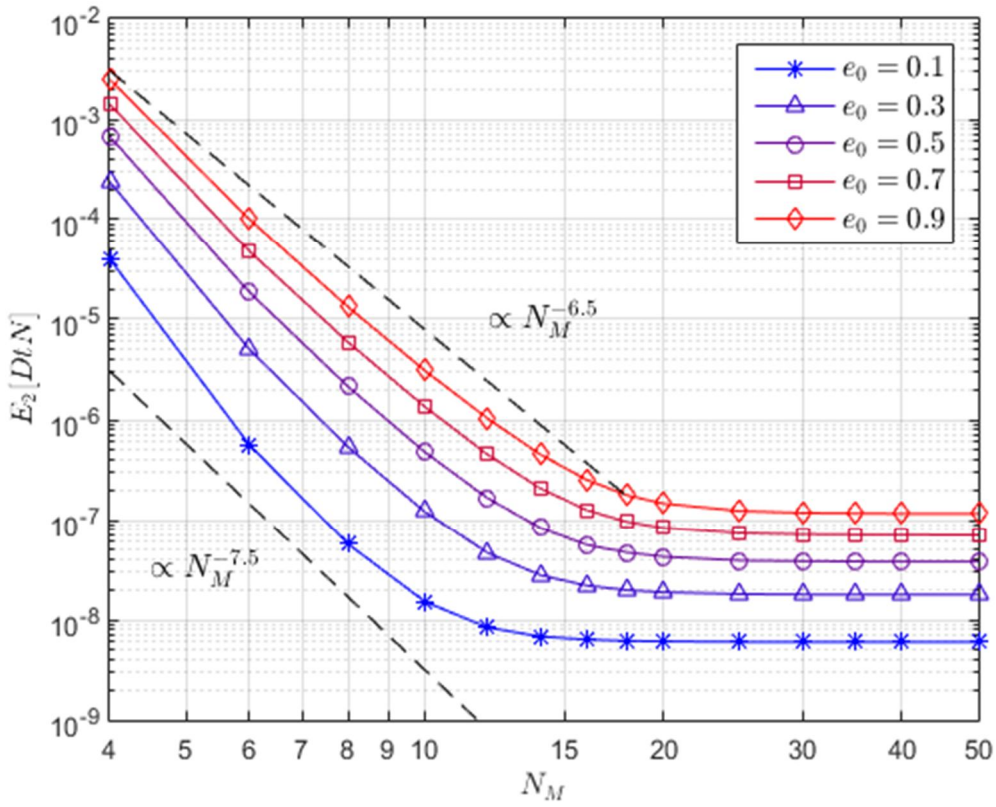

Figure 8: Presentation of the L^2- error of the DtN operator for a variety of different amplitudes of free-surface elevations.

As can be seen from Figure 7, all the cases reach a plateau of accuracy relatively fast with regard to the total number of used modes. As expected, the most linear case, where $e_0 = 0.1$, admits the highest accuracy for the DtN operator, where the most nonlinear case with $e_0 = 0.9$ has the worst relative error. Yet, the most linear case experiences a relative error of only an order of magnitude smaller than the worst case. This result showcases us that the present method's accuracy is not highly dependent on the nonlinearity of the problem. Many other models experience high drops of accuracy by raising the nonlinearity of the problem, especially those that are based on a petrubation of the linearized problem. Hence, this result seems to be encouraging for the ability of the model to handle problem with high nonlinearity (always without breaking of the wave though).

Note: In the previous paragraphs we stated that we wish to calculate the DtN operator (and furthermore the free-surface elevation and potential) with as much accuracy as we can. However, we should state that said accuracy was never meant to represent the accuracy of the problem compared with its physical counterpart in a long-time simulation. This low relative error is wanted for the purpose of the algorithm to be as stable as possible during long time simulations, so it will conserve energy and mass as best as it can during the simulation. It is well understood that the relative error of the method compared to a experimental solution or other fully nonlinear methods would be many magnitudes higher.

A remark regarding the value of the parameter μ_0

Throughout the discussion presented above, we never mentioned anything regarding the choice of the parameter μ_0. A theoretical justification regarding the optimal value of this parameter (for smaller relative error on the calculation of the DtN operator) will not be presented here. By trying different values we have found that for the case presented here the optimal value of this parameter is given by $\mu_0 = \frac{\omega^2}{g}$, where ω is the frequency of a wave with wavelength $l = 2\pi$, characterized by the dispersion relation of the linear water wave problem: $\omega = \sqrt{g\,k\tanh(k\,h_0)}$, with k being the wavenumber of the wave, and $h_0 = 1$ is the depth of the domain. To showcase this result, we present the L^2-error of the DtN operator, for a variety of used μ_0 values. The horizontal discretization of the problem consists of 256 points and a 4th finite difference scheme is used. In the following figure $\mu_0^* = \omega^2 / g$:

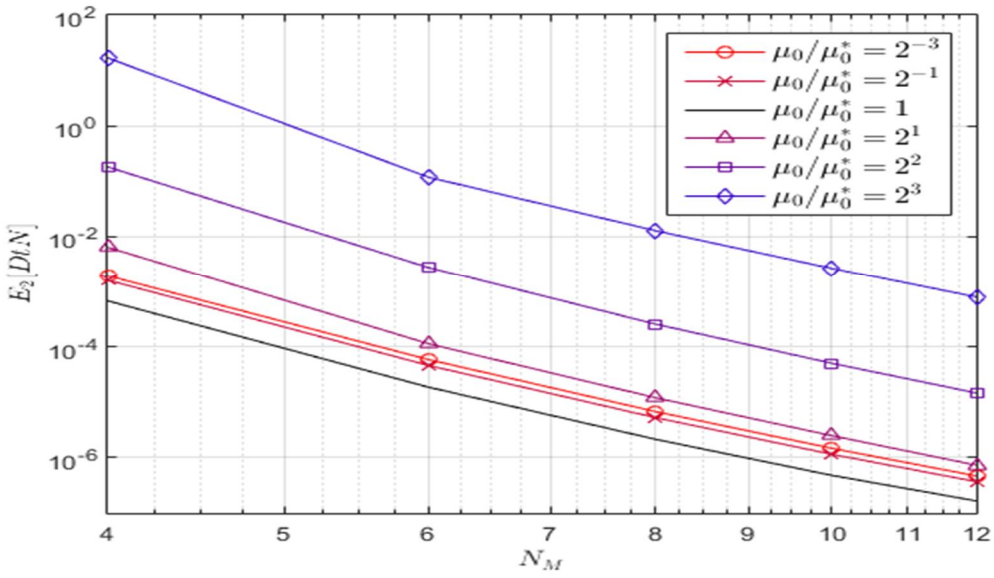

Figure 9: L^2- error fo the DtN operator for a various values of the parameter μ_0

3.3 Numerical Simulation of Solitary Waves in a closed wave tank

In section 3.2 we investigated the accuracy and efficiency of the substrate problem using an analytical example. Knowing that the substrate problem is solved without problem, we can now examine time dependent problems and be able to test the efficiency of the free-surface evolution equations. The main purpose of this section is to test the efficiency of the Hamiltonian Coupled Mode System (HCMS) in solving highly demanding physical problems. By demanding we mean a problem that is both rich in physical phenomena as well as demanding in its domain size whether that is the space domain or the time of the simulation. For these two purposes, the study of solitary waves comes as a natural decision. In order to be able to easily check the results in time, we assume a flat bottom. This way, at every moment we can easily compare the numerical solution with its theoretical counterpart. Solitary waves are waves that are not easily simulated by linearized or physically reduced models, therefore they are a very interesting test case for the current code. Furthermore, the modeling of such waves and their concerning behavior requires a very demanding discretization both in the time and in the space domain. As a result, models based in Boundary Element Methods require excessive amounts of computational time, rendering them an expensive (time-wise) solution. Hence, it is of great importance to highlight this method's ability to solve such cases with high precision and much lower computational time.

Solitary waves are defined as time-independent and periodic solutions of the water-wave problem, of infinite wavelength. As a result such waves propagate unchanged with a constant speed. The first documented encounter of a solitary wave is attributed to J. Scott Russell, who claimed to see such a wave in 1834 at the Edinburgh-Glasgow canal. Russell named the wave as "Wave of Translation" in the sense that there is significant net mass transport during the propagation of the wave. Russell's observations seemed to contradict the at the time established theories of hydrodynamics by Isaac Newton and Daniel Bernoulli. Since the existing models could not explain such a phenomenon many scientists of the era had trouble accepting Russell's observations. It would take till 1879 when Boussinesq and Lord Rayleigh published a theoretical treatment of solitons. Later, on 1895 D. Korteweg and C. de Vries will provide the known Korteweg-de Vries (KdV) equation, including solitary waves and periodic cnoidal wave solutions. The first simulation of solitary waves will come at 1965 by N. Zabusky and M. Kruskal who first documented the soliton behavior in media subject to KdV equations in a numerical investigation using a finite difference approach.

For the case of linear equations, such as the classical wave equation $u_{tt} - c^2 u_{xx} = 0$, the solutions produced by such a constraint have the arbitrary form: $u(x,t) = f(x-ct) = f(\xi)$. On the other hand a nonlinear equation will usually determine a restricted class of profiles which often play an important role in the solution of the initial value problem as $t \to \infty$. As one can read in the book (Drazin & Johnson, 1989):

"A travelling wave continually steepens and if allowed it will break and become multivalued. Similarly the effect of dispersion alone also produces a wave which forever changes its shape, but in the opposite sense (it spreads out). Perhaps these two effects many maintain a balance and produce a wave of permanent form."

Since no close form solutions exist for the classical water-wave problem, different solitary waves are produced from various simplified models where solitary wave solutions can be found analytically. Such known examples are the KdV equations and the Serre-Green-Naghdi (D Mitsotakis, Synolakis, & McGuiness, 2015) equations and other Boussinesq-type approximate models of the Euler equations. Our model as a non simplified one, cannot yield easily analytical solutions. Therefore, we must utilize numerically generated solutions of solitary waves. The method used here is the one presented in (Clamond & Dutykh, 2013), from which we will derive the initial free-surface elevation $\eta_0(x)$ and free-surface potential $\psi_0(x)$. In said paper, a fast method of numerically calculating gravity solitary surface waves of the full Euler equation in water of finite depth is developed. The method is based on Babenko's reformulation of the classical problem while for the numerical scheme it utilizes Petviashvili's iteration method. Their MATLAB code if freely provided.

For the simulations to follow, we consider the initial value problem presented below:

The nonlinear free-surface evolutionary equations:

$$\partial_t \eta = -\partial_x \eta\, \partial_x \psi + \left((\partial_x \eta)^2 + 1\right)\left(h_0^{-1} \mathcal{F}^{(M)}[\eta, h]\psi + \mu_0 \psi \right), \tag{3.19a}$$

$$\partial_t \psi = -g\eta - \frac{1}{2}(\partial_x \psi)^2 + \frac{1}{2}\left((\partial_x \eta)^2 + 1\right)\left(h_0^{-1} \mathcal{F}^{(M)}[\eta, h]\psi + \mu_0 \psi \right)^2, \tag{3.19b}$$

with initial values at $t = 0$:

$$\eta(x,0) = \eta_0 \qquad \psi(x,0) = \psi_0 \qquad x \in X\ , \tag{3.19c}$$

where $\mathcal{F}^{(M)}[\eta, h]\psi = \varphi_{-2}$ is the first element (the *free surface mode*) of the solution $\{\varphi_n\}_{n=-2}^{M}$ obtained from the boundary value problem on X , which is referred to as the substrate problem:

$$\sum_{m=-2}^{M} \mathrm{A}_{mn}\, \partial_x^2 \varphi_n + \mathrm{B}_{mn}\, \partial_x \varphi_n + \mathrm{C}_{mn} \varphi_n = 0\ ,\ m = -2, -1, ..., M-1\ ,\ x \in X\ , \tag{3.20a}$$

$$\sum_{n=-2}^{M} \varphi_n = \psi \tag{3.20b}$$

$$\left[\sum_{n=-2}^{M} \left(\partial_x \varphi_n\, \mathrm{A}_{mn} + \frac{1}{2}\left(\mathrm{B}_{mn} - \partial_x h \left[Z_m\, Z_n \right]_{z=-h} \right) \varphi_n \right) \right]_{x=a} = 0\ ,\ m = -2, ..., M-1 \tag{3.20c}$$

$$\left[\sum_{n=-2}^{M} \left(\partial_x \varphi_n\, \mathrm{A}_{mn} + \frac{1}{2}\left(\mathrm{B}_{mn} \varphi_n - \partial_x h \left[Z_m\, Z_n \right]_{z=-h} \right) \right) \right]_{x=b} = 0,\ m = -2, ..., M-1, \tag{3.20d}$$

with

$$\mathrm{A}_{mn} = \int_{-h}^{\eta} Z_n \, Z_m \, dz \tag{3.21a}$$

$$\mathrm{B}_{mn} = 2\int_{-h}^{\eta} \partial_x Z_n \, Z_m \, dz + \partial_x h \left[Z_m \, Z_n \right]_{z=-h} \tag{3.21b}$$

$$\mathrm{C}_{mn} = \int_{-h}^{\eta} (\partial_x^2 Z_n + \partial_z^2 Z_n) \, Z_m \, dz - \boldsymbol{N}_h \cdot \left[(\partial_x Z_n, \partial_z Z_n) \, Z_m \right]_{z=-h} \tag{3.21c}$$

Eqs (3.19a)-(3.19c) & (3.20a)-(3.20d) comprise the classical coupled nonlinear free-surface evolution equations and the linear substrate problem as presented in Section 1.4.

In this simulation we are mainly interested on whether the model retains the constant form of the solitary wave (its free-surface elevation and free-surface potential) as it propagates. Such error estimates shall be carried out using the following general formula:

$$E_2[F] = \frac{\left\| F(x, T; \Delta t) - F_{Initial}(x, T) \right\|_2}{\left\| F_{Initial}(x, T) \right\|_2} , \tag{3.22}$$

where $\|.\|_2$: is the L^2 norm and $F(x,t;\Delta t)$: is the quantity in discussion.

Another important aspect of the problem is the examination of the conservation of the total mass and Hamiltonian of the solitary wave over a long period of time. These quantities will be presented in the form:

$$ER[H] = \left| \frac{H(t) - H(t_0)}{H(t_0)} \right| , \qquad ER[M] = \left| \frac{M(t) - M(t_0)}{M(t_0)} \right| \tag{3.23a,b}$$

Where $H = \frac{1}{2}\int_X \left[\psi \, G[\eta, h]\psi + g\eta^2 \right] dx$ is the Hamiltonian of the system

while $M = \int_X \left(\eta(x;t) + h(x;t) \right) dx$ is the Mass of the system

We will display the aforementioned quantities in a systematic manner. We made a number of simulations changing a number of different parameters of the system. These parameters are the space and time steps: dx and dt, the number of modes of the system and the order of the finite difference scheme. This way we can understand how fine discretization and the number of modes the system needs to present satisfactory convergence and what finite difference scheme is the most efficient computational wise. The domain of the simulations is of depth $h_0 = 1$ and of length $100h_0$. The solitary wave is of amplitude $a/h_0 = 0.4$ and initially is centered $25h_0$ from the left lateral boundary. The length of the domain is not large enough for

the simulation to be thought as a long-time one. Yet, this case is only used for the purpose of deducting important conclusions for the accuracy of the method. The behavior that the error will exhibit for this domain will also be seen in bigger ones, hence in this step there is no need for a bigger domain. The modes used for these simulations will vary from 6 to 12. The horizontal and time spacing will also vary with the constraint that the Courant number of the system will always be equal to $C = c\frac{dt}{dx} = 0.5$, where $c = 3.69056\left[m/\sec \right]$, the propagation speed of the solitary wave. Results of these simulations are presented below

Maximum Error of Conservation of Mass of every simulation						
	$dx = 0.8$	$dx = 0.4$	$dx = 0.2$	$dx = 0.1$	$dx = 0.05$	$dx = 0.025$
$m = 4$	$1.014\cdot10^{-4}$	$3.002\cdot10^{-6}$	$7.248\cdot10^{-8}$	$2.406\cdot10^{-8}$	$1.421\cdot10^{-8}$	$5.3108\cdot10^{-9}$
$m = 6$	$9.257\cdot10^{-5}$	$2.392\cdot10^{-6}$	$3.312\cdot10^{-8}$	$2.312\cdot10^{-8}$	$1.578\cdot10^{-8}$	$1.8744\cdot10^{-9}$
$m = 8$	$9.110\cdot10^{-5}$	$2.332\cdot10^{-6}$	$3.124\cdot10^{-8}$	$2.093\cdot10^{-8}$	$1.874\cdot10^{-8}$	$3.0459\cdot10^{-9}$
$m = 10$	$9.064\cdot10^{-5}$	$2.314\cdot10^{-6}$	$3.686\cdot10^{-8}$	$2.124\cdot10^{-8}$	$1.515\cdot10^{-8}$	$4.6860\cdot10^{-9}$
$m = 12$	$9.044\cdot10^{-5}$	$2.304\cdot10^{-6}$	$3.499\cdot10^{-8}$	$1.843\cdot10^{-8}$	$1.515\cdot10^{-8}$	$7.6538\cdot10^{-9}$

Table 1: Conservation of Mass error of all simulations for Courant number $C = 0.5$

Maximum Error of Conservation of Hamiltonian of every simulation						
	$dx = 0.8$	$dx = 0.4$	$dx = 0.2$	$dx = 0.1$	$dx = 0.05$	$dx = 0.025$
$m = 4$	$1.737\cdot10^{-3}$	$7.848\cdot10^{-5}$	$1.719\cdot10^{-6}$	$3.361\cdot10^{-7}$	$1.616\cdot10^{-7}$	$1.119\cdot10^{-7}$
$m = 6$	$1.740\cdot10^{-3}$	$8.196\cdot10^{-5}$	$2.897\cdot10^{-6}$	$9.507\cdot10^{-8}$	$4.427\cdot10^{-9}$	$3.765\cdot10^{-9}$
$m = 8$	$1.739\cdot10^{-3}$	$8.199\cdot10^{-5}$	$2.908\cdot10^{-6}$	$9.767\cdot10^{-8}$	$6.540\cdot10^{-9}$	$1.378\cdot10^{-9}$
$m = 10$	$1.739\cdot10^{-3}$	$8.199\cdot10^{-5}$	$2.909\cdot10^{-6}$	$9.823\cdot10^{-8}$	$5.920\cdot10^{-9}$	$6.178\cdot10^{-9}$
$m = 12$	$1.739\cdot10^{-3}$	$8.199\cdot10^{-5}$	$2.914\cdot10^{-6}$	$9.851\cdot10^{-8}$	$7.101\cdot10^{-9}$	$1.138\cdot10^{-8}$

Table 2: Conservation of Hamiltonian error of all simulations for Courant number $C = 0.5$

Amplitude Error of Solitary Wave at the end of every simulation						
	$dx = 0.8$	$dx = 0.4$	$dx = 0.2$	$dx = 0.1$	$dx = 0.05$	$dx = 0.025$
$m = 4$	$-6.44\cdot10^{-2}$	$-5.09\cdot10^{-3}$	$-4.06\cdot10^{-3}$	$-1.69\cdot10^{-3}$	$-1.15\cdot10^{-3}$	$-1.03\cdot10^{-3}$
$m = 6$	$-6.39\cdot10^{-2}$	$-4.24\cdot10^{-3}$	$-3.25\cdot10^{-3}$	$-7.87\cdot10^{-4}$	$-2.09\cdot10^{-4}$	$-6.80\cdot10^{-5}$
$m = 8$	$-6.39\cdot10^{-2}$	$-4.23\cdot10^{-3}$	$-3.23\cdot10^{-3}$	$-7.70\cdot10^{-4}$	$-1.92\cdot10^{-4}$	$-5.04\cdot10^{-5}$
$m = 10$	$-6.39\cdot10^{-2}$	$-4.23\cdot10^{-3}$	$-3.23\cdot10^{-3}$	$-7.68\cdot10^{-4}$	$-1.90\cdot10^{-4}$	$-4.88\cdot10^{-5}$
$m = 12$	$-6.39\cdot10^{-2}$	$-4.23\cdot10^{-3}$	$-3.23\cdot10^{-3}$	$-7.68\cdot10^{-4}$	$-1.90\cdot10^{-4}$	$-4.85\cdot10^{-5}$

Table 3: Amplitude error of solitary wave at the end of the simulations for Courant number $C = 0.5$

The phase error of the solitary wave is smaller than the step of the horizontal discretization for every case. This means that the simulations did not last long enough for this error to have any physical meaning and as a result will not be presented here. From these results, we observe that the minimum error in the relative conservation of Mass and Hamiltonian is around 10^{-9}.

This threshold may be attributed to the nonlinearity of the problem. It should also be noted that the amplitude error is almost independent of the number of used modes. This error is mainly attributed to the low order representation of the free-surface elevation with the use of finite differences (first order polynomials between two consecutive horizontal points). Hence, it is logical when no horizontal point exists exactly where the center of the solitary wave should be, the wave to appear of lower amplitude. Since it is almost impossible for a horizontal control point to coincide with the center of the solitary wave, the solitary wave appears to have a slightly lower amplitude. This observation can be showcased from the fact that all measurements at Table 3 present smaller amplitudes than the theoretical amplitude of the wave.

We now proceed to do long time simulations for a domain of depth $h_0 = 1$ and of length $600h_0$. The amplitude of the solitary wave is chosen to be $a/h_0 = 0.4$. The wave is initially centered at $50h_0$ from the left lateral boundary of the domain. The initial data of the problem are taken from the Matlab code of (Clamond & Duthykh, 2013). The lateral boundaries of the domain are assumed to be fully reflecting walls. A 4th order finite difference scheme is utilized and 8 total modes are used. The horizontal discretization of the problem has a step $dx = 0.1h_0$ while the time-step is $dt = 0.02$. We present the conservation of Mass, the conservation of Momentum and Hamiltonian.

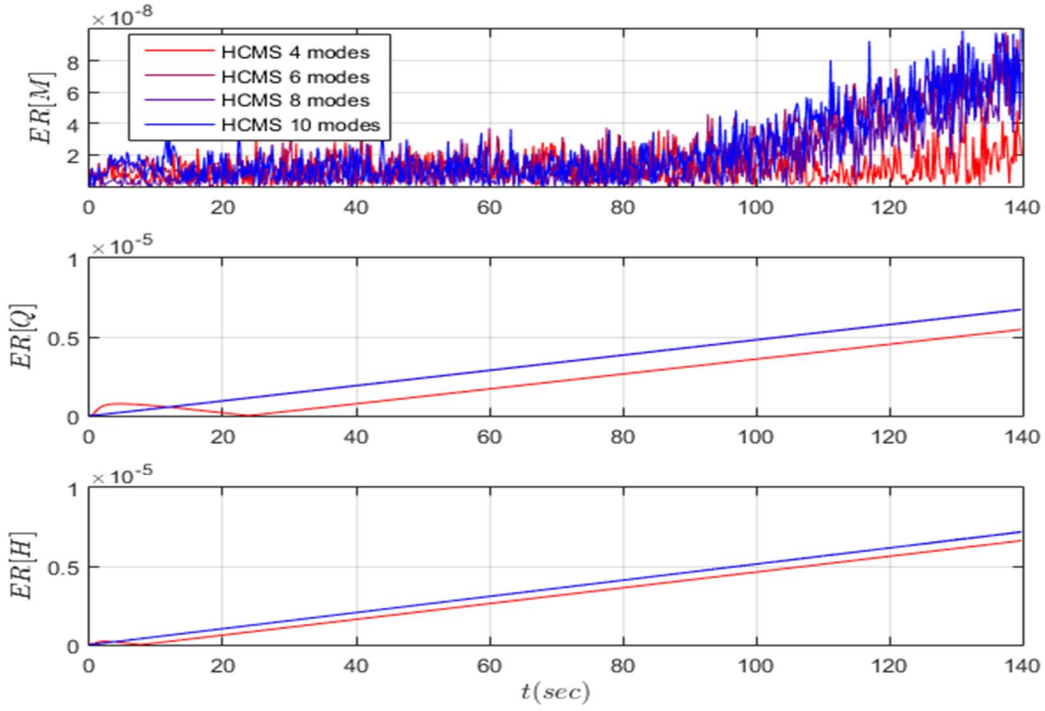

Figure 10: Conservation of Mass, Momentum and Hamiltonian for the long-time simulation.

As can be seen from the above results, the model can efficiently conserve the aforementioned quantities without for many modes. Only the solution for 4 modes appear to have a slightly different error for the conservation of the Momentum and the Hamiltonian, with all the other

cases been practically identical. We now move on to compare the free-surface elevation of these simulations for the last time-step. We also present the theoretical position for the solitary wave that can be calculated from the constant speed that is given by the code of (Clamond & Duthykh, 2013). The results are presented below:

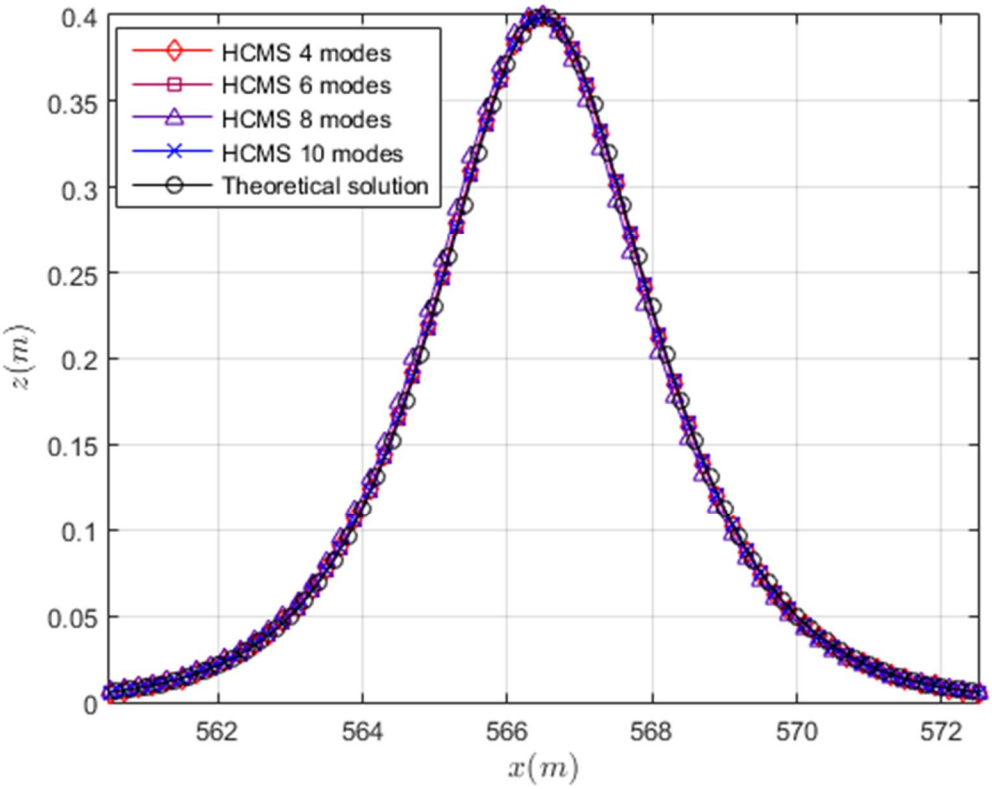

Figure 11: Comparison of free-surface elevation between simulations and the theoretical solution from the constant speed taken from (Clamond & Duthykh, 2013), at time $t = 139.98[\text{sec}]$

Once, again the results for the simulations are almost identical. This could mean that the spatial and time discretization that was used was very fine, resulting in early convergence (with regard to the number of modes) for the error of the method. Furthermore, we can also conclude that not many equations of the substrate problem are needed for such cases. Another, important trait of the model is the fact that no dispersive trail is developed as the solitary wave propagates. This result is presented in Figure 3 below for 4 different instants of the simulation. This trait is very positive and encouraging for the accuracy of the model, since many models exhibit the formation of a dispersive trail during the propagation of solitary waves, (i.e (Mitsotakis *et al.*, 2014)).

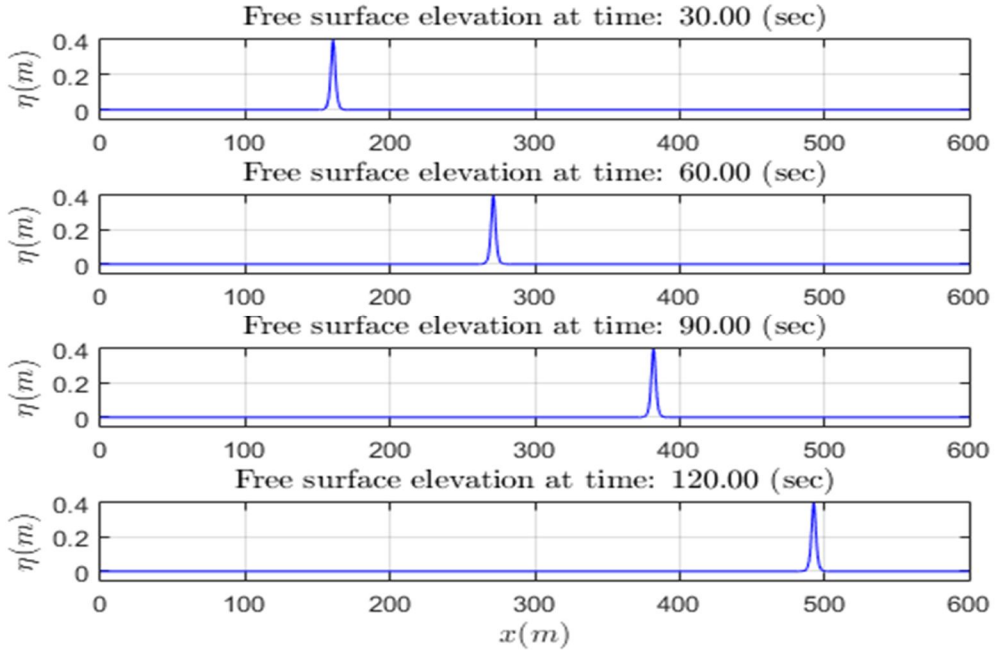

Figure 12: Free-surface elevation at given time instants for the simulation with 8 modes in total.

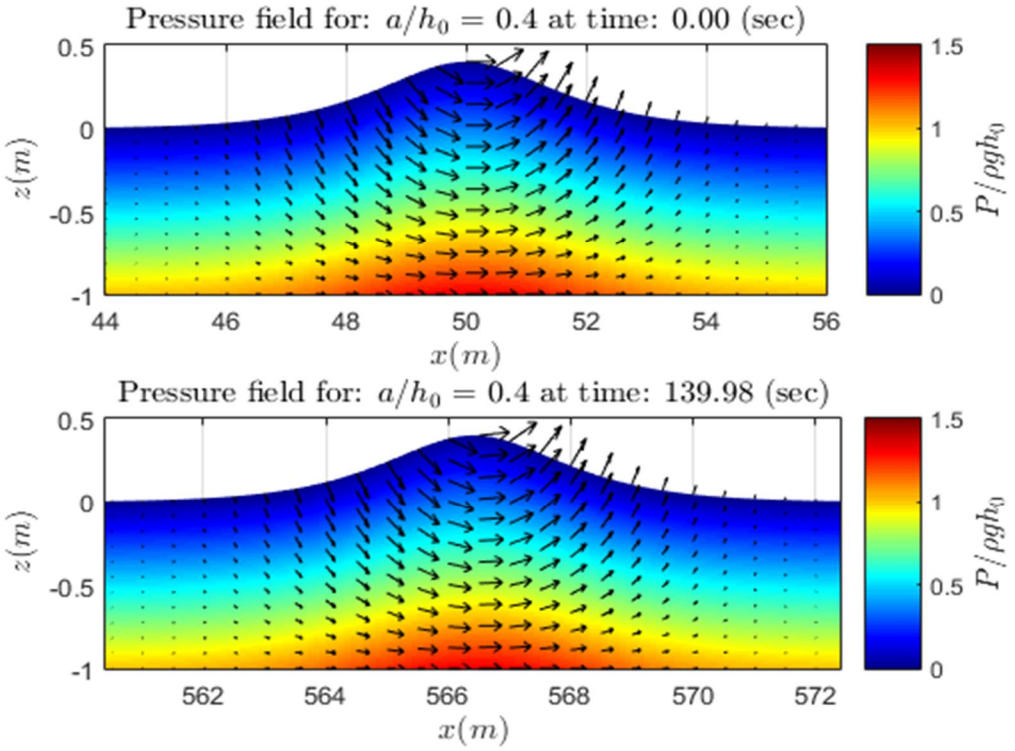

Figure 13: Comparison of the pressure and velocity field of a solitary wave for $a/h_0 = 0.4$ at different instants, using 8 modes.

Reflection of solitary waves on a vertical wall

We now proceed to present results for the case of reflection of solitary waves on a vertical wall. This case can be assumed equivalent to a head-on symmetric collision of two identical solitary wavers for the case of an irrotational, incompressible and inviscid flow. Such a problem will allow us to examine the validity and efficiency of the wall conditions we defined on the lateral boundaries of the domain. Also, it will test the behavior of the simulation to an abrupt rise in the nonlinearity of the problem. In papers like (Maxworthy, 1976) and (Chan & Street, 1970) experimental results we presented for the case of solitary symmetric collision and reflection on walls for a wide range of amplitudes. A comparison of the maximum run-up calculated by the simulation, for the various amplitudes, with these results is a way to evaluate whether the code can model effectively such highly nonlinear and sudden phenomena. These results can also be compared with simulations from other methods, such as the modified Serre-Green-Naghdi system presented in (D Mitsotakis et al., 2015), the series expansion of the Dirchlet to Neumann operator in (Craig, Guyenne, Hammack, Henderson, & Sulem, 2006), a KdV model presented in (Byatt-Smith, 1988), a Boundary Element method presented in (Cooker, Weidman, & Bale, 1997) and a Boundary Integral method presented in (Chambarel, Kharif, & Touboul, 2009). Furthermore, the conservation of mass and Hamiltonian throughout the simulations will be presented as a way to check the efficiency of the problem. Finally, the instantaneous wall-force from the collision will be presented as well as a comparison of results from the wall-reflection model and a symmetric collision since these two models are theoretically equivalent. An important note for these simulations can be found in the experimental report of Maxworthy, where for solitary waves of amplitudes larger than $a/h = 0.60$ a jet like formation is observed during the collision which breaks into individual drops. Such a phenomenon leads to a multivalued free-surface elevation and as such, our simulations are expected to break for these values of amplitudes (otherwise the simulation would model the problem incorrectly).

For the setup of this problem we assume a domain of depth $h_0 = 1$ and length $100\,h_0$. For the lateral boundary conditions we use the Robin type boundary conditions:

$$\sum_{n=-2}^{\infty}\left(\left[\partial_{x_1}\varphi_n\right]_{x_1=a}\mathrm{A}_{mn}^{(a)}+\left[\varphi_n\right]_{x_1=a}\mathrm{B}_{mn}^{(a)}\right)=0\,,\ n\geq -2\,, \tag{3.24}$$

The solitary wave is assumed to start from the middle of the domain and heading towards the right boundary of the domain. For the initial data of the problem we use once again the Matlab code of the method presented in (Clamond & Dutykh, 2013). Throughout all the simulations 4th order finite differences are used as well as 8 modes in total. The space and time discretization for amplitudes up to $a/h_0 = 0.35$ are $dx/h_0 = 0.05$ and $dt = 0.01$, while for higher amplitudes we halve the above steps. Finally we should mention that for the wave amplitude of $a/h_0 = 0.60$ the domain had a total length of $50h_0$ with the initial wave be centered at a distance of $30h_0$ measured from the left wall. We now compare the

maximum runup we calculated for the solitary waves at the wall with experimental results and other numerical models:

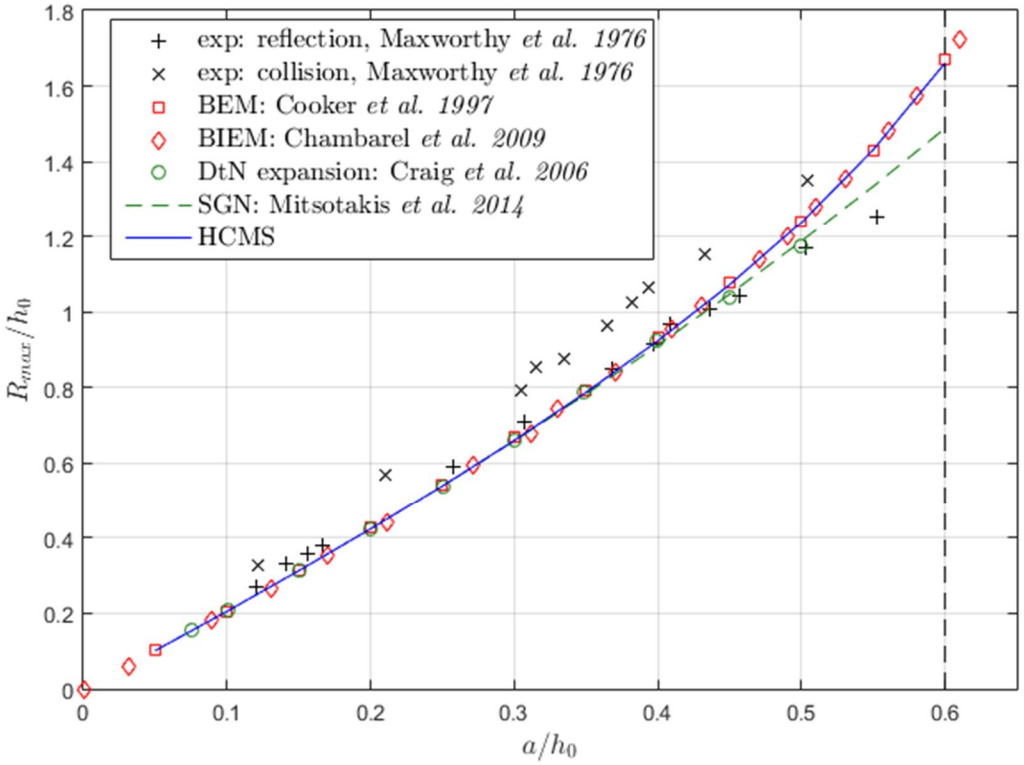

Figure 14: Comparison of Maximum run-up for wave collision of different simulations and experimental results.

From the above figure we can see that the experimental results deviate significantly from the numerical simulations, which are all based on the assumptions of irrotationality and inviscid flow. Furthermore, the experimental data show a significant difference for the maximum run-up for the case of a symmetrical wave collision and a wall-reflection. These differences may be attributed to viscosity and the inability to generate identical waves in a wave tank. As a result we conclude that a safer way to estimate the accuracy of our calculations is their comparison with the results derived from the fully nonlienear BEM models presented above. The BEM and BIEM models presented above are on a very good agreement with our simulations for all the amplitudes we could run. On the other hand the methods of Craig and Mitsotakis agree with ours until the amplitude $a/h = 0.40$ and deviate from ours after that. In addition, our assumption that we would be unable to simulate collisions for solitary waves of amplitude larger than $a/h = 0.60$ (in contrast with the BEM models) is verified from the above Figure. This behavior shows us the robustness of the model since it was able to simulate all the required cases until the physical aspects of the problem forbade it. Therefore, it is safe to assume that the break-down of our simulations after the amplitude $a/h = 0.60$ were not due to numerical instabilities of the discretized model. From these results, we can also assume that for other simulations we may be able to assume when waves break or overturn from the failure of the code (and attribute the failure to purely numerical reasons).

We now present the conservation of mass and energy for the above simulations:

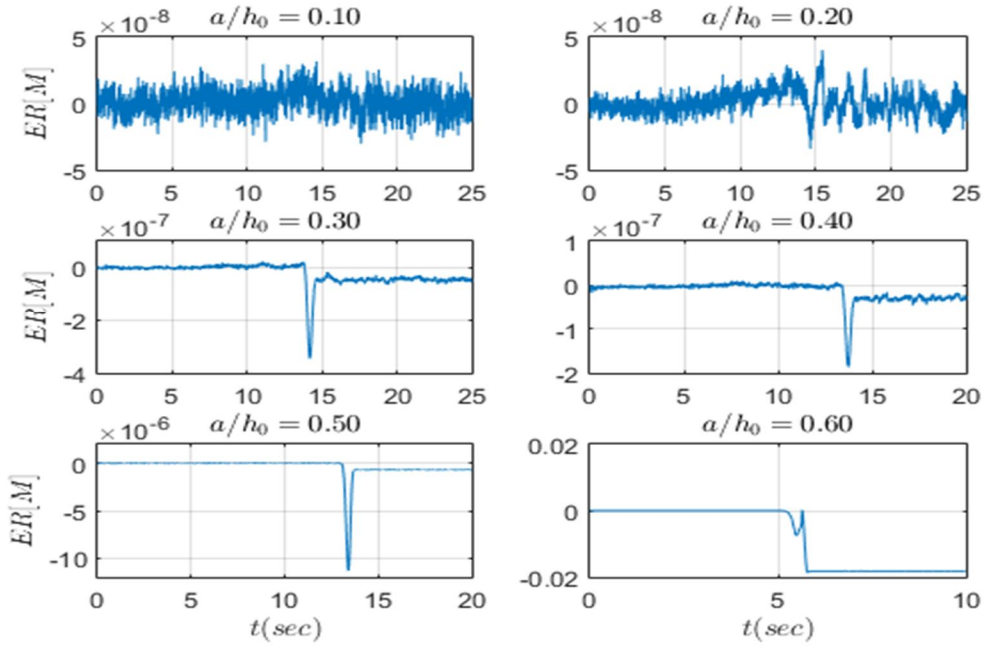

Figure 15a: Conservation of Mass in our simulations for a variety of amplitudes.

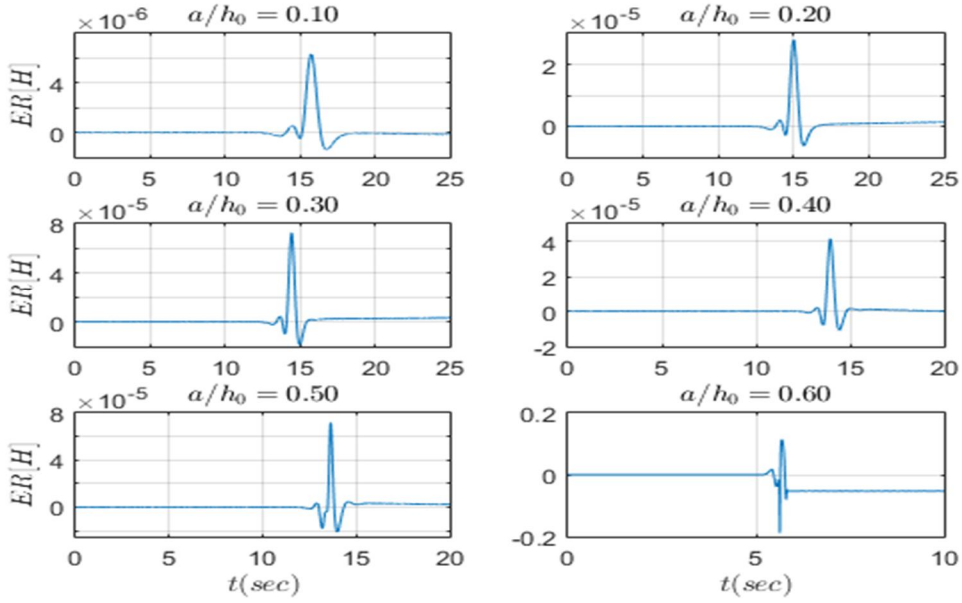

Figure 15b: Conservation of Hamiltonian in our simulations for a variety of amplitudes.

From the above figures we can observe that the conservation of Mass and Hamiltonian showcases a significant raise in the relative error during the reflection at the wall. This observation can be attributed to the sudden rise of the nonlinearity of the problem during the reflection. Furthermore, the conservation of Mass and Hamiltonian are both at satisfactory levels for all simulations until amplitude $a/h_0 = 0.55$. For amplitude $a/h_0 = 0.60$ the conservation of both quantities is severely hindered during the reflection at the wall and as a

result the simulation after the reflection at the wall cannot be deemed reliable. A relatively strange result is the accuracy at which we were able to calculate the maximum run-up for the case of $a/h_0 = 0.60$ in comparison with the BEM results, despite the drastic drop of the conservation of Mass and Hamiltonian. Another interesting result that needs to be presented is the change of amplitude the waves experience after the reflection as well as the dispersive trail that may be formed behind them. The results of the simulations are presented in the Figure below:

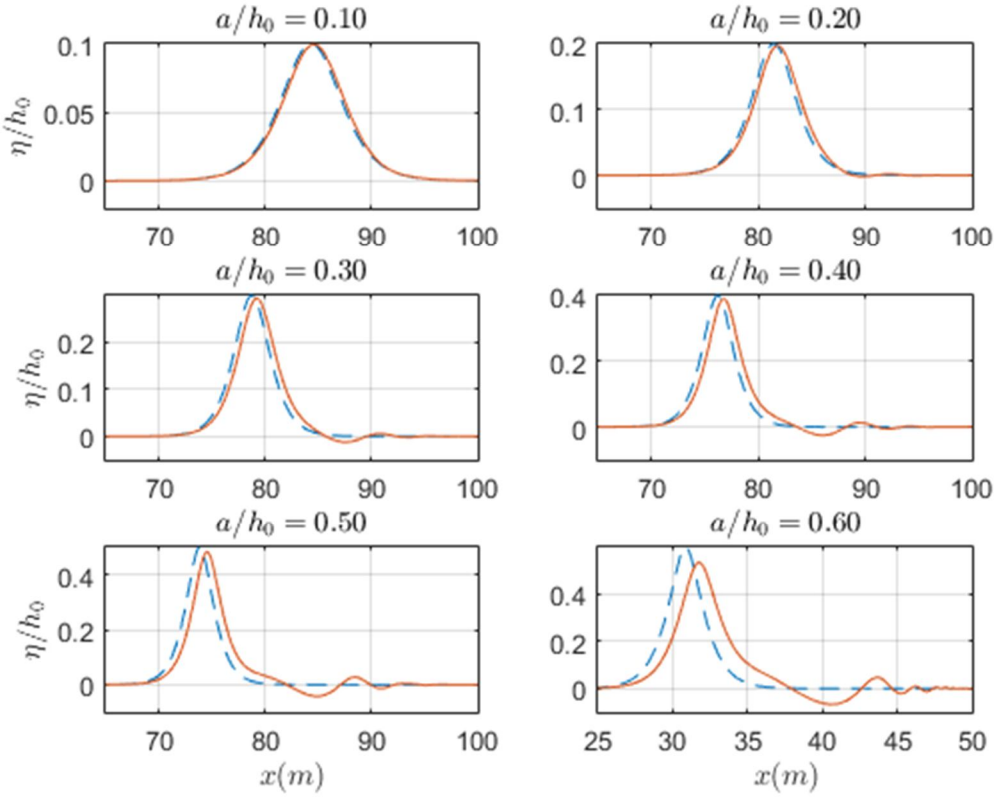

Figure 16: Comparing the resulted reflected wave (solid line) with the free-surface elevation of a perfect reflection (dashed line) at a given time.

Note: All comparisons are done at time $t = 20$, except for the case where $a/h_0 = 0.60$ and the results are presented for $t = 10$ because for that case the length of the domain is $50h_0$.

While the amplitude of the solitary wave rises, we observe a larger dispersive trail behind the reflected solitary wave. As a result, the amplitude of the reflected wave becomes significantly lower than the initial wave. However, the results for the case of $a/h_0 = 0.60$ cannot be perceived with much trust since the conservation of Mass and Hamiltonian were severely hindered during the reflection. Another quantity that is of great interest for practical applications is the force the solitary waves put upon the vertical wall. Such results can be used as extreme cases for coastal and offshore structures (due to the high amplitude and velocity of

the solitary waves). Below, we present results for the force applied on the wall due to the collision of the solitary wave:

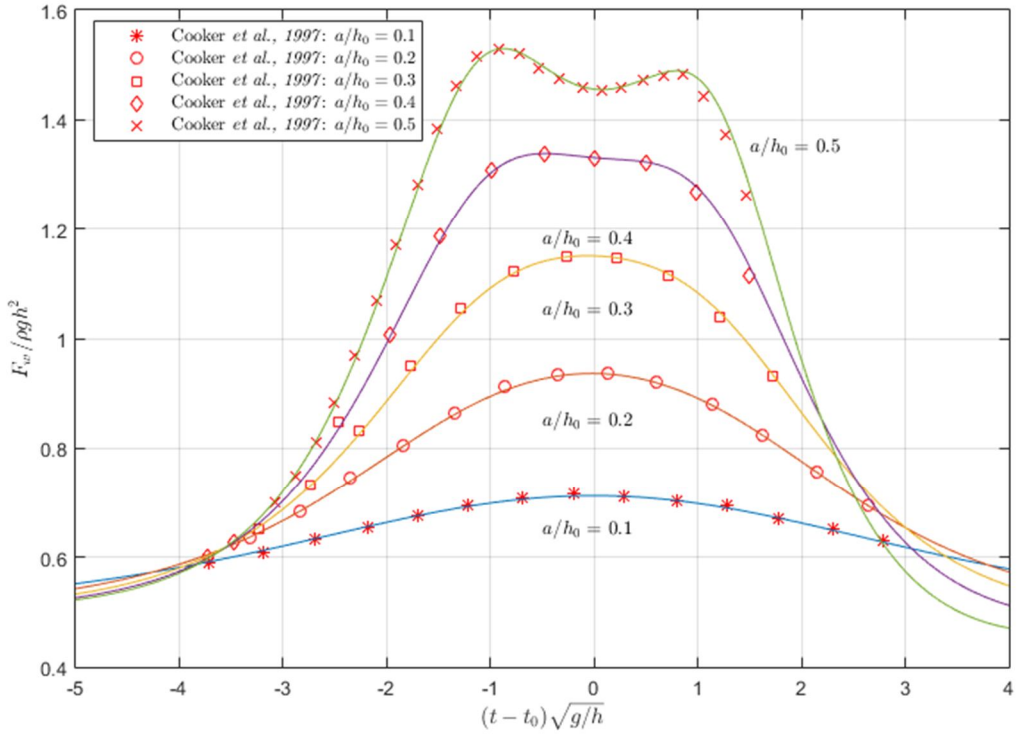

Figure 17: Comparison of instantaneous wall force during the collision from HCMS (solid line), and (Cooker et al., 1997) (BEM).

In the above Figure the instantaneous wall force is calculated as $F_W = \int_{-h}^{\eta} p\,dz$, where p is the pressure applied at the right wall and given by the formula:

$$\frac{p}{\rho} = -g\,z - \partial_t \Phi - \frac{1}{2}\left|\nabla\Phi\right|^2, \tag{3.25}$$

with the time t_0 being the time of the maximum run-up for every case.

From the above figure we can observe a very good agreement of our calculation with the numerical results derived by. We should also note that similar results were shown in (Chambarel, *et al.*, 2009), with the results being in perfect agreement with those of (Cooker, *et al.*, 1997). (with the exception that the paper of 2009, presents results for higher amplitudes). For solitary waves of amplitude $a/h_0 \le 0.3$, the maximum wall force is observed during the maximum run-up. For solitary waves of higher amplitude the maximum wall force occurs before the maximum run-up of the collision occurs. Cooker observed that the upsurging wave forms a narrow jet before the maximum run-up and that could be the cause of this maximum force. This observation was also confirmed by (Chambarel, *et al.*,

2009), while a sudden rise of the amplitude of the solitary wave can also be seen in our simulations. Furthermore, a second maximum of the pressure at the right wall is observed and as a result a second maximum of the wall force occurs. This behavior was able to be observed from our model as well. It should also be noted that the pressure of the fluid was calculated fairly simple, by differentiating the series expansion $\Phi(x,z;t)=\sum_{n=-2}^{M}\varphi_n(x;t)Z_n(z;t)$ by terms. Many of these space and time derivatives can be calculated analytically helping as minimized the error of an numerical differentiation scheme. Hence, the procedure of calculating the pressure and velocities of the fluid is straightforward and requires little computational time with this model (while it is a much more time consuming task for BEM models). In the figures below, we calculate the pressure and kinetic energy density as well as the horizontal and vertical velocity distributions for the case $a/h_0=0.5$ at the time of maximum runup:

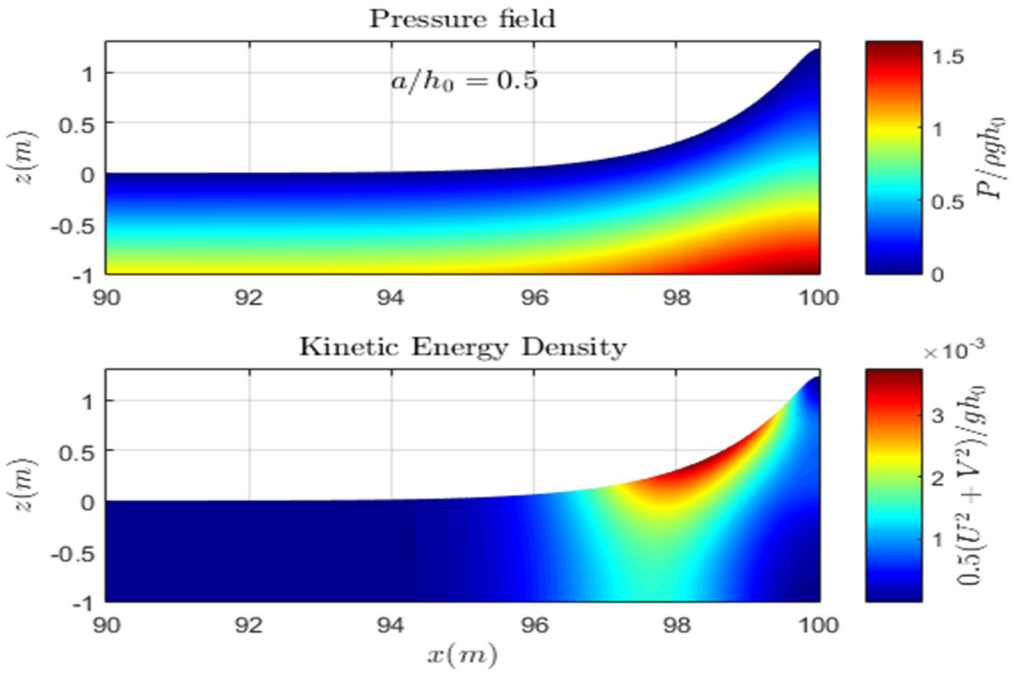

Figure 18a: Pressure and kinetic energy density during maximum runup for $a/h_0=0.5$

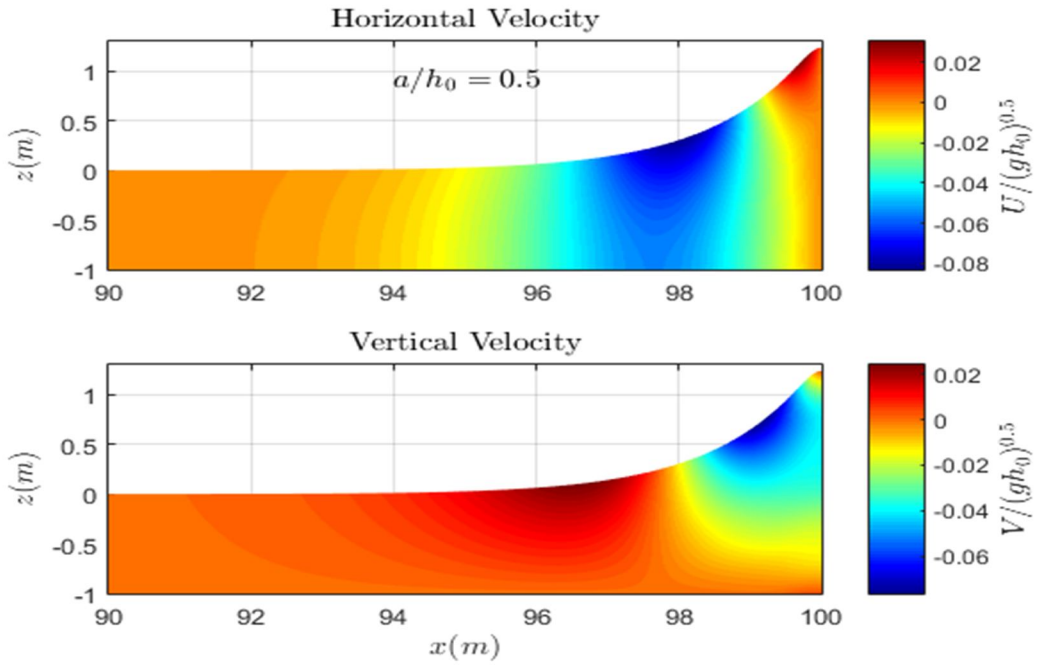

Figure 18b: Horizontal and vertical velocity during maximum runup for $a/h_0 = 0.5$

As said in the beginning of this subsection, the problem presented of the reflection of a wave from a vertical wall, is physically equivalent to a symmetric collision of two identical waves. For us to test the above statement for our model we simulate a symmetric collision of two solitary waves of amplitude $a/h_0 = 0.4$ and compare the history of the calculated free-surface elevation for the two simulations. The results presented below are identical ensuring the physical

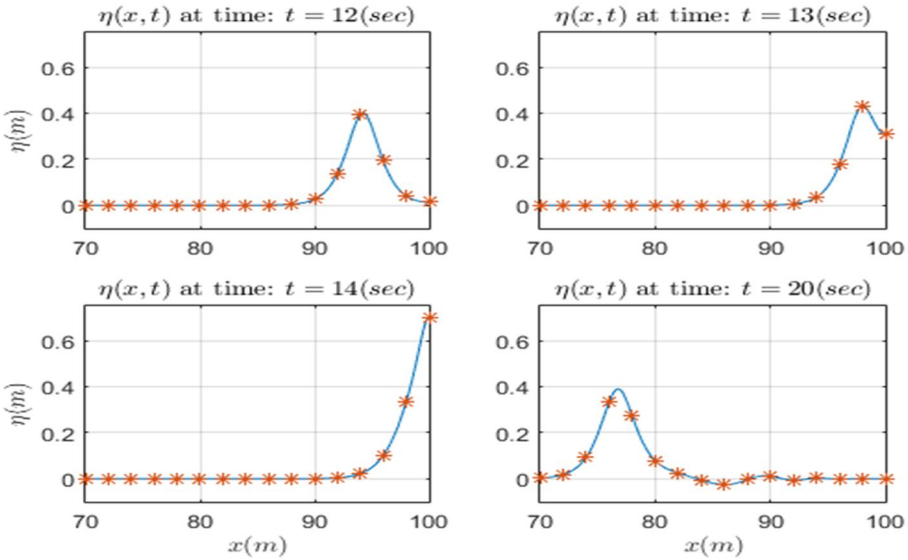

Figure 19: Free-surface elevation at given time for symmetric collision (solid line) and reflection to wall (*).

Asymmetric collision of solitary waves

We now simulate the case where two solitary waves of different amplitudes collide head-on. Such a problem cannot be modeled through a collision of a solitary wave with a fully reflecting wall since the problem is asymmetrical. We will present the cases for which numerical simulations are made in (Chambarel et al., 2009) and analytical results presented in (Su & Mirie, 1980). Four cases will be presented below for which we shall examine the maximum run-up and their conservation of Mass and Hamiltonian. The first case has a domain of depth $h_0 = 1$ and length $160h_0$. In this problem a wave of amplitude $a_l / h_0 = 0.4$ travelling from left to right, collides with a wave of amplitude $a_r / h_0 = 0.1$ travelling from right to left. The two solitary waves at centered at positions $x_r = 40h_0$ and $x_l = 120h_0$ respectively (measured from the left lateral boundary). For the other cases the depth of the domain is $h_0 = 1$ and of length $100h_0$. The two solitary waves are centered at positions $x_r = 25h_0$ and $x_l = 75h_0$ respectively (measured from the left lateral boundary). A 4th order finite difference scheme is used from the calculations with 8 modes in total. The horizontal discretizations has a step $dx = 0.05h_0$ while the time discretization of the problem has a time-step $dt = 0.01$. The initial data for these problems is again taken from the Matlab code of Clamond *et al*. The maximum run-up for the tested cases is presented below and compared with the papers mentioned above:

Left-to-Right Solitary wave	Right-to-Left Solitary wave	Maximum Run-Up		
		HCMS	Chambarel *et al.*	Su & Mirie
$a_l / h_0 = 0.4$	$a_r / h_0 = 0.1$	0.5234	0.5239	0.5275
$a_l / h_0 = 0.4$	$a_r / h_0 = 0.3$	0.7854	0.7867	0.7915
$a_l / h_0 = 0.5$	$a_r / h_0 = 0.25$	0.8411	0.8422	0.8477
$a_l / h_0 = 0.6$	$a_r / h_0 = 0.2$	0.8892	0.8903	0.8960

Table 4: Comparison of maximum run-up between the three methods for a variety of cases.

The results seem to be in good agreement with the ones presented in (Chambarel et al., 2009) and less with the results given by (Su & Mirie, 1980). The highest maximum run-up is given by Su & *et al* while the lowest maximum run-up is given by our method. Finally we present the conservation of Mass and Hamiltonian for all the above methods:

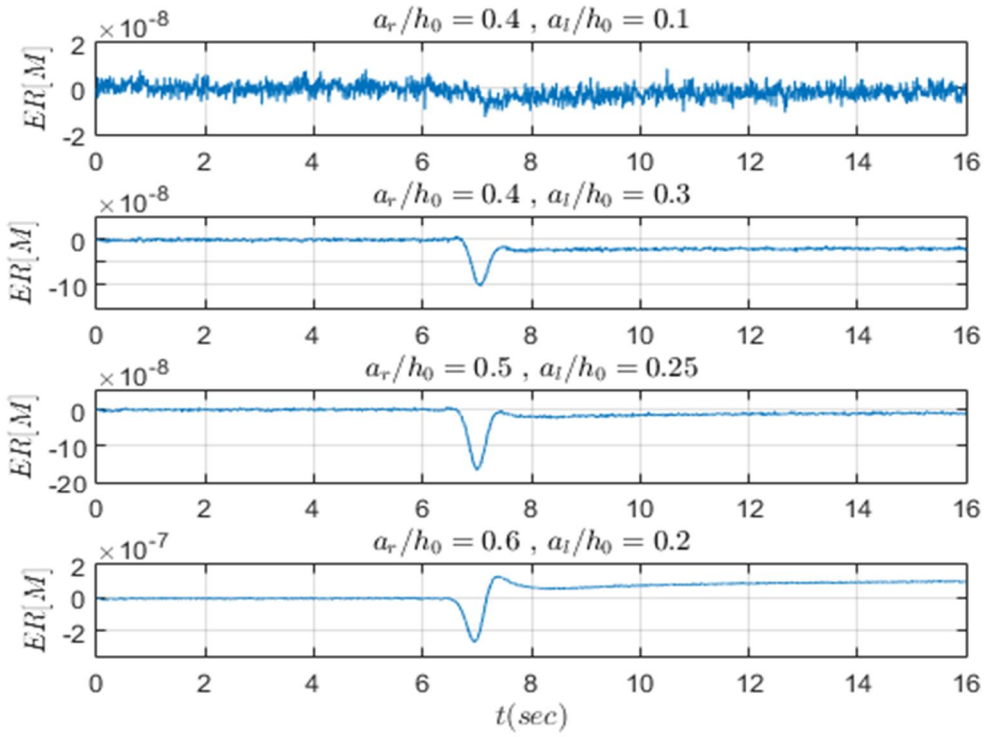

Figure 20a: Conservation of Mass for all the asymmetric collision cases.

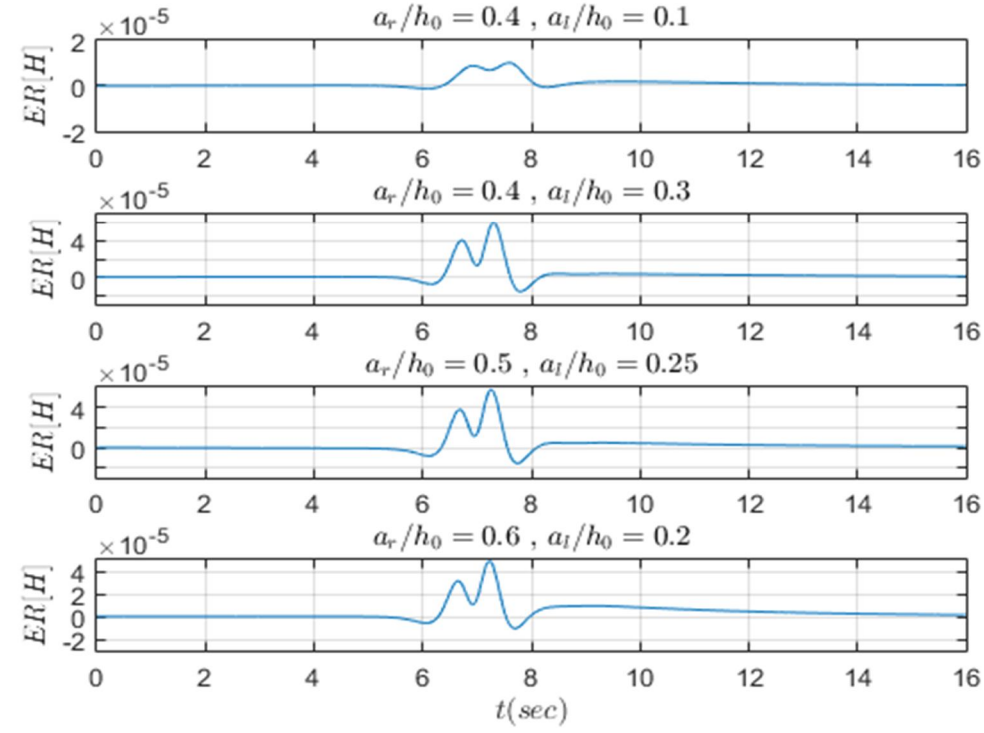

Figure 20b: Conservation of Hamiltonian for all the asymmetric collision cases.

3.4 Application on Variable Bottom Bathymetry

In this section we test the code on cases with variable bathymetry. In more detail, we concern ourselves with the propagation of solitary waves over abrupt changes in the seabed geometry, as well as geometries that lead to the breaking (or overturning) of the initial wave. We can therefore check the ability of the code to simulate problems in near breaking conditions (to sustain the physical consistency of the problem before the wave breaks or overturns). We present results concerning the conservation of Mass and Hamiltonian during the simulations and compare our results with experimental data whenever possible.

Solitary wave over a step

The first case we examine is a sudden decrease of the depth in the form of a step. This case was studied experimentally and numerically by (Seabra-Santos *et al.*, 1987) and results of our simulation will be compared with the corresponding experimental data presented in the aforementioned paper at certain stations. The domain of the problem has an initial depth of $h_0 = 0.2[m]$ and a length of $80[m]$. The step is located at position $x = 40[m]$ (the center of the domain) with the depth changing to $h_1 = 0.1[m]$. In theory our model cannot simulate problems with discontinuities on the bottom bathymetry. In the paper (Seabra-Santos *et al.*, 1987) for the numerical simulations, the authors (facing the same problem) used a sinusoidal approximation for the seabed's step with a total length of $0.60[m]$. For our simulation will shall utilize the same seabed, that is described in more detail as:

$$h(x) = \begin{cases} 0.2\,, & x \in [\,0, 39.7\,) \\ 0.15 - 0.05\sin\left(\pi \dfrac{x-40}{0.6}\right), & x \in [\,39.7, 40.3\,] \\ 0.1\,, & x \in (\,40.3, 80\,] \end{cases}, \tag{3.26}$$

The initial solitary wave has an amplitude $a/h_0 = 0.1825$ and is centered at the position $x = 37.5[m]$ (at the same position as in the numerical simulations of the paper mentioned above). The initial data is taken from the Matlab code of (Clamond & Duthykh, 2013). A 4^{th} order finite difference scheme is used together with 8 modes in total. The step of the horizontal space discretization is taken to be $dx = 0.008[m]$ and the time-step is taken as $dt = 0.0035[\text{sec}]$. We now present the conservation of Mass and Hamiltonian throughout the simulation:

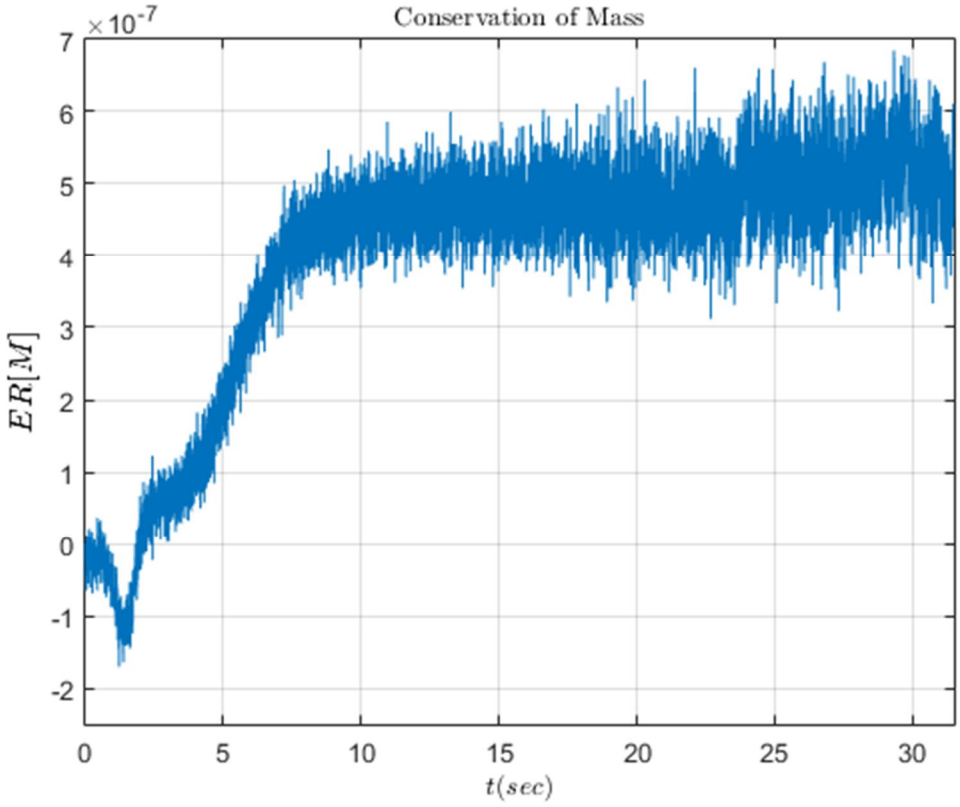

Figure 21a: Relative error of the Mass conservation for the simulation.

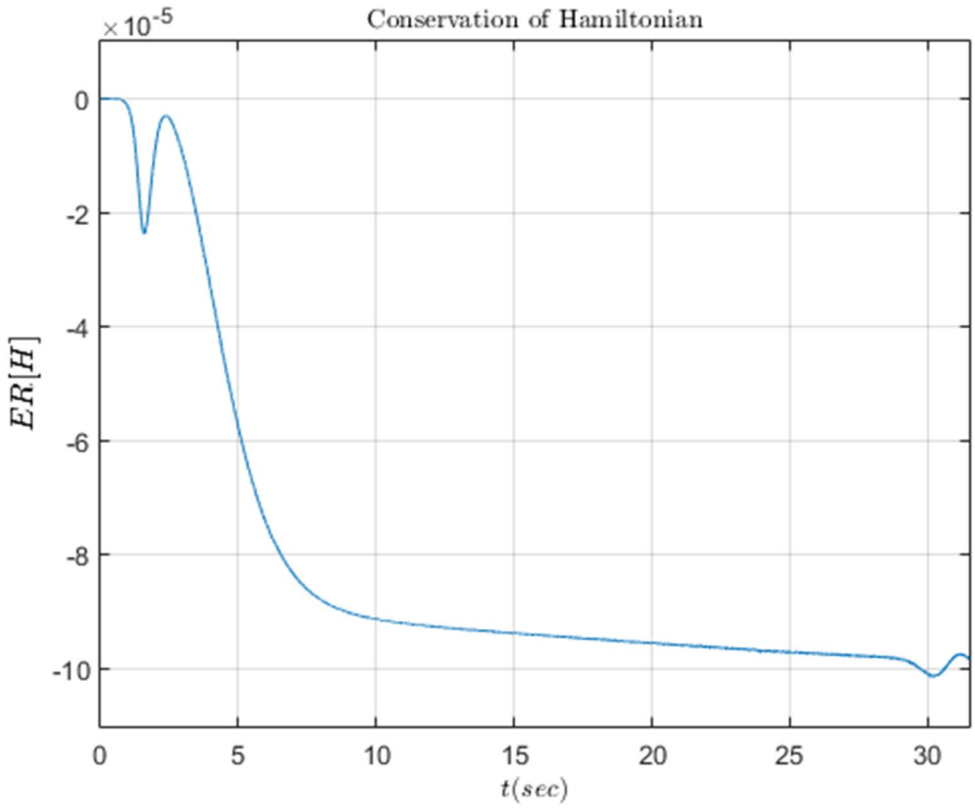

Figure 21b: Relative error of the Hamiltonian conservation for the simulation

The relative error of conservation of mass and Hamiltonian of the system appear to within acceptable limits. In Figure 21 we also present the time-evolution of the free-surface elevation of the problem (these results are used here for the examination of the conservation relative errors). The first (smaller) rise in the Hamiltonian error takes place during the reflection of a part of the solitary wave due to the step. The second and much larger rise in the error of the conservation of the Hamiltonian happens when the leading solitary wave breaks into two separate solitary waves. This sudden phenomenon appears to be the reason for this drop of accuracy as after this phenomenon error does not rises significantly. We also observe that the above phenomena have an effect on the conservation of Mass yet the magnitude of the error is much smaller. The break of the solitary wave once it passes in the shallow region is attributed to the sudden rise of nonlinearity. The initial solitary wave grows in amplitude, then grows in wavelength and as a result decreases in amplitude finally breaking into two solitary waves. The leading formed solitary wave has an amplitude $a_1 / h_1 = 0.624$ and the following solitary wave has an amplitude $a_2 / h_1 = 0.218$ with a dispersive trail following it. Even though the amplitudes of these solitary waves are much smaller than the amplitude of the initial wave, their non-dimensional amplitudes are quite larger. This result accounts for the sudden rise in the nonlinearity of the problem which as a result leads to the separation of the initial wave into two. Finally, the reflected wave, propagating to the left of the domain, forms a dispersive trail as the simulation evolves.

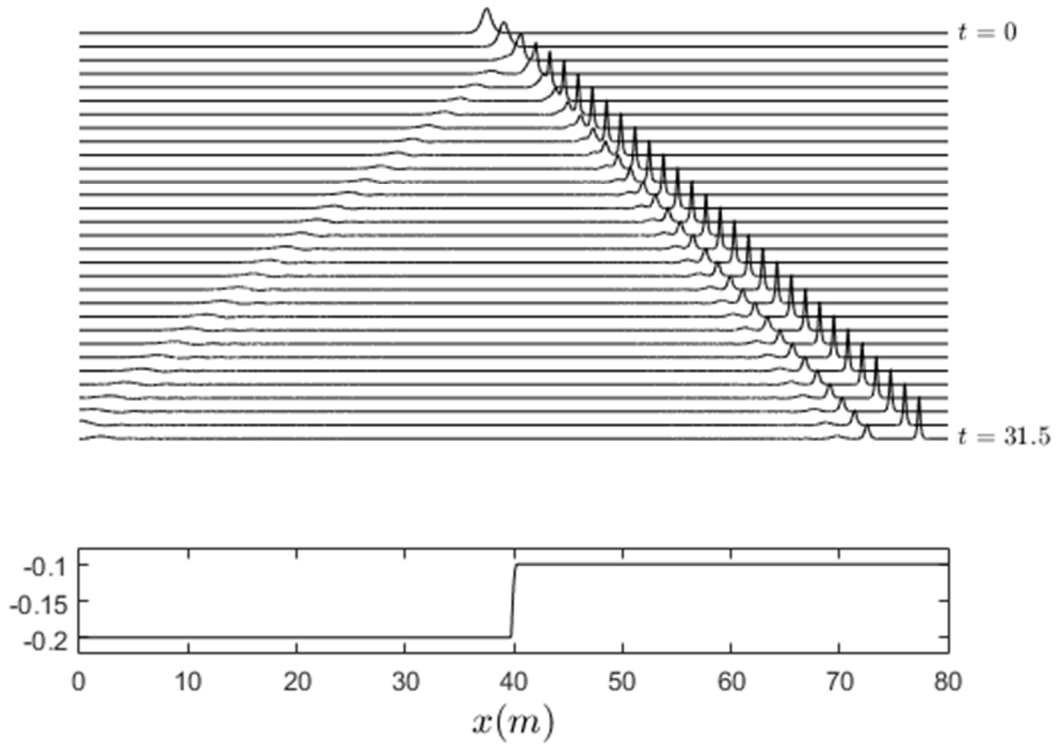

Figure 22: Evolution of the free-surface elevation as the solitary wave propagates.

In the paper (Seabra-Santos et al., 1987) experimental results were given for the case studied here, with the difference that the experiment lasts until $t = 10.74[\text{sec}]$. As a result we compare these results with our numerical data at given stations of the domain. From these figures we see that the experimental results produce waves that are slightly slower and of smaller amplitude, with these differences being more visible at the farthest stations. Furthermore, this difference is more visible in the case of the reflected wave train and much less for the case of the transmitted waves. As a result, the dissipation due to viscosity could explain this divergence between experimental and numerical results combined with the fact that solitary waves are much less affected by dissipation than regular periodic waves.

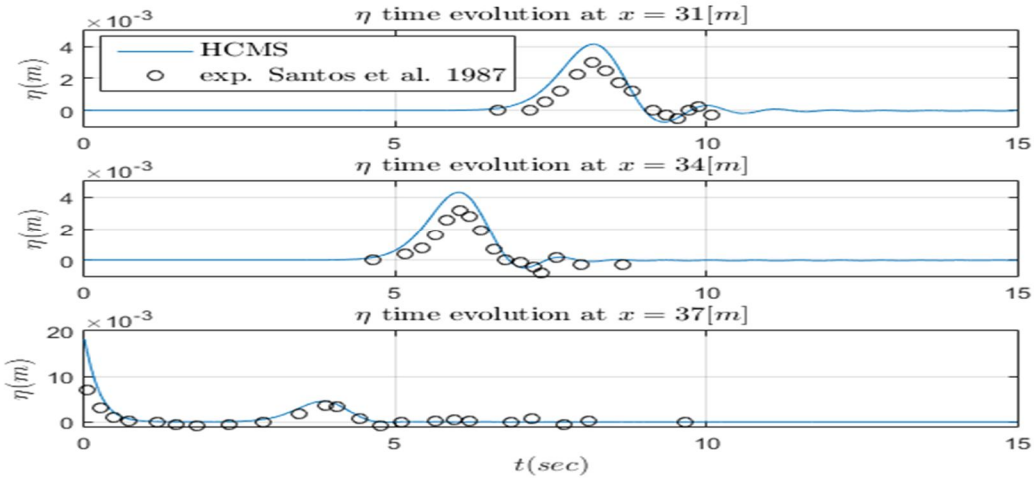

Figure 23a: Comparison of experimental data presented by Seabra-Santos et al. with numerical data of our model for the reflected waves.

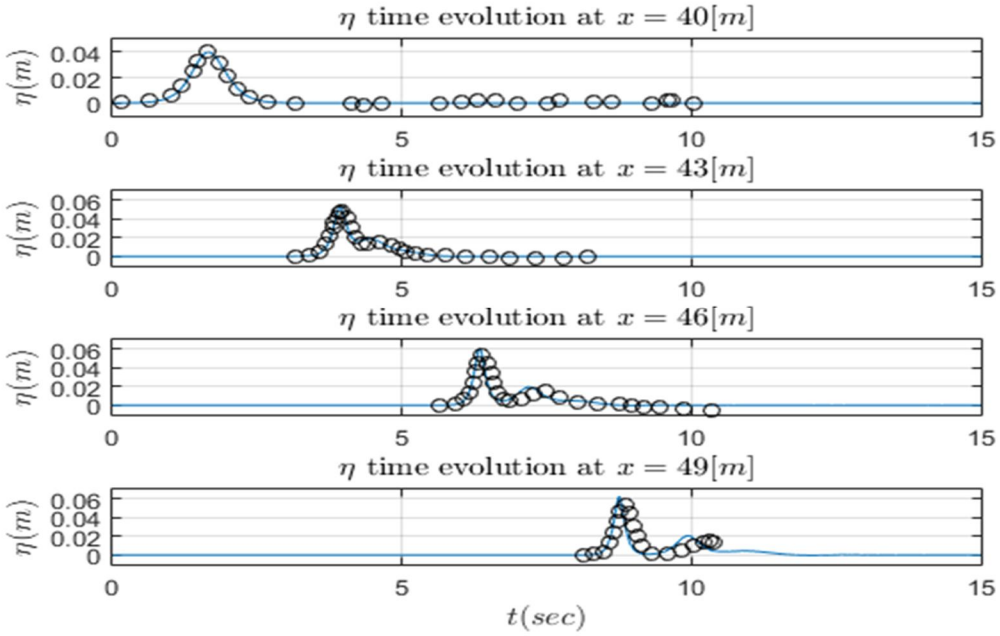

Figure 23b: Comparison of experimental data presented by Seabra-Santos et al. with numerical data of our model for incident and transmitted waves .

Shoaling of solitary waves over a plane beach

The propagation of a solitary wave (initially travelling over a flat bottom) over a plane beach that ends up to the shore line is called shoaling. It is obvious that in such a case, the solitary wave is bound to eventually break (and therefore end our simulation) before it reaches the shore line. The two aforementioned phenomena in nearshore areas are of great importance for the domain of coastal engineering. Especially the shoaling of solitary waves (granted their large energy and amplitudes) can act as an extreme design wave of coastal structures. In addition to the practical importance of shoaling, because before the breaking of the wave the problem experiences a rapid rise of its nonlinearity, such problems can be used to test the efficiency and accuracy of the simulation to approximate near breaking phenomena. To examine this problem, we shall simulate the experiments presented in (Grilli et al., 1994). Specifically, the first test case comprises of a domain of depth $h_0 = 1[m]$, length $L = 95[m]$ and a solitary wave of initial amplitude $a/h_0 = 0.20$ and centered at $x = 30[m]$ for $t = 0[\text{sec}]$. The sloping bottom has a slope of $1:35$, starts at $x = 60[m]$ and ends at $x = 95[m]$ (ending to a shore line). However, since the current model requires the depth always be greater than zero everywhere, the bottom geometry is slightly different than the one presented in (Grilli et al., 1994). It was established that for the method presented here to be valid, the total bathymetry at every horizontal point must be strictly positive (otherwise the Sturm-Liouville problem presented in Section 1.3 cannot be defined). As a result we alter the right end of the domain to end to a flat bottom of very small bathymetry. This alteration should not affect the results we will present since the breaking of the wave takes place before it reaches this area. The geometry configuration of the problem is presented below:

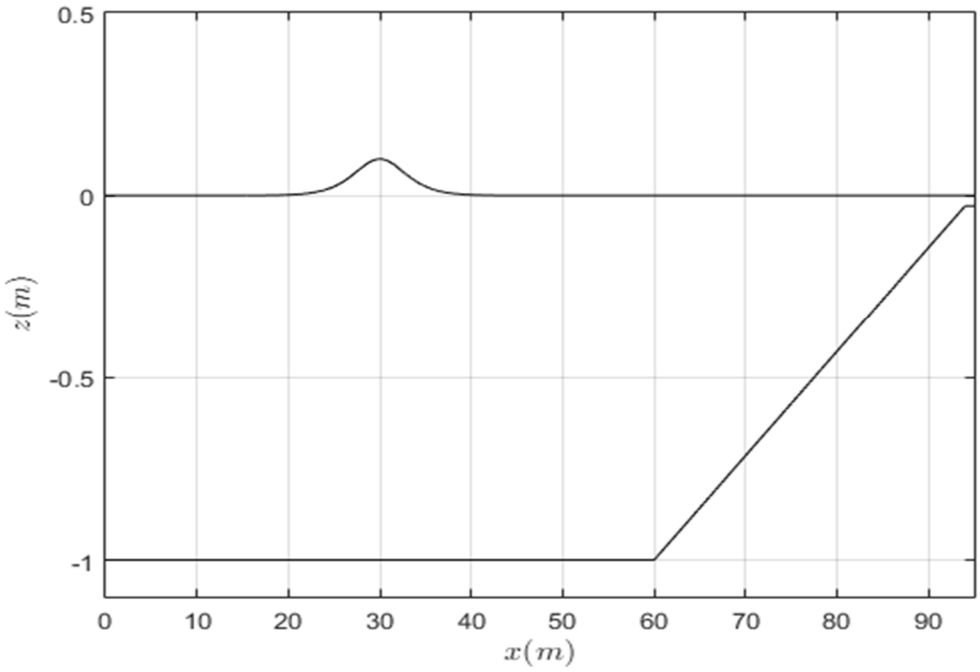

Figure 24: Initial free-surface elevation for the problem

For the simulations, a 4th order finite difference scheme is used, a horizontal step of $dx = 0.05[m]$ and a time-step of $dt = 0.01[\text{sec}]$ The total number of modes used for the simulation is $N_M = 8$. We compare our simulation with the free-surface elevation presented from the aforementioned experiment at certain stations. We shall also present numerical results from a BEM model presented in . The stations we will present are located at the positions:

Station	g_1	g_3	g_5	g_7	g_9
$x[m]$	80.96	82.55	83.66	84.68	85.95

Table 5: Positions of the stations for the measurement of the free-surface elevation.

The comparison for these stations is presented below:

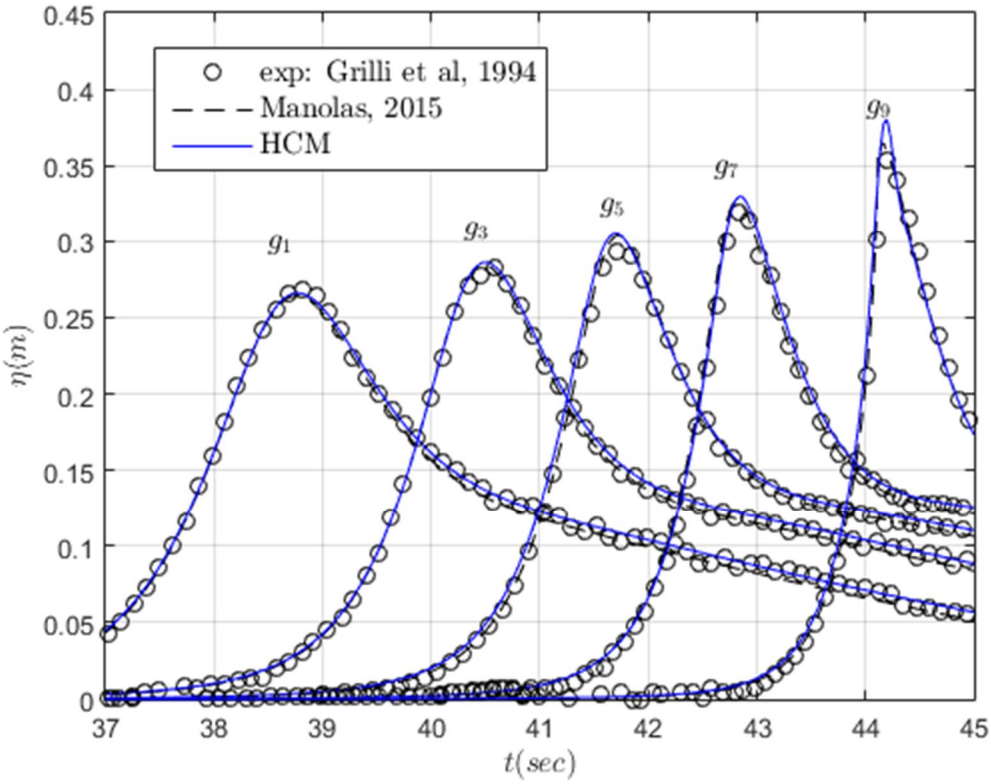

Figure 25: Comparison of the time series of free-surface elevation between the experimental results of (Grilli et al., 1994) BEM numerical results from (Manolas, 2015) and our simulation, at certain stations.

The results presented above, are in good agreement with the experimental data. At the stations g_5, g_7 and g_9 we observe a gradually rising (but always small) deviation from the experimental measurements. Hence, we can assume that the modeling of solitary waves shoaling with HCM (before breaking) is satisfactory. From this figure we also observe that the amplitude of the wave becomes a lot bigger than its initial amplitude as the wave propagates over the plane beach. This phenomenon can be illustrated in a more detailed manner in the following Figure, where we compare for a range of horizontal positions of the

domain the relative waveheight $H/h(x)$ where H is the maximum free-surface elevation over a specific horizontal position and $h(x)$ the bathymetry at the afore mentioned point. The comparison is done for 4 different cases, where the initial solitary wave amplitude is $a/h_0 = 0.10, 0.15, 0.20, 0.25$. The results are presented below:

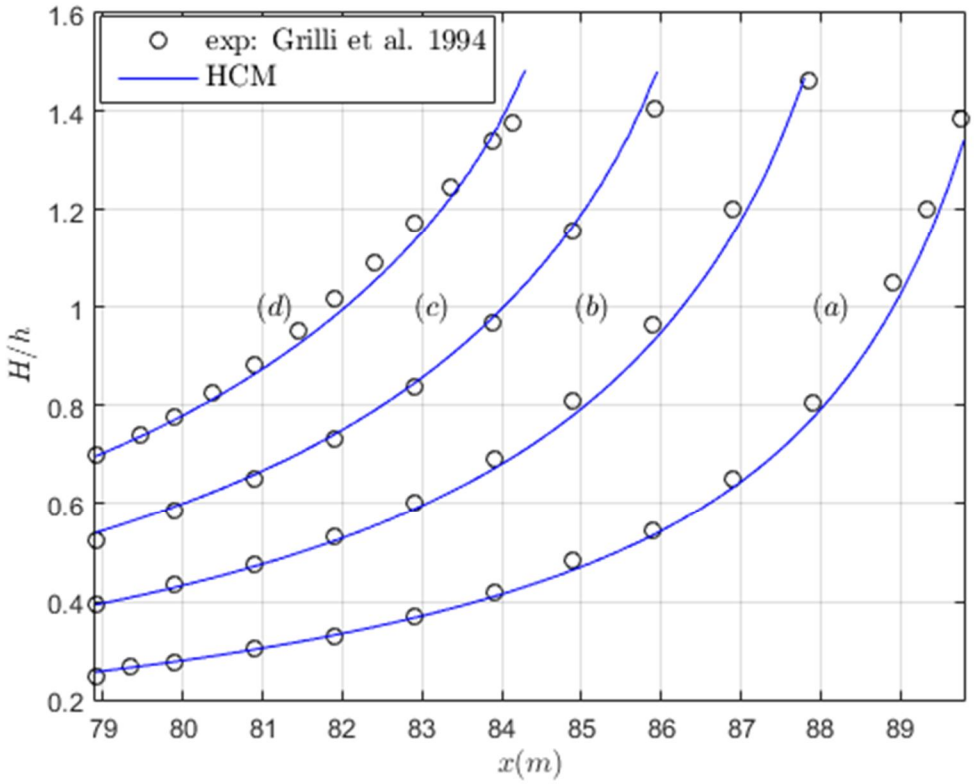

Figure 26: Comparison between experimental data and simulation regarding the relative wave height, for solitary waves of initial wave amplitude (a) 0.10, (b) 0.15, (c) 0.20, (d) 0.25.

The results of the simulation appear to be in good agreement with the experimental data. From this figure we also observe that the relative height for every initial wave amplitude, far exceeds the highest wave amplitude of 0.75 to 0.80 for symmetrical stable solitary waves over a constant depth. Hence, as it was mentioned also by the authors of the aforementioned paper, this result showcases that the stability limit of symmetrical solitary waves over a flat bottom cannot help as foresee the breaking limit for solitary waves that undergo asymmetrical deformation over a plane beach. Finally, for the case of $a/h_0 = 0.2$ experimentally the breaking of the wave was measured at $x_b = 86.27[m]$ while for the simulation the breaking was measured at $x_b = 86.60[m]$. The error between the two results is small enough (also considering that the experimental data showcase a 1% deviation near the breaking region). As a result, we can assume that potential theory is adequate in simulating shoaling of solitary waves over a mild plane beach while phenomena like bottom friction do not seem to affect the results in any significant matter.

Solitary wave over a submerged dike

We now examine a case where a solitary wave travels over a submerged dike. This problem is interesting for the fields of ocean and coastal engineering encompassing a variety of applications. Such cases are dike applications for preventing beach erosion as well as water waves propagating over coral reefs or continental shelf. Another use for these models is the simulation of water waves over a submerged breakwater. The goal of these structures is to reduce the transmitted wave energy by reflecting the waves and dissipating the incident wave energy by breaking up the waves. Such interactions of waves and submerged breakwaters has been studied extensively (see for example (Seabra-Santos et al., 1987), (Huang, Chang, & Hwung, 2003), (Lin, 2004)). The case we shall simulate is of depth $h_0 = 1.0$, and has a length of $200h_0$. The submerged dike has a height of $h_1 = 0.5$ and is placed in the area $x \in [90,110]$. The lateral boundaries of the domain are assumed to be fully reflecting walls. We simulate the problem for the case of initial solitary wave for amplitudes $a/h_0 = 0.15$ which is centered at position $x = 65[m]$. The initial data of the free-surface are taken by the Matlab code of Clamond *et al*. We use a 4^{th} order finite difference scheme and 8 modes in total. The horizontal step is taken equal to $dx = 0.1[m]$ and the time step is equal to $dt = 0.02[\text{sec}]$. Our first test for this case is to examine how abrupt we can make the dike without hindering the effectiveness of the model. Note that even though the approximation of the bottom bathymetry with the finite difference scheme can never be discontinuous, a sudden change in the geometry of the bottom can result in a blow up of its first and second horizontal derivatives. Such effects can result in a raise of the condition number of the matrix of the discretized substrate problem and as a result drastically raise the numerical error inserted to the simulation due to the linear solver. We should note however that most direct linear solvers are not affected easily by the condition number of the system. In an attempt to simulate the model as close as to its physical counterpart as possible we present the case where we use the bottom bathymetry:

$$h(x) = 1.0 - 0.5H(x-90)H(110-x)$$

but we set the horizontal derivatives of the bottom bathymetry equal to zero everywhere in the domain. We present the conservation of Mass and Hamiltonian for this case:

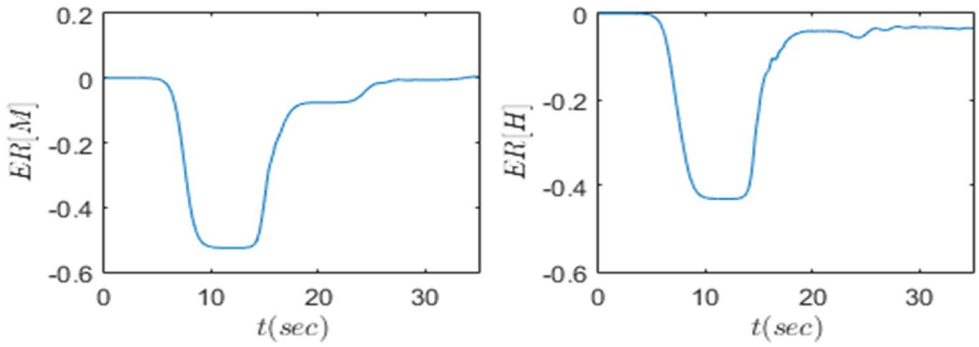

Figure 27: Relative error of Mass and Hamiltonian for abrupt bathymetry

The above results showcase that the abruptness of the geometry affects dramatically the accuracy of the model. It becomes therefore apparent that we need to simulate the problem with a more smooth geometry-approximation. For that reason we run the simulations for the bathymetries presented below:

$$h(x) = 0.75 - 0.25\tanh\left(\frac{x-90}{k}\right)H(x-80)H(100-x) + 0.25\tanh\left(\frac{x-110}{k}\right)H(x-100)H(120-x) + 0.25\left[H(90-x)+H(x-110)\right], \quad (3.2)$$

where the simulations are done for $k = 0.25, 0.50, 1.0$.

The relative error of the conservation of mass and Hamiltonian are presented below:

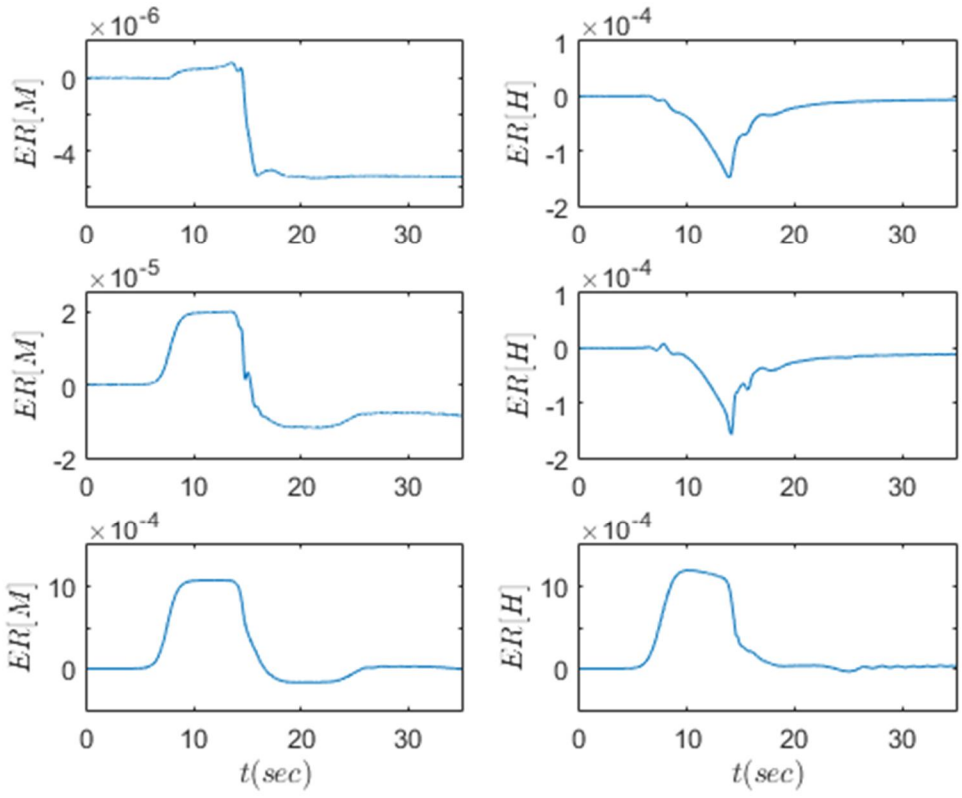

Figure 28: Relative conservation error for the case of $a/h_0 = 0.15$ with the first row representing the case $k = 1.0$, the second row the case $k = 0.5$ and the third row the case $k = 0.25$.

We see that for smoother bathymetries the relative error of the aforementioned quantities is a few orders of magnitudes better than for the abrupt cases. On all cases we observe initially a rise in the total mass of the system when the incident wave travels over the submerged dike. Such a phenomenon is not expected from the numerical scheme itself (since the Runge-Kutta method is dissipative) but maybe can be explained from the sudden rise of the free-surface elevation due to the dike. Yet, as expected, this increase of mass becomes less significant the smoother the bottom bathymetry becomes. Also, for all cases the total mass drops below the

initial mass when the incident wave leaves the submerged dike. This phenomenon may be explained form the fact that the solitary wave experienced a sudden decrease in amplitude due to the sudden deepening of the domain. We also observe that for both cases $k = 0.5$ and $k = 1.0$ the error of conservation of Hamiltonian is very similar while the respective error for the Mass is very different. This may be explained as a threshold for the accuracy of the error of the Hamiltonian due to the time and space discretization (perhaps the time-step is not small enough to capture the sudden decrease in amplitude effectively).

Finally, we present the time evolution of the problem for the case where $k = 0.5$.

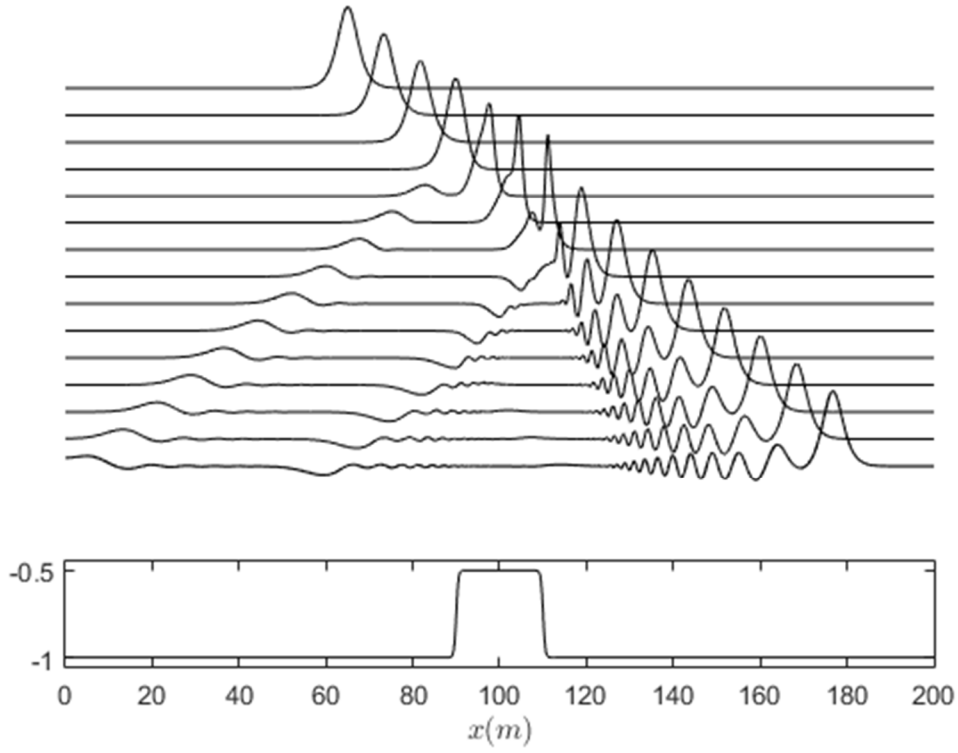

Figure 29: Time evolution of the free-surface for a solitary wave of $a/h_0 = 0.15$ with parameter $k = 0.5$.

From this figure we can observe that while the solitary wave passes over the left edge of the shelf, a part of it is reflected to the left of the domain, while the incident solitary wave starts to increase in amplitude and decrease in wavelength. This behavior continues until the solitary wave reaches the right edge of the shelf where part of it is again reflected to left while the solitary wave decreases in amplitude and develops a transmitted trail. We should also not that while the reflected waves are propagating the develop trails. Finally, once the solitary wave passes the shelf it decreases in amplitude and increases in wavelength.

Solitary wave over a sinusoidal variable bottom patch

We now investigate the effect of a rapidly variating bottom bathymetry on propagating solitary waves. For that purpose we utilize a sinusoidal bottom variation. Such bathymetries and their interaction with propagating regular periodic waves has been studied theoretically and experimentally in (Davies & Heathershaw, 1983) and (Davies & Heathershaw, 1984). In these papers it was observed that the reflection is strongest if the wavelength of the incident wave is equal to twice the wavelength of the periodic seabed variation. This phenomenon was characterized as the hydrodynamic equivalent of the so called *Bragg scattering*. Instead of using regular periodic waves as incident waves, we shall utilize a solitary wave to propagate over said bathymetry. In more detail, the domain of problem has a depth of $h_0 = 1.0[m]$ except for varying bottom patch of the form (8 ripples in total):

$$h(x) = h_0 - 0.3\sin(2\pi(x-580)/12.5)\ ,\ x \in [580, 680]$$

The total length of the domain is $1200[m]$. The lateral boundaries are assumed to be fully reflecting walls. The propagating solitary wave has an amplitude $a/h_0 = 0.4$ and it is initially centered at the position $x = 555[m]$. The initial data are taken again from the Matlab code of (Clamond & Duthykh, 2013). A 4^{th} order finite scheme is used for this problem as well as 8 total modes. The horizontal space discretization is $dx = 0.1[m]$ and the time discretization is $dt = 0.02[\text{sec}]$. As the solitary wave passes above the varying bottom irregular wave patterns are generated and propagate to both directions. These waves have a much smaller amplitude than the solitary wave. To the direction opposite to the propagation of the initial solitary wave, a reflected wave-train travels steadily. In the direction of the initial solitary wave's movement, a leading solitary wave (with smaller amplitude than the initial) propagates steadily while a rapidly changing wave-train follows it. Even though no experiments or numerical simulations could be found regarding such a case, this simulation was implemented to showcase the ability of the code to solve large problems in space and time as well as its ability to simulate problems were highly demanding physical phenomena occur.

The conservation of Mass and Hamiltonian of the simulation are presented in Figure: From this figure we can see that even though both quantities are conserved within acceptable limits, the conservation of mass experiences a much bigger error compared to the previous cases. This phenomenon can be attributed to the consecutive rapid changes in bathymetry during the propagation of the solitary wave (as the graph of the Mass conservation showcases). Furthermore, the very fast interaction of the wave and the bottom which results to sudden generation of reflected and trailing waves also accounts for this behavior. This rapid change in the geometry of the free-surface combined with the fact that the wavelength of these waves are a lot smaller than that of the solitary wave (and as a result are defined by less degrees of freedom) contribute to the raise of the error of the conservation of mass. Finally the time-history of the free-surface is presented.

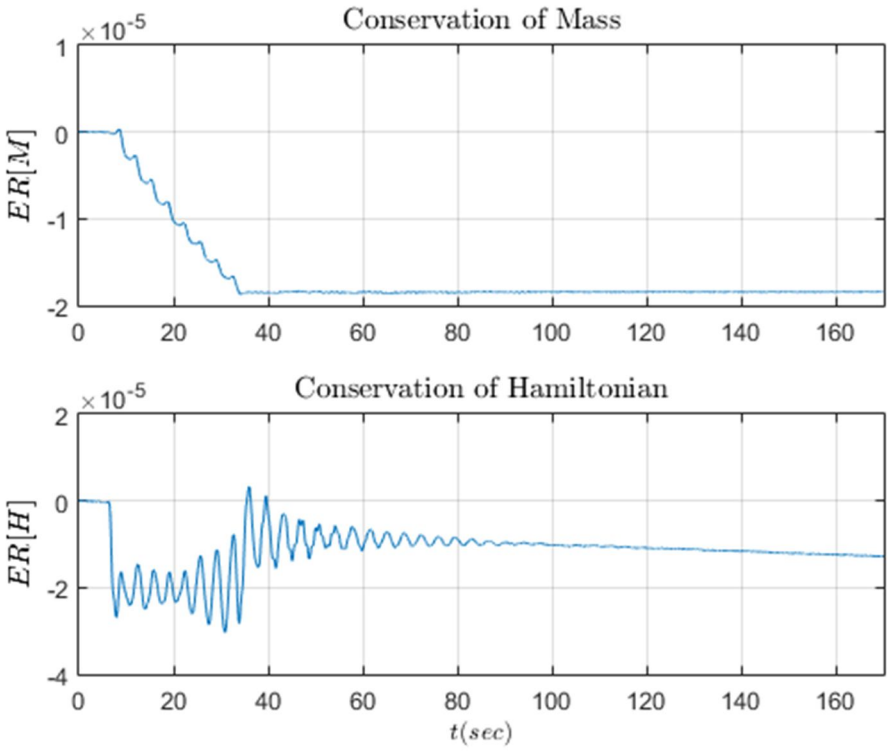

Figure 30: Conservation of Mass and Hamiltonian of the simulation.

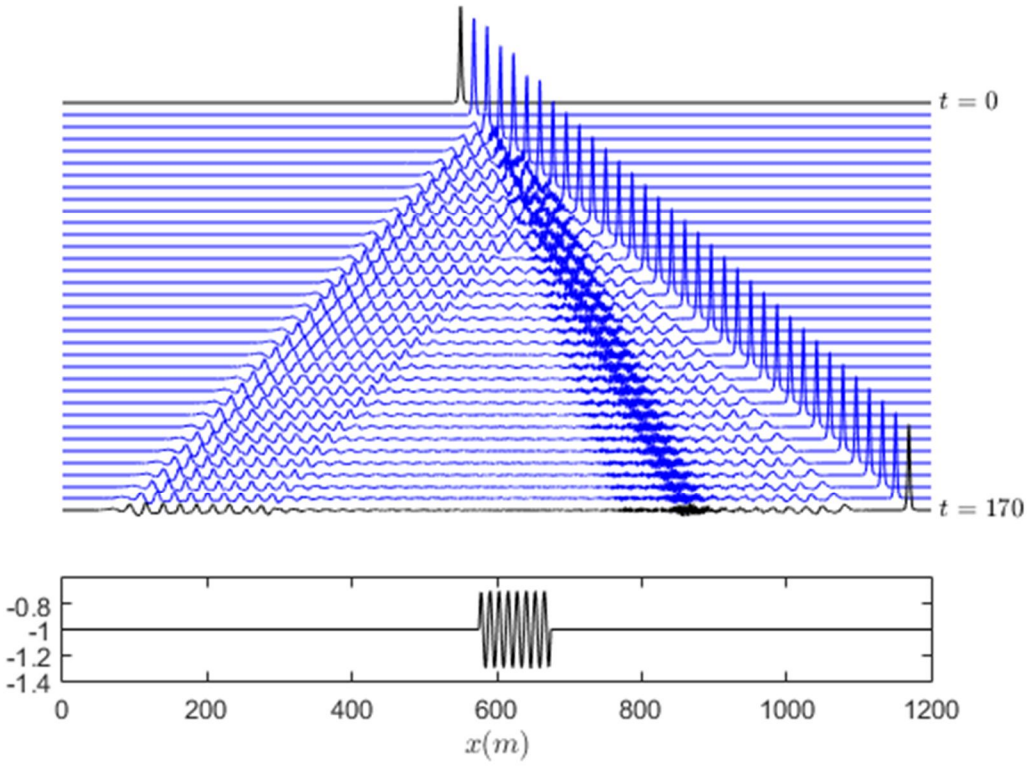

Figure 31: Time-clips of the propagation of a solitary wave of amplitude $a/h_0 = 0.3$ over 8 sinusoid ripples of amplitude 0.3 and wavelength 12.5 each.

3.5 Numerical Simulation of moving bottom

We now move on, to evaluate the efficiency of the HCMS in simulating problems that contain abrupt bottom movements. We begin by investigating the experiments presented in (Hammack, 1973). In this paper, Hammack addresses the generation and propagation of waves, in a rectangular tank of uniform depth, that were formed by an abruptly raised or lowered part of the bottom. Such an experiment constitutes a simplified model for the mechanisms of tsunami generation by means of an impulsive seafloor movement. For the first test-case we examine the raise of part of the bottom with an exponential movement. For the simulation, the domain of the problem is assumed 2D, with reference depth $h_0 = 1[m]$ and total horizontal length $L = 2500[m]$. The lateral boundaries of the domain are represented by fully-reflecting walls and they are located at the horizontal positions $x/h_0 = 0$ and $x/h_0 = 2500$. The moving block of the seafloor is located in the interval $x/h_0 \in [0, b]$ while the bed displacement in discussion is defined by the formula below:

$$h(x,t) = h_0 - \zeta_0\left(1 - e^{-at}\right)H(b - x), \quad x/h_0 \in [0, 2500], t \geq 0 \tag{3.27}$$

where $H(b - x)$ represents the Heaviside step function.

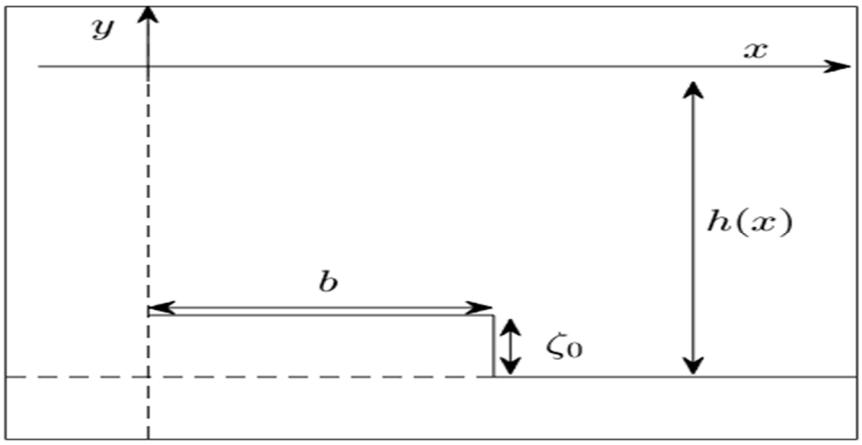

Figure 32: Geometric configuration of the moving part of the seafloor

The values of the parameters of Eq. (3.26) of the geometric configuration used here are presented below:

$$\zeta_0/h_0 = 0.1, \qquad b/h_0 = 12.2, \qquad a = 1.11/t_c \tag{3.28a,b,c}$$

where

$$t_c = 0.148 b/\sqrt{g h_o} \tag{3.28d}$$

Except for the experimental data presented by Hammack, for the parameter values of Eqs. (3.27), simulations have been presented by (Fuhrman & Madsen, 2009) where they utilized a

high-order Boussinesq model, and by (Benoit, et al., 2014) where they used a fully-nonlinear expansion of the velocity-potential. Both these simulations run for a much larger total time in comparison with the experimental data of Hammack, which results in the separation of the leading part of the disturbance into two distinct solitary waves. This result is in accordance with the prediction presented in (Hammack & Segur, 1974) with the exception that the authors predicted the formation of three distinct solitary waves.

The first step for the simulation is the inquiry needed to be done for the selection of space and time discretization that models the abrupt movement of the bottom without problem as well as the needed number of modes to be used (a parameter that determines the total nonlinearity and dispersion of the simulation). For that purpose, we start with what we think is the most important parameter of the current simulation, the time-step.

The time and space discretization used in (Benoit, et al., 2014), is

$$\Delta t\sqrt{g/h_0} = 0.2, \quad \text{and} \quad \Delta x/h_0 = 0.2 \tag{3.29a,b}$$

while, the corresponding parameters in (Fuhrman & Madsen, 2009) are:

$$\Delta t\sqrt{g/h_0} = 0.05 \quad \text{and} \quad \Delta x/h_0 = 0.25 \tag{3.30a,b}$$

From these values, we can deduce that the most crucial parameter for this simulation is the time-step of the method, due to the rapid bottom movement. For that purpose we begin with an investigation concerning the time-step needed for this simulation. Our main concern is whether the very abrupt dynamic phenomena that are observed during the movement of the bottom are efficiently captured. For that purpose we methodically decrease the time step used for the time interval that the movement of the bottom affects the free-surface. To define the end of this interval, we try to find the time in the previous simulations were the error of the Hamiltonian was less than 10^{-4}, or in more detail:

$$t^* = \max\left\{t \geq 0 : \left|\frac{H\left(t^*\right) - H\left(t_{final}\right)}{H\left(t_{final}\right)}\right| \leq 10^{-4}\right\}, \tag{3.31}$$

We estimate the above time to be at $t^*\sqrt{g/h_0} = 20$. Now, we run simulations for which the time step is choose to be $\Delta t\sqrt{g/h_0} = 0.2, 0.1, 0.05, 0.01, 0.005$, during the time interval $t\sqrt{g/h_0} \in [0, 20]$, while using a time step $\Delta t\sqrt{g/h_0} = 0.2$ for the rest of the simulation. The time step is chosen to be $\Delta x/h_0 = 0.2$, and the number of total modes is taken as $N_M = 6$. The results of said simulations are presented below for the first and last station that experimental results were shown in (Hammack, 1973):

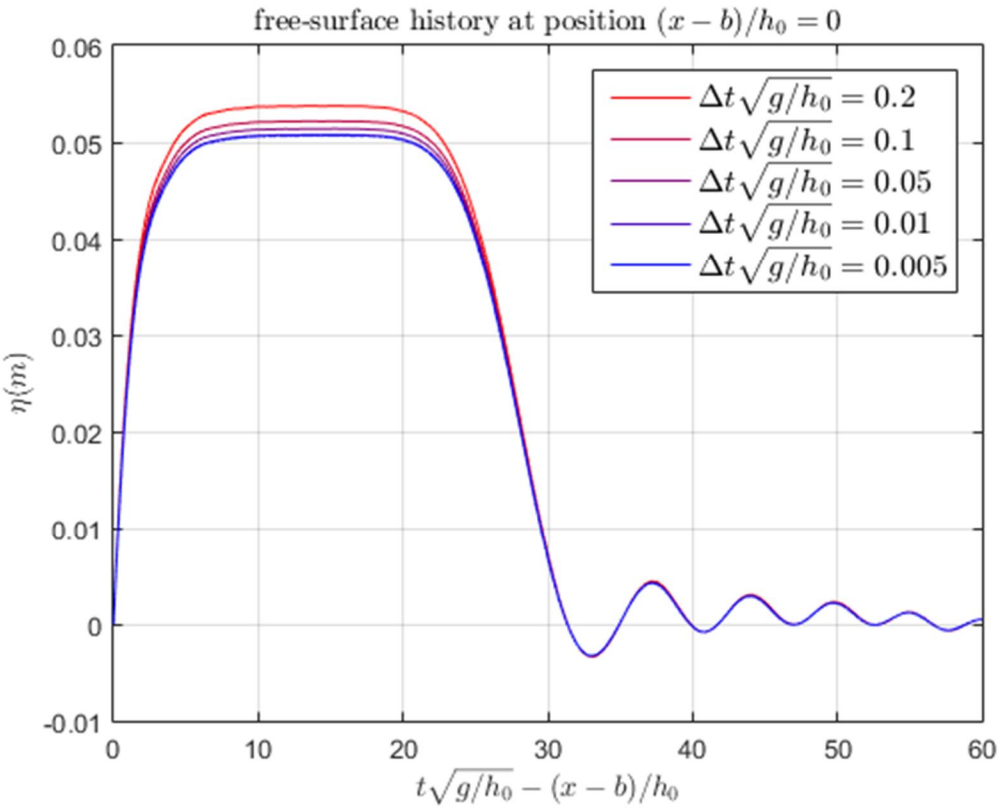

Figure 33a: Comparison of simulations with different time-steps at station $(x-b)/h_0 = 0$

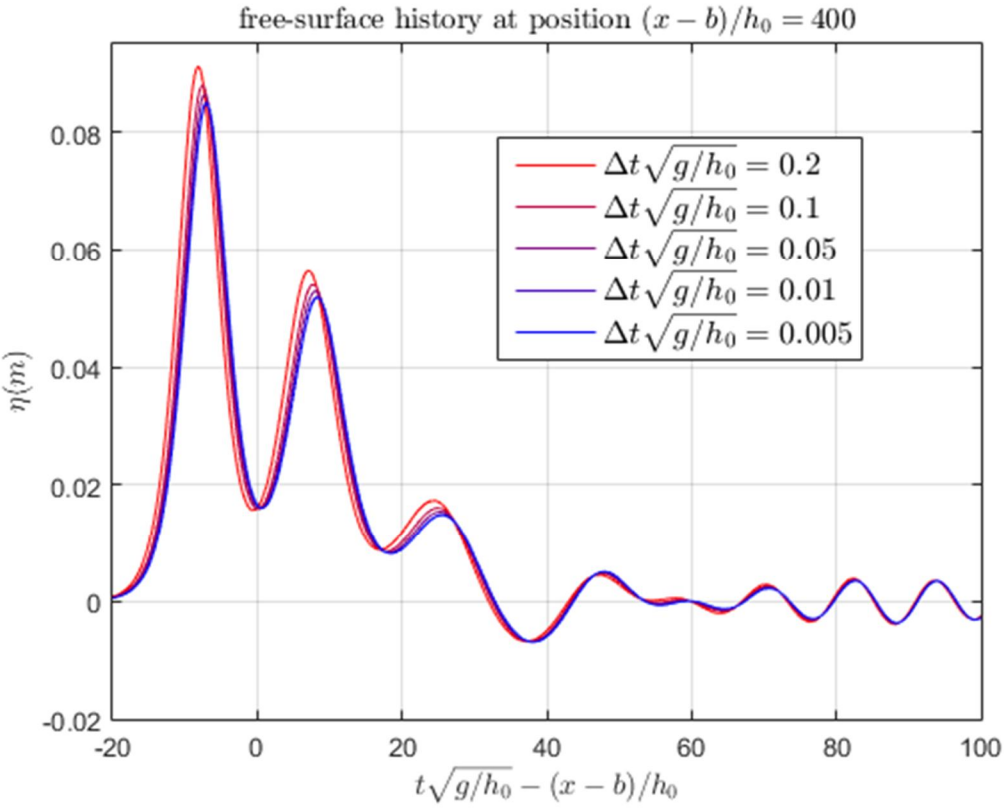

Figure 33b: Comparison of simulations with different time-steps at station $(x-b)/h_0 = 400$

We can see that the simulations gradually converge to a solution while the time-step is decreasing and hence we utilize the time-discretization used in the last simulation. We shall now investigate the number of needed total modes for the simulation. For that purpose, we present results for the cases of $N_M = 4, 6, 8$, with $\Delta x / h_0 = 0.2$, 4^{th} order finite differences and a time-discretization as described above. We present the free-surface elevation at certain stations (the stations used by (Hammack, 1973)), in the following figure.

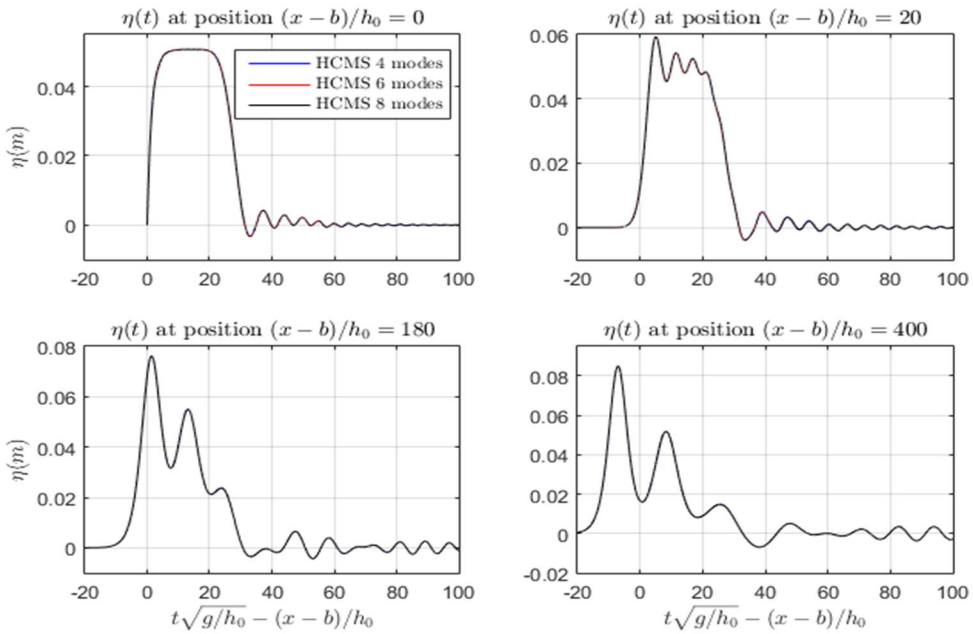

Figure 34a: Comparing simulations with different total modes at specific stations.

Significant differences are not observed between these simulations, leading us to believe that the time-step we shall use seems to be the most critical factor for the simulations. However, zooming in on the first station presented in Figure 21.a, we can observe the following difference between the simulations:

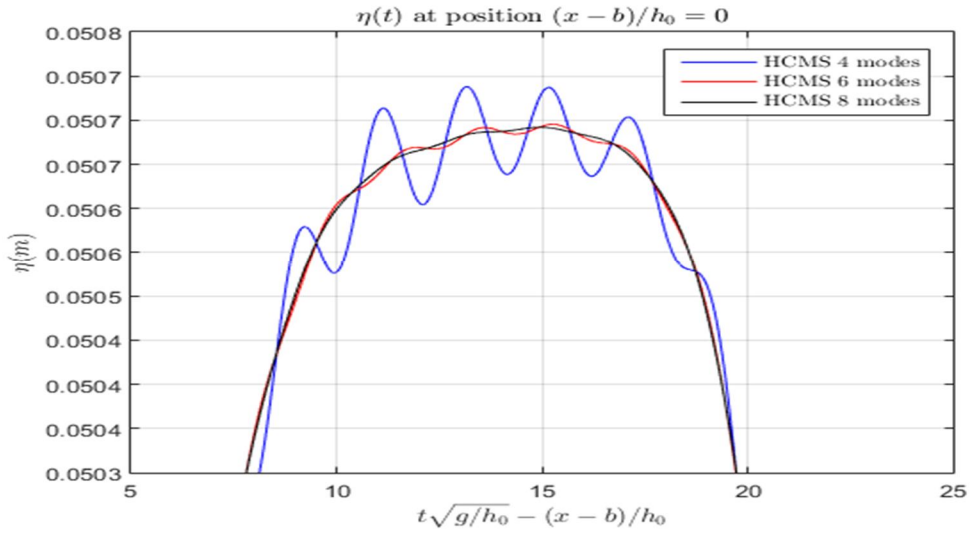

Figure 34b. Comparison of simulations with different total modes at the first station.

As can be seen, the simulation with 4 modes is a lot more oscillatory than the other 2. However free-surface elevation differences at the other stations are insignificant. Hence, we can see that using more than 6 modes does not have a significant improvement in the solution and as a result we shall utilize 8 modes for our simulation. We now present the comparison of our results with the experimental data and other simulations, using a time-step $\Delta t\sqrt{g/h_0} = 0.005$ for $t\sqrt{g/h_0} \leq 20$ and $\Delta t\sqrt{g/h_0} = 0.2$ afterwards while using 8 modes in total and a space discretization of $\Delta x/h_0 = 0.2$. The results of the experimental data, as well as the simulations of (Benoit, et al., 2014) and (Fuhrman & Madsen, 2009), are derived manually through a digitizer and as a result contain a relative error in their presentation. It is also noteworthy that the experimental data of Hammack, showcase waves with smaller amplitudes and as a result lower propagation velocities. Hence, as time progresses the simulations diverge from the experiment. Hammack also simulated the problem in discussion using the PBBM equation and measured significant differences with the experimental data which lead him to state:

"A possible explanation of the differences between theory and experiment is the presence of viscous energy losses and boundary stresses in the experimental measurements;"

The comparison is done in the 4 stations where measurements were taken from Hammack. results are presented below:

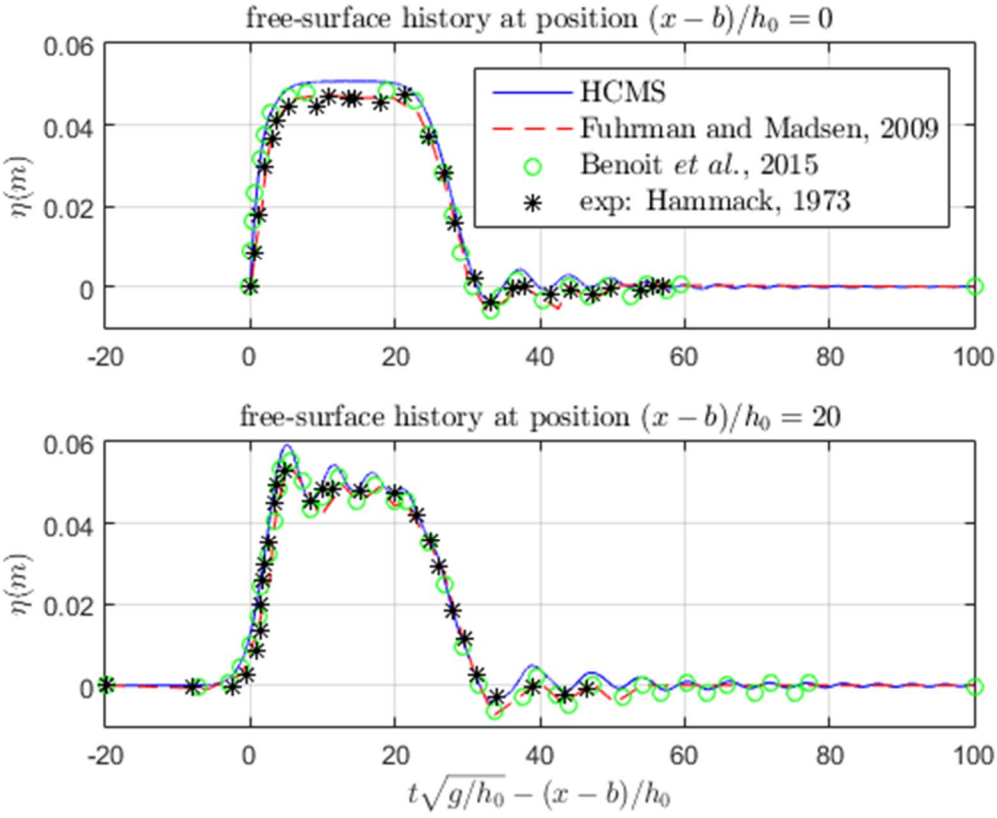

Figure 35a: Comparison of various simulations with experimental data on first two stations.

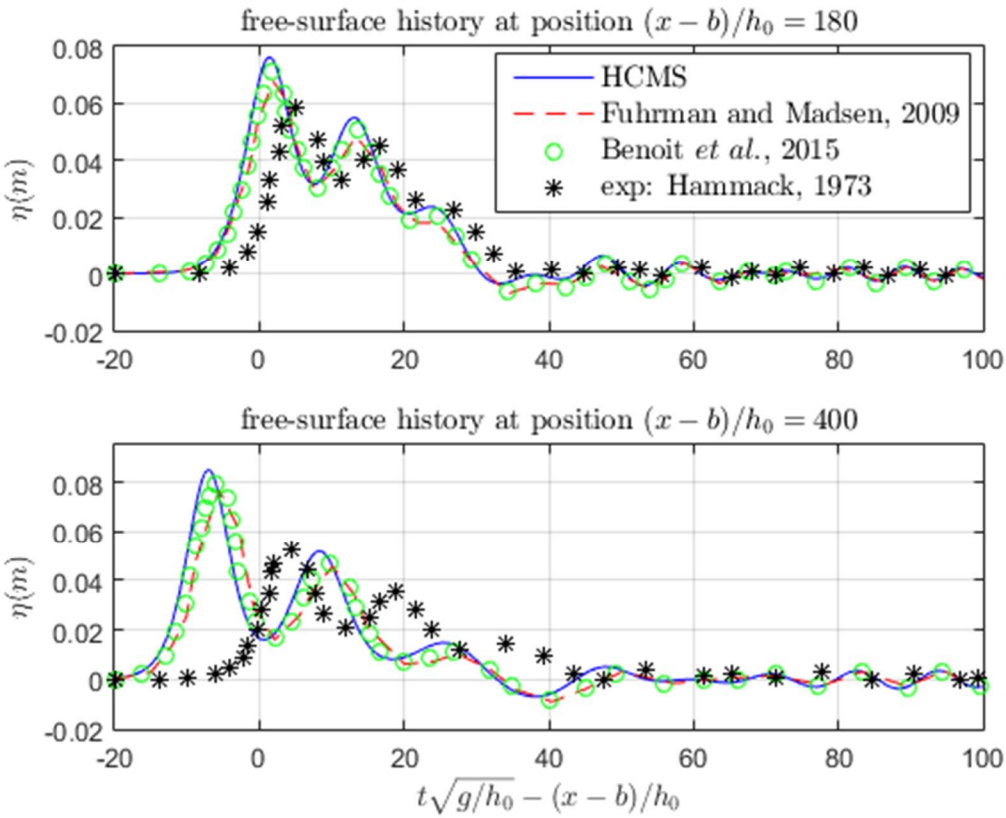

Figure 35b: Comparison of various simulations with experimental data on last two stations.

We can easily observe from the results that the leading waves of our simulation are slightly higher and as a result faster than the ones presented in the other two simulations. This divergence from the other results can be observed from the first station to the very last one. Furthermore, it is obvious that no simulation coincides with the experimental data at stations other than the first, an observation that showcases the dissipation present during the experiment. Trying to estimate the error of the measurements due to viscous losses, Hammack utilized Keulegan's theory (1948) (see (Keulegan, 1948)) for the viscous decay in amplitude of a single solitary wave propagating in the wave tank, he predicted that the amplitude of the leading wave should be around 57% larger than measured at station: $t\sqrt{g/h_0} - (x-b)/h_0 = 400$. Measuring the highest crest for the Hammack measurements at said station as $0.052[m]$, this theory predicts a wave with amplitude of $1.57 \cdot 0.052 = 0.082[m]$, with our crest measuring at $0.0844[m]$ and the crest given by Benoit & Yates being slightly under $0.080[m]$. Our divergence hence is not very significant from the predicted free-surface elevation by Hammack. Althought the experimental results of Hammack stop at distance $x/h_0 = 400$ from the raised bottom, continuing the propagation of the waves even further shows an interesting phenomenon, as the leading part of the disturbance separates into two solitary waves. This result was initially predicted by (Hammack & Segur, 1974) and verified numerically later by (Fuhrman & Madsen, 2009) and (Benoit & Yates, 2015). It should be noted though, that the asymptotic analysis by Hammack predicted the formation of 3 separate solitary waves, while numerical simulations of the aforementioned papers present exhibit only 2.

In the following figure we showcase the results taken from our simulation for long time propagation and compare it with the numerical results mentioned above:

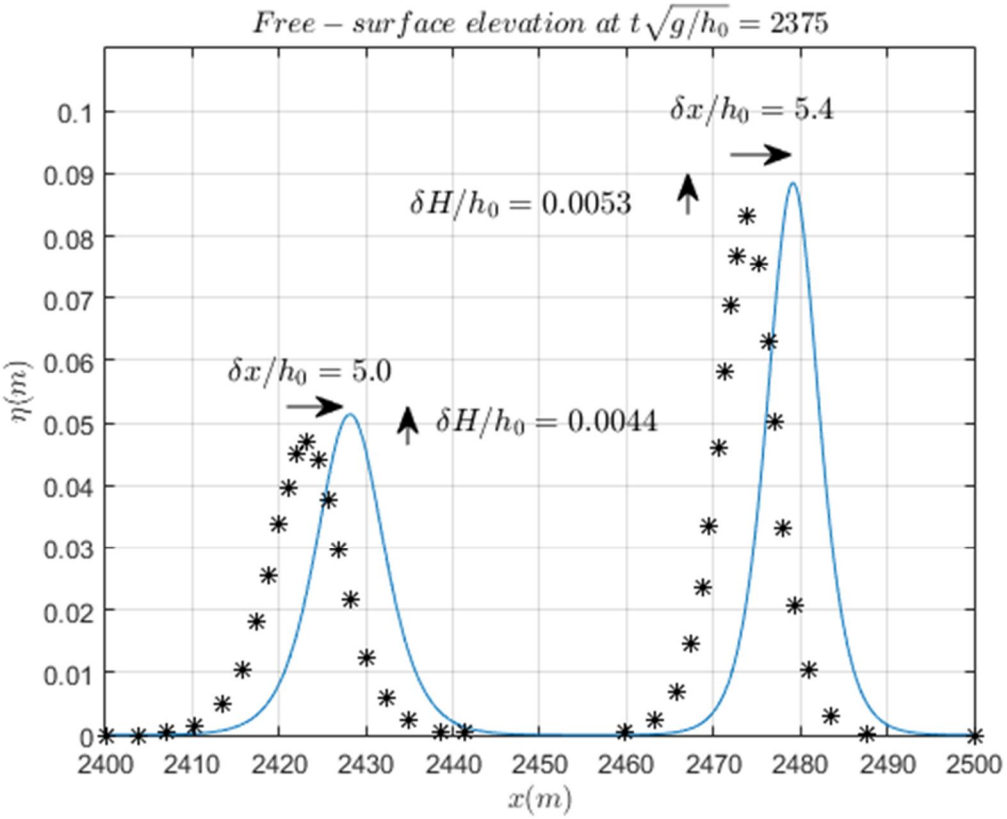

Figure 36: Comparison of the separated solitaries in long-time propagation, for our simulation (solid line), (Benoit, et al., 2014) (*)

We should also mention that in (Benoit, et al., 2014) their leading solitary wave at this instance has a difference of $\delta x/h_0 = 3.0$ and $\delta H/h_0 = 0.0266$ compared with (Fuhrman & Madsen, 2009). As expected, the formed solitary waves of our simulation are higher (and therefore faster) than the ones measured by the other simulations, a result mainly due to the initially higher rise of the free-surface of our simulation at the beginning of the phenomenon. A factor that was not investigated in this example and could play a role in the accuracy of the simulations, is the appropriate value of the parameter μ_0. For all the cases presented in the previous sections, we could always assume a wave of reference (usually the initial wave of each case) and choose the values of the parameter to be $\mu_0 = \omega^2/g$. Again, this result is not theoretically justified but it has been found numerically such a value to be efficient for the results of these simulations. However, in this case no initial or incident wave exists. For our simulations we chose the frequency of the solitary wave given in the far field by Benoit & Yates, for choosing the value of the parameter μ_0. However, a systematic study of this case for different values of the aforementioned parameter could showcase a better value that allows for more accurate simulations. Furthermore, the use an approximate seabed that does not showcase a step discontinuity may increase the accuracy of the results. Finally, a rise of the order of the finite difference scheme may play a role in the accuracy of the model. Ending, the

investigation of the current case we present results for the conservation of Mass and Hamiltonian throughout the simulation, assuming as reference values the one derived at the final time-step of our simulation. Results are presented below:

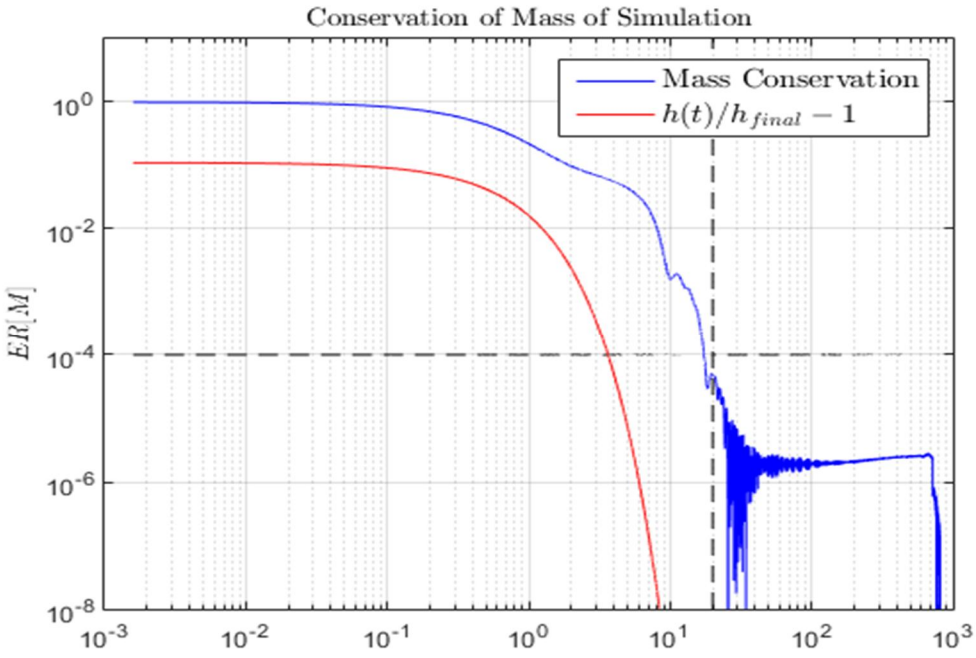

Figure 37a: Conservation of Mass of the system, for the duration of the simulation together with the moment of change for the time step (horizontal dashed line).

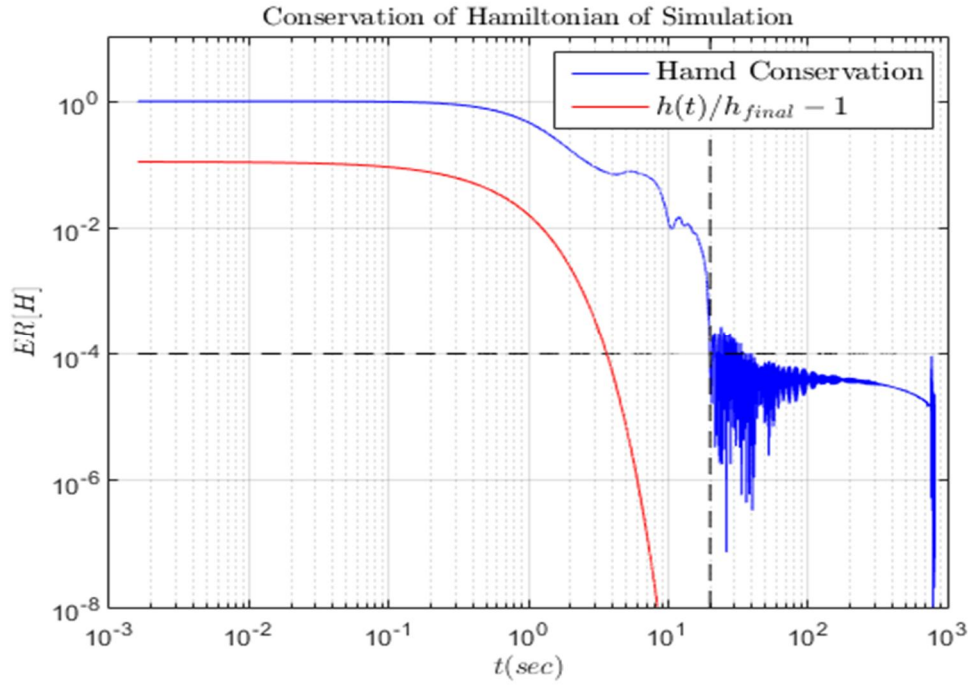

Figure 37b: Conservation of Mass of the system, for the duration of the simulation together with the moment of change for the time step (horizontal dashed line).

Hammack's downthrust experiment

Keeping the same geometric configuration, as presented in Figure 20, we now proceed to simulate the downwards abrupt movement of the bottom, an experiment done also by (Hammack, 1973). The parameters used for this case are presented below:

$$\zeta_0 / h_0 = -0.1, \qquad b / h_0 = 12.2, \qquad a = 1.11 / t_c \tag{3.32a,b,c}$$

$$t_c = 0.093 b / \sqrt{g h_o} \tag{3.32d}$$

For this case, we use exactly the same space and time discretization as used for the upthrust simulation before, where $\Delta x / h_0 = 0.2$ and $\Delta t \sqrt{g / h_0} = 0.005$ for the time interval $t \sqrt{g / h_0} \in [0, 20]$ and $\Delta t \sqrt{g / h_0} = 0.2$ for the rest of the simulation. Additionally, 6 modes are used (assuming that because the movement of the seabed is slower we don't need as many modes) and a 4th-order finite difference scheme is utilized. Finally, because no solitary waves are formed during this simulation, the domain is chosen to have a length of $L = 700 h_0$. We compare the free-surface elevation of the simulations at certain stations with the experimental data provided by Hammack and the high-order Boussinesq simulation executed by (Fuhrman & Madsen, 2009):

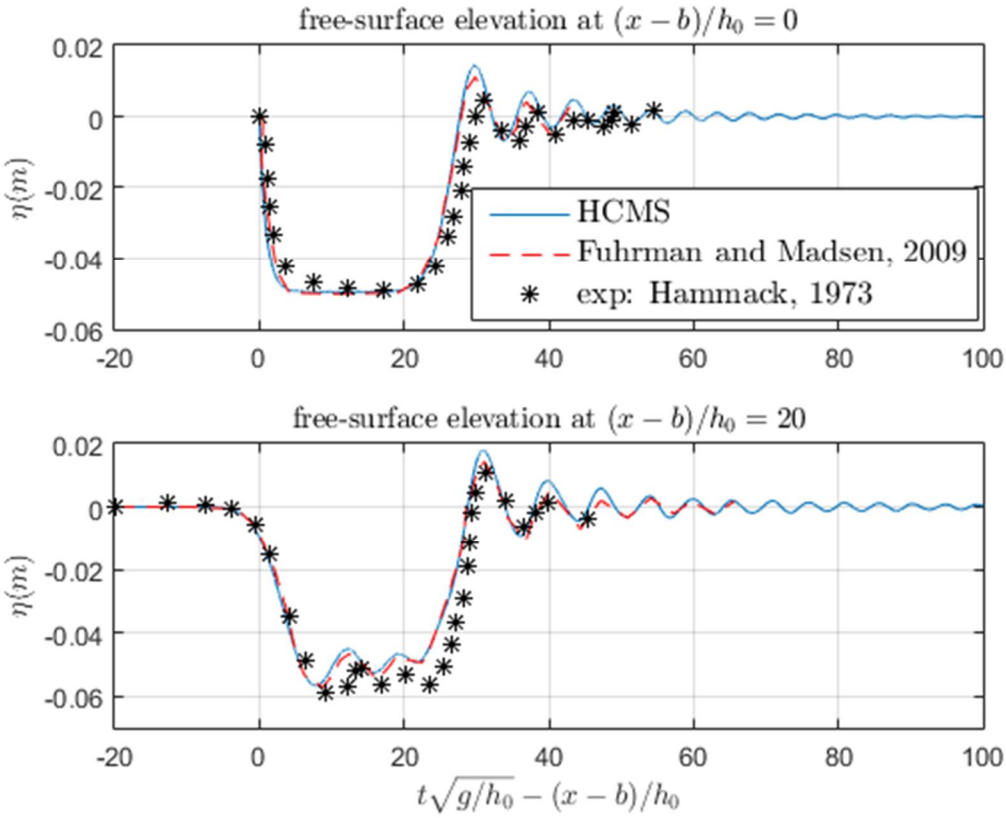

Figure 38a: Comparison of experimental data with various simulations at the first two stations

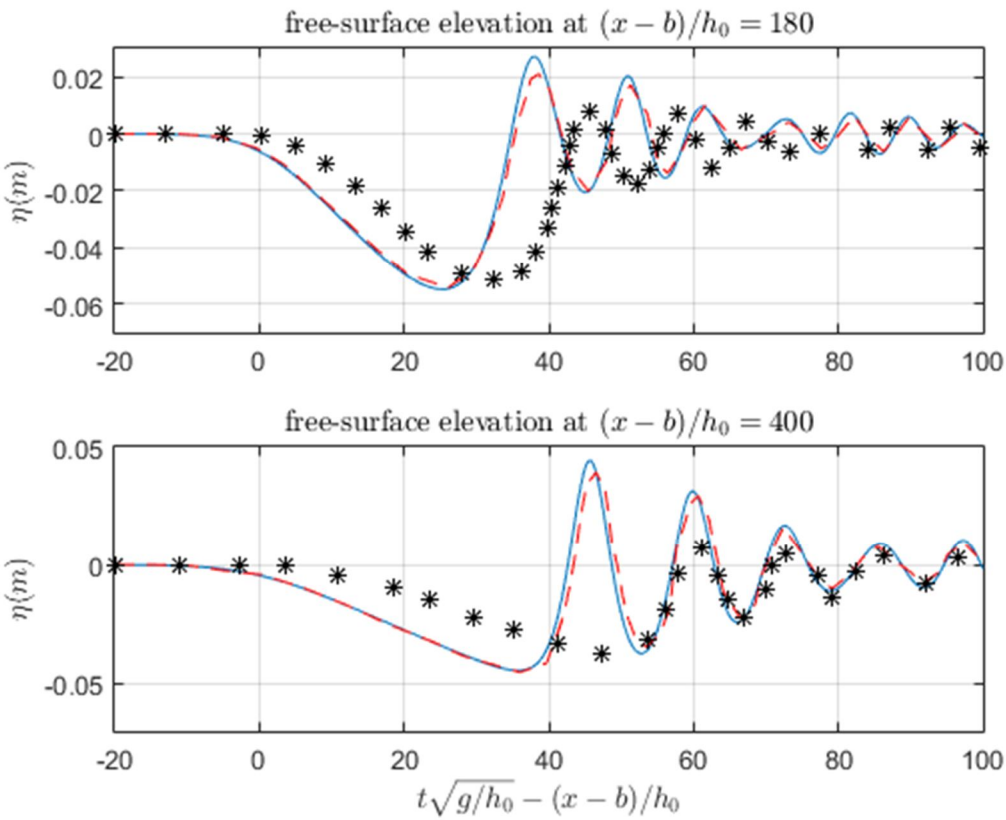

Figure 38b: Comparison of experimental data with various simulations at the last two stations

Once again, the experimental results diverge significantly from the simulations due to viscous effects. The wave amplitudes derived from our simulation are once again higher than the corresponding results of (Fuhrman & Madsen, 2009), yet with we should mention that for the previous case also the results of (Benoit, et al., 2014) gave slightly higher waves than the ones of the high-order Boussinesq model. Once, again the abruptness of the bathymetry may have played a role in the numerical results of our simulation together with the choice of the value of the parameter μ_0. Although these results showcase the potential of the model to simulate moving bottom problems more simulations need to be done to be able to better comprehend the accuracy of the method.

We should also mention that most moving bottom simulations in the literature, concern 3D geometries and hence cannot be modeled by the current code. However, the construction of a code able to solve 3D problems by utilizing the Finite Element method (and therefore the weak formulation of the problem) is in progress and results concerning more advanced moving bottom cases will be presented in the future.

Finally, we present the conservation of Mass and Hamiltonian during the simulation together with the seabed descend $1-h(t)/h_{final}$:

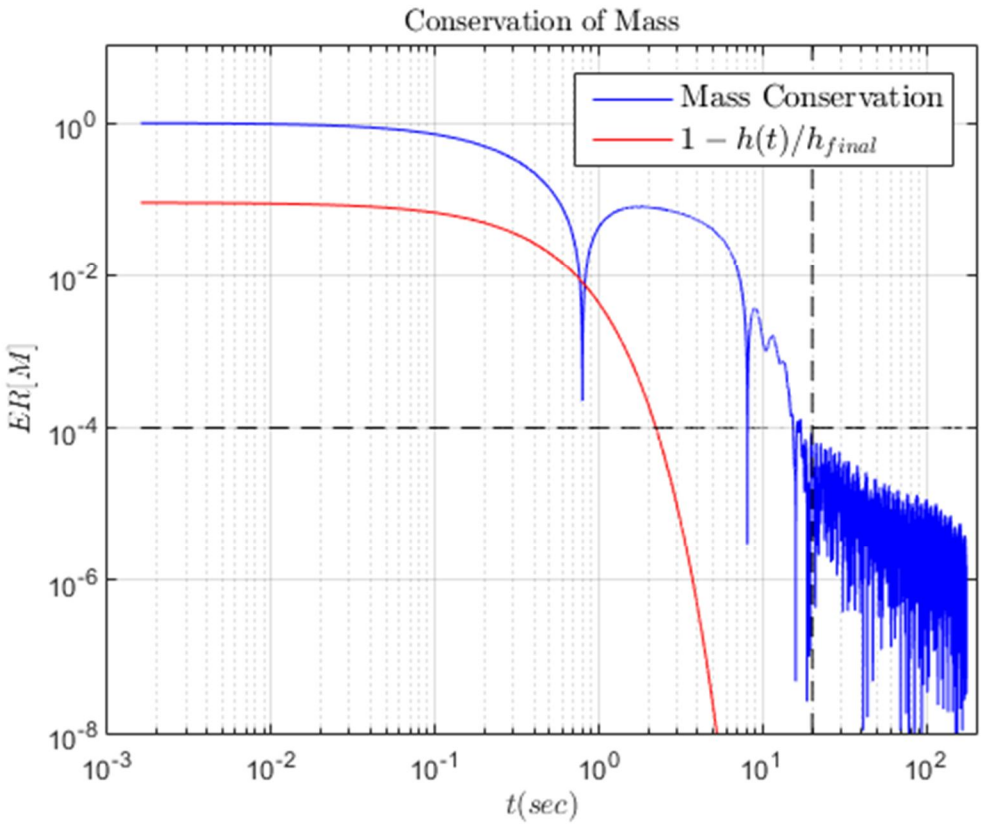

Figure 39a: Conservation of Mass during the simulation

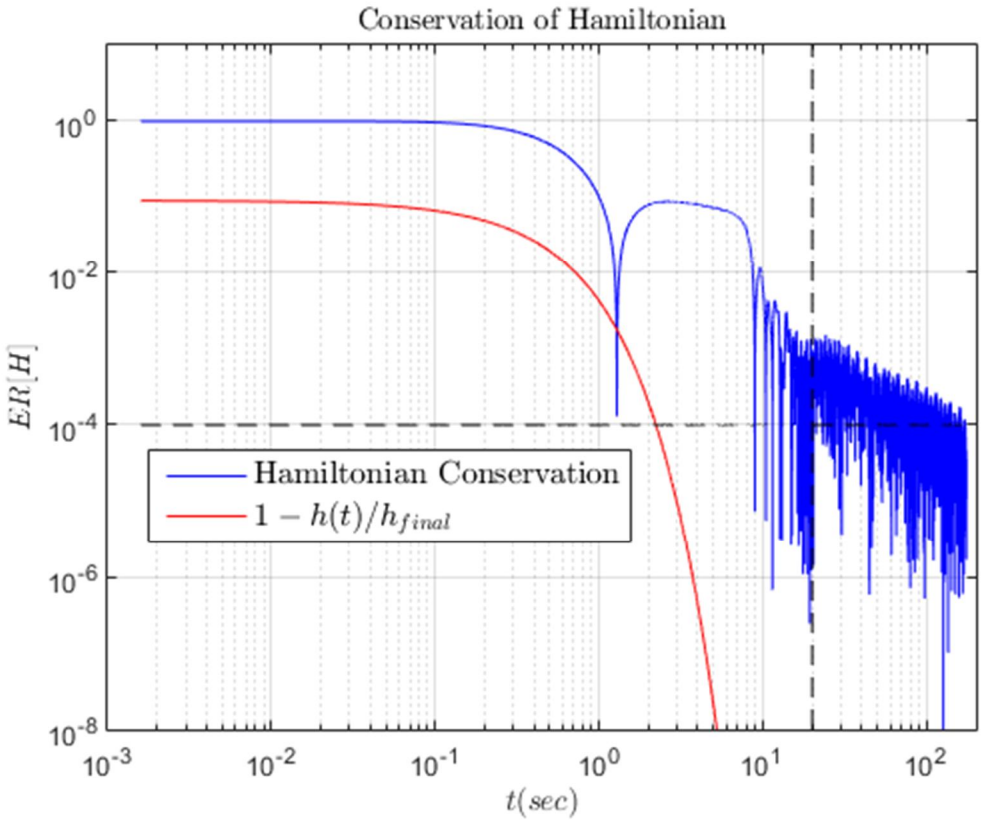

Figure 39b: Conservation of Hamiltonian during the simulation

PART II.

Appendices

Appendix A: Proof of Proposition 1, Section 2.1

Proposition 1, Section 2.1*: For* $n \geq 0$ *the first and second derivatives of* $k_n(H)$ *are given by the following equations:*

$$\partial_\eta k_n = \partial_h k_n = \partial_H k_n = \begin{cases} -\dfrac{k_0(k_0^2 - \mu_0^2)}{\mu_0 + H(k_0^2 - \mu_0^2)}, & n = 0 \\ \dfrac{k_n(k_n^2 + \mu_0^2)}{\mu_0 - H(k_n^2 + \mu_0^2)}, & n \geq 1 \end{cases}$$

$$\partial_H^2 k_n = -2\,\partial_H k_n \left\{ \mu_0 + \frac{\partial_H k_n}{k_n}\left(H\mu_0 - 1\right)\left(2 + H\frac{\partial_H k_n}{k_n}\right)\right\}, \; n \geq 0$$

$$\nabla_{\boldsymbol{x}} k_n = \partial_H k_n \cdot \nabla_{\boldsymbol{x}} H\,, \qquad \Delta_{\boldsymbol{x}} k_n = \partial_H^2 k_n \Delta_{\boldsymbol{x}} H + \partial_H k_n \left(\nabla_{\boldsymbol{x}} H\right)^2,$$

Proof: The wave numbers k_n, $n \in \{0,1,2,...\}$ are implicitly dependent on the free-surface elevation $\eta(\boldsymbol{x},t)$ and the bottom bathymetry $h(\boldsymbol{x},t)$. An observation that shall simplify the calculus that is to follow, can be derived from the dispersion relations:

$$f_0(\eta, h, k_0) = \mu_0 - k_0 \tanh\left[k_0(\eta + h)\right] = 0\,, \tag{A.1a}$$

$$f_n(\eta, h, k_n) = \mu_0 + k_n \tan\left[k_n(\eta + h)\right] = 0\,, n > 0\,, \tag{A.1b}$$

By setting $H(\boldsymbol{x};t) = \eta(\boldsymbol{x};t) + h(\boldsymbol{x};t)$, to symbolize the total bathymetry, one can easily verify that:

$$\partial_H f_n = \partial_\eta f_n = \partial_h f_n\,, n \in \{0,1,2,...\}\,, \tag{A.2a}$$

and as a result:

$$\partial_H k_n = \partial_\eta k_n = \partial_h k_n\,, n \in \{0,1,2,...\}\,, \tag{A.2b}$$

or in regard of the horizontal partial derivative:

$$\nabla_{\boldsymbol{x}} k_n = \partial_H k_n \nabla_{\boldsymbol{x}} H\,, n \in \{0,1,2,...\}\,, \tag{A.2c}$$

Therefore, we will only calculate the partial derivatives $\partial_H k_n$, $\partial_H^2 k_n$.

Calculation of first horizontal derivatives $\partial_H k_n$, $\nabla_{\boldsymbol{x}} k_n$, $n \in \{0,1,2,...\}$

The first step to such a calculation is the determination of the partial derivatives $\partial_H k_n$, $n \in \{0,1,2,...\}$. By applying the chain rule, to the functions f_n , $n \in \{0,1,2,...\}$, defined by Eqs. (A.1a) & (A.1b) we get

$$d_H f_n = \partial_H f_n + \partial_{k_n} f_n \, \partial_H k_n \ , \ n \in \{0,1,2,...\} \ , \tag{A.3a}$$

By also taking into account that $f_n = 0 = const$, we get

$$d_H f_n = 0 \ , \ n \in \{0,1,2,...\} \ , \tag{A.3b}$$

Combining Eqs. (A.3a) & (A.3b), we derive the formula:

$$\partial_H k_n = - \frac{\partial_H f_n}{\partial_{k_0} f_n} \ , \ n \in \{0,1,2,...\} \ , \tag{A.4}$$

The calculation of Eqs. (A.4) will be derived separately for the wavenumber corresponding to the propagating mode Z_0 and for the wavenumbers corresponding to the evanescent modes Z_n , $n > 0$.

Calculation of partial derivative $\partial_H k_0$

By straightforward differentiation of Eq. (A.1a) one easily finds

$$\partial_H f_0 = - k_0 [1 - \tanh^2 (k_0 H)] = - (k_0^2 - \mu_0^2) \ , \tag{A.5a}$$

$$\partial_{k_0} f_0 = - \tanh (k_0 H) - k_0 H \, [1 - \tanh^2 (k_0 H)] \Rightarrow$$

$$\partial_{k_0} f_0 = - \frac{\mu_0 + H (k_0^2 - \mu_0^2)}{k_0} \ , \tag{A.5b}$$

Therefore, using Eqs. (A.5a)-(A.5b) & (A.4) we get

$$\partial_H k_0 = - \frac{- (k_0^2 - \mu_0^2)}{- \dfrac{\mu_0 + H (k_0^2 - \mu_0^2)}{k_0}} = - \frac{k_0 (k_0^2 - \mu_0^2)}{\mu_0 + H (k_0^2 - \mu_0^2)} \tag{A.6}$$

Calculation of partial derivatives $\partial_H k_n$, $n \in \{1,2,...\}$

By straightforward differentiation of Eq. (A.1b) one easily finds:

$$\partial_H f_n = k_n [1 + \tan^2 (k_n H)] = k_n^2 + \mu_0^2 \tag{A.7a}$$

$$\partial_{k_n} f_n \;=\; \tan\left(k_n H\right) + k_n H\,[1+\tan^2\left(k_n H\right)] \Rightarrow$$

$$\partial_{k_n} f_n \;=\; -\frac{\mu_0 - H(k_n^2+\mu_0^2)}{k_n} \tag{A.7b}$$

Therefore, using Eqs. (A.7a)-(A.7b) & (A.4) we get:

$$\partial_H k_n \;=\; -\frac{k_n^2+\mu_0^2}{-\dfrac{\mu_0 - H(k_n^2+\mu_0^2)}{k_n}} \;=\; \frac{k_n(k_n^2+\mu_0^2)}{\mu_0 - H(k_n^2+\mu_0^2)} \tag{A.8}$$

Calculation of horizontal partial derivatives $\nabla_{\boldsymbol{x}} k_n$, $n \in \{0,1,2,...\}$

Finally, we arrive to the formulas:

$$\nabla_{\boldsymbol{x}} k_0 \;=\; \partial_H k_0 \nabla_{\boldsymbol{x}} H \;=\; -\frac{k_0(k_0^2-\mu_0^2)}{\mu_0 + H(k_0^2-\mu_0^2)} \nabla_{\boldsymbol{x}} H \tag{A.9a}$$

$$\nabla_{\boldsymbol{x}} k_n \;=\; \partial_H k_n \nabla_{\boldsymbol{x}} H \;=\; \frac{k_n(k_n^2+\mu_0^2)}{\mu_0 - H(k_n^2+\mu_0^2)} \nabla_{\boldsymbol{x}} H \;,\; n \;>\; 0 \tag{A.9b}$$

Calculation of second horizontal derivatives $\partial_H^2 k_n, \nabla_{\boldsymbol{x}}^2 k_n \;, n \in \{0,1,2,...\}$

The first step for said calculation is the derivation of the partial derivatives $\partial_H^2 k_n$, $n \in \{0,1,2,...\}$. Again, by applying the chain rule, to the functions f_n , $n \in \{0,1,2,...\}$, for their second derivatve we get:

$$d_{HH} f_n \;=\; \partial_{HH} f_n + 2\partial_{Hk_n} f_n \partial_H k_n + \partial_{k_n k_n} f_n (\partial_H k_n)^2 + \partial_{HH} k_n \partial_{k_n} f_n \;, \tag{A.10a}$$

By also taking into account that $f_n = 0 = const$, we get:

$$d_H^2 f_n \;=\; 0 \;,\; n \in \{0,1,2,...\} \;, \tag{A.10b}$$

Combining Eqs. (A.10a) & (A.10b), we derive the formula:

$$\partial_H^2 k_n \;=\; -\frac{\partial_H^2 f_n + 2\partial_{Hk_n} f_n \partial_H k_n + \partial_{k_n}^2 f_n (\partial_H k_n)^2}{\partial_{k_n} f_n} \;,\; n \in \{0,1,2,...\} \;, \tag{A.11}$$

The calculation of Eq. (11) will be derived separately for the wavenumber corresponding to the propagating mode Z_0 and for the wavenumbers corresponding to the evanescent modes Z_n , $n > 0$.

Calculation of partial derivative $\partial_H^2 k_0$

By straightforward differentiation of Eq. (A.1a) one easily finds:

$$\partial_H^2 f_0 \;=\; 2k_0^3 \tanh(k_0 H)[1-\tanh^2(k_0 H)] \;=\; 2\mu_0(k_0^2-\mu_0^2) \qquad \text{(A.12a)}$$

$$\partial_{Hk_0} f_0 \;=\; -2k_0[1-\tanh^2(k_0 H)] + 2k_0^2 H \tanh(k_0 H)[1-\tanh^2(k_0 H)] \Rightarrow$$

$$\partial_{Hk_0} f_0 \;=\; -2k_0[1-\tanh^2(k_0 H)](1-H\mu_0) \;=\; -2k_0(1-H\mu_0)\left(1-\frac{\mu_0^2}{k_0^2}\right) \qquad \text{(A.12b)}$$

$$\partial_{k_0}^2 f_0 \;=\; -2H[1-\tanh^2(k_0 H)] + 2k_0 H^2 \tanh(k_0 H)[1-\tanh^2(k_0 H)] \Rightarrow$$

$$\partial_{k_0}^2 f_0 \;=\; -2H[1-\tanh^2(k_0 H)](1-H\mu_0) \;=\; -2H(1-H\mu_0)\left(1-\frac{\mu_0^2}{k_0^2}\right) \qquad \text{(A.12c)}$$

Using Eqs. (A.12a)-(A.12c) we calculate the following quantities:

$$-\frac{\partial_H^2 f_0}{\partial_{k_0} f_0} \;=\; -\frac{2\mu_0(k_0^2-\mu_0^2)}{-\dfrac{\mu_0+H(k_0^2-\mu_0^2)}{k_0}} \;=\; \frac{2k_0\mu_0(k_0^2-\mu_0^2)}{\mu_0+H(k_0^2-\mu_0^2)} \;=\; -2\mu_0\partial_H k_0, \qquad \text{(A.13a)}$$

$$-\frac{2\partial_{Hk_0} f_0\,\partial_H k_0}{\partial_{k_0} f_0} \;=\; -\frac{-4k_0(1-H\mu_0)[1-1+\dfrac{\mu_0^2}{k_0^2}]\partial_H k_0}{-\dfrac{\mu_0+H(k_0^2-\mu_0^2)}{k_0}} \;=\; -\frac{4(1-H\mu_0)(k_0^2-\mu_0^2)\partial_H k_0}{\mu_0+H(k_0^2-\mu_0^2)} \Rightarrow$$

$$-\frac{2\partial_{Hk_0} f_0\,\partial_H k_0}{\partial_{k_0} f_0} \;=\; -\frac{4(1-H\mu_0)(k_0^2-\mu_0^2)\partial_H k_0}{\mu_0+H(k_0^2-\mu_0^2)} \;=\; 4(1-H\mu_0)\partial_H k_0\frac{\partial_H k_0}{k_0}, \qquad \text{(A.13b)}$$

$$-\frac{\partial_{k_0}^2 f_0(\partial_H k_0)^2}{\partial_{k_0} f_0} \;=\; -\frac{-2H(1-H\mu_0)(1-\dfrac{\mu_0^2}{k_0^2})(\partial_H k_0)^2}{-\dfrac{\mu_0+H(k_0^2-\mu_0^2)}{k_0}} \Rightarrow$$

$$-\frac{\partial_{k_0}^2 f_0(\partial_H k_0)^2}{\partial_{k_0} f_0} \;=\; -\frac{2H(1-H\mu_0)(k_0^2-\mu_0^2)(\partial_H k_0)^2}{k_0[\mu_0+H(k_0^2-\mu_0^2)]} \Rightarrow$$

$$-\frac{\partial^2_{k_0} f_0 (\partial_H k_0)^2}{\partial_{k_0} f_0} = 2H(1-H\mu_0)\partial_H k_0 (\frac{\partial_H k_0}{k_0})^2 \qquad \text{(A.13c)}$$

Finally we arrive at the formula:

$$\partial^2_H k_0 = -2\mu_0 \partial_H k_0 + 4(1-H\mu_0)\partial_H k_0 \frac{\partial_H k_0}{k_0} + 2H(1-H\mu_0)\partial_H k_0 (\frac{\partial_H k_0}{k_0})^2 \Rightarrow$$

$$\partial^2_H k_0 = 2\partial_H k_0 [-\mu_0 + 2(1-H\mu_0)\frac{\partial_H k_0}{k_0} + H(1-H\mu_0)(\frac{\partial_H k_0}{k_0})^2] \Rightarrow$$

$$\partial^2_H k_0 = 2\partial_H k_0 \{-\mu_0 + (1-H\mu_0)\frac{\partial_H k_0}{k_0}[2 + H\frac{\partial_H k_0}{k_0}]\} \qquad \text{(A.14)}$$

Calculation of partial derivatives $\partial^2_H k_n$, $n \in \{0,1,2,...\}$

By straightforward differentiation of Eq. (A.1b) one easily finds:

$$\partial^2_H f_n = -2k_n^3 \tan(k_n H)[1+\tan^2(k_n H)] = 2\mu_0 (k_n^2 + \mu_0^2) \qquad \text{(A.15a)}$$

$$\partial_{Hk_n} f_n = -2k_n [1+\tan^2(k_n H)] - 2k_n^2 H \tan(k_n H)[1+\tan^2(k_n H)] \Rightarrow$$

$$\partial_{Hk_n} f_n = -2k_n [1+\tan^2(k_n H)](1-H\mu_0) = -2k_n (1-H\mu_0)(1+\frac{\mu_0^2}{k_0^2}) \qquad \text{(A.15b)}$$

$$\partial^2_{k_n} f_n = -2H[1+\tan^2(k_n H)] - 2k_n H^2 \tan(k_n H)[1+\tan^2(k_n H)] \Rightarrow$$

$$\partial^2_{k_n} f_n = -2H[1+\tan^2(k_n H)](1-H\mu_0) = -2H(1-\mathrm{H}\mu_0)(1+\frac{\mu_0^2}{k_0^2}) \qquad \text{(A.15c)}$$

Using Eqs (A.15a)-(A.15c) we calculate the following quantities:

$$-\frac{\partial^2_H f_n}{\partial_{k_n} f_n} = -\frac{2\mu_0 (k_n^2+\mu_0^2)}{\frac{\mu_0 - H(k_n^2+\mu_0^2)}{k_n}} = -\frac{2k_n \mu_0 (k_n^2+\mu_0^2)}{\mu_0 - H(k_n^2+\mu_0^2)} = -2\mu_0 \partial_H k_n \qquad \text{(A.16a)}$$

$$-\frac{2\partial_{Hk_n} f_n \partial_H k_n}{\partial_{k_n} f_n} = -\frac{-4k_n (1-H\mu_0)(1+\frac{\mu_0^2}{k_0^2})\partial_H k_n}{\frac{\mu_0 - H(k_n^2+\mu_0^2)}{k_n}} = \frac{4(1-H\mu_0)(k_n^2+\mu_0^2)\partial_H k_n}{\mu_0 - H(k_n^2+\mu_0^2)} \Rightarrow$$

$$-\frac{2\partial_{Hk_n} f_n \partial_H k_n}{\partial_{k_n} f_n} = 4(1 - H\mu_0)\partial_H k_n \frac{\partial_H k_n}{k_n} \tag{A.16b}$$

$$-\frac{\partial^2_{k_n} f_n (\partial_H k_n)^2}{\partial_{k_n} f_n} = -\frac{-2H(1 - H\mu_0)(1 + \frac{\mu_0^2}{k_0^2})(\partial_H k_n)^2}{\frac{\mu_0 - H(k_n^2 + \mu_0^2)}{k_n}} \Rightarrow$$

$$-\frac{\partial^2_{k_n} f_n (\partial_H k_n)^2}{\partial_{k_n} f_n} = \frac{2H(1 - H\mu_0)(k_n^2 + \mu_0^2)(\partial_H k_n)^2}{k_n[\mu_0 - H(k_n^2 + \mu_0^2)]} \Rightarrow$$

$$-\frac{\partial^2_{k_n} f_n (\partial_H k_n)^2}{\partial_{k_n} f_n} = 2H(1 - H\mu_0)\partial_H k_n (\frac{\partial_H k_n}{k_n})^2 \tag{A.16c}$$

Finally we arrive at the formula:

$$\partial^2_H k_n = -2\mu_0 \partial_H k_n + 4(1 - H\mu_0)\partial_H k_n \frac{\partial_H k_n}{k_n} + 2H(1 - H\mu_0)\partial_H k_n (\frac{\partial_H k_n}{k_n})^2 \Rightarrow$$

$$\partial^2_H k_n = 2\partial_H k_n [-\mu_0 + 2(1 - H\mu_0)\frac{\partial_H k_n}{k_n} + H(1 - H\mu_0)(\frac{\partial_H k_n}{k_n})^2] \Rightarrow$$

$$\partial^2_H k_n = 2\partial_H k_n \{-\mu_0 + (1 - H\mu_0)\frac{\partial_H k_n}{k_n}[2 + H\frac{\partial_H k_n}{k_n}]\} \tag{A.17}$$

Finally by direct differentiation of the horizontal gradient $\nabla_{\boldsymbol{x}} k_n$, we have

$$\nabla^2_{\boldsymbol{x}} k_n = \partial_H k_n \nabla^2_{\boldsymbol{x}} H + \partial^2_H k_n \left(\nabla_{\boldsymbol{x}} H\right)^2, \; n \in \{0,1,2,...\} \tag{A.18}$$

Thus the proof is complete. □

Appendix B: Spatial derivatives of the vertical functions

Abstract: The purpose of this note is the calculation of the Z_n first and second space derivatives. These calculations are essential for the analytical computation of the integral coefficients that arise in the substrate problem.

Introduction - needed formulas:

We begin by writing the formulas for the additional modes:

The *free-surface mode*:

$$Z_{-2} = \frac{\mu_0 h_0 + 1}{2 h_0}\frac{(z+h)^2}{H} - \frac{\mu_0 h_0 + 1}{2 h_0} H + 1 = a_2 \frac{(z+h)^2}{H} + 1 - a_2 H , \tag{B.1a}$$

and the *sloping-bottom mode*:

$$Z_{-1} = a_1 \frac{(z+h)^2}{H} + \frac{z+h}{h_0} + 1 - a_2 H , \tag{B.1b}$$

where:

$$a_1 = \frac{\mu_0 h_0 - 1}{2 h_0} , \qquad a_2 = \frac{\mu_0 h_0 + 1}{2 h_0}$$

Then, the formulas of the $L^2 -$ basis modes are presented again

$$Z_0 = \frac{\cosh\left[k_0 (z + h) \right]}{\cosh(k_0 H)} , \tag{B.1c}$$

$$Z_n = \frac{\cos\left[k_n (z + h) \right]}{\cos(k_n H)} , \; n = 1, 2, \ldots , \tag{B.1d}$$

where, the parameters k_n , $n \geq 0$ are calculated through the formulas:

$$\mu_0 - k_0 \tanh[k_0 H] = 0 \qquad \text{and} \quad \mu_0 + k_n \tan[k_n H] = 0$$

Note: The k_n parameters are functions of the free-surface elevation and the bottom bathymetry. Therefore, they are better written as $k_n = k_n(\boldsymbol{x}, t; \eta, h)$, a representation that is omitted for simplification of the formulas.

Next, we rewrite the W_n functions, that will be used for the formulas to follow:

$$W_0 = \frac{\sinh\left[k_0\left(z+h\right)\right]}{\cosh\left(k_0 H\right)}, \tag{A.2a}$$

$$W_n = \frac{\sin\left[k_n\left(z+h\right)\right]}{\cos\left(k_n H\right)}, \; n=1,2,\ldots, \tag{A.2b}$$

Finally, we present the partial derivatives of the k_n parameters with respect to the total bathymetry $H\left(\boldsymbol{x};t\right)$.

$$\partial_H k_n = \begin{cases} -\dfrac{k_0\left(k_0^2-\mu_0^2\right)}{\mu_0+H\left(k_0^2-\mu_0^2\right)}, \; n=0 \\ \dfrac{k_n\left(k_n^2+\mu_0^2\right)}{\mu_0-H\left(k_n^2+\mu_0^2\right)}, \; n=1,2,\ldots \end{cases} \tag{B.3}$$

First horizontal derivatives of the additional modes.

The gradient of the *sloping-bottom mode* is easily obtained through straightforward differentiation:

$$\nabla_{\boldsymbol{x}} Z_{-1} = \nabla_{\boldsymbol{x}}\left(a_1\frac{(z+h)^2}{H}+\frac{z+h}{h_0}-a_2 H+1\right)\Rightarrow$$

$$\nabla_{\boldsymbol{x}} Z_{-1} = 2a_1\frac{(z+h)}{H}\nabla_{\boldsymbol{x}} h - a_1\frac{(z+h)^2}{H^2}\partial_x H+\frac{\partial_x h}{h_0}-a_2\nabla_{\boldsymbol{x}} H\Rightarrow$$

$$\nabla_{\boldsymbol{x}} Z_{-1} = \frac{1}{h_0}\nabla_{\boldsymbol{x}} h - a_2\nabla_{\boldsymbol{x}} H+\frac{2a_1}{H}\nabla_{\boldsymbol{x}} h(z+h)-\frac{a_1}{H^2}\nabla_{\boldsymbol{x}} H(z+h)^2, \tag{B.4a}$$

Again, the gradient of the *free-surface mode* is easily calculated:

$$\nabla_{\boldsymbol{x}} Z_{-2} = \nabla_{\boldsymbol{x}}\left(a_2\frac{(z+h)^2}{H}-a_2 H+1\right)\Rightarrow$$

$$\nabla_{\boldsymbol{x}} Z_{-2} = 2a_2\frac{(z+h)}{H}\nabla_{\boldsymbol{x}} h - a_2\frac{(z+h)^2}{H^2}\nabla_{\boldsymbol{x}} H-a_2\nabla_{\boldsymbol{x}} H\Rightarrow$$

$$\nabla_{\boldsymbol{x}} Z_{-2} = -a_2\,\partial_x H+\frac{2a_2\,\partial_x h}{H}(z+h)-\frac{a_2\,\partial_x H}{H^2}(z+h)^2, \tag{B.4b}$$

First horizontal derivatives of the vertical $L^2(-h,\eta)-$ basis.

The calculation of the gradient of the propagating and evanescent modes requires taking into account their implicit $\boldsymbol{x}-$ dependence from the free-surface $\eta(\boldsymbol{x};t)$, the bottom bathymetry $h(\boldsymbol{x},t)$ and the parameter k_n. Therefore, such a calculation is better done by utilizing the chain rule. Specifically, we can write:

$$\nabla_{\boldsymbol{x}} Z_n = (\partial_\eta Z_n + \partial_{k_n} Z_n \partial_H k_n)\nabla_{\boldsymbol{x}}\eta + (\partial_h Z_n + \partial_{k_n} Z_n \partial_H k_n)\nabla_{\boldsymbol{x}} h \tag{B.5}$$

Hence, for the calculation of the horizontal gradient of the $L^2(-h,\eta)-$ modes, one needs to calculate the partial derivatives shown at the right hand side of formula (B.5).

For the propagating mode $n=0,$ we obtain:

$$\partial_\eta Z_0 = -\frac{k_0\cosh[k_0(z+h)]\sinh(k_0 H)}{\cosh^2(k_0 H)} = -\mu_0 Z_0\,, \tag{B.6a}$$

$$\partial_h Z_0 = \frac{k_0\sinh[k_0(z+h)]}{\cosh(k_0 H)} - \frac{k_0\cosh[k_0(z+h)]\sinh(k_0 H)}{\cosh^2(k_0 H)} = k_0 W_0 - \mu_0 Z_0\,, \tag{B.6b}$$

$$\partial_{k_0} Z_0 = \frac{(z+h)\sinh[k_0(z+h)]}{\cosh[k_0 H]} - \frac{H\cosh[k_0(z+h)]\sinh[k_0 H]}{\cosh^2[k_0 H]} \Rightarrow$$

$$\partial_{k_0} Z_0 = (z+h)W_0 - \frac{H\mu_0}{k_0} Z_0\,, \tag{B.6c}$$

Replacing formulas (B.6a), (B.6b) & (B.6c) to formula (B.5), we get

for the first term of the right side of equation (B.5)

$$\partial_\eta Z_0 + \partial_{k_0} Z_0 \partial_H k_0 = -\mu_0 Z_0 + \partial_H k_0 (z+h)W_0 - H\mu_0 \frac{\partial_H k_0}{k_0} Z_0 \Rightarrow$$

$$\partial_\eta Z_0 + \partial_{k_0} Z_0 \partial_H k_0 = -\mu_0[1 + H\frac{\partial_H k_0}{k_0}]Z_0 + \partial_H k_0 (z+h)W_0\,, \tag{B.7a}$$

for the second term of the right side of equation (B.5):

$$\partial_h Z_0 + \partial_{k_0} Z_0 \partial_H k_0 = k_0 W_0 - \mu_0 Z_0 + \partial_H k_0 (z+h)W_0 - H\mu_0 \frac{\partial_H k_0}{k_0} Z_0 \Rightarrow$$

$$\partial_h Z_0 + \partial_{k_0} Z_0 \partial_H k_0 = -\mu_0[1 + H\frac{\partial_H k_0}{k_0}]Z_0 + k_0 W_0 + \partial_H k_0 (z+h)W_0 \tag{B.7b}$$

Therefore we have:

$$\nabla_{\boldsymbol{x}} Z_0 = -\mu_0[1 + H\frac{\partial_H k_0}{k_0}]\nabla_{\boldsymbol{x}} H Z_0 + \partial_H k_0 \nabla_{\boldsymbol{x}} H(z+h)W_0 + k_0 \nabla_{\boldsymbol{x}} hW_0 , \tag{B.8}$$

Finally, we can write the gradient of Z_0 in the following form:

$$\nabla_{\boldsymbol{x}} Z_0 = \boldsymbol{F}_0^{(1)} Z_0 + \boldsymbol{F}_0^{(2)} W_0 + \boldsymbol{F}_0^{(3)}(z+h)W_0 \tag{B.9}$$

For $n>0$, we have:

$$\partial_\eta Z_n = \frac{k_n \cos[k_n(z+h)]\sin(k_n H)}{\cos^2(k_n H)} = -\mu_0 Z_n , \tag{B.10a}$$

$$\partial_h Z_n = k_n \frac{-\sin[k_n(z+h)]}{\cos(k_n H)} + \frac{k_n \cos[k_n(z+h)]\sin(k_n H)}{\cos^2(k_n H)} = -k_n W_n - \mu_0 Z_n , \tag{B.10b}$$

$$\partial_{k_n} Z_n = (z+h)\frac{-\sin[k_n(z+h)]}{\cos(k_n H)} + \frac{H\cos[k_n(z+h)]\sin(k_n H)}{\cos^2(k_n H)} \Rightarrow$$

$$\partial_{k_n} Z_n = -(z+h) W_n - \frac{H\mu_0}{k_n} Z_n , \tag{B.10c}$$

Replacing formulas (B.10a), (B.10b) & (B.10c) to formula (B.5), we obtain:

for the first term of the right side of equation (B.5):

$$\partial_\eta Z_n + \partial_{k_n} Z_n \partial_H k_n = -\mu_0 Z_n - \partial_H k_n (z+h)W_n - H\mu_0 \frac{\partial_H k_n}{k_n} Z_n \Rightarrow$$

$$\partial_\eta Z_n + \partial_{k_n} Z_n \partial_H k_n = -\mu_0[1 + H\frac{\partial_H k_n}{k_n}]Z_n - \partial_H k_n (z+h)W_n , \tag{B.11a}$$

for the second term of the right side of equation (B.5):

$$\partial_h Z_n + \partial_{k_n} Z_n \partial_H k_n = -k_n W_n - \mu_0 Z_n - \partial_H k_n (z+h)W_n - H\mu_0 \frac{\partial_H k_n}{k_n} Z_n \Rightarrow$$

$$\partial_h Z_n + \partial_{k_n} Z_n \partial_H k_n = -\mu_0[1 + H\frac{\partial_H k_n}{k_n}]Z_n - k_n W_n - \partial_H k_n (z+h)W_n , \tag{B.11b}$$

Therefore we have:

$$\nabla_{\boldsymbol{x}} Z_n = -\mu_n[1 + H\frac{\partial_H k_n}{k_n}]\nabla_{\boldsymbol{x}} H Z_n - \partial_H k_n \nabla_{\boldsymbol{x}} H(z+h) W_n - k_n \nabla_{\boldsymbol{x}} hW_n , \tag{B.12}$$

Finally we can write the gradient of Z_n in the following form:

$$\partial_x Z_n = \boldsymbol{F}_n^{(1)} Z_n - \boldsymbol{F}_n^{(2)} W_n - \boldsymbol{F}_n^{(3)} (z+h) W_n \,, \tag{B.13}$$

The coefficients of the formulas (B.13) and (B.9) are

$$\boldsymbol{F}_n^{(1)} = -\mu_0 [1 + H \frac{\partial_H k_n}{k_n}] \nabla_{\boldsymbol{x}} H \,, n = 0,1,2,\ldots, \tag{B.14a}$$

$$\boldsymbol{F}_n^{(2)} = k_n \nabla_{\boldsymbol{x}} h \,, n = 0,1,2,\ldots, \tag{B.14b}$$

$$\boldsymbol{F}_n^{(3)} = \partial_H k_n \nabla_{\boldsymbol{x}} H \,, n = 0,1,2,\ldots, \tag{B.14c}$$

First horizontal derivatives of the W_n functions.

This part acts as proof for Proposition 2, Section 2.1. As stated before, our main objective in this section is to write the horizontal space derivatives of the $Z_n -$ functions in a way that will enhance the computational efficiency of an implementation of the HCM method, to a parallel program. In the case of the space derivatives, our main concern, with respect to computational efficiency, is the fast computation of the analytical formulas of the integral coefficients. The representation used in this section has the following desirable attributes that render our computations both efficient and easily checkable. Firstly, this representation visibly separates the x and z dependency of said derivatives making the analytical integrations easier. Secondly, In both the second and first horizontal derivatives the z-dependent terms (the terms to be integrated) are the same. This fact will later allow us to calculate separately these basic integrals and use them for the calculation of the integral coefficients. Such a process greatly enhances the performance of the code since it prohibits us from calculating more than once quantities that appear in many formulas.

From chain rule we get:

$$\nabla_{\boldsymbol{x}} W_n = (\partial_\eta W_n + \partial_{k_n} W_n \partial_H k_n) \nabla_{\boldsymbol{x}} \eta + (\partial_h W_n + \partial_{k_n} W_n \partial_H k_n) \nabla_{\boldsymbol{x}} h \tag{B.15}$$

Calculating the partial derivatives of the right side of the formula (B.15) we have:

For $n=0$

$$\partial_\eta W_0 = -\frac{k_0 \sinh[k_0 (z+h)] \sinh(k_0 H)}{\cosh^2(k_0 H)} = -\mu_0 W_0, \tag{B.16a}$$

$$\partial_h W_0 = \frac{k_0 \cosh[k_0 (z+h)]}{\cosh(k_0 H)} - \frac{k_0 \sinh[k_0 (z+h)] \sinh(k_0 H)}{\cosh^2(k_0 H)} = k_0 Z_0 - \mu_0 W_0, \tag{B.16b}$$

$$\partial_{k_0} W_0 = \frac{(z+h) \cosh[k_0 (z+h)]}{\cosh(k_0 H)} - \frac{H \sinh[k_0 (z+h)] \sinh(k_0 H)}{\cosh^2(k_0 H)} \Rightarrow$$

$$\partial_{k_0} W_0 = (z+h) Z_0 - \frac{H \mu_0}{k_0} W_0, \tag{B.16c}$$

Replacing formulas (B.16a), (B.16b) & (B.16c) to formula (B.15), we get

for the first term of the right side of equation (B.5)

$$\partial_\eta W_0 + \partial_{k_0} W_0 \partial_H k_0 = -\mu_0 W_0 + \partial_H k_0 (z+h) Z_0 - H \mu_0 \frac{\partial_H k_0}{k_0} W_0 \Rightarrow$$

$$\partial_\eta W_0 + \partial_{k_0} W_0 \partial_H k_0 = -\mu_0 [1 + H \frac{\partial_H k_0}{k_0}] W_0 + \partial_H k_0 (z+h) Z_0, \tag{B.17a}$$

for the second term of the right side of equation (B.5):

$$\partial_h W_0 + \partial_{k_0} W_0 \partial_H k_0 = k_0 Z_0 - \mu_0 W_0 + \partial_H k_0 (z+h) Z_0 - H \mu_0 \frac{\partial_H k_0}{k_0} W_0 \Rightarrow$$

$$\partial_h W_0 + \partial_{k_0} W_0 \partial_H k_0 = -\mu_0 [1 + H \frac{\partial_H k_0}{k_0}] W_0 + k_0 Z_0 + \partial_H k_0 (z+h) Z_0, \tag{B.17b}$$

Therefore we have

$$\nabla_{\boldsymbol{x}} W_0 = -\mu_0 [1 + H \frac{\partial_H k_0}{k_0}] \nabla_{\boldsymbol{x}} H W_0 + \partial_H k_0 \nabla_{\boldsymbol{x}} H (z+h) Z_0 + k_0 \nabla_{\boldsymbol{x}} h Z_0, \tag{B.18}$$

Finally, we can write the gradient of the W_0 in the following form:

$$\nabla_{\boldsymbol{x}} W_0 = \boldsymbol{F}_0^{(1)} W_0 + \boldsymbol{F}_0^{(2)} Z_0 + \boldsymbol{F}_0^{(3)} (z+h) Z_0 \tag{B.19}$$

For $n>0$:

$$\partial_\eta W_n = -\frac{k_n (\sin[k_n (z+h)])(-\sin(k_n H))}{\cos^2(k_n H)} = k_n \tan(k_n H) W_n = -\mu_0 W_n, \tag{B.20a}$$

$$\partial_h W_n = \frac{k_n \cos[k_n (z+h)]}{\cos(k_n H)} + \frac{k_n (\sin[k_n (z+h)]) \sin(k_n H)}{\cos^2(k_n H)} = k_n Z_n - \mu_0 W_n, \tag{B.20b}$$

$$\partial_{k_n} W_n = \frac{(z+h)\cos[k_n (z+h)]}{\cos(k_n H)} - \frac{H (\sin[k_n (z+h)])(-\sin(k_n H))}{\cos^2(k_n H)} \Rightarrow$$

$$\partial_{k_n} W_n = (z+h) Z_n - \frac{H \mu_0}{k_n} W_n \tag{B.20c}$$

Replacing formulas (B.20a), (B.20b) & (B.20c) to formula (B.15), we get:

for the first term of the right side of equation (B.5):

$$\partial_\eta W_n + \partial_{k_n} W_n \partial_H k_n = -\mu_0 W_n + \partial_H k_n (z+h) Z_n - H \mu_0 \frac{\partial_H k_n}{k_n} W_n \Rightarrow$$

$$\partial_\eta W_n + \partial_{k_n} W_n \partial_H k_n = -\mu_0 [1 + H \frac{\partial_H k_n}{k_n}] W_n + \partial_H k_n (z+h) Z_n \tag{B.21a}$$

for the second term of the right side of equation (B.5):

$$\partial_h W_n + \partial_{k_n} W_n \partial_H k_n = k_n Z_n - \mu_0 W_n + \partial_H k_n (z+h) Z_n - H \mu_0 \frac{\partial_H k_n}{k_n} W_n \Rightarrow$$

$$\partial_h W_n + \partial_{k_n} W_n \partial_H k_n = -\mu_0 [1 + H \frac{\partial_H k_n}{k_n}] W_n + k_n Z_n + \partial_H k_n (z+h) Z_n , \tag{B.21b}$$

Therefore we have:

$$\nabla_{\boldsymbol{x}} W_n = -\mu_n [1 + H \frac{\partial_H k_n}{k_n}] \nabla_{\boldsymbol{x}} H W_n + \partial_H k_n \nabla_{\boldsymbol{x}} H (z+h) Z_n + k_n \nabla_{\boldsymbol{x}} h Z_n , \tag{B.22}$$

Finally, we can write the gradient of the W_n in the following form:

$$\nabla_{\boldsymbol{x}} W_n = \boldsymbol{F}_n^{(1)} W_n + \boldsymbol{F}_n^{(2)} Z_n + \boldsymbol{F}_n^{(3)} (z+h) Z_n , \tag{B.23}$$

Second horizontal derivatives of the additional modes.

As with the first horizontal derivatives of the *sloping bottom mode*, one can easily obtain the second with straightforward differentiation:

$$\Delta_{\boldsymbol{x}} Z_{-1} = \nabla_{\boldsymbol{x}} \cdot (\nabla_{\boldsymbol{x}} Z_{-1}) \Rightarrow$$

$$\Delta_{\boldsymbol{x}} Z_{-1} = \nabla_{\boldsymbol{x}} \cdot (\frac{1}{h_0} \nabla_{\boldsymbol{x}} h - a_2 \nabla_{\boldsymbol{x}} H + \frac{2 a_1}{H} \nabla_{\boldsymbol{x}} h (z+h) - \frac{a_1 \nabla_{\boldsymbol{x}} H}{H^2} (z+h)^2) \Rightarrow$$

$$\begin{aligned} \Delta_{\boldsymbol{x}} Z_{-1} = {} & \frac{\Delta_{\boldsymbol{x}} h}{h_0} - a_2 \Delta_{\boldsymbol{x}} H + \frac{2 a_1}{H} \Delta_{\boldsymbol{x}} h (z+h) + \frac{2 a_1 (\nabla_{\boldsymbol{x}} h)^2}{H} - \\ & - \frac{2 a_1 \nabla_{\boldsymbol{x}} h \nabla_{\boldsymbol{x}} H}{H^2} (z+h) - \frac{a_1 \partial_x^2 H}{H^2} (z+h)^2 - \frac{2 a_1 \nabla_{\boldsymbol{x}} H \nabla_{\boldsymbol{x}} h}{H^2} (z+h) + \\ & + \frac{2 a_1 (\nabla_{\boldsymbol{x}} H)^2}{H^3} (z+h)^2 \Rightarrow \end{aligned}$$

$$\begin{aligned}\Delta_x Z_{-1} &= (\frac{\Delta_x h}{h_0} - a_2\,\Delta_x H + \frac{2a_1(\nabla_x h)^2}{H}) + \\ &+ (\frac{2a_1\partial_x^2 h}{H} - \frac{4a_1\nabla_x h\nabla_x H}{H^2})(z+h) + \\ &+ (\frac{2a_1(\nabla_x H)^2}{H^3} - \frac{a_1\cdot\partial_x^2 H}{H^2})\,(z+h)^2\end{aligned} \tag{B.24}$$

Similarly, the second horizontal derivatives of the *free-surface mode* are calculated by the same method:

$$\Delta_x Z_{-2} = \nabla_x\cdot(\nabla_x Z_{-2}) \Rightarrow$$

$$\Delta_x Z_{-2} = \nabla_x\cdot(-a_2\nabla_x H + \frac{2a_2\nabla_x h}{H}(z+h) - \frac{a_2\nabla_x H}{H^2}(z+h)^2) \Rightarrow$$

$$\begin{aligned}\Delta_x Z_{-2} &= -a_2\Delta_x H + \frac{2a_2(\nabla_x h)^2}{H} + \frac{2a_2\partial_x^2 h}{H}(z+h) - \frac{2a_2\nabla_x h\nabla_x H}{H^2}(z+h) - \\ &- \frac{2a_2\nabla_x H\nabla_x h}{H^2}(z+h) + \frac{2a_2(\nabla_x H)^2}{H^3}(z+h)^2 - \frac{a_2\Delta_x H}{H^2}(z+h)^2\end{aligned}$$

$$\begin{aligned}\Delta_x Z_{-2} &= (\frac{2a_2(\nabla_x h)^2}{H} - a_2\Delta_x H) + (\frac{2a_2\Delta_x h}{H} - \frac{4a_2\nabla_x h\nabla_x H}{H})(z+h) + \\ &+ (\frac{2a_2(\nabla_x H)^2}{H^2} - \frac{a_2\Delta_x H}{H})(z+h)^2\end{aligned}, \tag{B.25}$$

Second horizontal derivatives of the $L^2(-h,\eta)-$ basis modes.

To obtain the Laplacian of the propagating and evanescent modes, we take the gradient of $\nabla_x Z_n$. The gradient of these modes is, as was the case with the modes themselves, implicitly $\boldsymbol{x}-$ dependent through its dependence on the free-surface $\eta(\boldsymbol{x};t)$, bottom bathymetry $h(\boldsymbol{x};t)$ and the parameter k_n. Therefore, as with the first derivatives in section 2.2, we will use the chain rule:

For $n=0$:

Applying the chain rule we get:

$$\Delta_x Z_0 = \nabla_x\cdot(\nabla_x Z_0) = \nabla_x\cdot(\boldsymbol{F}_0^{(1)} Z_0 + \boldsymbol{F}_0^{(2)} W_0 + \boldsymbol{F}_0^{(3)}(z+h)W_0) \Rightarrow$$

$$\Delta_x Z_0 = \boldsymbol{F}_0^{(1)}\cdot\nabla_x Z_0 + [\boldsymbol{F}_0^{(2)} + (z+h)\boldsymbol{F}_0^{(3)}]\cdot\nabla_x W_0 + \left(\nabla_x\cdot\boldsymbol{F}_0^{(1)}\right)Z_0 + \\ + [\nabla_x\cdot\boldsymbol{F}_0^{(2)} + (z+h)\nabla_x\cdot\boldsymbol{F}_0^{(3)}]\,W_0 + \left(\boldsymbol{F}_0^{(3)}\cdot\nabla_x h\right)W_0 \Rightarrow$$

$$\Delta_x Z_0 = \boldsymbol{F}_0^{(1)}\cdot[\boldsymbol{F}_0^{(1)} Z_0 + \boldsymbol{F}_0^{(2)} W_0 + \boldsymbol{F}_0^{(3)}(z+h)W_0] + \\ + [\boldsymbol{F}_0^{(2)} + (z+h)\boldsymbol{F}_0^{(3)}]\cdot[\boldsymbol{F}_0^{(1)} W_0 + \boldsymbol{F}_0^{(2)} Z_0 + \boldsymbol{F}_0^{(3)}(z+h)Z_0] + \\ + \left(\nabla_x\cdot\boldsymbol{F}_0^{(1)}\right)Z_0 + [\nabla_x\cdot\boldsymbol{F}_0^{(2)} + (z+h)\nabla_x\cdot\boldsymbol{F}_0^{(3)}]W_0 + \left(\boldsymbol{F}_0^{(3)}\cdot\nabla_x h\right)W_0 \Rightarrow$$

$$\Delta_x Z_0 = \left|\boldsymbol{F}_0^{(1)}\right|^2 Z_0 + \boldsymbol{F}_0^{(1)}\cdot[\boldsymbol{F}_0^{(2)} + (z+h)\boldsymbol{F}_0^{(3)}]W_0 + \\ + \boldsymbol{F}_0^{(1)}\cdot[\boldsymbol{F}_0^{(2)} + (z+h)\boldsymbol{F}_0^{(3)}]W_0 + [\boldsymbol{F}_0^{(2)} + (z+h)\boldsymbol{F}_0^{(3)}]^2 Z_0 + \\ + \nabla_x\cdot\boldsymbol{F}_0^{(1)} Z_0 + [\nabla_x\cdot\boldsymbol{F}_0^{(2)} + (z+h)\nabla_x\cdot\boldsymbol{F}_0^{(3)}]W_0 + \left(\boldsymbol{F}_0^{(3)}\cdot\nabla_x h\right)W_0 \Rightarrow$$

$$\Delta_x Z_0 = \{\left|\boldsymbol{F}_0^{(1)}\right|^2 + [\boldsymbol{F}_0^{(2)} + \boldsymbol{F}_0^{(3)}(z+h)]^2 + \nabla_x\cdot\boldsymbol{F}_0^{(1)}\}Z_0 + \\ + \{2\,\boldsymbol{F}_0^{(1)}\cdot[\boldsymbol{F}_0^{(2)} + \boldsymbol{F}_0^{(3)}(z+h)] + \nabla_x\cdot\boldsymbol{F}_0^{(2)} + \\ + \nabla_x\cdot\boldsymbol{F}_0^{(3)}\cdot(z+h) + \boldsymbol{F}_0^{(3)}\cdot\nabla_x h\}W_0 \Rightarrow$$

$$\Delta_x Z_0 = [\left|\boldsymbol{F}_0^{(1)}\right|^2 + \left|\boldsymbol{F}_0^{(2)}\right|^2 + \nabla_x\cdot\boldsymbol{F}_0^{(1)}]Z_0 + [2\,\boldsymbol{F}_0^{(2)}\cdot\boldsymbol{F}_0^{(3)}](z+h)Z_0 + \\ + \left|\boldsymbol{F}_0^{(3)}\right|^2(z+h)^2 Z_0 + [2\,\boldsymbol{F}_0^{(2)}\cdot\boldsymbol{F}_0^{(1)} + \nabla_x\cdot\boldsymbol{F}_0^{(2)} + \boldsymbol{F}_0^{(3)}\cdot\nabla_x h]W_0 + , \\ + [2\,\boldsymbol{F}_0^{(3)}\cdot\boldsymbol{F}_0^{(1)} + \nabla_x\cdot\boldsymbol{F}_0^{(3)}](z+h)W_0 \qquad \text{(B.26)}$$

Equation (B.26) can be written as:

$$\Delta_x Z_0 = G_0^{(1)} Z_0 + G_0^{(2)}(z+h)Z_0 + G_0^{(3)}(z+h)^2 Z_0 + \\ + G_0^{(4)} W_0 + G_0^{(5)}(z+h)W_0 \qquad \text{(B.27)}$$

where:

$$G_0^{(1)} = \left|\boldsymbol{F}_0^{(1)}\right|^2 + \left|\boldsymbol{F}_0^{(2)}\right|^2 + \nabla_x\cdot\boldsymbol{F}_0^{(1)}, \qquad \text{(B.28a)}$$

$$G_0^{(2)} = 2\,\boldsymbol{F}_0^{(2)}\cdot\boldsymbol{F}_0^{(3)}, \qquad \text{(B.28b)}$$

$$G_0^{(3)} = \left|\boldsymbol{F}_0^{(3)}\right|^2, \qquad \text{(B.28c)}$$

$$G_0^{(4)} = 2\,\boldsymbol{F}_0^{(2)}\cdot\boldsymbol{F}_0^{(1)} + \nabla_x\cdot\boldsymbol{F}_0^{(2)} + \boldsymbol{F}_0^{(3)}\cdot\nabla_x h, \qquad \text{(B.28d)}$$

$$G_0^{(5)} = 2\,\boldsymbol{F}_0^{(3)}\cdot\boldsymbol{F}_0^{(1)} + \nabla_x\cdot\boldsymbol{F}_0^{(3)}, \qquad \text{(B.28e)}$$

For $n>0$:

Again, applying the chain rule we get:

$$\Delta_{\boldsymbol{x}} Z_n = \nabla_{\boldsymbol{x}} \cdot (\nabla_{\boldsymbol{x}} Z_n) = \nabla_{\boldsymbol{x}} \cdot (\boldsymbol{F}_n^{(1)} Z_n - \boldsymbol{F}_n^{(2)} W_n - \boldsymbol{F}_n^{(3)} (z+h) W_n) \Rightarrow$$

$$\Delta_{\boldsymbol{x}} Z_n = \boldsymbol{F}_n^{(1)} \cdot \nabla_{\boldsymbol{x}} Z_n - [\boldsymbol{F}_n^{(2)} + (z+h)\boldsymbol{F}_n^{(3)}] \cdot \nabla_{\boldsymbol{x}} W_n + \left(\nabla_{\boldsymbol{x}} \cdot \boldsymbol{F}_n^{(1)}\right) Z_n + \\ - [\nabla_{\boldsymbol{x}} \cdot \boldsymbol{F}_n^{(2)} + (z+h)\nabla_{\boldsymbol{x}} \cdot \boldsymbol{F}_n^{(3)}] W_n - \left(\boldsymbol{F}_n^{(3)} \cdot \nabla_{\boldsymbol{x}} h\right) W_n \Rightarrow$$

$$\Delta_{\boldsymbol{x}} Z_n = \boldsymbol{F}_n^{(1)} \cdot [\boldsymbol{F}_n^{(1)} Z_n - \boldsymbol{F}_n^{(2)} W_n - \boldsymbol{F}_n^{(3)} (z+h) W_n] - \\ - [\boldsymbol{F}_n^{(2)} + (z+h)\boldsymbol{F}_n^{(3)}] \cdot [\boldsymbol{F}_n^{(1)} W_n + \boldsymbol{F}_n^{(2)} Z_n + \boldsymbol{F}_n^{(3)} (z+h) Z_n] + \\ + \left(\nabla_{\boldsymbol{x}} \cdot \boldsymbol{F}_n^{(1)}\right) Z_n - [\nabla_{\boldsymbol{x}} \cdot \boldsymbol{F}_n^{(2)} + (z+h)\nabla_{\boldsymbol{x}} \cdot \boldsymbol{F}_n^{(3)}] W_n - \left(\boldsymbol{F}_n^{(3)} \cdot \nabla_{\boldsymbol{x}} h\right) W_n \Rightarrow$$

$$\Delta_{\boldsymbol{x}} Z_n = \left|\boldsymbol{F}_n^{(1)}\right|^2 Z_n - \boldsymbol{F}_n^{(1)} \cdot [\boldsymbol{F}_n^{(2)} + (z+h)\boldsymbol{F}_n^{(3)}] W_n - \\ - \boldsymbol{F}_n^{(1)} \cdot [\boldsymbol{F}_n^{(2)} + (z+h)\boldsymbol{F}_n^{(3)}] W_n - [\boldsymbol{F}_n^{(2)} + (z+h)\boldsymbol{F}_n^{(3)}]^2 Z_n + \\ + \left(\nabla_{\boldsymbol{x}} \cdot \boldsymbol{F}_n^{(1)}\right) Z_n - [\nabla_{\boldsymbol{x}} \cdot \boldsymbol{F}_n^{(2)} + (z+h)\nabla_{\boldsymbol{x}} \cdot \boldsymbol{F}_n^{(3)}] W_n - \left(\boldsymbol{F}_n^{(3)} \cdot \nabla_{\boldsymbol{x}} h\right) W_n \Rightarrow$$

$$\Delta_{\boldsymbol{x}} Z_n = \{\left|\boldsymbol{F}_n^{(1)}\right|^2 - [\boldsymbol{F}_n^{(2)} + \boldsymbol{F}_n^{(3)} (z+h)]^2 + \nabla_{\boldsymbol{x}} \cdot \boldsymbol{F}_n^{(1)}\} Z_0 + \\ + \{-2\boldsymbol{F}_n^{(1)} \cdot [\boldsymbol{F}_n^{(2)} + \boldsymbol{F}_n^{(3)} (z+h)] - \nabla_{\boldsymbol{x}} \cdot \boldsymbol{F}_n^{(2)} - \\ - \nabla_{\boldsymbol{x}} \cdot \boldsymbol{F}_n^{(3)} (z+h) - \boldsymbol{F}_n^{(3)} \cdot \nabla_{\boldsymbol{x}} h\} W_n \Rightarrow$$

$$\Delta_{\boldsymbol{x}} Z_n = [\left|\boldsymbol{F}_n^{(1)}\right|^2 - \left|\boldsymbol{F}_n^{(2)}\right|^2 + \nabla_{\boldsymbol{x}} \cdot \boldsymbol{F}_n^{(1)}] Z_n - [2\boldsymbol{F}_n^{(2)} \cdot \boldsymbol{F}_n^{(3)}](z+h) Z_n - \\ - \left|\boldsymbol{F}_n^{(3)}\right|^2 (z+h)^2 Z_n - [2\boldsymbol{F}_n^{(2)} \cdot \boldsymbol{F}_n^{(1)} + \nabla_{\boldsymbol{x}} \cdot \boldsymbol{F}_n^{(2)} + \boldsymbol{F}_n^{(3)} \cdot \nabla_{\boldsymbol{x}} h] W_n -, \\ - [2\boldsymbol{F}_n^{(3)} \cdot \boldsymbol{F}_n^{(1)} + \nabla_{\boldsymbol{x}} \cdot \boldsymbol{F}_n^{(3)}](z+h) W_n \tag{B.29}$$

Equation (B.26) can be written as:

$$\Delta_{\boldsymbol{x}} Z_n = G_n^{(1)} Z_n + G_n^{(2)} (z+h) Z_n + G_n^{(3)} (z+h)^2 Z_n + \\ + G_n^{(4)} W_n + G_n^{(5)} (z+h) W_n \quad , \tag{B.30}$$

where:

$$G_n^{(1)} = \left|\boldsymbol{F}_n^{(1)}\right|^2 - \left|\boldsymbol{F}_n^{(2)}\right|^2 + \nabla_{\boldsymbol{x}} \cdot \boldsymbol{F}_n^{(1)}, \tag{B.31a}$$

$$G_n^{(2)} = -2\boldsymbol{F}_n^{(2)} \cdot \boldsymbol{F}_n^{(3)}, \tag{B.31b}$$

$$G_n^{(3)} = -\left|\boldsymbol{F}_n^{(3)}\right|^2, \tag{B.31c}$$

$$G_n^{(4)} = -2\boldsymbol{F}_n^{(2)} \cdot \boldsymbol{F}_n^{(1)} - \nabla_{\boldsymbol{x}} \cdot \boldsymbol{F}_n^{(2)} - \boldsymbol{F}_n^{(3)} \cdot \nabla_{\boldsymbol{x}} h \tag{B.31d}$$

$$G_n^{(5)} = -2\,\boldsymbol{F}_n^{(3)}\cdot\boldsymbol{F}_n^{(1)} - \nabla_{\boldsymbol{x}}\cdot\boldsymbol{F}_n^{(3)} \tag{B.31e}$$

First & Second vertical derivatives of the additional modes.

As with the horizontal derivatives of the *free-surface mode*, one can easily obtain the vertical ones with straightforward differentiation:

$$\partial_z Z_{-2} = \partial_z\left(a_2\frac{(z+h)^2}{H} - a_2 H + 1\right) = \frac{2a_2}{H}(z+h) \tag{B.32a}$$

$$\partial_z^2 Z_{-2} = \partial_z(\partial_z Z_{-2}) = \partial_z\left(\frac{2a_2}{H}(z+h)\right) = \frac{2a_2}{H} \tag{B.32b}$$

Equivalently, the horizontal derivatives of the *sloping bottom mode*, one can easily obtain the vertical ones with straightforward differentiation:

$$\partial_z Z_{-1} = \partial_z\left(a_1\frac{(z+h)^2}{H} + \frac{(z+h)}{h_0} - a_1 H + 1\right) = \frac{2a_1}{H}(z+h) + \frac{1}{h_0} \tag{B.33a}$$

$$\partial_z^2 Z_{-1} = \partial_z(\partial_z Z_{-1}) = \partial_z\left(\frac{2a_1}{H}(z+h) + \frac{1}{h_0}\right) = \frac{2a_1}{H} \tag{B.33b}$$

First & second vertical derivatives of the vertical $L^2(-h,\eta)-$ *basis*

The calculation of the vertical derivatives of the *propagating mode* can be seen below:

$$\partial_z Z_0 = \partial_z\left(\frac{\cosh\left(k_0(z+h)\right)}{\cosh\left(k_0 H\right)}\right) = k_0\frac{\sinh\left(k_0(z+h)\right)}{\cosh\left(k_0 H\right)} = k_0 W_0 \tag{B.34a}$$

$$\partial_z^2 Z_0 = \partial_z(k_0 W_0) = k_0^2\frac{\cosh\left(k_0(z+h)\right)}{\cosh\left(k_0 H\right)} = k_0^2 Z_0 \tag{B.34b}$$

Similarly, the calculation of the vertical derivatives of the *evanescent modes* can be seen below:

$$\partial_z Z_n = \partial_z\left(\frac{\cos\left(k_n(z+h)\right)}{\cos\left(k_n H\right)}\right) = -k_n\frac{\sin\left(k_n(z+h)\right)}{\cos\left(k_n H\right)} = k_n W_n \tag{B.35a}$$

$$\partial_z^2 Z_n = \partial_z(k_n W_n) = -k_n^2\frac{\cos\left(k_n(z+h)\right)}{\cos\left(k_n H\right)} = -k_n^2 Z_n \tag{B.35b}$$

Appendix C: A Detailed calculation of basic integrals

Calculation of basic integrals $J(s;Z_n)$ *and* $J(s;W_n)$

The calculation of said integrals will be done in the following way:

For the integrals $J(s;Z_{-2})$ and $J(s;Z_{-1})$ we will derive general analytical expressions. For the remaining integrals, we will first calculate the formulae with zero polynomial part. Then, we will derive recursive formulae, with respect to the polynomial degree.

For the vertical function corresponding to the free-surface additional mode:

$$J(s;Z_{-2}) = \int_{z=-h}^{z=\eta} (z+h)^s Z_{-2}\, dz = \frac{a_2}{H}\int_{z=-h}^{z=\eta} (z+h)^{s+2}\, dz + (1-a_2 H)\int_{z=-h}^{z=\eta} (z+h)^s\, dz \Rightarrow$$

$$J(s;Z_{-2}) = \frac{a_2}{3+s}H^{s+2} + (1-a_2 H)\frac{H^{s+1}}{1+s} = \frac{1}{1+s}H^{s+1} - \frac{2a_2}{(s+3)(s+1)}H^{s+2}, \quad \text{(C.1a)}$$

For the vertical function corresponding to the sloping-bottom additional mode:

$$J(s;Z_{-1}) = \int_{z=-h}^{z=\eta} (z+h)^s Z_{-1}\, dz = \frac{a_1}{H}\int_{z=-h}^{z=\eta} (z+h)^{s+2}\, dz + \frac{1}{h_0}\int_{z=-h}^{z=\eta} (z+h)^{s+1}\, dz + (1-a_2 H)\int_{z=-h}^{z=\eta} (z+h)^s\, dz \Rightarrow$$

$$J(s;Z_{-1}) = \frac{1}{s+1}H^{s+1} + \left[\frac{1}{(s+2)h_0} + \frac{a_1}{(s+3)} - \frac{a_2}{(s+1)}\right]H^{s+2}, \quad \text{(C.1b)}$$

Now we calculate the remaining basic integrals for zero polynomial degree:

For the integral corresponding to the propagating mode and its conjugate function:

$$J(0;Z_0) = \int_{z=-h}^{z=\eta} Z_0\, dz = \int_{z=-h}^{z=\eta} \frac{\partial_z W_0}{k_0}\, dz = \frac{\left[W_0\right]_{z=-h}^{z=\eta}}{k_0} = \frac{\tanh(k_0 H)}{k_0} \Rightarrow$$

$$J(0;Z_0) = \frac{\mu_0}{k_0^2}, \quad \text{(C.2a)}$$

$$J(0;W_0) = \int_{z=-h}^{z=\eta} W_0\, dz = \int_{z=-h}^{z=\eta} \frac{\partial_z Z_0}{k_0}\, dz = \frac{\left[Z_0\right]_{z=-h}^{z=\eta}}{k_0} = \frac{1-\frac{1}{\cosh(k_0 H)}}{k_0}, \quad \text{(C.2b)}$$

For the integrals corresponding to the evanescent modes and their conjugate functions:

$$J(0;Z_n) = \int_{z=-h}^{z=\eta} Z_n\,dz = \int_{z=-h}^{z=\eta} \frac{-\partial_z W_n}{k_n}dz = -\frac{\left[W_n\right]_{z=-h}^{z=\eta}}{k_n} = \frac{\tan\left(k_n H\right)}{k_n} \Rightarrow$$

$$J(0;Z_n) = -\frac{\mu_0}{k_n^2}, \tag{C.3a}$$

$$J(0;W_n) = \int_{z=-h}^{z=\eta} W_n\,dz = \int_{z=-h}^{z=\eta} \frac{\partial_z Z_n}{k_n}dz = \frac{\left[Z_n\right]_{z=-h}^{z=\eta}}{k_n} = \frac{1-\frac{1}{\cos\left(k_n H\right)}}{k_n}, \tag{C.3b}$$

Finally we derive the following recursive formulae:

For the basic integrals of the form $J(s;Z_0)$, we have:

$$J(s;Z_0) = \int_{z=-h}^{z=\eta} (z+h)^s Z_0\,dz = \int_{z=-h}^{z=\eta} (z+h)^s \frac{\partial_z W_0}{k_0}dz \Rightarrow$$

$$J(s;Z_0) = \frac{\left[(z+h)^s W_0\right]_{z=-h}^{z=\eta}}{k_0} - \frac{s}{k_0}\int_{z=-h}^{z=\eta} (z+h)^{s-1} W_0\,dz \Rightarrow$$

$$J(s;Z_0) = \frac{H^s \tanh\left(k_0 H\right)}{k_0} - \frac{s}{k_0}J(s-1;W_0) = H^s\frac{\mu_0}{k_0^2} - \frac{s}{k_0}J(s-1;W_0) \Rightarrow$$

$$J(s;Z_0) = H^s J(0;Z_0) - \frac{s}{k_0}J(s-1;W_0), \tag{C.4a}$$

For the basic integrals of the form $J(s;Z_n)$, $n \geq 1$, we have:

$$J(\mathrm{s};Z_n) = \int_{z=-h}^{z=\eta} (z+h)^s Z_n\,dz = \int_{z=-h}^{z=\eta} (z+h)^s \frac{-\partial_z W_n}{k_n}dz \Rightarrow$$

$$J(s;Z_n) = -\frac{\left[(z+h)^s W_n\right]_{z=-h}^{z=\eta}}{k_n} + \frac{s}{k_n}\int_{z=-h}^{z=\eta} (z+h)^{s-1} W_n\,dz \Rightarrow$$

$$J(s;Z_n) = \frac{H^s \tan\left(k_n H\right)}{k_n} + \frac{s}{k_n}J(s-1;W_n) = -H^s\frac{\mu_0}{k_n^2} + \frac{s}{k_n}J(s-1;W_n) \Rightarrow$$

$$J(s;Z_n) = H^s J(0;Z_n) + \frac{s}{k_n}J(\mathrm{s}-1;W_n), \tag{C.4b}$$

For the basic integrals of the form $J(s;W_0)$, we have:

$$J(s;W_0) = \int_{z=-h}^{z=\eta} (z+h)^s W_0\, dz = \int_{z=-h}^{z=\eta} (z+h)^s \frac{\partial_z Z_0}{k_0} dz \Rightarrow$$

$$J(s;W_0) = \frac{\left[(z+h)^s Z_0\right]_{z=-h}^{z=\eta}}{k_0} - \frac{s}{k_0} \int_{z=-h}^{z=\eta} (z+h)^{s-1} Z_0\, dz \Rightarrow$$

$$J(s;W_0) = \frac{H^s \left(1 - \frac{1}{\cosh(k_0 H)}\right)}{k_0} - \frac{s}{k_0} J(s-1;Z_0) \Rightarrow$$

$$J(s;W_0) = H^s J(0;W_0) - \frac{s}{k_0} J(s-1;Z_0), \tag{C.5a}$$

For the basic integrals of the form $J(s;W_n)$, $n \geq 1$, we have:

$$J(s;W_n) = \int_{z=-h}^{z=\eta} (z+h)^s W_n\, dz = \int_{z=-h}^{z=\eta} (z+h)^s \frac{\partial_z Z_n}{k_n} dz \Rightarrow$$

$$J(s;W_n) = \frac{\left[(z+h)^s Z_n\right]_{z=-h}^{z=\eta}}{k_n} - \frac{s}{k_n} \int_{z=-h}^{z=\eta} (z+h)^{s-1} Z_n\, dz \Rightarrow$$

$$J(s;W_n) = \frac{H^s \left(1 - \frac{1}{\cos(k_n H)}\right)}{k_n} - \frac{s}{k_n} J(s-1;Z_n) \Rightarrow$$

$$J(s;W_n) = H^s J(0;W_n) - \frac{s}{k_n} J(s-1;Z_n), \tag{C.5b}$$

The calculation of the basic integrals of the form $J(s;Z_m Z_n)$, $J(s;W_n Z_m)$ and $J(s;W_n W_m)$ will be done in the following way: First we will derive the formulae of said basic integrals for $s = 0$ and then we will derive recursive relations for the integrals with non-zero polynomial degree.

Calculation of basic integrals $J(0;Z_m Z_n)$

For $m = -2$, $n \geq -2$ & $m \geq -2$, $n = -2$:

$$J(0;Z_{-2},Z_m) = \int_{-h}^{\eta} Z_{-2} Z_m \, dz = \int_{-h}^{\eta} (a_2 \frac{(z+h)^2}{H} - a_2 H + 1) Z_m \, dz \Rightarrow$$

$$J(0;Z_{-2},Z_m) = \frac{a_2}{H} \int_{-h}^{\eta} (z+h)^2 Z_m \, dz + (1 - a_2 H) \int_{-h}^{\eta} Z_m \, dz \Rightarrow$$

$$J(0;Z_{-2},Z_m) = \frac{a_2}{H} J(2;Z_m) + (1 - a_2 H) J(0;Z_m), \tag{C.6a}$$

For $m = -1$, $n \geq -2$ & $m \geq -2$, $n = -1$:

$$J(0;Z_{-1},Z_m) = \int_{-h}^{\eta} Z_{-1} Z_m \, dz = \int_{-h}^{\eta} (a_1 \frac{(z+h)^2}{H} + \frac{z+h}{h_0} - a_2 H + 1) Z_m \, dz \Rightarrow$$

$$J(0;Z_{-1},Z_m) = \frac{a_1}{H} \int_{-h}^{\eta} (z+h)^2 Z_m \, dz + \frac{1}{h_0} \int_{-h}^{\eta} (z+h) Z_m \, dz + (1 - a_2 H) \int_{-h}^{\eta} Z_m \, dz \Rightarrow$$

$$J(0;Z_{-1},Z_m) = \frac{a_1}{H} J(2;Z_m) + \frac{1}{h_0} J(1;Z_m) + (1 - a_2 H) J(0;Z_m), \tag{C.6b}$$

For $m = 0$, $n = 0$:

$$J(0;Z_0,Z_0) = \int_{-h}^{\eta} Z_0 Z_0 \, dz = \int_{-h}^{\eta} \frac{\partial_z W_0}{k_0} Z_0 \, dz = \frac{\left[W_0 Z_0\right]_{z=-h}^{z=\eta}}{k_0 \cosh(k_0 H)} - \int_{-h}^{\eta} W_0 W_0 \, dz \Rightarrow$$

$$J(0;Z_0,Z_0) = \frac{\tanh(k_0 H)}{k_0} - \int_{-h}^{\eta} W_0^2 \, dz = \frac{\mu_0}{k_0^2} + \int_{-h}^{\eta} [\frac{1}{\cosh^2(k_0 H)} - Z_0^2] dz \Rightarrow$$

$$J(0;Z_0,Z_0) = \frac{\mu_0}{k_0^2} + \frac{H}{\cosh^2(k_0 H)} - \int_{-h}^{\eta} Z_0^2 \, dz = \frac{\mu_0}{k_0^2} + \frac{H(k_0^2 - \mu_0^2)}{k_0^2} - J(0;Z_0,Z_0) \Rightarrow$$

$$J(0;Z_0,Z_0) = \frac{\mu_0 + H(k_0^2 - \mu_0^2)}{2k_0^2}, \tag{C.6c}$$

For $m = n > 0$:

$$J(0;Z_m,Z_m) = \int_{-h}^{\eta} Z_m Z_m\,dz = \int_{-h}^{\eta} \frac{-\partial_z W_m}{k_m} Z_m\,dz = -\frac{\left[W_m Z_m\right]_{z=-h}^{z=\eta}}{k_m} + \int_{-h}^{\eta} W_m W_m\,dz \Rightarrow$$

$$J(0;Z_m,Z_m) = \frac{\tan(k_m H)}{k_m} + \int_{-h}^{\eta} W_m^2\,dz = \frac{-\mu_0}{k_m^2} + \int_{-h}^{\eta} [\frac{1}{\cos^2(k_m H)} - Z_m^2]\,dz \Rightarrow$$

$$J(0;Z_m,Z_m) = \frac{-\mu_0}{k_m^2} + \frac{H}{\cos^2(k_m H)} - \int_{-h}^{\eta} Z_m^2\,dz = \frac{-\mu_0}{k_m^2} + \frac{H}{\cos^2(k_m H)} - J(0;Z_m,Z_m) \Rightarrow$$

$$2J(0;Z_m,Z_m) = \frac{-\mu_0}{k_m^2} + \frac{H(k_m^2+\mu_0^2)}{k_m^2} \Rightarrow$$

$$J(0;Z_m,Z_m) = \frac{H}{2} + \frac{-\mu_0 + H\,\mu_0^2}{2}\frac{1}{k_m^2}, \tag{C.6d}$$

For $m,n \geq 0 \wedge m \neq n$:

Because the vertical functions Z_n $n \geq 0$ are the eigenfunctions of a Sturm-Liouville problem, we know from the theory of such problems that they form an orthogonal base on $L^2(-h,\eta)$. As a result we have the formula:

$$J(0;Z_n,Z_m) = 0, \tag{C.6e}$$

Calculation of basic integrals $J(0;W_n Z_m)$

For $m = -2$, $n \geq 0$:

$$J(0;W_n,Z_{-2}) = \int_{-h}^{\eta} W_n Z_{-2}\,dz = \int_{-h}^{\eta} [a_2\frac{(z+h)^2}{H} - a_2 H + 1] W_n\,dz \Rightarrow$$

$$J(0;W_n,Z_{-2}) = \frac{a_2}{H}\int_{-h}^{\eta} (z+h)^2 W_n\,dz + (1-a_2 H)\int_{-h}^{\eta} W_n\,dz \Rightarrow$$

$$J(0;W_n,Z_{-2}) = \frac{a_2}{H} J(2;W_n) + (1-a_2 H) J(0;W_n), \tag{C.7a}$$

For $m = -1$, $n \geq 0$:

$$J(0;W_n,Z_{-1}) = \int_{-h}^{\eta} W_0 Z_{-1}\,dz = \int_{-h}^{\eta} (a_1\frac{(z+h)^2}{H} + \frac{z+h}{h_0} - a_2 H + 1)W_0\,dz \Rightarrow$$

$$J(0;W_n,Z_{-1}) = \frac{a_1}{H}\int_{-h}^{\eta}(z+h)^2 W_0\,dz + \frac{1}{h_0}\int_{-h}^{\eta}(z+h)W_0\,dz + (1-a_2 H)\int_{-h}^{\eta} W_0\,dz \Rightarrow$$

$$J(0;W_n,Z_{-1}) = \frac{a_1}{H}J(2;W_0) + \frac{1}{h_0}J(1;W_0) + (1-a_2 H)J(0;W_0), \tag{C.7b}$$

For $m = n = 0$:

$$J(0;W_0,Z_0) = \int_{-h}^{\eta} W_0 Z_0\,dz = \int_{-h}^{\eta} W_0\frac{\partial_z W_0}{k_0}dz = \frac{[W_0 W_0]_{z=-h}^{z=\eta}}{k_0} - \int_{-h}^{\eta} Z_0 W_0\,dz \Rightarrow$$

$$J(0;W_0,Z_0) = \tanh(k_0 H)\frac{\tanh(k_0 H)}{k_0} - \int_{-h}^{\eta} Z_0 W_0\,dz = \frac{\mu_0^2}{k_0^3} - J(0;W_0,Z_0) \Rightarrow$$

$$2J(0;W_0,Z_0) = \frac{\mu_0^2}{k_0^3} \Rightarrow$$

$$J(0;W_0,Z_0) = \frac{\mu_0^2}{2k_0^3}, \tag{C.7c}$$

For $n = 0$, $m \geq 1$:

$$J(0;W_0,Z_m) = \int_{-h}^{\eta} W_0 Z_m\,dz = \int_{-h}^{\eta} W_0\frac{\partial_z W_m}{k_m}dz = \frac{[W_0 W_m]_{z=-h}^{z=\eta}}{k_m} - \frac{k_0}{k_m}\int_{-h}^{\eta} Z_0 W_m\,dz \Rightarrow$$

$$J(0;W_0,Z_m) = \tanh(k_0 H)\frac{\tan(k_m H)}{k_m} - \frac{k_0}{k_m}\int_{-h}^{\eta} Z_0\frac{(-\partial_z Z_m)}{k_m}dz \Rightarrow$$

$$J(0;W_0,Z_m) = -\frac{\mu_0^2}{k_m^2 k_0} + \frac{k_0}{k_m^2}[Z_0 Z_m]_{z=-h}^{z=\eta} - \frac{k_0^2}{k_m^2}\int_{-h}^{\eta} W_0 Z_m\,dz \Rightarrow$$

$$J(0;W_0,Z_m) = -\frac{\mu_0^2}{k_m^2 k_0} + \frac{k_0}{k_m^2}[1 - \frac{1}{\cosh(k_0 H)\cos(k_m H)}] - \frac{k_0^2}{k_m^2}J(0;W_0,Z_m) \Rightarrow$$

$$(\frac{k_0^2+k_m^2}{k_m^2})J(0;W_0,Z_m) = -\frac{\mu_0^2}{k_m^2 k_0} + \frac{k_0}{k_m^2}[1 - \frac{1}{\cosh(k_0 H)\cos(k_m H)}] \Rightarrow$$

$$J(0;W_0,Z_m) = -\frac{\mu_0^2}{(k_0^2+k_m^2)k_0} + \frac{k_0}{k_0^2+k_m^2}[1-\frac{1}{\cosh(k_0 H)\cos(k_m H)}], \qquad \text{(C.7d)}$$

For $n \geq 1$, $m = 0$:

$$J(0;W_n,Z_0) = \int_{-h}^{\eta} W_n Z_0\, dz = \int_{-h}^{\eta} W_n \frac{\partial_z W_0}{k_0} dz = \frac{[W_n W_0]_{z=-h}^{z=\eta}}{k_0} - \frac{k_n}{k_0}\int_{-h}^{\eta} Z_n W_0\, dz \Rightarrow$$

$$J(0;W_n,Z_0) = \tan[k_n H]\frac{\tanh[k_0 H]}{k_0} - \frac{k_n}{k_0}\int_{-h}^{\eta} Z_n W_0\, dz = -\frac{\mu_0^2}{k_0^2 k_n} - \frac{k_n}{k_0}\int_{-h}^{\eta} Z_n \frac{\partial_z Z_0}{k_0} dz \Rightarrow$$

$$J(0;W_n,Z_0) = -\frac{\mu_0^2}{k_0^2 k_n} - \frac{k_n}{k_0^2}[Z_n Z_0]_{z=-h}^{z=\eta} - \frac{k_n^2}{k_0^2}\int_{-h}^{\eta} W_n Z_0\, dz \Rightarrow$$

$$J(0;W_n,Z_0) = -\frac{\mu_0^2}{k_0^2 k_n} - \frac{k_n}{k_0^2}[1-\frac{1}{\cos(k_n H)\cosh(k_0 H)}] - \frac{k_n^2}{k_0^2}J(0;W_n,Z_0) \Rightarrow$$

$$(\frac{k_n^2+k_0^2}{k_0^2})J(0;W_n,Z_0) = -\frac{\mu_0^2}{k_0^2 k_n} - \frac{k_n}{k_0^2}[1-\frac{1}{\cos(k_n H)\cosh(k_0 H)}] \Rightarrow$$

$$J(0;W_n,Z_0) = -\frac{\mu_0^2}{(k_n^2+k_0^2)k_n} - \frac{k_n}{k_n^2+k_0^2}[1-\frac{1}{\cos(k_n H)\cosh(k_0 H)}], \qquad \text{(C.7e)}$$

For $m,n \geq 1 \wedge m \neq n$:

$$J(0;W_n,Z_m) = \int_{-h}^{\eta} W_n Z_m\, dz = \int_{-h}^{\eta} W_n \frac{\partial_z W_m}{k_m} dz = \frac{[W_n W_m]_{z=-h}^{z=\eta}}{k_m} - \frac{k_n}{k_m}\int_{-h}^{\eta} Z_n W_m\, dz \Rightarrow$$

$$J(0;W_n,Z_m) = \tan(k_n H)\frac{\tan(k_m H)}{k_m} - \frac{k_n}{k_m}\int_{-h}^{\eta} Z_n W_m\, dz \Rightarrow$$

$$J(0;W_n,Z_m) = -\frac{\mu_0^2}{k_m^2 k_n} - \frac{k_n}{k_m}\int_{-h}^{\eta} Z_n \frac{(-\partial_z Z_m)}{k_m} dz = -\frac{\mu_0^2}{k_m^2 k_n} + \frac{k_n}{k_m^2}[Z_n Z_m]_{z=-h}^{z=\eta} + \frac{k_n^2}{k_m^2}\int_{-h}^{\eta} W_n Z_m\, dz \Rightarrow$$

$$J(0;W_n,Z_m) = -\frac{\mu_0^2}{k_m^2 k_n} + \frac{k_n}{k_m^2}[1-\frac{1}{\cos(k_n H)\cos(k_m H)}] + \frac{k_n^2}{k_m^2}J(0;W_n,Z_m) \Rightarrow$$

$$(\frac{k_m^2-k_n^2}{k_m^2})J(0;W_n,Z_m) = -\frac{\mu_0^2}{k_m^2 k_n} + \frac{k_n}{k_m^2}[1-\frac{1}{\cos(k_n H)\cos(k_m H)}] \Rightarrow$$

$$J(0;W_n,Z_m) = \frac{\mu_0^2}{(k_n^2-k_m^2)k_n} - \frac{k_n}{k_n^2-k_m^2}[1-\frac{1}{\cos(k_n H)\cos(k_m H)}], \qquad \text{(C.7f)}$$

For $n = m \geq 1$:

$$J(0;W_m,Z_m)=\int_{-h}^{\eta} W_m\,Z_m\,dz=\int_{-h}^{\eta} W_m\,\frac{\partial_z W_m}{k_m}\,dz=\frac{[W_m\,W_m]_{z=-h}^{z=\eta}}{k_m}-\int_{-h}^{\eta} Z_m\,W_m\,dz\Rightarrow$$

$$J(0;W_m,Z_m)=\tan(k_m H)\frac{\tan(k_m H)}{k_m}-J(0;W_m,Z_m)\Rightarrow$$

$$2J(0;W_m,Z_m)=\frac{\mu_0^2}{k_m^3}\Rightarrow$$

$$J(0;W_m,Z_m)=\frac{\mu_0^2}{2k_m^3}, \tag{C.7g}$$

Calculation of basic integrals $J(0;W_n W_m)$

For $m = n = 0$:

$$J(0;W_0,W_0)=\int_{-h}^{\eta} W_0\,W_0\,dz=\int_{-h}^{\eta} W_0\,\frac{\partial_z Z_0}{k_0}\,dz=\frac{[W_0\,Z_0]_{z=-h}^{z=\eta}}{k_0}-\int_{-h}^{\eta} Z_0\,Z_0\,dz\Rightarrow$$

$$J(0;W_0,W_0)=\frac{\tanh(k_0 H)}{k_0}-J(0;Z_0,Z_0)=\frac{\mu_0}{k_0^2}-\frac{\mu_0+H(k_0^2-\mu_0^2)}{2k_0^2}\Rightarrow$$

$$J(0;W_0,W_0)=\frac{\mu_0-H(k_0^2-\mu_0^2)}{2k_0^2}, \tag{C.8a}$$

For $n = 0$, $m \geq 1$ & $n \geq 1$, $m = 0$:

$$J(0;W_n,W_0)=\int_{-h}^{\eta} W_n\,W_0\,dz=\int_{-h}^{\eta} W_n\,\frac{\partial_z Z_0}{k_0}\,dz=\frac{[W_n\,Z_0]_{z=-h}^{z=\eta}}{k_0}-\frac{k_n}{k_0}\int_{-h}^{\eta} Z_n\,Z_0\,dz\Rightarrow$$

$$J(0;W_n,W_0)=\frac{\tan(k_n H)}{k_0}-\frac{k_n}{k_0}J(0;Z_n,Z_0)=-\frac{\mu_0}{k_0\,k_n}+\frac{k_n}{k_0}0\Rightarrow$$

$$J(0;W_n,W_0)=-\frac{\mu_0}{k_0\,k_n}, \tag{C.8b}$$

For $n = m \geq 1$:

$$J(0;W_m,W_m)=\int_{-h}^{\eta} W_m W_m\, dz=\int_{-h}^{\eta} W_m \frac{(-\partial_z Z_m)}{k_m} dz=-\frac{[W_m Z_m]_{z=-h}^{z=\eta}}{k_m}+\int_{-h}^{\eta} Z_m Z_m\, dz \Rightarrow$$

$$J(0;W_m,W_m)=-\frac{\tan(k_m H)}{k_m}+J(0;Z_m,Z_m)=\frac{\mu_0}{k_m^2}+\frac{-\mu_0+H(k_m^2+\mu_0^2)}{2k_m^2} \Rightarrow$$

$$J(0;W_m,W_m) = \frac{\mu_0 + H(k_m^2+\mu_0^2)}{2k_m^2}, \tag{C.8c}$$

For $m,n \geq 1 \wedge m \neq n$:

$$J(0;W_n,W_m)=\int_{-h}^{\eta} W_n W_m\, dz=\int_{-h}^{\eta} W_n \frac{(-\partial_z Z_m)}{k_m} dz=-\frac{[W_n Z_m]_{z=-h}^{z=\eta}}{k_m}+\frac{k_n}{k_m}\int_{-h}^{\eta} Z_n Z_m\, dz \Rightarrow$$

$$J(0;W_n,W_m)=-\frac{\tan(k_n H)}{k_m}+\frac{k_n}{k_m}J(0;Z_n,Z_m)=\frac{\mu_0}{k_m k_n}+\frac{k_n}{k_m}0 \Rightarrow$$

$$J(0;W_n,W_m) = \frac{\mu_0}{k_m k_n}, \tag{C.8d}$$

Having derived the above formulas we can now conclude the calculation of the basic integrals using the following recursive formulae:

Calculation of basic integrals $J(s; Z_m Z_n)$, $s \geq 1$

For $m = n = 0$:

$$J(s;Z_0,Z_0)=\int_{-h}^{\eta}(z+h)^s\,Z_0\,Z_0\,dz=\int_{-h}^{\eta}(z+h)^s\,Z_0\,\frac{\partial_z W_0}{k_0}\,dz\Rightarrow$$

$$J(s;Z_0,Z_0)=\frac{\left|(z+h)^s\,Z_0\,W_0\right|_{z=-h}^{z=\eta}}{k_0}-\int_{-h}^{\eta}(z+h)^s\,W_0\,W_0\,dz-\frac{s\int_{-h}^{\eta}(z+h)^{s-1}\,Z_0\,W_0\,dz}{k_0}\Rightarrow$$

$$J(s;Z_0,Z_0)=\frac{H^s\tanh[k_0\,H]}{k_0}+\int_{-h}^{\eta}\frac{(z+h)^s}{\cosh^2[k_0\,H]}dz-J(\mathrm{s};Z_0,Z_0)-\frac{s\,J(\mathrm{s-1};Z_0,W_0)}{k_0}\Rightarrow$$

$$2\,J(s;Z_0,Z_0)=\frac{H^s\,\mu_0}{k_0^2}+\frac{H^{s+1}}{(s+1)\cosh^2[k_0\,H]}-\frac{s\,k_0\,J(\mathrm{s-1};Z_0,W_0)}{k_0^2}\Rightarrow$$

$$J(s;Z_0,Z_0)=-\frac{s\,k_0\,J(\mathrm{s-1};Z_0,W_0)}{2\,k_0^2}+\frac{H^s[(\mathrm{s+1})\,\mu_0+H\,(k_0^2-\mu_0^2)]}{2\,(\mathrm{s+1})\,k_0^2}\Rightarrow$$

$$J(s;Z_0,Z_0)=-\frac{s\,k_0\,J(\mathrm{s-1};Z_0,W_0)}{2\,k_0^2}+\frac{H^s\,s\,\mu_0}{2(\mathrm{s+1})\,k_0^2}+\frac{H^s[\mu_0+H\,(k_0^2-\mu_0^2)]}{2(\mathrm{s+1})\,k_0^2}\Rightarrow$$

$$J(s;Z_0,Z_0)=-\frac{s}{2k_0}J(s-1;Z_0,W_0)+\frac{H^s}{s+1}J(0;Z_0,Z_0)+\frac{H^s\,s}{2(s+1)}J(0;Z_0),\ \text{(C.9a)}$$

For $m = 0$, $n \geq 1$:

$$J(\mathrm{s};\mathrm{Z}_n,\mathrm{Z}_0)=\int_{-h}^{\eta}(z+h)^s\,\mathrm{Z}_n\,\mathrm{Z}_0\,dz=\int_{-h}^{\eta}(z+h)^s\,\mathrm{Z}_n\,\frac{\partial_z W_0}{k_0}\,dz\Rightarrow$$

$$J(\mathrm{s};\mathrm{Z}_n,\mathrm{Z}_0)=\frac{\left[(z+h)^s\,\mathrm{Z}_n\,W_0\right]_{z=-h}^{z=\eta}}{k_0}+\frac{k_n}{k_0}\int_{-h}^{\eta}(z+h)^s\,W_n\,W_0\,dz-\frac{s\int_{-h}^{\eta}(z+h)^{s-1}\,\mathrm{Z}_n\,W_0\,dz}{k_0}\Rightarrow$$

$$J(\mathrm{s};\mathrm{Z}_n,\mathrm{Z}_0)=\frac{H^s\tanh[k_0\,H]}{k_0}+\frac{k_n}{k_0}\int_{-h}^{\eta}(z+h)^s\,W_n\,\frac{\partial_z Z_0}{k_0}\,dz-\frac{s\,J(\mathrm{s}-1;\mathrm{Z}_n,W_0)}{k_0}\Rightarrow$$

$$J(\mathrm{s};\mathrm{Z}_n,\mathrm{Z}_0)=\frac{H^s\,\mu_0}{k_0^2}+\frac{k_n}{k_0^2}\left[(z+h)^s\,W_n\,Z_0\right]_{z=-h}^{z=\eta}-\frac{k_n^2}{k_0^2}J(\mathrm{s};\mathrm{Z}_n,\mathrm{Z}_0)-$$

$$-\frac{s\,k_n\,J(\mathrm{s}-1;W_n,Z_0)+s\,k_0\,J(\mathrm{s}-1;\mathrm{Z}_n,W_0)}{k_0^2}\Rightarrow$$

$$\left(\frac{k_0^2+k_n^2}{k_0^2}\right)J(\mathrm{s};\mathrm{Z}_n,\mathrm{Z}_0)=\frac{H^s\,\mu_0}{k_0^2}-\frac{H^s\,\mu_0}{k_0^2}-s\,\frac{k_n\,J(\mathrm{s}-1;W_n,Z_0)+k_0\,J(\mathrm{s}-1;\mathrm{Z}_n,W_0)}{k_0^2}\Rightarrow$$

$$J(s;Z_n,Z_0)\;=\;-\,s\,\frac{k_n\,J(s-1;W_n,Z_0)+k_0\,J(s-1;\mathrm{Z}_n,W_0)}{k_0^2+k_n^2},\qquad\text{(C.9b)}$$

For $m=n\geq 1$:

$$J(\mathrm{s};\mathrm{Z}_m,\mathrm{Z}_m)=\int_{-h}^{\eta}(z+h)^s\,\mathrm{Z}_m\,\mathrm{Z}_m\,dz=\int_{-h}^{\eta}(z+h)^s\,\mathrm{Z}_m\,\frac{\partial_z W_m}{k_m}\,dz\Rightarrow$$

$$J(\mathrm{s};\mathrm{Z}_m,\mathrm{Z}_m)=\frac{\left[(z+h)^s\,\mathrm{Z}_m\,W_m\right]_{z=-h}^{z=\eta}}{k_m}+\int_{-h}^{\eta}(z+h)^s\,W_m\,W_m\,dz-\frac{s\int_{-h}^{\eta}(z+h)^{s-1}\,\mathrm{Z}_m\,W_m\,dz}{k_m}\Rightarrow$$

$$J(\mathrm{s};\mathrm{Z}_m,\mathrm{Z}_m)=\frac{\tan[k_m\,H]H^s}{k_m}+\int_{-h}^{\eta}\frac{(z+h)^s}{\cos^2[k_m\,H]}\,dz-J(\mathrm{s};\mathrm{Z}_m,\mathrm{Z}_m)-\frac{s\,J(\mathrm{s}-1;\mathrm{Z}_m,W_m)}{k_m}\Rightarrow$$

$$2\,J(\mathrm{s};\mathrm{Z}_m,\mathrm{Z}_m)=\frac{-\mu_0\,H^s-s\,k_m\,J(s-1;\mathrm{Z}_m,W_m)}{k_m^2}+\frac{H^{s+1}}{(s+1)\cos^2[k_m\,H]}\Rightarrow$$

$$J(\mathrm{s};\mathrm{Z}_m,\mathrm{Z}_m)=\frac{-\mu_0\,H^s-s\,k_m\,J(s-1;\mathrm{Z}_m,W_m)}{2\,k_m^2}+\frac{H^{s+1}(k_m^2+\mu_0^2)}{2(s+1)\,k_m^2}\Rightarrow$$

$$J(\mathrm{s};\mathrm{Z}_m,\mathrm{Z}_m)=-\frac{s\,k_m\,J(s-1;\mathrm{Z}_m,W_m)}{2\,k_m^2}+\frac{H^s[-(s+1)\,\mu_0+H\,(k_m^2+\mu_0^2)]}{2\,(s+1)\,k_m^2}\Rightarrow$$

$$J(\mathrm{s};\mathrm{Z}_m,\mathrm{Z}_m)=-\frac{s\,k_m\,J(s-1;\mathrm{Z}_m,W_m)}{2\,k_m^2}-\frac{s\,H^s\,\mu_0}{2\,(s+1)\,k_m^2}+\frac{H^s[-\mu_0+H\,(k_m^2+\mu_0^2)]}{2\,(s+1)\,k_m^2}\Rightarrow$$

$$J(s;\mathrm{Z}_m,\mathrm{Z}_m)\;=\;-\frac{s}{2\,k_m}J(s-1;\mathrm{Z}_m,W_m)+\frac{H^s}{(s+1)}\,J(0;\mathrm{Z}_m,\mathrm{Z}_m)+\frac{s\,H^s}{2\,(s+1)}J(0;\mathrm{Z}_m)\quad,\tag{C.9c}$$

For $m,n>0\;\wedge\;m\neq n$:

$$J(\mathrm{s};\mathrm{Z}_n,\mathrm{Z}_m)=\int_{-h}^{\eta}(z+h)^s\,\mathrm{Z}_n\,\mathrm{Z}_m\,dz=\int_{-h}^{\eta}(z+h)^s\,\mathrm{Z}_n\,\frac{\partial_z W_m}{k_m}\,dz\Rightarrow$$

$$J(\mathrm{s};\mathrm{Z}_n,\mathrm{Z}_m)=\frac{\left|(z+h)^s\,\mathrm{Z}_n\,W_m\right|_{z=-h}^{z=\eta}}{k_m}+\frac{k_n}{k_m}\int_{-h}^{\eta}(z+h)^s\,W_n\,W_m\,dz-\frac{s\int_{-h}^{\eta}(z+h)^{s-1}\,\mathrm{Z}_n\,W_m\,dz}{k_m}\Rightarrow$$

$$J(\mathrm{s};\mathrm{Z}_n,\mathrm{Z}_m)=\frac{H^s\tan\left(k_m\;H\right)}{k_m}+\frac{k_n}{k_m}\int_{-h}^{\eta}(z+h)^s\,W_n\,\frac{\left(-\partial_z\,\mathrm{Z}_m\right)}{k_m}\,dz-\frac{s\,J(\mathrm{s}-1;\mathrm{Z}_n,W_m)}{k_m}\Rightarrow$$

$$J(\mathrm{s};\mathrm{Z}_n,\mathrm{Z}_m)=-\frac{H^s\,\mu_0}{k_m^2}-\frac{k_n}{k_m^2}\left|(z+h)^s\,W_n\,\mathrm{Z}_m\right|_{z=-h}^{z=\eta}+\frac{k_n^2}{k_m^2}\int_{-h}^{\eta}(z+h)^s\,\mathrm{Z}_n\,\mathrm{Z}_m\,dz-$$

$$-\frac{s\,k_m\,J(\mathrm{s}-1;\mathrm{Z}_n,W_m)-s\,k_n\,J(\mathrm{s}-1;W_n,\mathrm{Z}_m)}{k_m^2}\Rightarrow$$

$$\left(\frac{k_m^2-k_n^2}{k_m^2}\right)J(\mathrm{s};\mathrm{Z}_n,\mathrm{Z}_m)=-\frac{H^s\,\mu_0}{k_m^2}+\frac{H^s\,\mu_0}{k_m^2}-\frac{s\,k_m\,J(\mathrm{s}-1;\mathrm{Z}_n,W_m)-s\,k_n\,J(\mathrm{s}-1;W_n,\mathrm{Z}_m)}{k_m^2}\Rightarrow$$

$$J(s;\mathrm{Z}_n,\mathrm{Z}_m)\;=\;s\frac{k_n\,J(s-1;W_n,\mathrm{Z}_m)-k_m\,J(s-1;\mathrm{Z}_n,W_m)}{k_m^2-k_n^2}\,,\tag{C.9d}$$

Calculation of basic integrals $J(s;W_n Z_m)$, s ≥ 1

For $m = n = 0$:

$$J(\mathrm{s};W_0,\mathrm{Z}_0)=\int_{-h}^{\eta}(z+h)^s W_0 \mathrm{Z}_0\,dz=\int_{-h}^{\eta}(z+h)^s W_0\frac{\partial_z W_0}{k_0}dz\Rightarrow$$

$$J(\mathrm{s};W_0,\mathrm{Z}_0)=\frac{\left[(z+h)^s W_0 W_0\right]_{z=-h}^{z=\eta}}{k_0}-\int_{-h}^{\eta}(z+h)^s \mathrm{Z}_0 W_0\,dz-\frac{s\int_{-h}^{\eta}(z+h)^{s-1}W_0 W_0\,dz}{k_0}\Rightarrow$$

$$2J(\mathrm{s};W_0,\mathrm{Z}_0)=\frac{H^s\tanh[k_0 H]\tanh[k_0 H]}{k_0}-\frac{s\,J(\mathrm{s}-1;W_0,W_0)}{k_0}\Rightarrow$$

$$J(\mathrm{s};W_0,\mathrm{Z}_0)=-\frac{s\,J(\mathrm{s}-1;W_0,W_0)}{2k_0}+\frac{H^s\mu_0^2}{2k_0^3}\Rightarrow$$

$$J(s;W_0,Z_0)=-\frac{s}{2k_0}J(s-1;W_0,W_0)+H^s J(0;W_0,Z_0)\,, \qquad \text{(C.10a)}$$

For $m \geq 1$, $n = 0$:

$$J(\mathrm{s};W_0,Z_m)=\int_{-h}^{\eta}(z+h)^s W_0 Z_m\,dz=\int_{-h}^{\eta}(z+h)^s W_0\frac{\partial_z W_m}{k_m}dz\Rightarrow$$

$$J(\mathrm{s};W_0,Z_m)=\frac{\left[(z+h)^s W_0 W_m\right]_{z=-h}^{z=\eta}}{k_m}-\frac{k_0}{k_m}\int_{-h}^{\eta}(z+h)^s Z_0 W_m\,dz-\frac{s\int_{-h}^{\eta}(z+h)^{s-1}W_0 W_m\,dz}{k_m}\Rightarrow$$

$$J(\mathrm{s};W_0,Z_m)=\frac{H^s\tanh[k_0 H]\tan[k_m H]}{k_m}-\frac{k_0}{k_m}\int_{-h}^{\eta}(z+h)^s Z_0\frac{(-\partial_z Z_m)}{k_m}dz-\frac{s\,J(\mathrm{s}-1;W_0,W_m)}{k_m}\Rightarrow$$

$$J(\mathrm{s};W_0,Z_m)=-\frac{H^s\mu_0^2}{k_m^2 k_0}+\frac{k_0}{k_m^2}\left[(z+h)^s Z_0 Z_m\right]_{z=-h}^{z=\eta}-\frac{k_0^2}{k_m^2}J(\mathrm{s};W_0,Z_m)-$$

$$-\frac{s\,k_m J(\mathrm{s}-1;W_0,W_m)+s\,k_0 J(\mathrm{s}-1;Z_0,Z_m)}{k_m^2}\Rightarrow$$

$$\left(\frac{k_m^2+k_0^2}{k_m^2}\right)J(\mathrm{s};W_0,\mathrm{Z}_m)=\frac{H^s(k_0^2-\mu_0^2)}{k_m^2 k_0}-\frac{s\,k_m J(\mathrm{s}-1;W_0,W_m)+s\,k_0 J(\mathrm{s}-1;\mathrm{Z}_0,\mathrm{Z}_m)}{k_m^2}\Rightarrow$$

$$J(\mathrm{s};W_0,\mathrm{Z}_m)=\frac{H^{s-1}\left[H(k_0^2-\mu_0^2)+\mu_0\right]}{(k_m^2+k_0^2)k_0}-\frac{H^{s-1}\mu_0}{(k_m^2+k_0^2)k_0}-s\frac{k_m J(\mathrm{s}-1;W_0,W_m)}{k_m^2+k_0^2}\Rightarrow$$

$$J(\mathrm{s};W_0,\mathrm{Z}_m)=\frac{2H^{s-1}k_0J(0;Z_0,Z_0)}{k_m^2+k_0^2}+\frac{H^{s-1}k_mJ(0;W_0,W_m)}{k_m^2+k_0^2}-s\frac{k_m J(\mathrm{s}-1;W_0,W_m)}{k_m^2+k_0^2}\Rightarrow$$

$$J(s;W_0,Z_m)=\frac{2H^{s-1}k_0J(0;Z_0,Z_0)}{k_m^2+k_0^2}+\frac{k_m\left(H^{s-1}J(0;W_0,W_m)-sJ(s-1;W_0,W_m)\right)}{k_m^2+k_0^2}, \tag{C.10b}$$

For $m=0$, $n\geq 1$:

$$J(\mathrm{s};W_n,Z_0)=\int_{-h}^{\eta}(z+h)^s W_n Z_0\,dz=\int_{-h}^{\eta}(z+h)^s W_n\frac{\partial_z W_0}{k_0}dz\Rightarrow$$

$$J(\mathrm{s};W_n,Z_0)=\frac{\left[(z+h)^s W_n W_0\right]_{z=-h}^{z=\eta}}{k_0}-\frac{k_n}{k_0}\int_{-h}^{\eta}(z+h)^s Z_n W_0\,dz-\frac{s\int_{-h}^{\eta}(z+h)^{s-1}W_nW_0\,dz}{k_0}\Rightarrow$$

$$J(\mathrm{s};W_n,Z_0)=\frac{H^s\tanh[k_0H]\tan[k_nH]}{k_0}-\frac{k_n}{k_0}\int_{-h}^{\eta}(z+h)^s Z_n\frac{\partial_z Z_0}{k_0}dz-\frac{sJ(\mathrm{s}-1;W_n,W_0)}{k_0}\Rightarrow$$

$$J(\mathrm{s};W_n,Z_0)=-\frac{H^s\mu_0^2}{k_0^2k_n}-\frac{k_n}{k_0}\int_{-h}^{\eta}(z+h)^s Z_n\frac{\partial_z Z_0}{k_0}dz-\frac{sk_0J(\mathrm{s}-1;W_n,W_0)}{k_0^2}\Rightarrow$$

$$J(\mathrm{s};W_n,Z_0)=-\frac{H^s\mu_0^2}{k_0^2k_n}-\frac{k_n}{k_0^2}\left[(z+h)^s Z_nZ_0\right]_{z=-h}^{z=\eta}-\frac{k_n^2}{k_0^2}J(\mathrm{s};W_n,Z_0)+$$

$$+\frac{sk_nJ(\mathrm{s}-1;Z_n,Z_0)-sk_0J(\mathrm{s}-1;W_n,W_0)}{k_0^2}\Rightarrow$$

$$(\frac{k_0^2+k_n^2}{k_0^2})J(\mathrm{s};W_n,Z_0)=-\frac{H^s(\mu_0^2+k_n^2)}{k_0^2k_n}+s\frac{k_nJ(\mathrm{s}-1;Z_n,Z_0)-k_0J(\mathrm{s}-1;W_n,W_0)}{k_0^2}\Rightarrow$$

$$J(\mathrm{s};W_n,Z_0)=-s\frac{k_0J(\mathrm{s}-1;W_n,W_0)}{k_0^2+k_n^2}-\frac{H^s(\mu_0^2+k_n^2)}{(k_0^2+k_n^2)k_n}\Rightarrow$$

$$J(\mathrm{s};W_n,Z_0)=-s\frac{k_0J(\mathrm{s}-1;W_n,W_0)}{k_0^2+k_n^2}-\frac{H^{s-1}\left[H(\mu_0^2+k_n^2)-\mu_0\right]}{(k_0^2+k_n^2)k_n}-\frac{H^{s-1}\mu_0}{(k_0^2+k_n^2)k_n}\Rightarrow$$

$$J(\mathrm{s};W_n,Z_0)=-s\frac{k_0J(\mathrm{s}-1;W_n,W_0)}{k_0^2+k_n^2}-\frac{2H^{s-1}k_nJ(0;Z_n,Z_n)}{k_0^2+k_n^2}+\frac{H^{s-1}k_0J(0;W_n,W_0)}{k_0^2+k_n^2}\Rightarrow$$

$$J(s;W_n,Z_0)=\frac{k_0\left(H^{s-1}J(0;W_n,W_0)-sJ(s-1;W_n,W_0)\right)}{k_0^2+k_n^2}-\frac{2H^{s-1}k_nJ(0;Z_n,Z_n)}{k_0^2+k_n^2}, \tag{C.10c}$$

For $m = n > 0$:

$$J(\mathrm{s};W_m,\mathrm{Z}_m)=\int_{-h}^{\eta}(z+h)^s W_m\,\mathrm{Z}_m\,dz=\int_{-h}^{\eta}(z+h)^s W_m\frac{\partial_z W_m}{k_m}dz\Rightarrow$$

$$J(\mathrm{s};W_m,\mathrm{Z}_m)=\frac{\left\lfloor(z+h)^s W_m W_m\right\rfloor_{z=-h}^{z=\eta}}{k_m}-\int_{-h}^{\eta}(z+h)^s\,\mathrm{Z}_m W_m\,dz-\frac{s\int_{-h}^{\eta}(z+h)^{s-1}W_m W_m\,dz}{k_m}\Rightarrow$$

$$2\,J(\mathrm{s};W_m,\mathrm{Z}_m)=\frac{H^s\tan^2[k_m H]}{k_m}-\frac{s\,J(\mathrm{s}-1;W_m,W_m)}{k_m}\Rightarrow$$

$$J(\mathrm{s};W_m,\mathrm{Z}_m)=-\frac{s\,J(\mathrm{s}-1;W_m,W_m)}{2k_m}+\frac{H^s\mu_0^2}{2k_m^3}\Rightarrow$$

$$J(s;W_m,Z_m)\;=\;-H^s J(0;W_m,Z_m)-\frac{s}{2k_m}J(s-1;W_m,W_m)\;, \qquad \text{(C.10d)}$$

For $m\,,\ n>0\ \wedge\ m\neq n$:

$$J(\mathrm{s};W_n,Z_m)=\int_{-h}^{\eta}(z+h)^s W_n\,Z_m\,dz=\int_{-h}^{\eta}(z+h)^s W_n\frac{\partial_z W_m}{k_m}dz\Rightarrow$$

$$J(\mathrm{s};W_n,Z_m)=\frac{\left\lfloor(z+h)^s W_n W_m\right\rfloor_{z=-h}^{z=\eta}}{k_m}-\frac{k_n}{k_m}\int_{-h}^{\eta}(z+h)^s Z_n W_m\,dz-\frac{s\int_{-h}^{\eta}(z+h)^{s-1}W_n W_m\,dz}{k_m}\Rightarrow$$

$$J(\mathrm{s};W_n,Z_m)=\frac{H^s\tan\left(k_n H\right)\tan\left(k_m H\right)}{k_m}-\frac{k_n}{k_m}\int_{-h}^{\eta}(z+h)^s Z_n\frac{\left(-\partial_z Z_m\right)}{k_m}dz-\frac{s\,J(\mathrm{s}-1;W_n,W_m)}{k_m}\Rightarrow$$

$$J(\mathrm{s};W_n,Z_m)=\frac{H^s\mu_0^2}{k_m^2 k_n}+\frac{k_n}{k_m^2}\left\lfloor(z+h)^s Z_n Z_m\right\rfloor_{z=-h}^{z=\eta}+\frac{k_n^2}{k_m^2}J(\mathrm{s};W_n,\mathrm{Z}_m)-$$

$$-\frac{s\,k_m J(\mathrm{s}-1;W_n,W_m)+s\,k_n J(\mathrm{s}-1;Z_n,Z_m)}{k_m^2}\Rightarrow$$

$$\left(\frac{k_m^2-k_n^2}{k_m^2}\right)J(\mathrm{s};W_n,Z_m)=\frac{H^s\mu_0^2}{k_m^2 k_n}+\frac{k_n^2 H^s}{k_m^2 k_n}-s\frac{k_m J(\mathrm{s}-1;W_n,W_m)+k_n J(\mathrm{s}-1;Z_n,Z_m)}{k_m^2}\Rightarrow$$

$$J(\mathrm{s};W_n,Z_m)=\frac{H^{s-1}\mu_0}{(k_m^2-k_n^2)k_n}-\frac{H^{s-1}\left[\mu_0-H(k_n^2+\mu_0^2)\right]}{(k_m^2-k_n^2)k_n}-s\frac{k_m J(\mathrm{s}-1;W_n,W_m)}{k_m^2-k_n^2}\Rightarrow$$

$$(\mathrm{s};W_n,Z_m)=\frac{H^{s-1}k_m J(0;W_n,W_m)}{k_m^2-k_n^2}-\frac{2H^{s-1}k_n J(0;Z_n,Z_n)}{k_m^2-k_n^2}-s\frac{k_m J(\mathrm{s}-1;W_n,W_m)}{k_m^2-k_n^2}\Rightarrow$$

$$J(s;W_n,Z_m)\;=\;\frac{k_m\left(J(0;W_n,W_m)H^{s-1}\;-s\,J(s-1;W_n,W_m)\right)-2k_n H^{s-1}J(0;\,Z_n,Z_n)}{k_m^2\;-k_n^2}$$

(C.10e

Calculation of basic integrals $J(s;W_n W_m)$, $s \geq 1$

For $m = n = 0$:

$$J(\mathrm{s};W_0,W_0)=\int_{-h}^{\eta}(z+h)^s W_0 W_0\,dz=\int_{-h}^{\eta}(z+h)^s W_0\frac{\partial_z Z_0}{k_0}dz \Rightarrow$$

$$J(\mathrm{s};W_0,W_0)=\frac{\left[(z+h)^s W_0 Z_0\right]_{z=-h}^{z=\eta}}{k_0}-\int_{-h}^{\eta}(z+h)^s Z_0 Z_0\,dz-\frac{s\int_{-h}^{\eta}(z+h)^{s-1}W_0 Z_0\,dz}{k_0}\Rightarrow$$

$$J(\mathrm{s};W_0,W_0)=\frac{H^s\tanh\left(k_0 H\right)}{k_0}-\int_{-h}^{\eta}(z+h)^s\left[\frac{1}{\cosh^2\left(k_0 H\right)}+W_0^2\right]dz-\frac{s\,J(\mathrm{s}-1;W_0,\mathrm{Z}_0)}{k_0}\Rightarrow$$

$$2J(\mathrm{s};W_0,W_0)=\frac{H^s\mu_0}{k_0^2}-\frac{H^{s+1}}{(\mathrm{s}+1)\cosh^2\left(k_0 H\right)}-\frac{s\,J(\mathrm{s}-1;W_0,\mathrm{Z}_0)}{k_0}\Rightarrow$$

$$J(\mathrm{s};W_0,W_0)=\frac{H^s\mu_0}{2k_0^2}-\frac{H^{s+1}(k_0^2-\mu_0^2)}{2(\mathrm{s}+1)k_0^2}-\frac{s\,J(\mathrm{s}-1;W_0,\mathrm{Z}_0)}{2k_0}\Rightarrow$$

$$J(s;W_0,W_0)=-\frac{s\,J(s-1;W_0,\mathrm{Z}_0)}{2k_0}+\frac{H^s[(s+1)\mu_0-H(k_0^2-\mu_0^2)]}{2k_0^2}\,, \qquad \text{(C.11a)}$$

For $n = 0$, $m \geq 1$ & $n \geq 1$, $m = 0$:

$$J(\mathrm{s};W_n,W_0)=\int_{-h}^{\eta}(z+h)^s W_n W_0\,dz=\int_{-h}^{\eta}(z+h)^s W_n\frac{\partial_z Z_0}{k_0}dz\Rightarrow$$

$$J(\mathrm{s};W_n,W_0)=\frac{\left[(z+h)^s W_n Z_0\right]_{z=-h}^{z=\eta}}{k_0}-\frac{k_n}{k_0}\int_{-h}^{\eta}(z+h)^s Z_n Z_0\,dz-\frac{s\int_{-h}^{\eta}(z+h)^{s-1}W_n Z_0\,dz}{k_0}\Rightarrow$$

$$J(\mathrm{s};W_n,W_0)=\frac{H^s\tan\left(k_n H\right)}{k_0}-\frac{k_n}{k_0}\int_{-h}^{\eta}(z+h)^s Z_n\frac{\partial_z W_0}{k_0}dz-\frac{s\,J(\mathrm{s}-1;W_n,\mathrm{Z}_0)}{k_0}\Rightarrow$$

$$J(\mathrm{s};W_n,W_0)=-\frac{H^s\mu_0}{k_0 k_n}-\frac{k_n}{k_0^2}\left[(z+h)^s Z_n W_0\right]_{z=-h}^{z=\eta}-\frac{k_n^2}{k_0^2}\int_{-h}^{\eta}(z+h)^s W_n W_0\,dz+$$

$$+s\frac{k_n J(\mathrm{s}-1;Z_n,W_0)-k_0 J(\mathrm{s}-1;W_n,\mathrm{Z}_0)}{k_0^2}\Rightarrow$$

$$J(\mathrm{s};W_n,W_0)=-\frac{H^s\mu_0}{k_0 k_n}-\frac{k_n H^s\tanh\left(k_0 H\right)}{k_0^2}-\frac{k_n^2}{k_0^2}J(\mathrm{s};W_n,W_0)+$$

$$+s\frac{k_n J(\mathrm{s}-1;Z_n,W_0)-k_0 J(\mathrm{s}-1;W_n,\mathrm{Z}_0)}{k_0^2}\Rightarrow$$

$$(\frac{k_0^2+k_n^2}{k_0^2})\,J(\mathrm{s};W_n,W_0)=-\frac{H^s\,k_0^2\,\mu_0}{k_0^3\,k_n}-\frac{k_n^2\,H^s\,\mu_0}{k_0^3\,k_n}+$$
$$+s\,\frac{k_n\,J(\mathrm{s}-1;Z_n,W_0)-k_0\,J(\mathrm{s}-1;W_n,Z_0)}{k_0^2}\Rightarrow$$
$$J(\mathrm{s};W_n,W_0)=-\frac{H^s\,\mu_0\,(k_0^2+k_n^2)\,\mu_0}{k_0\,k_n\,(k_0^2+k_n^2)}+s\,\frac{k_n\,J(\mathrm{s}-1;Z_n,W_0)-k_0\,J(\mathrm{s}-1;W_n,Z_0)}{k_0^2}\Rightarrow$$

$$J(s;W_n,W_0)\;=\;s\,\frac{k_n\,J(s-1;Z_n,W_0)-k_0\,J(s-1;W_n,Z_0)}{k_0^2}-\frac{H^s\,\mu_0^2}{k_0\,k_n}\;, \qquad \text{(C.11b)}$$

For $m\,,\;n\geq 1\;\wedge\;m\neq n$:

$$J(\mathrm{s};W_n,W_m)=\int_{-h}^{\eta}(z+h)^s\,W_n\,W_m\,dz=\int_{-h}^{\eta}(z+h)^s\,W_n\,\frac{(-\partial_z Z_m)}{k_m}\,dz\Rightarrow$$
$$J(\mathrm{s};W_n,W_m)=-\frac{\left[(z+h)^s\,W_n\,Z_m\right]_{z=-h}^{z=\eta}}{k_m}+\frac{k_n}{k_m}\int_{-h}^{\eta}(z+h)^s\,Z_n\,Z_m\,dz+\frac{s\int_{-h}^{\eta}(z+h)^{s-1}\,W_n\,Z_m\,dz}{k_m}\Rightarrow$$
$$J(\mathrm{s};W_n,W_m)=-\frac{H^s\tan(k_n\,H)}{k_m}+\frac{k_n}{k_m}\int_{-h}^{\eta}(z+h)^s\,Z_n\,\frac{\partial_z W_m}{k_m}\,dz+\frac{s\,J(\mathrm{s}-1;W_n,Z_m)}{k_m}\Rightarrow$$

$$J(\mathrm{s};W_n,W_m)=\frac{H^s\,\mu_0}{k_m\,k_n}+\frac{k_n}{k_m^2}\left[(z+h)^s\,Z_n\,W_m\right]_{z=-h}^{z=\eta}+\frac{k_n^2}{k_m^2}\int_{-h}^{\eta}(z+h)^s\,W_n\,W_m\,dz+$$
$$+s\,\frac{k_m\,J(\mathrm{s}-1;W_n,Z_m)-k_n\,J(\mathrm{s}-1;Z_n,W_m)}{k_m^2}\Rightarrow$$
$$J(\mathrm{s};W_n,W_m)=\frac{H^s\,\mu_0}{k_m\,k_n}+\frac{k_n\,H^s\tan(k_m\,H)}{k_m^2}+\frac{k_n^2}{k_m^2}J(\mathrm{s};W_n,W_m)+$$
$$+s\,\frac{k_m\,J(\mathrm{s}-1;W_n,Z_m)-k_n\,J(\mathrm{s}-1;Z_n,W_m)}{k_m^2}\Rightarrow$$
$$(\frac{k_m^2-k_n^2}{k_m^2})\,J(\mathrm{s};W_n,W_m)=\frac{H^s\,k_m^2\,\mu_0}{k_m^3\,k_n}-\frac{k_n^2\,H^s\,\mu_0}{k_m^3\,k_n}+$$
$$+s\,\frac{k_m\,J(\mathrm{s}-1;W_n,Z_m)-k_n\,J(\mathrm{s}-1;Z_n,W_m)}{k_m^2}\Rightarrow$$
$$J(\mathrm{s};W_n,W_m)=\frac{H^s\,\mu_0\,(k_m^2-k_n^2)}{k_m\,k_n\,(k_m^2-k_n^2)}+s\,\frac{k_m\,J(\mathrm{s}-1;W_n,Z_m)-k_n\,J(\mathrm{s}-1;Z_n,W_m)}{k_m^2-k_n^2}\Rightarrow$$

$$J(s;W_n,W_m)\;=\;s\,\frac{k_m\,J(s-1;W_n,Z_m)-k_n\,J(s-1;Z_n,W_m)}{k_m^2-k_n^2}+\frac{H^s\,\mu_0}{k_m\,k_n}\;, \qquad \text{(C.11c)}$$

For $m = n > 0$:

$$J(\mathrm{s};W_m,W_m)=\int_{-h}^{\eta}(z+h)^s W_m W_m\,dz=\int_{-h}^{\eta}(z+h)^s W_m\frac{(-\partial_z \mathrm{Z}_m)}{k_m}dz\Rightarrow$$

$$J(\mathrm{s};W_m,W_m)=-\frac{\left[(z+h)^s W_m \mathrm{Z}_m\right]_{z=-h}^{z=\eta}}{k_m}+\int_{-h}^{\eta}(z+h)^s \mathrm{Z}_m \mathrm{Z}_m\,dz+\frac{s\int_{-h}^{\eta}(z+h)^{s-1} W_m \mathrm{Z}_m\,dz}{k_m}\Rightarrow$$

$$J(\mathrm{s};W_m,W_m)=-\frac{H^s\tan[k_m H]}{k_m}+\int_{-h}^{\eta}(z+h)^s\left[\frac{1}{\cos^2[k_m H]}-W_m^2\right]dz+\frac{s\,J(\mathrm{s}-1;W_m,\mathrm{Z}_m)}{k_m}\Rightarrow$$

$$2\,J(\mathrm{s};W_m,W_m)=\frac{H^s\mu_0}{k_m^2}+\frac{H^{s+1}}{(\mathrm{s}+1)\cos^2[k_m H]}+\frac{s\,J(\mathrm{s}-1;W_m,\mathrm{Z}_m)}{k_m}\Rightarrow$$

$$J(\mathrm{s};W_m,W_m)=\frac{H^s\mu_0}{2k_m^2}+\frac{H^{s+1}(k_m^2+\mu_0^2)}{2(\mathrm{s}+1)k_m^2}+\frac{s\,J(\mathrm{s}-1;W_m,\mathrm{Z}_m)}{2k_m}\Rightarrow$$

$$J(s;W_m,W_m)=\frac{s\,J(s-1;W_m,Z_m)}{2k_m}+\frac{H^s[(s+1)\mu_0+H(k_m^2+\mu_0^2)]}{2(s+1)k_m^2}\,, \qquad \text{(C.11d)}$$

Appendix D: Detailed asymptotics of matrix coefficients

In this Section, we calculate in detail the asymptotic behavior of the matrix coefficients presented in Chapter 2. This appendix supplements the results presented in Section 2.3 with detailed derivations. As a result, the asymptotic behavior of the functions $\boldsymbol{F}_n^{(i)}$, $n \geq 1$ and $G_n^{(i)}$, $n \geq 1$ as well as that of the basic integrals will be presented in order to calculate the asymptotic formulae of the matrix coefficients.

Before we calculate said asymptotics, we prove Proposition 2 from Section 2.3

Proposition 2: *The asymptotic behavior of the partial derivatives $\partial_H k_n$ and $\partial_H^2 k_n$ are given by the following relations:*

$$\partial_H k_n = -\frac{n\pi}{H^2} - \frac{H\mu_0^2}{n\pi} + O(n^{-2}), \tag{D.1a}$$

$$\partial_H^2 k_n = 2\frac{n\pi}{H^3} + O(n^{-1}), \tag{D.1b}$$

The following limits are also true:

$$\lim_{n\to\infty} \frac{\partial_H k_n}{k_n} = -\frac{1}{H}, \qquad \lim_{n\to\infty} \frac{\nabla_{\boldsymbol{x}} k_n}{k_n} = -\frac{\nabla_{\boldsymbol{x}} H}{H} \tag{D.1c}$$

$$\lim_{n\to\infty} \frac{\partial_H^2 k_n}{k_n} = \frac{2}{H^2}, \qquad \lim_{n\to\infty} \frac{\Delta_{\boldsymbol{x}} k_n}{k_n} = \frac{2(\nabla_{\boldsymbol{x}} H)^2}{H^2} - \frac{\Delta_{\boldsymbol{x}} H}{H} \tag{D.1d}$$

Proof: For the first partial derivative $\partial_H k_n$ we utilize Eq (4a) of Proposition 1, Section 2.1:

$$\partial_H k_n = \frac{k_n(k_n^2 + \mu_0^2)}{\mu_0 - H(k_n^2 + \mu_0^2)}$$

Imploring the asymptotic behavior of k_n, $n \geq 1$ from Proposition 1, Section 2.3:

$$\partial_H k_n = \frac{(\frac{n\pi}{H} + O(n^{-1}))(\frac{n^2\pi^2}{H^2} + O(1) + \mu_0^2)}{\mu_0 - H(\frac{n^2\pi^2}{H^2} + O(1) + \mu_0^2)} \Rightarrow$$

$$\partial_H k_n = \frac{\frac{n^3\pi^3}{H^3} + O(n)}{-H\frac{n^2\pi^2}{H^2} + O(1)} = -\frac{n\pi}{H^2} + O(n^{-1})$$

From this relation we can also prove (B.1c) as

$$\lim_{n\to\infty}\frac{\partial_H k_n}{k_n} = \lim_{n\to\infty}\frac{-\frac{n\pi}{H^2}+O(n^{-1})}{\frac{n\pi}{H}+O(n^{-1})} = -\frac{1}{H}$$

$$\lim_{n\to\infty}\frac{\nabla_{\boldsymbol{x}} k_n}{k_n} = \lim_{n\to\infty}\frac{\partial_H k_n}{k_n}\nabla_{\boldsymbol{x}} H = \lim_{n\to\infty}\frac{-\frac{n\pi}{H^2}+O(n^{-1})}{\frac{n\pi}{H}+O(n^{-1})}\nabla_{\boldsymbol{x}} H = -\frac{\nabla_{\boldsymbol{x}} H}{H}$$

To prove now Eq (B.1b) we implore Eq (4b) of Proposition 1, Section 2.1:

$$\partial_H^2 k_n = -2\,\partial_H k_n\left\{\mu_0 + \frac{\partial_H k_n}{k_n}\left(H\mu_0 - 1\right)\left(2 + H\frac{\partial_H k_n}{k_n}\right)\right\},$$

Imploring the asymptotic behavior of k_n, $n \geq 1$ from Proposition, Section 2.3:

$$\partial_H^2 k_n = -2\left(-\frac{n\pi}{H^2}+O(n^{-1})\right)\left\{\mu_0 + \left(-\frac{1}{H}+O(n^{-2})\right)\left(H\mu_0 - 1\right)\left(2 + H\left(-\frac{1}{H}+O(n^{-2})\right)\right)\right\} \Rightarrow$$

$$\partial_H^2 k_n = 2\frac{n\pi}{H^3}+O(n^{-1})$$

From this relation we can also prove B(1.d) as:

$$\lim_{n\to\infty}\frac{\partial_H^2 k_n}{k_n} = \lim_{n\to\infty}\frac{2\frac{n\pi}{H^3}+O(n^{-1})}{\frac{n\pi}{H}+O(n^{-1})} = \frac{2}{H^2}$$

$$\lim_{n\to\infty}\frac{\Delta_{\boldsymbol{x}} k_n}{k_n} = \lim_{n\to\infty}\left[\frac{\partial_H k_n}{k_n}\Delta_{\boldsymbol{x}} H + \frac{\partial_H^2 k_n}{k_n}(\nabla_{\boldsymbol{x}} H)^2\right] = \frac{2\,(\nabla_{\boldsymbol{x}} H)^2}{H^2} - \frac{\Delta_{\boldsymbol{x}} H}{H}$$

which finishes the proof. □

Then we proceed to calculate the asymptotic behavior of the functions $\boldsymbol{F}_n^{(i)}$, $n \geq 1$ and $G_n^{(i)}$, $n \geq 1$.

Asymptotics of $\boldsymbol{F}_n^{(i)},\ n \geq 1$ *and* $G_n^{(i)},\ n \geq 1$

For the functions $\boldsymbol{F}_n^{(i)},\ n \geq 1$ making use of the Propositions of Chapter 2, will make use of Proposition 1 & 2, of Section 2.3. In more detail:

$$\boldsymbol{F}_n^{(1)} = -\mu_0\left(1 + H\frac{\partial_H k_n}{k_n}\right)\nabla_{\boldsymbol{x}} H = -\mu_0\left(1 - H\left(\frac{1}{H} + \frac{H^2\mu_0^2}{n^2\pi^2} + O\left(n^{-4}\right)\right)\right)\nabla_{\boldsymbol{x}} H \Rightarrow$$

$$\boldsymbol{F}_n^{(1)} = \frac{H^3\mu_0^3}{n^2\pi^2}\nabla_{\boldsymbol{x}} H + O\left(n^{-4}\right) \tag{D.2a}$$

$$\boldsymbol{F}_n^{(2)} = k_n\nabla_{\boldsymbol{x}} h = \frac{n\pi}{H}\nabla_{\boldsymbol{x}} h - \frac{\mu_0 H}{n\pi}\nabla_{\boldsymbol{x}} h + O(n^{-2}) \tag{D.2b}$$

$$\boldsymbol{F}_n^{(3)} = \partial_H k_n\nabla_{\boldsymbol{x}} H = -\frac{n\pi}{H^2}\nabla_{\boldsymbol{x}} H - \frac{H\mu_0^2}{n\pi}\nabla_{\boldsymbol{x}} H + O(n^{-2}) \tag{D.2c}$$

For the functions $G_n^{(i)},\ n \geq 1$, defined by Eqs. (2.22) of Chapter 2, we again utilize the Propositions stated above and the asymptotic behavior of Eqs. (D.2) derived for the $\boldsymbol{F}_n^{(i)},\ n \geq 1$. Furthermore, we need to calculate some spatial derivatives of the functions $\boldsymbol{F}_n^{(i)},\ n \geq 1$ which can be computed by means of direct differentiation of Eqs (2.22), Section 2.1.

$$G_n^{(1)} = \left|\boldsymbol{F}_n^{(1)}\right|^2 - \left|\boldsymbol{F}_n^{(2)}\right|^2 + \nabla_{\boldsymbol{x}}\cdot\boldsymbol{F}_n^{(1)} = \left|\boldsymbol{F}_n^{(1)}\right|^2 - \left|\boldsymbol{F}_n^{(2)}\right|^2 - \mu_0\left(1 + H\frac{\partial_H k_n}{k_n}\right)\Delta_{\boldsymbol{x}} H$$
$$-\mu_0\frac{\partial_H k_n}{k_n}\left|\nabla_{\boldsymbol{x}} H\right|^2 - \mu_0\left(1 + H\frac{\partial_{HH} k_n}{k_n} - H\frac{\left(\partial_H k_n\right)^2}{k_n^2}\right)\left|\nabla_{\boldsymbol{x}} H\right|^2 \Rightarrow$$

$$G_n^{(1)} = \frac{H^6\mu_0^6}{n^4\pi^4}\left|\nabla_{\boldsymbol{x}} H\right|^2 + O(n^{-6}) - \frac{n^2\pi^2}{H^2}\left|\nabla_{\boldsymbol{x}} h\right|^2 + O(1) - \mu_0\left(1 - 1 - \frac{H^3\mu_0^2}{n^2\pi^2} - O(n^{-4})\right)\Delta_{\boldsymbol{x}} H$$
$$-\frac{\mu_0}{H}\left|\nabla_{\boldsymbol{x}} H\right|^2 - \mu_0\left(1 + \frac{2}{H} - 1\right)\left|\nabla_{\boldsymbol{x}} H\right|^2 \Rightarrow$$

$$G_n^{(1)} = \frac{H^6\mu_0^6}{n^4\pi^4}\left|\nabla_{\boldsymbol{x}} H\right|^2 - \frac{n^2\pi^2}{H^2}\left|\nabla_{\boldsymbol{x}} h\right|^2 + \mu_0\frac{H^3\mu_0^2}{n^2\pi^2}\Delta_{\boldsymbol{x}} H - \frac{\mu_0}{H}\left|\nabla_{\boldsymbol{x}} H\right|^2 - \mu_0\frac{2}{H}\left|\nabla_{\boldsymbol{x}} H\right|^2 \Rightarrow$$

$$G_n^{(1)} = -\frac{n^2\pi^2}{H^2}\left|\nabla_{\boldsymbol{x}} h\right|^2 + O(1), \tag{D.3a}$$

For $i = 2$, utilizing Eqs. (B.2b) & (B.2c) we have:

$$G_n^{(2)} = -2\boldsymbol{F}_n^{(2)}\cdot\boldsymbol{F}_n^{(3)} = 2\frac{n^2\pi^2}{H^3}\nabla_{\boldsymbol{x}}H\cdot\nabla_{\boldsymbol{x}}h + O(1), \tag{D.3b}$$

For $i = 3$, utilizing Eq. (B.2c) we have:

$$G_n^{(3)} = -\left|\boldsymbol{F}_n^{(3)}\right|^2 = -\frac{n^2\pi^2}{H^4}\left|\nabla_{\boldsymbol{x}}H\right|^2 + O(1), \tag{D.3c}$$

For $i = 4$, utilizing Eqs (B.2a), (B.2b) & (19b) of Section 2.1, we have:

$$G_n^{(4)} = 2\boldsymbol{F}_n^{(2)}\cdot\boldsymbol{F}_n^{(1)} + \nabla_{\boldsymbol{x}}\cdot\boldsymbol{F}_n^{(2)} + \nabla_{\boldsymbol{x}}h\cdot\boldsymbol{F}_n^{(3)} = 2\boldsymbol{F}_n^{(2)}\cdot\boldsymbol{F}_n^{(1)} + \nabla_{\boldsymbol{x}}h\cdot\boldsymbol{F}_n^{(3)}$$
$$+ \partial_H k_n\nabla_{\boldsymbol{x}}H\cdot\nabla_{\boldsymbol{x}}h + k_n\Delta_{\boldsymbol{x}}h \Rightarrow$$

$$G_n^{(4)} = \frac{n\pi}{H}\frac{H^3\mu_0^3}{n^2\pi^2}\nabla_{\boldsymbol{x}}h\cdot\nabla_{\boldsymbol{x}}H - \frac{n\pi}{H^2}\nabla_{\boldsymbol{x}}h\cdot\nabla_{\boldsymbol{x}}H$$
$$- \frac{n\pi}{H^2}\nabla_{\boldsymbol{x}}h\cdot\nabla_{\boldsymbol{x}}H + \frac{n\pi}{H}\Delta_{\boldsymbol{x}}h \Rightarrow$$

$$G_n^{(4)} = \frac{n\pi}{H}\left(\Delta_{\boldsymbol{x}}h - \frac{2}{H}\nabla_{\boldsymbol{x}}h\cdot\nabla_{\boldsymbol{x}}H\right) + O(1), \tag{D.3d}$$

For $i = 5$ utilizing Eqs. (B.2a), (B.2c) & (19c) of Section 2.1, we have:

$$G_n^{(5)} = 2\boldsymbol{F}_n^{(3)}\cdot\boldsymbol{F}_n^{(1)} + \nabla_{\boldsymbol{x}}\cdot\boldsymbol{F}_n^{(3)} = 2\boldsymbol{F}_n^{(3)}\cdot\boldsymbol{F}_n^{(1)} + \partial_{HH}k_n\left|\nabla_{\boldsymbol{x}}H\right|^2 + \partial_H k_n\Delta_{\boldsymbol{x}}H \Rightarrow$$

$$G_n^{(5)} = -2\frac{n\pi}{H^2}\frac{H^3\mu_0^3}{n^2\pi^2}\left|\nabla_{\boldsymbol{x}}H\right|^2 + 2\frac{n\pi}{H^3}\left|\nabla_{\boldsymbol{x}}H\right|^2 - \frac{n\pi}{H^2}\Delta_{\boldsymbol{x}}H + O(1) \Rightarrow$$

$$G_n^{(5)} = +\frac{n\pi}{H^2}\left(\frac{2}{H}\left|\nabla_{\boldsymbol{x}}H\right|^2 - \Delta_{\boldsymbol{x}}H\right) + O(1), \tag{D.3e}$$

Asymptotics of basic integrals $J(s;Z_n)$ and $J(s;W_n)$

Utilizing Eqs (??) of Section 2.2 we have:

$$J(0;Z_n) = -\frac{\mu_0}{k_n^2} = -\frac{\mu_0 H^2}{n^2\pi^2} + O(n^{-3}) \tag{D.4a}$$

$$J(0;W_n) = \frac{\frac{1}{\cos(k_n H)} - 1}{k_n} = \begin{cases} \frac{\mu_0^2 H^3}{4n^3\pi^3} + O(n^{-5}) & ,n \text{ even} \\ -\frac{2H}{n\pi} + O(n^{-3}) & ,n \text{ odd} \end{cases}$$

(D.4b)

To state the asymptotic behavior of all the other such basic integrals we state the following Lemma that provides general formulae for the calculation of their leading term.

Lemma 1: *The asymptotic behavior of basic integrals* $J(s;Z_n)$ *and* $J(s;W_n)$ *with* $s \geq 1$ *is given by the following formulae:*

$$J(s;Z_n) = \begin{cases} -\frac{\mu_0 H^{s+2}}{n^2\pi^2} + O(n^{-4}) & ,n \text{ even} \\ -\frac{H^{s+1}}{n^2\pi^2}(\mu_0 H + 2s) + O(n^{-4}) & ,n \text{ odd} \end{cases} \quad \text{(D.5a)}$$

$$J(s;W_n) = \begin{cases} \frac{\mu_0 H^{s+2}}{n^3\pi^3}\left(\frac{\mu_0 H}{4} + s\right) + O(n^{-5}) & ,n \text{ even} \\ -\frac{2H^{s+1}}{n\pi} + O(n^{-3}) & ,n \text{ odd} \end{cases} \quad \text{(D.5b)}$$

Proof: We first prove these formulae for $s = 1$.

Utilizing the recursive relations (33b) of Section 2.2 and Eqs. (B.4), we have

$$J(1;Z_n) = H J(0;Z_n) + \frac{1}{k_n} J(0;W_n) \Rightarrow$$

$$J(1;Z_n) = -H\frac{\mu_0 H^2}{n^2\pi^2} + \frac{H}{n\pi}\begin{cases} \frac{\mu_0^2 H^3}{4n^3\pi^3} + O(n^{-5}) & ,n \text{ even} \\ -\frac{2H}{n\pi} + O(n^{-3}) & ,n \text{ odd} \end{cases} \Rightarrow$$

$$J(1;Z_n) = \begin{cases} -\frac{\mu_0 H^3}{n^2\pi^2} + O(n^{-4}) & ,n \text{ even} \\ -\frac{H^2}{n^2\pi^2}(\mu_0 H + 2) + O(n^{-4}) & ,n \text{ odd} \end{cases} \quad \text{(D.6a)}$$

and using Eq. (34b) and Eqs (B.4):

$$J(1;W_n) = H J(0;W_n) - \frac{1}{k_n} J(0;Z_n) \Rightarrow$$

$$J(1;W_n) = H\begin{cases} \dfrac{\mu_0^2 H^3}{4n^3\pi^3} + O(n^{-5}) & ,n \text{ even} \\ -\dfrac{2H}{n\pi} + O(n^{-3}) & ,n \text{ odd} \end{cases} + \frac{H}{n\pi}\frac{\mu_0 H^2}{n^2\pi^2} \Rightarrow$$

$$J(1;W_n) = \begin{cases} \dfrac{\mu_0 H^3}{n^3\pi^3}\left(\dfrac{\mu_0 H}{4}+1\right) + O(n^{-5}) & ,n \text{ even} \\ -\dfrac{2H^2}{n\pi} + O(n^{-3}) & ,n \text{ odd} \end{cases}$$

(D.6b)

Now let us assume that Eqs. (D.5) hold for $s-1$. Then from the recursive relation (2.33b) of Chapter 2, we have:

$$J(s;Z_n) = H^s J(0;Z_n) + \frac{s}{k_n} J(\mathrm{s}-1;W_n) \Rightarrow$$

$$J(s;Z_n) = -H^s\frac{\mu_0 H^2}{n^2\pi^2} + \frac{sH}{n\pi}\begin{cases} \dfrac{\mu_0 H^{s+1}}{n^3\pi^3}\left(\dfrac{\mu_0 H}{4}+s-1\right) + O(n^{-5}) & ,n \textit{ even} \\ -\dfrac{2H^s}{n\pi} + O(n^{-3}) & ,n \textit{ odd} \end{cases} \Rightarrow$$

$$J(s;Z_n) = \begin{cases} -\dfrac{\mu_0 H^{s+2}}{n^2\pi^2} + O(n^{-4}) & ,n \text{ even} \\ -\dfrac{H^{s+1}}{n^2\pi^2}\left(\mu_0 H + 2s\right) + O(n^{-4}) & ,n \text{ odd} \end{cases}$$

which proves Eq. (D.5a).

Now, from the recursive relation (2.34b) of Chapter 2, we have:

$$J(s;W_n) = H^s J(0;W_n) - \frac{s}{k_n} J(s-1;Z_n) \Rightarrow$$

$$J(s;W_n) = H^s \begin{cases} \dfrac{\mu_0^2 H^3}{4n^3\pi^3} + O(n^{-5}) & ,n \text{ even} \\ -\dfrac{2H}{n\pi} + O(n^{-3}) & ,n \text{ odd} \end{cases} - \frac{sH}{n\pi} \begin{cases} -\dfrac{\mu_0 H^{s+1}}{n^2\pi^2} + O(n^{-4}) & ,n \text{ even} \\ -\dfrac{H^s}{n^2\pi^2}\left(\mu_0 H + 2s - 2\right) + O(n^{-4}) & ,n \text{ odd} \end{cases} \Rightarrow$$

$$J(s;W_n) = \begin{cases} \dfrac{\mu_0 H^{s+2}}{n^3\pi^3}\left(\dfrac{\mu_0 H}{4} + s\right) + O(n^{-5}) & ,n \text{ even} \\ -\dfrac{2H^{s+1}}{n\pi} + O(n^{-3}) & ,n \text{ odd} \end{cases}$$

which proves Eq. (D.5b) and thus concludes the proof. □

Asymptotic behavior of $J(0;Z_n,Z_m)$ integrals

In this case we note that the basic integrals are symmetric with respect to the indexes n,m. As a result the asymptotic behavior of the limit $\lim_{m\to\infty} J(0;Z_m,Z_n)$ is the same as the limit $\lim_{m\to\infty} J(0;Z_n,Z_m)$, and therefore only the calculation of one of the in needed.

$$J(0;Z_{-2},Z_n) = \frac{a_2}{H}J(2;Z_n) + (1-a_2H)J(0;Z_n) \Rightarrow$$

$$J(0;Z_{-2},Z_n) = \frac{a_2}{H} \begin{cases} -\dfrac{\mu_0 H^4}{n^2\pi^2} + O(n^{-4}) & ,n \text{ even} \\ -\dfrac{H^3}{n^2\pi^2}\left(\mu_0 H + 4\right) + O(n^{-4}) & ,n \text{ odd} \end{cases} - (1-a_2H)\frac{\mu_0 H^2}{n^2\pi^2} \Rightarrow$$

$$J(0;Z_{-2},Z_n) = \begin{cases} -\dfrac{\mu_0 H^2}{n^2\pi^2} + O(n^{-4}) & ,n \text{ even} \\ (4a_2 - \mu_0)\dfrac{H^2}{n^2\pi^2} + O(n^{-4}) & ,n \text{ odd} \end{cases} \quad \text{(D.7a)}$$

$$J(0;Z_{-1},Z_n) = \frac{a_1}{H}J(2;Z_n) + \frac{1}{h_0}J(1;Z_n) + (1-a_2H)J(0;Z_n) \Rightarrow$$

$$J(0;Z_{-1},Z_n) = \frac{a_1}{H}\begin{cases} -\dfrac{\mu_0 H^4}{n^2\pi^2} + O(n^{-4}) & ,n \text{ even} \\ -\dfrac{H^3}{n^2\pi^2}(\mu_0 H + 4) + O(n^{-4}) & ,n \text{ odd} \end{cases}$$

$$+ \frac{1}{h_0}\begin{cases} -\dfrac{\mu_0 H^3}{n^2\pi^2} + O(n^{-4}) & ,n \text{ even} \\ -\dfrac{H^2}{n^2\pi^2}(\mu_0 H + 2) + O(n^{-4}) & ,n \text{ odd} \end{cases} - (1 - a_2 H)\frac{\mu_0 H^2}{n^2\pi^2} \Rightarrow$$

$$J(0;Z_{-1},Z_n) = \begin{cases} \dfrac{\mu_0 H^2}{n^2\pi^2}\left(-a_1 H + \dfrac{H}{h_0} + a_2 H - 1\right) + O(n^{-4}) & ,n \text{ even} \\ -\dfrac{H^2}{n^2\pi^2}\left(\begin{array}{l} a_1(\mu_0 H + 4) + \dfrac{\mu_0 H + 2}{h_0} \\ -a_2\mu_0 H + \mu_0 \end{array}\right) + O(n^{-4}) & ,n \text{ odd} \end{cases} \tag{D.7b}$$

$$J(0;Z_m,Z_n) = 0 \ , m \neq n \ , \ m,n \geq 0 \tag{D.7c}$$

$$J(0;Z_n,Z_n) = \frac{-\mu_0 + H(k_n^2 + \mu_0^2)}{2k_n^2} = \frac{H}{2} + H^2\mu_0\frac{H\mu_0 - 1}{2n^2\pi^2 + O(n^{-2})} + \Rightarrow$$

$$J(0;Z_n,Z_n) = \frac{H}{2} + O(n^{-2}) \tag{D.7d}$$

Asymptotic behavior of $J(0;W_n,Z_m)$ integrals

$$J(0;W_n,Z_{-2}) = \frac{a_2}{H}J(2;W_n) + (1 - a_2 H)J(0;W_n) \Rightarrow$$

$$J(0;W_n,Z_{-2}) = \frac{a_2}{H}\begin{cases} \dfrac{\mu_0 H^4}{n^3\pi^3}\left(\dfrac{\mu_0 H}{4} + 2\right) + O(n^{-5}) & ,n \text{ even} \\ -\dfrac{2H^3}{n\pi} + O(n^{-3}) & ,n \text{ odd} \end{cases} + (1 - a_2 H)\begin{cases} \dfrac{\mu_0^2 H^3}{4n^3\pi^3} + O(n^{-5}) & ,n \text{ even} \\ -\dfrac{2H}{n\pi} + O(n^{-3}) & ,n \text{ odd} \end{cases} \Rightarrow$$

$$J(0;W_n,Z_{-2}) = \begin{cases} \dfrac{\mu_0 H^3}{n^3\pi^3}\left(a_2\left(\dfrac{\mu_0 H}{4} + 2\right) + (1 - a_2 H)\mu_0\right) + O(n^{-5}) & ,n \text{ even} \\ -\dfrac{2H}{n\pi} + O(n^{-3}) & ,n \text{ odd} \end{cases} \tag{D.8a}$$

$$J(0;W_n,Z_{-1}) = \frac{a_1}{H}J(2;W_n) + \frac{1}{h_0}J(1;W_n) + (1-a_2H)J(0;W_n) \Rightarrow$$

$$J(0;W_n,Z_{-1}) \xrightarrow{n\to\infty} \frac{a_1}{H}\begin{cases} \frac{\mu_0 H^4}{n^3\pi^3}\left(\frac{\mu_0 H}{4}+2\right)+O(n^{-5}) & ,n \text{ even} \\ -\frac{2H^3}{n\pi}+O(n^{-3}) & ,n \text{ odd} \end{cases}$$

$$+\frac{1}{h_0}\begin{cases} \frac{\mu_0 H^3}{n^3\pi^3}\left(\frac{\mu_0 H}{4}+1\right)+O(n^{-5}) & ,n \text{ even} \\ -\frac{2H^2}{n\pi}+O(n^{-3}) & ,n \text{ odd} \end{cases} + (1-a_2H)\begin{cases} \frac{\mu_0^2 H^3}{4n^3\pi^3}+O(n^{-5}) & ,n \text{ even} \\ -\frac{2H}{n\pi}+O(n^{-3}) & ,n \text{ odd} \end{cases} \Rightarrow$$

$$J(0;W_n,Z_{-1}) = \begin{cases} \frac{\mu_0 H^3}{n^3\pi^3}\left(\frac{a_1\mu_0}{4}+2a_1+\frac{\mu_0 H}{4h_0}+\frac{1}{h_0}+(1-a_2H)\frac{\mu_0}{4}\right)+O(n^{-5}) & ,n \text{ even} \\ -\frac{2H}{n\pi}\left(a_1H+\frac{H}{h_0}+1-a_2H\right)+O(n^{-3}) & ,n \text{ odd} \end{cases} \quad \text{(D.8b)}$$

$$J(0;W_n,Z_0) = -\frac{\mu_0^2}{(k_n^2+k_0^2)k_n} - \frac{k_n}{k_n^2+k_0^2}\left[1-\frac{1}{\cos(k_nH)\cosh(k_0H)}\right] \Rightarrow$$

$$J(0;W_n,Z_0) = -\frac{\mu_0^2}{\frac{n^3\pi^3}{H^3}+O(n)} - \frac{\frac{n\pi}{H}+O(n^{-1})}{\frac{n^2\pi^2}{H^2}+O(1)}\left[1-\frac{(-1)^n}{\cosh(k_0H)}\right] \Rightarrow$$

$$J(0;W_n,Z_0) = -\frac{H}{n\pi}\left[1-\frac{(-1)^n}{\cosh(k_0H)}\right]+O(n^{-3}) \quad \text{(D.8c)}$$

$$J(0;W_0,Z_m) = -\frac{\mu_0^2}{(k_0^2+k_m^2)k_0} + \frac{k_0}{k_0^2+k_m^2}\left[1-\frac{1}{\cosh(k_0H)\cos(k_mH)}\right] \Rightarrow$$

$$J(0;W_0,Z_m) = -\frac{\mu_0^2}{\frac{m^2\pi^2}{H^2}k_0+O(1)} + \frac{k_0}{\frac{m^2\pi^2}{H^2}+O(1)}\left[1-\frac{(-1)^m}{\cosh(k_0H)}\right] \Rightarrow$$

$$J(0;W_0,Z_m) = \frac{H^2}{m^2\pi^2+O(1)}\left(-\frac{\mu_0^2}{k_0}+k_0\left[1-\frac{(-1)^m}{\cosh(k_0H)}\right]\right) \quad \text{(D.8d)}$$

$$J(0;W_n,Z_m) = \frac{\mu_0^2}{(k_n^2-k_m^2)k_n} + \frac{k_n}{k_n^2-k_m^2}[1-\frac{1}{\cos(k_m H)}] + \frac{1}{\cos(k_m H)}\frac{k_n[1-\frac{1}{\cos(k_n H)}]}{k_n^2-k_m^2} \Rightarrow$$

$$J(0;W_n,Z_m) = \frac{\mu_0^2}{(k_n^2-k_m^2)k_n} - \frac{k_n}{k_n^2-k_m^2}[1-\frac{1}{\cos(k_n H)\cos(k_m H)}]$$

For $m \to \infty$ we have:

$$J(0;W_n,Z_m) = \frac{\mu_0^2}{-\frac{m^2\pi^2}{H^2}k_n + O(1)} + \frac{k_n}{-\frac{m^2\pi^2}{H^2} + O(1)}[1-(-1)^n\left[1+\frac{\mu_0^2 H^2}{4n^2\pi^2} + O(m^{-4})\right]]$$

$$+(-1)^n\frac{k_n[1-\frac{1}{\cos(k_n H)}]}{-\frac{m^2\pi^2}{H^2} + O(1)} \Rightarrow$$

$$J(0;W_n,Z_m) = -\frac{\mu_0^2 H^2}{m^2\pi^2 k_n + O(1)} - \frac{k_n H^2}{m^2\pi^2 + O(1)}[1-(-1)^n\left[1+\frac{\mu_0^2 H^2}{4m^2\pi^2} + O(m^{-4})\right]]$$

$$-(-1)^n\frac{H^2 k_n[1-\frac{1}{\cos(k_n H)}]}{m^2\pi^2 + O(1)} \Rightarrow$$

$$J(0;W_n,Z_m) = -\frac{H^2}{m^2\pi^2}\left(\frac{\mu_0^2}{k_n} + k_n\left[1-(-1)^n\right] - (-1)^n k_n[1-\frac{1}{\cos(k_n H)}]\right), \qquad \text{(D.8e)}$$

$$+O(m^{-4})$$

For $n \to \infty$ we have:

$$J(0;W_n,Z_m) = \frac{\mu_0^2}{\frac{n^3\pi^3}{H^3} + O(n)} + \frac{\frac{n\pi}{H} + O(n^{-2})}{\frac{n^2\pi^2}{H^2} + O(1)}[1-\frac{1}{\cos(k_m H)}]$$

$$+\frac{1}{\cos(k_m H)}\frac{\frac{n\pi}{H}[1-(-1)^n\left[1+\frac{\mu_0^2 H^2}{4\pi^2 n^2} + O\left(n^{-4}\right)\right]]}{\frac{n^2\pi^2}{H^2} + O(1)} \Rightarrow$$

$$J(0;W_n,Z_m) = \frac{\mu_0^2 H^3}{n^3\pi^3} + \frac{H}{n\pi}[1-\frac{1}{\cos(k_m H)}] + \frac{1}{\cos(k_m H)}\frac{H\left[1-(-1)^n\right]}{n\pi} \Rightarrow$$

$$J(0;W_n,Z_m) = \frac{H}{n\pi}[1+\frac{(-1)^n}{\cos(k_m H)}] + O(n^{-3}), \qquad \text{(D.8f)}$$

For $m = n - c$, $n \to \infty$ we have:

$$J(0;W_n,Z_m) = \frac{\mu_0^2}{(\frac{n^2\pi^2}{H^2} - \frac{(n-c)^2\pi^2}{H^2})\frac{n\pi}{H} + O(n)} - \frac{\frac{n\pi}{H} + O(1)}{\frac{n^2\pi^2}{H^2} - \frac{(n-c)^2\pi^2}{H^2} + O(1)}$$
$$[1 - (-1)^{n+n-c}\left[1 + \frac{\mu_0^2 H^2}{4\pi^2 n^2} + O\left(n^{-4}\right)\right]\left[1 + \frac{\mu_0^2 H^2}{4\pi^2 (n-c)^2} + O\left(n^{-4}\right)\right]] \Rightarrow$$

$$J(0;W_n,Z_m) = \frac{\mu_0^2}{\frac{2n^2 c\pi^3}{H^3} + O(n)} - \frac{\frac{n\pi}{H} + O(1)}{\frac{2nc\pi^2}{H^2} + O(1)}[1 - (-1)^{2n-c}\left[1 + \frac{\mu_0^2 H^2}{2\pi^2 n^2} + O\left(n^{-4}\right)\right]] \Rightarrow$$

$$J(0;W_n,Z_m) = \frac{\mu_0^2 H^3}{2n^2 c\pi^3} - \frac{H}{2c\pi}[1 - (-1)^{2n-c}\left[1 + \frac{\mu_0^2 H^2}{2\pi^2 n^2} + O\left(n^{-4}\right)\right]] \Rightarrow$$

$$J(0;W_n,Z_m) = \begin{cases} \frac{\mu_0^2 H^3}{4c\pi^3 n^2} + O(n^{-4}) & ,c \text{ even} \\ -\frac{H}{c\pi} + O(n^{-2}) & ,c \text{ odd} \end{cases}$$

$$J(0;W_m,Z_m) = \frac{\mu_0^2}{2k_m^3} = \frac{\mu_0^2 H^3}{2m^3\pi^3} + O(m^{-5}), \qquad \text{D.8g)}$$

Asymptotic behavior of $J(0;W_n,W_m)$ integrals

$$J(0;W_n,W_0) = -\frac{\mu_0}{k_0 k_n} = -\frac{\mu_0 H}{k_0 n\pi} + O(n^{-2}) \qquad \text{(D.9a)}$$

$$J(0;W_n,W_m) = \frac{\mu_0}{k_m k_n} = \frac{\mu_0 H}{k_m n\pi} + O(n^{-2}), \qquad \text{as } n \to \infty \qquad \text{(D.9b)}$$

$$J(0;W_n,W_m) = \frac{\mu_0 H}{k_n m\pi} + O(m^{-2}), \qquad \text{as } m \to \infty, \qquad \text{(D.9d)}$$

$$J(0;W_n,W_m) = \frac{\mu_0 H^2}{n^2\pi^2} + O(n^{-4}), \qquad \text{as } n-m = c \wedge n \to \infty, \qquad \text{(D.9e)}$$

$$J(0;W_n,W_n) = \frac{\mu_0 + H(k_n^2 + \mu_0^2)}{2k_n^2} = \frac{H}{2} + \frac{\mu_0 + H\mu_0^2}{2k_n^2} \Rightarrow$$

$$J(0;W_n,W_n) = \frac{H}{2} + H^2\frac{\mu_0 + H\mu_0^2}{2n^2\pi^2} + O(n^{-4}) \tag{D.8f}$$

Now we can proceed on the asymptotics of the matrix coefficients $A_{m,n}$, $B_{m,n}$, $C_{m,n}$. For that purpose we will use the Eqs (2.26) and (2.27) of Chapter 2, Section 2. It should also be noted that the asymptotic behavior of the coefficients $A_{m,n}$ can readily be found in Eqs (D.6) and so their formulae will not be explicitly written. For the other coefficients we will exploit the aforementioned relations (2.26) and (2.27), the asymptotic behavior of the basic integrals and the functions $\boldsymbol{F}_n^{(i)}$, $n\geq 1$ and $G_n^{(i)}$, $n\geq 1$, calculated in this Appendix, as well as the asymptotic behavior of the wave numbers k_n as was presented in Proposition 2 of Section 2.3.

Asymptotics of matrix coefficients $B_{m,n}$

$$B_{m,-2} = \boldsymbol{F}_{-2}^{(0)}\, J(0;Z_m) + \boldsymbol{F}_{-2}^{(1)} J(1;Z_m) + \boldsymbol{F}_{-2}^{(2)}\, J(2;Z_m) + \nabla_{\boldsymbol{x}} h\left[Z_m Z_{-2}\right]_{-h} \Rightarrow$$

$$B_{m,-2} = -\boldsymbol{F}_{-2}^{(0)}\frac{\mu_0 H^2}{m^2\pi^2} + \boldsymbol{F}_{-2}^{(1)}\begin{cases} -\dfrac{\mu_0 H^3}{m^2\pi^2} & ,n \text{ even} \\ -\dfrac{H^2}{m^2\pi^2}\left(\mu_0 H + 2\right) & ,n \text{ odd} \end{cases}$$

$$+ \boldsymbol{F}_{-2}^{(2)}\begin{cases} -\dfrac{\mu_0 H^4}{m^2\pi^2} & ,\mathrm{mod}(n,2)=0 \\ -\dfrac{H^3}{m^2\pi^2}\left(\mu_0 H + 4\right) & ,\mathrm{mod}(n,2)=1 \end{cases} + (-1)^m \nabla_{\boldsymbol{x}} h\left[Z_{-2}\right]_{-h} \Rightarrow$$

$$B_{m,-2} = (-1)^m (1 - a_2 H)\nabla_{\boldsymbol{x}} h + O(m^{-2}), \tag{D.9a}$$

$$B_{m,-1} = \boldsymbol{F}_{-1}^{(0)}\, J(0;Z_m) + \boldsymbol{F}_{-1}^{(1)} J(1;Z_m) + \boldsymbol{F}_{-1}^{(2)}\, J(2;Z_m) + \nabla_{\boldsymbol{x}} h\left[Z_m Z_{-1}\right]_{-h} \Rightarrow$$

$$B_{m,-1} = \boldsymbol{F}_{-1}^{(0)}\frac{\mu_0 H^2}{m^2\pi^2} + \boldsymbol{F}_{-1}^{(1)}\begin{cases} -\dfrac{\mu_0 H^3}{m^2\pi^2} & ,n \text{ even} \\ -\dfrac{H^2}{m^2\pi^2}\left(\mu_0 H + 2\right) & ,n \text{ odd} \end{cases}$$

$$+ \boldsymbol{F}_{-1}^{(2)}\begin{cases} -\dfrac{\mu_0 H^4}{m^2\pi^2} & ,n \text{ even} \\ -\dfrac{H^3}{m^2\pi^2}\left(\mu_0 H + 4\right) & ,n \text{ odd} \end{cases} + (-1)^m \nabla_{\boldsymbol{x}} h\left[Z_{-1}\right]_{-h} \Rightarrow$$

$$B_{m,-1} = (-1)^m (1 - a_2 H)\nabla_x h + O(m^{-2}), \qquad \text{(D.9b)}$$

$$B_{m,0} = 2\left(\boldsymbol{F}_0^{(2)} J(0; W_0 Z_m) + \frac{2k_0}{k_m^2 + k_0^2} \boldsymbol{F}_0^{(3)} J(0; Z_0 Z_0) \right) + \nabla_x h \left[Z_m Z_0 \right]_{-h} \Rightarrow$$

$$B_{m,0} = 2\left(\boldsymbol{F}_0^{(2)} \frac{H^2}{m^2 \pi^2} \left(-\frac{\mu_0^2}{k_0} + k_0 [1 - \frac{(-1)^m}{\cosh(k_0 H)}] \right) + \frac{2k_0 H^2}{m^2 \pi^2 + k_0^2} \boldsymbol{F}_0^{(3)} J(0; Z_0 Z_0) \right)$$

$$+ (-1)^m \nabla_x h \left[Z_0 \right]_{-h} \Rightarrow$$

$$B_{m,0} = (-1)^m \frac{\nabla_x h}{\cosh(k_0 H)} + O(m^{-2}), \qquad \text{(D.9c)}$$

$$B_{-2,n} = 2\boldsymbol{F}_n^{(1)} J(0; Z_n, Z_{-2}) + 2\boldsymbol{F}_n^{(2)} J(0; W_n, Z_{-2}) +$$

$$+ 2\boldsymbol{F}_n^{(3)} [\frac{a_2}{H} J(3; W_n) + (1 - a_2 H) J(1; W_n)] + \nabla_x h \frac{(1 - a_2 H)}{\cos(k_n H)} \Rightarrow$$

$$B_{-2,n} = 2\frac{H^3 \mu_0^3}{n^2 \pi^2} \nabla_x H \begin{cases} -\dfrac{\mu_0 H^2}{n^2 \pi^2} & , n \text{ even} \\ (4a_2 - \mu_0) \dfrac{H^2}{n^2 \pi^2} & , n \text{ odd} \end{cases}$$

$$+ 2\frac{n\pi}{H} \nabla_x h \begin{cases} \dfrac{\mu_0 H^3}{n^3 \pi^3} \left(a_2 \left(\dfrac{\mu_0 H}{4} + 2 \right) + (1 - a_2 H)\mu_0 \right) & , n \text{ even} \\ -\dfrac{2H}{n\pi} & , n \text{ odd} \end{cases}$$

$$- 2\frac{n\pi}{H^2} \nabla_x H [\frac{a_2}{H} \begin{cases} \dfrac{\mu_0 H^5}{n^3 \pi^3} \left(\dfrac{\mu_0 H}{4} + 3 \right) & , n \text{ even} \\ -\dfrac{2H^4}{n\pi} & , n \text{ odd} \end{cases}$$

$$+ (1 - a_2 H) \begin{cases} \dfrac{\mu_0 H^3}{n^3 \pi^3} \left(\dfrac{\mu_0 H}{4} + 1 \right) & , n \text{ even} \\ -\dfrac{2H^2}{n\pi} & , n \text{ odd} \end{cases}] + (-1)^m (1 - a_2 H) \nabla_x h \Rightarrow$$

$$B_{-2,n} = (-1)^n (1 - a_2 H)\nabla_x h + \begin{cases} 0 & , n \text{ even} \\ 4\nabla_x H - 4\nabla_x h & , n \text{ odd} \end{cases} + O(n^{-2}) \qquad \text{(D.9d)}$$

$$B_{-1,n} = 2\,\boldsymbol{F}_n^{(1)}\,J(0;Z_n,Z_{-1}) + 2\,\boldsymbol{F}_n^{(2)}\,J(0;W_n,Z_{-1}) +$$

$$+2\,\boldsymbol{F}_n^{(3)}\left[\frac{a_1}{H}J(3;W_n) + \frac{1}{h_0}J(2;W_n) + (1-a_2\,H)\,J(1;W_n)\right] + \nabla_x h\,\frac{(1-a_2\,H)}{\cos(k_n\,H)} \Rightarrow$$

$$B_{-1,n} = 2\frac{H^3\,\mu_0^3}{n^2\,\pi^2}\nabla_x H\begin{cases}\dfrac{\mu_0\,H^2}{n^2\,\pi^2}\left(-a_1\,H + \dfrac{H}{h_0} + a_2\,H - 1\right) & ,\mathrm{mod}(n,2)=0\\ -\dfrac{H^2}{n^2\,\pi^2}\left(a_1(\mu_0\,H+4) + \dfrac{\mu_0\,H+2}{h_0} - a_2\,\mu_0\,H + \mu_0\right) & ,\mathrm{mod}(n,2)=1\end{cases}$$

$$+\,2\frac{n\,\pi}{H}\nabla_x h\begin{cases}\dfrac{\mu_0\,H^3}{n^3\,\pi^3}\left(\dfrac{a_1\,\mu_0}{4} + 2\,a_1 + \dfrac{\mu_0\,H}{4\,h_0} + \dfrac{1}{h_0} + (1-a_2\,H)\dfrac{\mu_0}{4}\right) & ,\mathrm{mod}(n,2)=0\\ -\dfrac{2\,H}{n\,\pi}\left(a_1\,H + \dfrac{H}{h_0} + 1 - a_2\,H\right) & ,\mathrm{mod}(n,2)=1\end{cases}$$

$$-\,2\frac{n\,\pi}{H^2}\nabla_x H\left[\frac{a_1}{H}\begin{cases}\dfrac{\mu_0\,H^5}{n^3\,\pi^3}\left(\dfrac{\mu_0\,H}{4}+3\right) & ,\mathrm{mod}(n,2)=0\\ -\dfrac{2H^4}{n\,\pi} & ,\mathrm{mod}(n,2)=1\end{cases} + \frac{1}{h_0}\begin{cases}\dfrac{\mu_0\,H^4}{n^3\,\pi^3}\left(\dfrac{\mu_0\,H}{4}+2\right) & ,\mathrm{mod}(n,2)=0\\ -\dfrac{2H^3}{n\,\pi} & ,\mathrm{mod}(n,2)=1\end{cases}\right.$$

$$\left.+\,(1-a_2\,H)\begin{cases}\dfrac{\mu_0\,H^3}{n^3\,\pi^3}\left(\dfrac{\mu_0\,H}{4}+1\right) & ,\mathrm{mod}(n,2)=0\\ -\dfrac{2H^2}{n\,\pi} & ,\mathrm{mod}(n,2)=1\end{cases}\right] + (-1)^n\,\nabla_x h\,(1-a_2\,H) \Rightarrow$$

$$B_{-1,n} = (-1)^n\,\nabla_x h\,(1-a_2\,H) + \begin{cases}0 & ,n\ \text{even}\\ -4\left(a_1\,H + \dfrac{H}{h_0} + 1 - a_2\,H\right)\nabla_x h & \\ +\,4\left(a_1 + \dfrac{H}{h_0}\,1 - a_2\,H\right)\nabla_x H & ,n\ \text{odd}\end{cases} + O(n^{-2}) \qquad \text{(D.9e)}$$

$$B_{0,n} = 2\left(-\boldsymbol{F}_n^{(2)}\,J(0;W_n\,Z_0) + \frac{k_n}{k_0^2+k_n^2}\boldsymbol{F}_n^{(3)}\,J(0;Z_n\,Z_n)\right) + \nabla_x h\,[Z_0\,Z_n]_{-h} \Rightarrow$$

$$B_{0,n} = 2\left(\frac{n\,\pi}{H}\nabla_x h\frac{H}{n\,\pi} - \frac{\dfrac{n\,\pi}{H}}{k_0^2 + \dfrac{n^2\,\pi^2}{H^2}}\frac{n\,\pi}{H^2}\nabla_x H\frac{H}{2}\right) + (-1)^n\frac{\nabla_x h}{\cosh(k_0\,H)} \Rightarrow$$

$$B_{0,n} = \left[2 + \frac{(-1)^n}{\cosh(k_0\,H)}\right]\nabla_x h - \nabla_x H + O(n^{-2}) \qquad \text{(D.9f)}$$

$$B_{m,m} = 2\left(\boldsymbol{F}_m^{(1)} J(0; Z_m Z_m) + \left(\boldsymbol{F}_m^{(3)} - \boldsymbol{F}_m^{(2)} \right) J(0; W_m Z_m) + \frac{1}{2k_m} \boldsymbol{F}_m^{(3)} J(0; W_m W_m) \right) +$$
$$+ \nabla_{\boldsymbol{x}} h \left[Z_m Z_m \right]_{-h}, \Rightarrow$$

$$B_{m,m} = 2\left(\frac{H^3 \mu_0^3}{m^2 \pi^2} \nabla_{\boldsymbol{x}} H \frac{H}{2} + \left(-\frac{m\pi}{H^2} \nabla_{\boldsymbol{x}} H - \frac{m\pi}{H} \nabla_{\boldsymbol{x}} h \right) \frac{\mu_0^2 H^3}{2 m^3 \pi^3} - \frac{H}{2m\pi} \frac{m\pi}{H^2} \nabla_{\boldsymbol{x}} H \frac{H}{2} \right) + \nabla_{\boldsymbol{x}} h \Rightarrow$$

$$B_{m,m} = \nabla_{\boldsymbol{x}} h - \frac{1}{2} \nabla_{\boldsymbol{x}} H + O(m^{-2}) \qquad \text{(D.9g)}$$

$$B_{m,n} = 2\left(- \boldsymbol{F}_n^{(2)} J(0; W_n Z_m) + \frac{2k_n}{k_m^2 - k_n^2} \boldsymbol{F}_n^{(3)} J(0; Z_n Z_n) \right) + \nabla_{\boldsymbol{x}} h \left[Z_m Z_n \right]_{-h} \Rightarrow$$

For $n \to \infty$ we have:

$$B_{m,n} = 2\left(-\frac{n\pi}{H} \nabla_{\boldsymbol{x}} h \frac{H}{n\pi} [1 + \frac{(-1)^n}{\cos(k_m H)}] - \frac{2\frac{n\pi}{H}}{k_m^2 - \frac{n^2\pi^2}{H^2}} \frac{n\pi}{H^2} \frac{H}{2} \nabla_{\boldsymbol{x}} H \right) + (-1)^n \frac{\nabla_{\boldsymbol{x}} h}{\cos(k_m H)} \Rightarrow$$

$$B_{m,n} = 2\nabla_{\boldsymbol{x}} H - 2\nabla_{\boldsymbol{x}} h + O(n^{-2}) \qquad \text{(D.9h)}$$

For $m \to \infty$ we have:

$$B_{m,n} = 2\boldsymbol{F}_n^{(2)} \frac{H^2}{m^2 \pi^2} \left(\frac{\mu_0^2}{k_n} + k_n \left[1 - (-1)^n \right] - (-1)^m k_n [1 - \frac{1}{\cos(k_n H)}] \right)$$
$$+ \frac{4k_n}{\frac{m^2\pi^2}{H^2} - k_n^2} \boldsymbol{F}_n^{(3)} J(0; Z_n Z_n) + (-1)^m \frac{\nabla_{\boldsymbol{x}} h}{\cos(k_n H)} \Rightarrow$$

$$B_{m,n} = (-1)^m \frac{\nabla_{\boldsymbol{x}} h}{\cos(k_n H)} + O(m^{-2}) \qquad \text{(D.9i)}$$

For $m = n - c$, $n \to \infty$ we have:

$$B_{m,n} = 2\left(-\frac{n\pi}{H}\nabla_x h \frac{H}{n\pi}[1 + \frac{(-1)^n}{\cos(k_m H)}] - \frac{2\frac{n\pi}{H}}{k_m^2 - \frac{n^2\pi^2}{H^2}} \frac{n\pi}{H^2}\frac{H}{2}\nabla_x H \right) + (-1)^n \frac{\nabla_x h}{\cos(k_m H)} \Rightarrow$$

$$B_{m,n} = 2\left(-\left(\frac{n\pi}{H}\nabla_x h + O(n^{-1})\right) \begin{cases} \frac{\mu_0^2 H^3}{4c\pi^3 n^2} + O(n^{-4}) & ,c \text{ even} \\ -\frac{H}{c\pi} + O(n^{-2}) & ,c \text{ odd} \end{cases} - \right.$$
$$\left. - \frac{2\frac{n\pi}{H} + O(n^{-1})}{\frac{(n-c)^2\pi^2}{H^2} - \frac{n^2\pi^2}{H^2}} \frac{n\pi}{H^2}\nabla_x H \frac{H}{2} \right) + \nabla_x h\,(-1)^{2n-c}\left[1 + O\left(n^{-2}\right)\right] \Rightarrow$$

$$B_{m,n} = 2\left(\begin{cases} -\frac{\mu_0^2 H^2}{4c\pi^2 n}\nabla_x h + O(n^{-4}) & ,c \text{ even} \\ \frac{n}{c}\nabla_x h + O(n^{-2}) & ,c \text{ odd} \end{cases} + \frac{nH}{2c}\nabla_x H \right) + \nabla_x h\,(-1)^{2n-c} \Rightarrow$$

$$B_{m,n} = \begin{cases} \frac{nH}{c}\nabla_x H + O(1) & ,c \text{ even} \\ \frac{n}{c}\left[H\nabla_x H + 2\nabla_x h\right] + O(n^{-2}) & ,c \text{ odd} \end{cases}, \qquad \text{D(9.j)}$$

Asymptotics of matrix coefficients $C_{m,n}$

$$C_{m,-2} = \left(G_{-2}^{(0)} + \frac{2a_2}{H}\right) J(0; Z_m) + G_{-2}^{(1)} J(1; Z_m) + G_{-2}^{(2)} J(2; Z_m) - \nabla_x h \cdot \boldsymbol{F}_{-2}^{(0)}\left[Z_m\right]_{-h} \Rightarrow$$

$$C_{m,-2} = -\left(G_{-2}^{(0)} + \frac{2a_2}{H}\right)\frac{\mu_0 H^2}{m^2\pi^2} + G_{-2}^{(1)} \begin{cases} -\frac{\mu_0 H^3}{m^2\pi^2} & ,m \text{ even} \\ -\frac{H^2}{m^2\pi^2}(\mu_0 H + 2) & ,m \text{ odd} \end{cases}$$
$$+ G_{-2}^{(2)} \begin{cases} -\frac{\mu_0 H^4}{m^2\pi^2} & ,m \text{ even} \\ -\frac{H^3}{m^2\pi^2}(\mu_0 H + 4) & ,m \text{ odd} \end{cases} - (-1)^m \nabla_x h \cdot \boldsymbol{F}_{-2}^{(0)} \Rightarrow$$

$$C_{m,-2} = -(-1)^m \nabla_{\boldsymbol{x}} h \cdot \boldsymbol{F}_{-2}^{(0)} + O(m^{-1}) \tag{D.10a}$$

$$C_{m,-1} = \left(G_{-1}^{(0)} + \frac{2a_1}{H} \right) J(0; Z_m) + G_{-1}^{(1)} J(1; Z_m) + G_{-1}^{(2)} J(2; Z_m) - \nabla_{\boldsymbol{x}} h \cdot \boldsymbol{F}_{-1}^{(0)} [Z_m]_{-h} \Rightarrow$$

$$C_{m,-1} = -\left(G_{-1}^{(0)} + \frac{2a_1}{H} \right) \frac{\mu_0 H^2}{m^2 \pi^2} + G_{-1}^{(1)} \begin{cases} -\dfrac{\mu_0 H^3}{m^2 \pi^2} & , m \text{ even} \\ -\dfrac{H^2}{m^2 \pi^2} (\mu_0 H + 2) & , m \text{ odd} \end{cases}$$

$$+ G_{-1}^{(2)} \begin{cases} -\dfrac{\mu_0 H^4}{m^2 \pi^2} & , m \text{ even} \\ -\dfrac{H^3}{m^2 \pi^2} (\mu_0 H + 4) & , m \text{ odd} \end{cases} - (-1)^m \nabla_{\boldsymbol{x}} h \cdot \boldsymbol{F}_{-1}^{(0)} \Rightarrow$$

$$C_{m,-1} = -(-1)^m \nabla_{\boldsymbol{x}} h \cdot \boldsymbol{F}_{-1}^{(0)} + O(m^{-1}) \tag{D.10b}$$

$$C_{m,0} = \left(-G_0^{(3)} \frac{4k_0^2}{\left(k_0^2 + k_m^2\right)^2} + G_0^{(5)} \frac{2k_0}{k_m^2 + k_0^2} \right) J(0; Z_0 Z_0)$$

$$+ G_0^{(3)} \frac{4k_m^2}{\left(k_0^2 + k_m^2\right)^2} J(0; Z_m Z_m) + \left(-G_0^{(2)} \frac{k_0}{k_0^2 + k_m^2} + G_0^{(4)} \right) J(0; W_0 Z_m)$$

$$- G_0^{(2)} \frac{k_m}{k_0^2 + k_m^2} J(0; W_m Z_0) - \nabla_{\boldsymbol{x}} h \cdot \boldsymbol{F}_n^{(1)} [Z_0 Z_m]_{-h}$$

$$C_{m,0} = \left(-G_0^{(3)} \frac{4k_0^2}{\left(k_0^2 + \dfrac{m^2 \pi^2}{H^2}\right)^2} + G_0^{(5)} \frac{2k_0}{\dfrac{m^2 \pi^2}{H^2} + k_0^2} \right) J(0; Z_0 Z_0)$$

$$+ G_0^{(3)} \frac{4\dfrac{m^2 \pi^2}{H^2}}{\left(k_0^2 + \dfrac{m^2 \pi^2}{H^2}\right)^2} \frac{H}{2} + \left(-G_0^{(2)} \frac{k_0}{k_0^2 + \dfrac{m^2 \pi^2}{H^2}} + G_0^{(4)} \right) \frac{H^2}{m^2 \pi^2} \left(-\frac{\mu_0^2}{k_0} + k_0 [1 - \frac{(-1)^m}{\cosh(k_0 H)}] \right)$$

$$+ G_0^{(2)} \frac{\dfrac{m\pi}{H}}{k_0^2 + \dfrac{m^2 \pi^2}{H^2}} \frac{H}{m\pi} [1 - \frac{(-1)^m}{\cosh(k_0 H)}] - (-1)^m \nabla_{\boldsymbol{x}} h \cdot \frac{\boldsymbol{F}_n^{(1)}}{\cosh(k_0 H)} \Rightarrow$$

$$C_{m,0} = -(-1)^m \nabla_{\boldsymbol{x}} h \cdot \frac{\boldsymbol{F}_n^{(1)}}{\cosh(k_0 H)} O(m^{-1}) \tag{D.10c}$$

$$C_{-2,n} = G_n^{(1)} J(0; Z_n, Z_{-2}) + G_n^{(4)} J(0; W_n, Z_{-2}) + [(1 - a_2 H) G_n^{(2)}] J(1; Z_n) +$$
$$+ [(1 - a_2 H) G_n^{(3)}] J(2; Z_n) + [\frac{a_2}{H} G_n^{(2)}] J(3; Z_n) + [\frac{a_2}{H} G_n^{(3)}] J(4; Z_n) +$$
$$+ [(1 - a_2 H) G_n^{(5)}] J(1; W_n) + [\frac{a_2}{H} G_n^{(5)}] J(3; W_n) - \frac{F_n^{(1)} (a_2 H - 1)}{\cos(k_n H)} \nabla_x h \Rightarrow$$

$$C_{-2,n} = O(1) \qquad \text{(D.10d)}$$

$$C_{-1,n} = [G_n^{(1)} - k_n^2] J(0; Z_n, Z_{-1}) + G_n^{(4)} J(0; W_n, Z_{-1}) + [(1 - a_2 H) G_n^{(2)}] J(1; Z_n) +$$
$$+ [\frac{1}{h_0} G_n^{(2)} + (1 - a_2 H) G_n^{(3)}] J(2; Z_n) + [\frac{a_1}{H} G_n^{(2)} + \frac{1}{h_0} G_n^{(3)}] J(3; Z_n) + \frac{a_1}{H} G_n^{(3)} J(4; Z_n) +$$
$$+ (1 - a_2 H) G_n^{(5)} J(1; W_n) + \frac{1}{h_0} G_n^{(5)} J(2; W_n) + \frac{a_1}{H} G_n^{(5)} J(3; W_n) + \frac{F_n^{(1)} (1 - a_2 H)}{\cos(k_n H)} \nabla_x h \Rightarrow$$

$$C_{-1,n} = O(1) \qquad \text{(D.10e)}$$

$$C_{0,n} = [\frac{k_n}{k_n^2 + k_0^2} G_n^{(2)} + G_n^{(4)}] J(0; W_n, Z_0) - \frac{k_0}{k_n^2 + k_0^2} G_n^{(2)} J(0; W_0, Z_n) -$$
$$- [\frac{2 k_0}{k_n^2 + k_0^2}]^2 G_n^{(3)} J(0; Z_0, Z_0) + [\left(\frac{2 k_n}{k_n^2 + k_0^2}\right)^2 G_n^{(3)} + \frac{2 k_n}{k_n^2 + k_0^2} G_n^{(5)}] J(0; Z_n, Z_n) +$$
$$+ \frac{F_n^{(1)}}{\cosh(k_0 H) \cos(k_n H)} \cdot \nabla_x h \Rightarrow$$

$$C_{0,n} = -[\frac{\frac{n\pi}{H}}{\frac{n^2\pi^2}{H^2} + k_0^2} 2 \frac{n^2\pi^2}{H^3} \nabla_x H \cdot \nabla_x h + \frac{n\pi}{H} \left(\Delta_x h - \frac{2}{H} \nabla_x h \cdot \nabla_x H \right)] \frac{H}{n\pi} [1 - \frac{(-1)^n}{\cosh(k_0 H)}]$$
$$+ [- \left(\frac{2 \frac{n\pi}{H}}{\frac{n^2\pi^2}{H^2} + k_0^2} \right)^2 \frac{n^2\pi^2}{H^4} |\nabla_x H|^2 + \frac{2 \frac{n\pi}{H}}{\frac{n^2\pi^2}{H^2} + k_0^2} \frac{n\pi}{H^2} \left(\frac{2}{H} |\nabla_x H|^2 - \Delta_x H \right)] \frac{H}{2} \Rightarrow$$

$$C_{0,n} = -[\frac{2}{H} \nabla_x H \cdot \nabla_x h + \left(\Delta_x h - \frac{2}{H} \nabla_x h \cdot \nabla_x H \right)] [1 - \frac{(-1)^n}{\cosh(k_0 H)}]$$
$$+ [- \frac{2}{H} |\nabla_x H|^2 + \left(\frac{2}{H} |\nabla_x H|^2 - \Delta_x H \right)] \Rightarrow$$

$$C_{0,n} = -\Delta_x h [1 - \frac{(-1)^n}{\cosh(k_0 H)}] - \Delta_x H + O(n^{-1}), \qquad \text{(D.10f)}$$

$$C_{m,n} = -\left(G_n^{(3)} \frac{4k_n^2}{\left(k_m^2 - k_n^2\right)^2} + G_n^{(5)} \frac{2k_n}{k_m^2 - k_n^2} \right) J(0; Z_n Z_n)$$
$$+ \left(G_n^{(2)} \frac{k_n}{k_m^2 - k_n^2} + G_n^{(4)} \right) J(0; W_n Z_m) - G_n^{(2)} \frac{k_m}{k_m^2 - k_n^2} J(0; Z_n W_m)$$
$$- G_n^{(3)} \frac{4k_m^2}{\left(k_m^2 - k_n^2\right)^2} J(0; Z_m Z_m) - \nabla_{\boldsymbol{x}} h \cdot \boldsymbol{F}_n^{(1)} \left[Z_n Z_m \right]_{-h}$$

For $n \to \infty$ we have:

$$C_{m,n} = -\left(-\frac{n^2 \pi^2}{H^4} \left| \nabla_{\boldsymbol{x}} H \right|^2 \frac{4H^2}{n^2 \pi^2} - \frac{n\pi}{H^2} \left(\frac{2}{H} \left| \nabla_{\boldsymbol{x}} H \right|^2 - \Delta_{\boldsymbol{x}} H \right) \frac{2H}{n\pi} \right) \frac{H}{2}$$
$$+ \left(-2 \frac{n^2 \pi^2}{H^3} \nabla_{\boldsymbol{x}} H \cdot \nabla_{\boldsymbol{x}} h \frac{H}{n\pi} + \frac{n\pi}{H} \left(\Delta_{\boldsymbol{x}} h - \frac{2}{H} \nabla_{\boldsymbol{x}} h \cdot \nabla_{\boldsymbol{x}} H \right) \right) \frac{H}{n\pi} [1 + \frac{(-1)^n}{\cos(k_m H)}] \Rightarrow$$

$$C_{m,n} = -\left(\frac{4}{H} \left| \nabla_{\boldsymbol{x}} H \right|^2 + \Delta_{\boldsymbol{x}} H \right) + \left(-\frac{4}{H} \nabla_{\boldsymbol{x}} H \cdot \nabla_{\boldsymbol{x}} h + \Delta_{\boldsymbol{x}} h \right) [1 + \frac{(-1)^n}{\cos(k_m H)}] + O(n^{-1})$$

For $m \to \infty$ we have:

$$C_{m,n} = -\frac{(-1)^m}{\cos(k_n H)} \nabla_{\boldsymbol{x}} h \cdot \boldsymbol{F}_n^{(1)} + O(m^{-1}) \,, \qquad \text{(D.10g)}$$

For $m = n - c$, $n \to \infty$ we have:

$$C_{m,n} = \left(\frac{n^2\pi^2}{H^4}\left|\nabla_{\boldsymbol{x}} H\right|^2 \frac{4\dfrac{n^2\pi^2}{H^2}}{\left(\dfrac{(n-c)^2\pi^2}{H^2} - \dfrac{n^2\pi^2}{H^2}\right)^2} - \frac{n\pi}{H^2}\left(\frac{2}{H}\left|\nabla_{\boldsymbol{x}} H\right|^2 - \Delta_{\boldsymbol{x}} H\right) \frac{\dfrac{n\pi}{H}}{\dfrac{(n-c)^2\pi^2}{H^2} - \dfrac{n^2\pi^2}{H^2}} \right) \frac{H}{2}$$

$$+ \left(2\frac{n^2\pi^2}{H^3}\nabla_{\boldsymbol{x}} H\cdot\nabla_{\boldsymbol{x}} h \frac{\dfrac{n\pi}{H}}{\dfrac{(n-c)^2\pi^2}{H^2} - \dfrac{n^2\pi^2}{H^2}} + \frac{n\pi}{H}\left(\Delta_{\boldsymbol{x}} h - \frac{2}{H}\nabla_{\boldsymbol{x}} h\cdot\nabla_{\boldsymbol{x}} H\right) \right) \begin{cases} \dfrac{\mu_0^2 H^3}{4c\pi^3 n^2} + O(n^{-4}) & ,c \text{ even} \\ -\dfrac{H}{c\pi} + O(n^{-2}) & ,c \text{ odd} \end{cases}$$

$$- 2\frac{n^2\pi^2}{H^3}\nabla_{\boldsymbol{x}} H\cdot\nabla_{\boldsymbol{x}} h \frac{\dfrac{(n-c)\pi}{H}}{\dfrac{(n-c)^2\pi^2}{H^2} - \dfrac{n^2\pi^2}{H^2}} \begin{cases} -\dfrac{\mu_0^2 H^3}{4c\pi^3 n^2} + O(n^{-4}) & ,c \text{ even} \\ \dfrac{H}{c\pi} + O(n^{-2}) & ,c \text{ odd} \end{cases}$$

$$+ \frac{n^2\pi^2}{H^4}\left|\nabla_{\boldsymbol{x}} H\right|^2 \frac{4\dfrac{(n-c)^2\pi^2}{H^2}}{\left(\dfrac{(n-c)^2\pi^2}{H^2} - \dfrac{n^2\pi^2}{H^2}\right)^2} \frac{H}{2} - \nabla_{\boldsymbol{x}} h\cdot\nabla_{\boldsymbol{x}} H \frac{H^3\mu_0^3}{n^2\pi^2}(-1)^{2n-c} \Rightarrow$$

$$C_{m,n} = \left(\frac{n^2}{c^2 H^2}\left|\nabla_{\boldsymbol{x}} H\right|^2 + \frac{n}{2cH}\left(\frac{2}{H}\left|\nabla_{\boldsymbol{x}} H\right|^2 - \Delta_{\boldsymbol{x}} H\right) \right) \frac{H}{2}$$

$$+ \left(-\frac{n^2\pi}{cH^2}\nabla_{\boldsymbol{x}} H\cdot\nabla_{\boldsymbol{x}} h + \frac{n\pi}{H}\left(\Delta_{\boldsymbol{x}} h - \frac{2}{H}\nabla_{\boldsymbol{x}} h\cdot\nabla_{\boldsymbol{x}} H\right) \right) \begin{cases} \dfrac{\mu_0^2 H^3}{4c\pi^3 n^2} + O(n^{-4}) & ,c \text{ even} \\ -\dfrac{H}{c\pi} + O(n^{-2}) & ,c \text{ odd} \end{cases}$$

$$+ \frac{n^2\pi}{cH^2}\nabla_{\boldsymbol{x}} H\cdot\nabla_{\boldsymbol{x}} h \begin{cases} -\dfrac{\mu_0^2 H^3}{4c\pi^3 n^2} + O(n^{-4}) & ,c \text{ even} \\ \dfrac{H}{c\pi} + O(n^{-2}) & ,c \text{ odd} \end{cases}$$

$$+ \frac{n^2}{c^2 H^2}\left|\nabla_{\boldsymbol{x}} H\right|^2 \frac{H}{2} - \nabla_{\boldsymbol{x}} h\cdot\nabla_{\boldsymbol{x}} H \frac{H^3\mu_0^3}{n^2\pi^2}(-1)^{2n-c} \Rightarrow$$

$$C_{m,n} = \frac{n^2}{2c^2 H}\left|\nabla_{\boldsymbol{x}} H\right|^2 + \begin{cases} -\dfrac{\mu_0^2 H}{4c^2\pi^2}\nabla_{\boldsymbol{x}} H\cdot\nabla_{\boldsymbol{x}} h + O(n^{-4}) & ,c \text{ even} \\ \dfrac{n^2}{c^2 H}\nabla_{\boldsymbol{x}} H\cdot\nabla_{\boldsymbol{x}} h + O(n^{-2}) & ,c \text{ odd} \end{cases}$$

$$+ \begin{cases} -\dfrac{\mu_0^2 H}{4c^2\pi^2}\nabla_{\boldsymbol{x}} H\cdot\nabla_{\boldsymbol{x}} h + O(n^{-4}) & ,c \text{ even} \\ \dfrac{n^2}{c^2 H}\nabla_{\boldsymbol{x}} H\cdot\nabla_{\boldsymbol{x}} h + O(n^{-2}) & ,c \text{ odd} \end{cases} + \frac{n^2}{c^2 H^2}\left|\nabla_{\boldsymbol{x}} H\right|^2\frac{H}{2} \Rightarrow$$

$$C_{m,n} = \begin{cases} \dfrac{n^2}{c^2 H}\left|\nabla_{\boldsymbol{x}} H\right|^2 + O(n^{-2}) & ,c \text{ even} \\ \dfrac{n^2}{c^2 H}\left[\left|\nabla_{\boldsymbol{x}} H\right|^2 + 2\nabla_{\boldsymbol{x}} H\cdot\nabla_{\boldsymbol{x}} h\right] + O(n^{-2}) & ,c \text{ odd} \end{cases}, \tag{D.10h}$$

$$C_{m,m} = \left(G_m^{(1)} + G_m^{(2)}\frac{H}{2} + G_m^{(3)}\frac{H^2}{3}\right)J(0;Z_m Z_m) + \left(G_m^{(2)}\frac{H}{4} + G_m^{(3)}\frac{H^2}{3}\right)J(0;Z_m) +$$
$$+\left(-G_m^{(2)}\frac{1}{2k_m} + G_m^{(3)}\frac{H}{k_m} + G_m^{(4)} - G_m^{(5)}H\right)J(0;W_m Z_m) +$$
$$+\left(G_m^{(3)}\frac{1}{2k_m^2} - G_m^{(5)}\frac{1}{2k_m}\right)J(0;W_m W_m) - \nabla_{\boldsymbol{x}} h\cdot\boldsymbol{F}_m^{(1)}\left[Z_m Z_m\right]_{-h} \Rightarrow$$

$$C_{m,m} = \left(-\frac{n^2\pi^2}{H^2}\left|\nabla_{\boldsymbol{x}} h\right|^2 + 2\frac{n^2\pi^2}{H^3}\nabla_{\boldsymbol{x}} H\cdot\nabla_{\boldsymbol{x}} h\frac{H}{2} - \frac{n^2\pi^2}{H^4}\left|\nabla_{\boldsymbol{x}} H\right|^2\frac{H^2}{3}\right)\frac{H}{2} \Rightarrow$$

$$C_{m,m} = \frac{2n^2\pi^2}{H}\left(-\left|\nabla_{\boldsymbol{x}} h\right|^2 + \nabla_{\boldsymbol{x}} H\cdot\nabla_{\boldsymbol{x}} h - \frac{1}{3}\left|\nabla_{\boldsymbol{x}} H\right|^2\right), \tag{D.10i}$$

Conclusions & Future Work

The main goal of this thesis was the implementation of the HCM method to a parallel C++ code enabling the efficient simulation of problems defined on large domains. For that purpose, new analytical formulae for the matrix coefficients $A_{mn}, \mathbf{B}_{mn}, C_{mn}$ were derived allowing for a more efficient (computation-wise) method of their calculation. Furthermore, use of arbitrary order of finite differences was actualized and results regarding their error estimates were presented for 2nd order up to 12th order. This step comes as an expansion to the 4th order (and serial) Matlab code that existed before this work. In addition, the parallelization of the code was implemented allowing for fast simulations regarding large problems not possible to be simulated before. Regarding the expansion of the HCM method to a wider range of problems, the equations of the system were derived for a moving seabed, with numerical results being to close proximity with simulations of other models. Also, the effectiveness of the method in calculating forces acted on a vertical wall, caused by a solitary wave, was presented with the numerical results being in very good agreement with those of BEM codes. Finally, asymptotic estimates concerning the matrix coefficients $A_{mn}, \mathbf{B}_{mn}, C_{mn}$, with regard to indexes m, n, were also calculated, a step necessary for future studies concerning the behavior of the substrate problem.

Regarding **future work** on the Hamiltonian Coupled Mode method, we begin by stating that the development of a 3D code is already in progress. The aforementioned code implements the Finite Elements Method, allowing us to also study the problem through a high-order representation of the fields. Furthermore, practice of symplectic time-integration methods appears as an interesting addition to the numerical study of the problem. Concerning a more theoretical aspect, usage of the asymptotic behavior of the matrix coefficients $A_{mn}, \mathbf{B}_{mn}, C_{mn}$ is a necessary and appealing step towards the theoretical justification of the truncated model in use. In addition, systematic study of other truncated models may give rise to approaches with better error estimate and behavior. Finally, a study concerning the optimal value of the parameter μ_0 for an arbitrary simulation may lead to better numerical results as well as decrease the (already low) total number of modes or horizontal points for satisfactory results.

Except for advancements regarding the model described in this work, the HCM method can be expanded to problems with richer physics. This could either mean trivial physical expansions, like the introduction of surface tension, or much more interesting cases like wave-current interactions. To go even further, introduction of vorticity to the problem could allow for more interesting cases to be modeled. Finally, wave-body interactions (a highly practical set of problems) could also be explored, although hybrid methods, incorporating for example BEM near the bodies, may be required for such problems.

Bibliography:

Athanassoulis, G. A., & Belibassakis, K. A. (1998). Water-wave green's function for a 3D uneven-bottom problem with different depths at. In *IUTAM Symposium on Computational Methods for Unbounded Domains* (pp. 21–32).

Athanassoulis, G. A., & Belibassakis, K. A. (1999). A consistent coupled-mode theory for the propagation of small-amplitude water waves over variable bathymetry regions. *Journal of Fluid Mechanics*, *389*, 275–301.

Athanassoulis, G. A., & Belibassakis, K. A. (2000). A Complete Modal Expansion of the Wave Potential and Its Application to Linear and Nonlinear Water-Wave Problems. *Rogue Waves*, 73–90.

Athanassoulis, G. A., & Belibassakis, K. A. (2002). A Coupled-Mode, Fully-dispersive, Weakly-nonlinear Model for Water Waves over a General Bathymetry. In *21st International Conference on Offshore Mechanics and Arctic Engineering* (Vol. 3, pp. 48–55).

Athanassoulis, G. A., & Belibassakis, K. A. (2003). Rapidly-Convergent Local-Mode Representations for Wave Propagation and Scattering in Curved-Boundary Waveguides. In *Mathematical and Numerical Aspects of Wave Propagation WAVES* (pp. 451–456).

Athanassoulis, G. A., & Belibassakis, K. A. (2007). New evolution equations for non-linear water waves in general bathymetry with application to steady travelling solutions in constant, but arbitrary, depth. *Discrete and Continuous Dynamical Systems- Series A*, (SUPPL.), 75–84. http://doi.org/10.3934/proc.2007.2007.75

Athanassoulis, G. A., Belibassakis, K. A., & Livaditi, E. L. (1998). AN ENHANCED COUPLED - MODE THEORY FOR SOUND PROPAGATION OVER AN ARBITRARY BOTTOM TOPOGRAPHY. In *Proceedings of the Fourth European Conference on Underwater Acoustics, ECUA 1998* (pp. 1–6).

Athanassoulis, G. A., & Papoutsellis, C. E. (2015). New form of the Hamiltonian equations for the nonlinear water-wave problem, based on a new representation of the DtN operator, and some applications. In *Proceedings of the 34th International Conference on Ocean, Offshore and Arctic Engineering*.

Athanassoulis, G. A., Papoutsellis, C. E., & Belibassakis, K. A. (2016). A new Hamiltonian formulation of the nonlinear water-wave problem over arbitrary bathymetry, based on an exact vertical series expansion of the wave potential. *To Be Published*.

Barré de Saint-Venant, A. J. C. (1871). Théorie du mouvement non permanent des eaux, avec application aux crues des rivières et à l'introduction des marées dans leurs lits. *Comptes Rendus Des Séances de l'Académie Des Sciences*, *73*, 237–240.

Belibassakis, K. A., Athanassoulis, G. A., & Gerostathis, T. P. (2001). A coupled-mode model for the refraction-diffraction of linear waves over steep three-dimensional bathymetry. *Applied Ocean Research*, *23*, 319–336. Retrieved from file:///C:/Users/Christos/AppData/Local/Mendeley Ltd./Mendeley Desktop/Downloaded/Belibassakis, Athanassoulis, Gerostathis - 2001 - A coupled-mode model for the refraction-diffraction of linear waves over steep three-d.pdf

Belibassakis, K. A., Gerostathis, T. P., & Athanassoulis, G. A. (2011). A coupled-mode model for water wave scattering by horizontal, non-homogeneous current in general bottom topography. *Applied Ocean Research*, *33*(4), 384–397. http://doi.org/10.1016/j.apor.2011.05.004

Benoit, M., & Yates, M. L. (2015). Development and validation of a phase- resolving potential-flow model for nonlinear and dispersive waves in coastal areas. In *Summer school "Wave propagation in complex media."* Corsica, France.

Berkhoff, J. C. W. (1972). Refraction-Diffraction, Computation of Combined. In *Proc. 13th Int. Conf. on Coastal Eng., ASCE* (pp. 471–490). http://doi.org/10.1111/j.1600-0447.1951.tb04161.x

Bingham, H. B., & Zhang, H. (2007). On the accuracy of finite difference solutions for nonlinear water waves. *Journal of Engineering Mathematics*, *58*, 211–228. Retrieved from file:///C:/Users/Christos/AppData/Local/Mendeley Ltd./Mendeley Desktop/Downloaded/Bingham, Zhang - 2007 - On the accuracy of finite difference solutions for nonlinear water waves.pdf

Birkhoff, G., & Rota, G. (1989). *Ordinary Differential Equations* (4th ed.). John Wiley & Sons, Inc.

Boussinesq, J. (1872). Théorie des ondes et des remous qui se propagent le long d'un canal rectangulaire horizontal, en communiquant au liquide contenu dans ce canal des vitesses sensiblement pareilles de la surface au fond. *Journal de Mathématiques Pures et Appliquées*, 55–108.

Bridges, T. J., & Donaldson, N. M. (2011). Variational principles for water waves from the viewpoint of a time-dependent moving mesh. *Mathematika*, *57*(1), 147–173.

Byatt-Smith, J. G. B. (1988). The reflection of a solitary wave by a vertical wall. *Journal of Fluid Mechanics*, *197*, 503–521. http://doi.org/10.1017/S0022112088003349

Cai, X., Langtangen, H. ., Nielsen, B. ., & Tveito, A. (1998). A Finite Element Method for Fully Nonlinear. *Journal of Computational Physicsu*, *143*, 544–568. http://doi.org/DOI: 10.1006/jcph.1998.9997

Chambarel, J., Kharif, C., & Touboul, J. (2009). Head-on collision of two solitary waves and residual falling jet formation. *Nonlinear Processes in Geophysics*, *16*, 111–122. http://doi.org/10.5194/npg-16-111-2009

Chamberlain, P. G., & Porter, D. (1995). The modified mild-slope equation. *Journal of Fluid Mechanics*, *291*, 393.

Chan, R. K. C., & Street, R. L. (1970). A computer study of finite-amplitude water waves. *Journal of Computational Physics*, *6*(1), 68–94. http://doi.org/10.1016/0021-9991(70)90005-7

Clamond, D., & Dutykh, D. (2013). Fast accurate computation of the fully nonlinear solitary surface gravity waves. *Computers & Fluids*, *84*, 35–38.

Clamond, D., & Grue, J. (2001). A fast method for fully nonlinear water-wave computations. *Journal of Fluid Mechanics*, *447*, 337–355. http://doi.org/10.1017/S0022112001006000

Coddington, E. a., & Levinson, N. (1955). Theory of Ordinary Differential Equations. New York: McGraw-Hill Inc.

Cooker, M. J., Weidman, P. D., & Bale, D. S. (1997). Reflection of a high-amplitude solitary wave at a vertical wall. *Journal of Fluid Mechanics*, *342*, 141–158. http://doi.org/10.1017/S002211209700551X

Craig, W., Guyenne, P., Hammack, J., Henderson, D., & Sulem, C. (2006). Solitary water wave interactions. *Physics of Fluids*, *18*(5), 57106. http://doi.org/10.1063/1.2205916

Craig, W., & Sulem, C. (1993). Numerical Simulation of Gravity Waves. *Journal of Computational Physics*, *108*, 73–83.

Craik, A. D. D. (2004). the Origins of Water Wave Theory. *Annual Review of Fluid Mechanics*, *36*(1), 1–28. http://doi.org/10.1146/annurev.fluid.36.050802.122118

Davies, A. G., & Heathershaw, A. D. (1983). Surface wave propagation over sinusoidally varying topography: theory and observation.

Davies, A. G., & Heathershaw, A. D. (1984). Surface-wave propagation over sinusoidally varying topography. *Journal of Fluid Mechanics*, *144*, 419–443. http://doi.org/doi:10.1017/S0022112084001671

Davis, T. a. (2006). *Direct Methods for Sparse Linear Systems*. (N. J. Higham, Ed.). http://doi.org/10.1137/1.9780898718881

Dommermuth, D. G., & Yue, D. K. P. (1987). A high-order spectral method for the study of nonlinear gravity waves. *J. Fluid Mech.*, *184*, 267–288.

Drazin, P. G., & Johnson, R. S. (1989). *Solitions: an introduction*. Cambridge University Press.

Dutykh, D., & Clamond, D. (2012). Modified Shallow Water Equations for significantly varying bottoms. *ArXiv*, *0*, 30. http://doi.org/10.1016/j.apm.2016.06.033

Elsgolc, L. D. (1961). *Calculus of Variations*. Mineola, New York: Dover Publications, Inc.

Engsig-Karup, A. P., Bingham, H. B., & Lindberg, O. (2009). An efficient flexible-order model for 3D nonlinear water waves. *Journal of Computational Physics*, *228*(6), 2100–2118. http://doi.org/10.1016/j.jcp.2008.11.028

Fazioli, C., & Nicholls, D. P. (2010). Stable computation of the functional variation of the Dirichlet–Neumann operator. *Journal of Computational Physics*, *229*(3), 906–920. http://doi.org/10.1016/j.jcp.2009.10.021

Fuhrman, D. R., & Madsen, P. A. (2009). Tsunami generation, propagation, and run-up with a high-order Boussinesq model. *Coastal Engineering*, *56*(7), 747–758. http://doi.org/10.1016/j.coastaleng.2009.02.004

Gagarina, E., Ambati, V. R., van der Vegt, J. J. W., & Bokhove, O. (2014). Variational space–time (dis)continuous Galerkin method for nonlinear free surface water waves. *Journal of Computational Physics*, *275*, 459–483. http://doi.org/10.1016/j.jcp.2014.06.035

Gelfand, I. M., & Fomin, S. V. (1963). *Calculus of Variations*. (R. A. Silverman, Ed.).

Mineola, New York: Dover Publications, Inc.

Gouin, M., Ducrozet, G., & Ferrant, P. (2015). Development and validation of a non-linear spectral model for water waves over variable depth. *European Journal of Mechanics, B/Fluids*, *57*, 115–128. http://doi.org/10.1016/j.euromechflu.2015.12.004

Green, A. E., & Naghdi, P. M. (1976). A derivation of equations for wave propagation in water of variable depth. *Journal of Fluid Mechanics*, *78*(02), 237. http://doi.org/10.1017/S0022112076002425

Grilli, S. T., Guyenne, P., & Dias, F. (2001). A fully non-linear model for three-dimensional overturning waves over an arbitrary bottom. *International Journal for Numerical Methods in Fluids*, *35*(7), 829–867.

Grilli, S. T., Skourup, J., & Svendsen, I. A. (1989). An efficient boundary element method for nonlinear water waves. *Engineering Analysis with Boundary Elements*.

Grilli, S. T., Subramanya, R., Svendsen, I. a., & Veeramony, J. (1994). Shoaling of Solitary Waves on Plane Beaches. *Journal of Waterway, Port, Coastal, and Ocean Engineering*, *120*(6), 609–628. http://doi.org/10.1061/(ASCE)0733-950X(1994)120:6(609)

Hammack, J. L. (1973). A note on tsunamis: their generation and propagation in an ocean of uniform depth. *Journal of Fluid Mechanics*, *60*, 769. http://doi.org/10.1017/S0022112073000479

Hammack, J. L., & Segur, H. (1974). The Korteweg-de Vries equation and water waves. Part 2. Comparison with experiments. *Journal of Fluid Mechanics*, *65*(02), 289–314. http://doi.org/10.1017/S002211207400139X

Huang, C. J., Chang, H. H., & Hwung, H. H. (2003). Structural permeability effects on the interaction of a solitary wave and a submerged breakwater. *Coastal Engineering*, *49*(1-2), 1–24. http://doi.org/10.1016/S0378-3839(03)00034-6

Isobe, M., & Abohadima, S. (1998). Numerical model of fully-nonlinear wave refraction and diffraction. In *Coastal Engineering* (Vol. 26).

Johnson, R. S. (1997). *A Modern Introduction to the Mathematical Theory of Water Waves*. *A Modern Introduction to the Mathematical Theory of Water Waves*. Cambridge University Press.

Kantorovich, L., & Krylov, V. (1958). *Approximate Methods of Higher Analysis*. New York: Interscience Publishers, Inc.

Klopman, G., Van Groesen, B., & Dingemans, M. W. (2010). A variational approach to Boussinesq modelling of fully nonlinear water waves. *Journal of Fluid Mechanics*, *657*(2010), 36–63.

Korteweg, D. J., & de Vries, G. (1895). On the change of form of long waves advancing in a rectangular canal, and on a new type of long stationary waves. *Philosophical Magazine Series 5*, *39*(240), 422–443. http://doi.org/10.1080/14786449508620739

Kreiss, H.-O., & Oliger, J. (1972). Comparison of accurate methods for the integration of hyperbolic equations. *Tellus*, *24*(3), 199–215. http://doi.org/10.1111/j.2153-3490.1972.tb01547.x

Lannes, D. (2013). *The Water Waves Problem*. Providence, Rhode Island: American Mathematical Society.

Leszek Gasinski, & Papageorgiou, N. S. (2005). *Nonlinear Analysis, Volume 9*. *Analysis and Applications* (Vol. 9). Taylor & Francis Group, LLC.

Lin, P. (2004). A numerical study of solitary wave interaction with rectangular obstacles. *Coastal Engineering*, *51*(1), 35–51. http://doi.org/10.1016/j.coastaleng.2003.11.005

Liu, Y., & Yue, D. (1998). On generalized Bragg scattering of surface waves by bottom ripples. *Journal of Fluid Mechanics*, *356*, 297–326. http://doi.org/10.1017/S0022112097007969

Longuet-Higgins, M. S., & Cokelet, E. D. (1976). The Deformation of Steep Surface Waves on Water. I. A Numerical Method of Computation. *Proceedings of the Royal Society A: Mathematical, Physical and Engineering Science*, *350*(1660), 1–26. http://doi.org/10.1098/rspa.1976.0092

Luke, J. C. (1967). A variational principle for a fluid with a free surface. *J. Fluid Mech.*, *27*(02), 395–397.

Madsen, P. A., Fuhrman, D. R., & Schäffer, H. A. (2008). On the solitary wave paradigm for tsunamis. *Journal of Geophysical Research: Oceans*, *113*(12). http://doi.org/10.1029/2008JC004932

Manolas, D. (2015). *Development of simulation tools for the integrated analysis of offshore wind turbines*. National Technical University of Athens.

Massel, S. R. (1993). Extended refraction-diffraction equation for surface waves. *Coastal Engineering*, *19*, 97–126.

Maxworthy, T. (1976). Experiments on collisions between solitary waves. *Journal of Fluid Mechanics*, *76*(01), 177–185. http://doi.org/10.1017/S0022112076003194

Milder, D. M. (1969). Ray and Wave Invariants for SOFAR Channel Propagation. *The Journal of the Acoustical Society of America*, *46*(April 1969), 1259–1263.

Mitsotakis, D., Dutykh, D., & Carter, J. (2014). On the nonlinear dynamics of the travelling-wave solutions of the Serre equations. *Arxiv*.

Mitsotakis, D., Synolakis, C., & McGuiness, M. (2015). A MODIFIED GALERKIN / FINITE ELEMENT METHOD FOR THE NUMERICAL SOLUTION OF THE SERRE-GREEN-NAGHDI SYSTEM. *Arxiv*, 12. Retrieved from http://arxiv.org/abs/1505.0779

Nicholls, D. P., & Reitich, F. (2001). Stability of High-Order Perturbative Methods for the Computation of Dirichlet–Neumann Operators. *Journal of Computational Physics*, *170*(1), 276–298. http://doi.org/10.1006/jcph.2001.6737

Nwogu, O. (1993). Alternative Form of Boussinesq Equations for Nearshore Wave Propagation. *Journal of Waterway, Port, Coastal, and Ocean Engineering*, *119*(6), 618–638. http://doi.org/10.1061/(ASCE)0733-950X(1993)119:6(618)

Papoutsellis, C. E. (2016). *Nonlinear water waves over varying bathymetry: Theoretical and*

numerical study using variational methods. National Technical University of Athens.

Petrov, A. A. (1964). Variational Statement of the Problem of Liquid Motion in a Container of Finite Dimensions. *Journal of Applied Mathematics and Mechanics*, *28*(4), 754–758.

Pierce, A. D. (1965). Extension of the Method of Normal Modes to Sound Propagation in an Almost-Stratified Medium. *The Journal of the Acoustical Society of America*, *37*, 19. http://doi.org/10.1121/1.1909303

Porter, D., & Staziker, D. (1995). Extensions of the mild-slope equation. *Journal of Fluid Mechanics*, *300*, 367–382.

Rayleigh, Lord. (1876). On waves. *Phil. Mag.*, *1*, 257–279.

Rycroft, C. H., & Wilkening, J. (2013). Computation of three-dimensional standing water waves. *Journal of Computational Physics*, *255*, 612–638. http://doi.org/10.1016/j.jcp.2013.08.026

Saad, Y. (2003). *Iterative Methods for Sparse Linear Systems Second Edition Yousef Saad* (2nd ed.). http://doi.org/10.2277/0898715342

Seabra-Santos, F. J., Renouard, D. P., & Temperville, A. M. (1987). Numerical and experimental study of the transformation of a solitary wave over a shelf or isolated obstacle. *Journal of Fluid Mechanics*, *176*, 117–134. http://doi.org/10.1017/S0022112087000594

Serre, F. (1953). Contribution {à} l'{é}tude des {é}coulements permanents et variables dans les canaux. *La Houille Blanche*, *8*(9), 830–872.

Stoker, J. J. (1957). *Water Waves: The Mathematical Theory With Applications*. Interscience Publishers, Inc.

Stokes, G. (1847). On the theory of oscillatory waves. *Trans Cambridge Philos Soc*, *8*, 441–473.

Su, C. H., & Mirie, R. M. (1980). On head-on collisions between two solitary waves. *J. Fluid Mech.*, *98*, 509–525.

Wehausen, J. V., & Laitone, E. V. (1960). *Surface Waves*. (S. Flugge, Ed.). Springer-Verlag.

West, B. J., Brueckner, K. A., & Janda, R. S. (1987). A New Numerical Method for Surface Hydrodynamics. *Journal of Geophysical Research: Oceans*, *92*, 11,803–11,824.

Whitham, G. B. (1974). *Linear and Nonlinear Waves*. New York: John Wiley & Sons, Inc.

Xing, Y., & Shu, C. W. (2005). High order finite difference WENO schemes with the exact conservation property for the shallow water equations. *Journal of Computational Physics*, *208*(1), 206–227. http://doi.org/10.1016/j.jcp.2005.02.006

Yates, M. L., & Benoit, M. (2015). Accuracy and efficiency of two numerical methods of solving the potential flow problem for highly nonlinear and dispersive water waves. *International Journal for Numerical Methods in Fluids*, *77*(10), 616–640.

Zakharov, V. E. (1968). Stability of Periodic Waves of Finite Amplitude on the Surface of Deep Fluid. *Journal of Applied Mechanics and Technical Physics*, *9*(2), 190–194.